Spring 2018

Seismic Site Response of Partially Saturated Soil Layers

Morteza Mirshekari
University of New Hampshire, Durham

Seismic Site Response of Partially Saturated Soil Layers

BY

Morteza Mirshekari

B.Sc. University of Tehran, 2010

M.Sc. University of Tehran, 2013

DISSERTATION

Submitted to the University of New Hampshire

in Partial Fulfillment of

the Requirements for the Degree of

Doctor of Philosophy

in

Civil Engineering

May 2018

This dissertation has been examined and approved in partial fulfillment of the requirements for the degree of Doctor of Philosophy in Civil Engineering by:

Dissertation Director, Dr. Majid Ghayoomi
Assistant Professor of Civil and Environmental Engineering

Dr. Jean Benoit
Professor of Civil and Environmental Engineering

Dr. Ricardo Medina
Associate Professor of Civil and Environmental Engineering

Dr. Margaret Boettcher
Associate Professor of Earth Sciences

Dr. James Kaklamanos
Assistant Professor of Civil Engineering
Merrimack College

On January 31, 2017.

Original approval signatures are on file with the University of New Hampshire Graduate School.

Acknowledgment

First and foremost, I would like to express my deepest gratitude and appreciation to my parents who supported me throughout my life. Without their unconditional support and encouragement to pursue my dreams, this work would have not been possible.

I would like to acknowledge Professor Majid Ghayoomi, whose title was my adviser, but his role was far beyond that in my life. I have found Professor Ghayoomi a phenomenal teacher, a friend, an inspiration, and a role model in my life, who guided me throughout different aspects of my journey towards this degree.

I am grateful to the members of my dissertation committee Professors Jean Benoit, Ricardo Medina, Margaret Boettcher, and James Kaklamanos, whose recommendations helped us to improve the quality of this research.

During this research, I received significant assistance from TSC members at UNH, for the renovation, reoperation, and modification of the centrifuge facility. In particular, I would like to thank James Abare, John Ahern, Scott Campbell, Kevan Carpenter, and Christopher Levesque for their contribution to this project.

I would especially like to thank my dear friend Amir Golalipour for his lifetime true friendship. "A good friend knows all your best stories; a best friend has lived them with you."

Lastly, I would like to thank my friends at University of New Hampshire, especially Amin Borghei, Reza Ebadi, Masoud Mousavi, Pegah Jarast, and Shokoufeh Zargar for their friendships and supports during the course of this Ph.D. study.

Table of Contents

List of Tables

List of Figures

ABSTRACT

SEISMIC SITE RESPONSE OF PARTIALLY SATURATED SOIL LAYERS

by

Morteza Mirshekari

University of New Hampshire, May, 2018

Accurate prediction of seismic ground response plays a vital role in earthquake-resistant, sustainable, and cost-effective design of infrastructure. Seismic response of unsaturated soil layers may differ from that of saturated or dry soil deposits. Importantly, surficial soil layers are often partially water-saturated, however, site-specific design procedures only consider ground in either dry or fully saturated conditions. Further, seasonal water table fluctuation introduces additional uncertainty in site-specific response analysis. This research investigates the effect of soil-water interaction on seismic site response of soil layers both experimentally and numerically. To that end, initially, preliminary numerical analyses were performed using the DEEPSOIL software considering uniform suction profiles where partial saturation was considered by changing the unit weight and dynamic soil properties as a function of degree of saturation. Further, a set of centrifuge experiments were conducted to study the influence of partial saturation on seismic response of sand layers under scaled Northridge and Kobe earthquake motions. Steady state infiltration was implemented to control and provide uniform degrees of saturation profiles in depth. Partial saturation led to higher surface-to-base motion intensity amplification than dry conditions; especially in low period ranges. On average, the amplification of peak ground acceleration was inversely proportional to degree of saturation at surface, demonstrating higher amplifications at lower degrees of saturation. It also varied with depth, showing higher values for unsaturated conditions near the ground level. The lateral deformation and surface settlement of partially saturated sand layers with higher stiffness were generally lower than that in dry soil. Although neglecting the effect of partial saturation in sand layers might be conservative with respect to seismic deformations, it may result in underestimating the surface design acceleration spectra. To assess the uncertainty in site response analysis due to water table fluctuation, further parametric analyses were performed using DEEPSOIL program. Water table fluctuations considerably affected the seismic response of sand and silt layers, with a more significant divergence in sandy soils. Variations in small-strain shear modulus and unit weight, due to water table fluctuation, led to considerable change in site response, while the change in damping and modulus reduction factor caused insignificant difference in acceleration amplification, mainly due to the incompetency of their formulations to account for partial saturation.

CHAPTER I

INTRODUCTION

1.1. Research Motivation

Earthquakes impose severe life-threatening and detrimental risks to communities throughout the globe. According to the recent United States Geological Survey (USGS) earthquake hazard maps (Petersen et al. 2014), almost half of Americans are prone to potentially destructive strong ground motions. Considering the potential level of casualties and financial loss due to the ground shakings (e.g. 49 billion dollars of financial loss and 57 deaths only due to the 1994 Northridge earthquake with a moment magnitude of 6.7), even minor advances in earthquake science and engineering could be valuable. Seismic site response of partially saturated soil layers may vary from that of fully saturated or dry conditions (Ghayoomi et al. 2013, Mirshekari and Ghayoomi 2017). Shallow soil layers are mostly partially saturated with the exception of regions with high water table. In addition, due to the seasonal variation of the ground water level, the degree of saturation of soil layers may vary significantly throughout the year.

Partially saturated soils (which can be interchangeably called unsaturated soils) are stiffer than dry or saturated soils due to the presence of capillary suction forces that attract adjacent soil grains (Lu & Likos 2006); as schematically illustrated in Figure 1-2. This will lead to different dynamic soil properties including small-strain and strain-dependent shear modulus and damping (Mancuso et al. 2002, Ng et al. 2009, Ghayoomi and McCartney 2011, Hoyos et al. 2015, Ghayoomi et al. 2017) which, in turn, impacts the wave propagation mechanisms in partially saturated soils (Yang and Sato 2000). As a result, seismic site response in dry, partially saturated, or fully saturated soil layers may differ as a function of degree of saturation (Yang & Sato 2000, D'Onza et al. 2008, Ghayoomi et al. 2011, Mirshekari and Ghayoomi 2017).

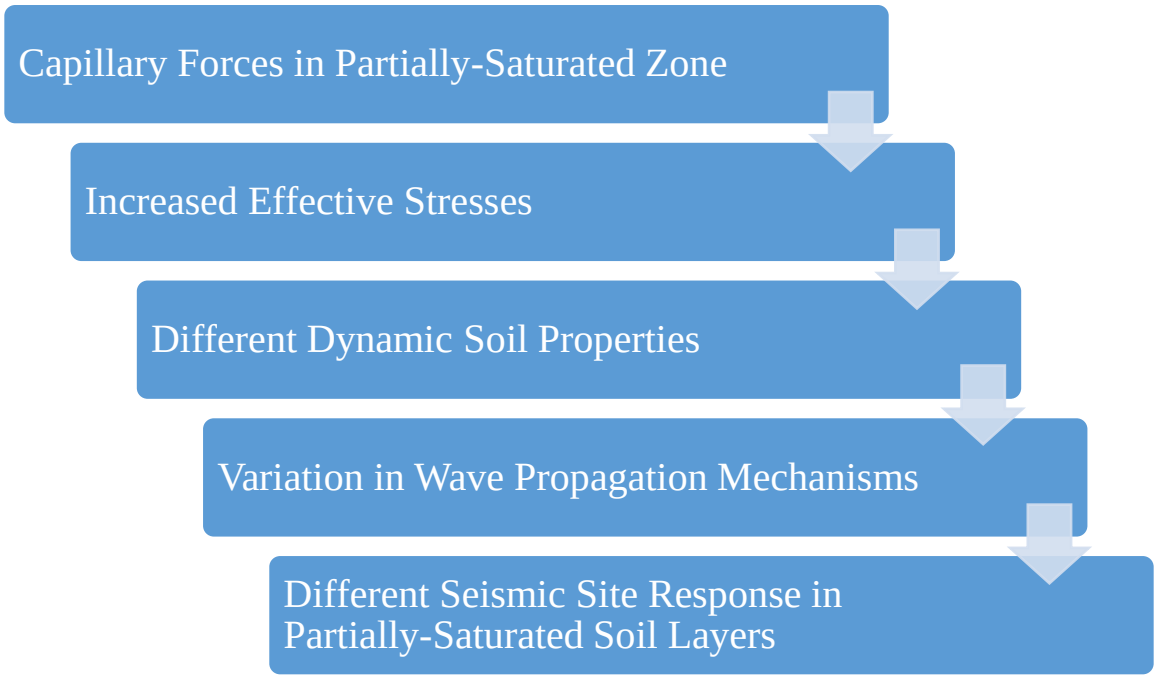

Figure 1-1. A conceptual diagram showing the influence of partial saturation on seismic site response

Assuming soils in either dry or fully saturated conditions has been believed to result in more conservative solutions because matric suction in unsaturated soils increases the ground stiffness. Therefore, although the effect of partial saturation on site response has been recognized in

previous research, partial saturation has not been directly considered in the state-of-the-practice site response analysis. However, recent investigations on site response in unsaturated soils showed that this assumption might not be always reasonable (Ghayoomi and McCartney 2012). Further, the influence of the degree of saturation on seismic response analysis is often considered by incorporating the in-situ measured shear wave velocity of shallow unsaturated soil layers. However, the extent of this influence might be beyond the suction-dependency of the dynamic soil properties where the wave propagation mechanisms may vary (Yang 2006). Thus, recognizing this difference would be essential in assessing the uncertainty in projected site response where well-documented laboratory seismic site response data as well as predictive numerical models in partially saturated soils are still needed. To this end, this research project aims to fill this gap with potential goal of a more reliable evaluation of seismic hazards.

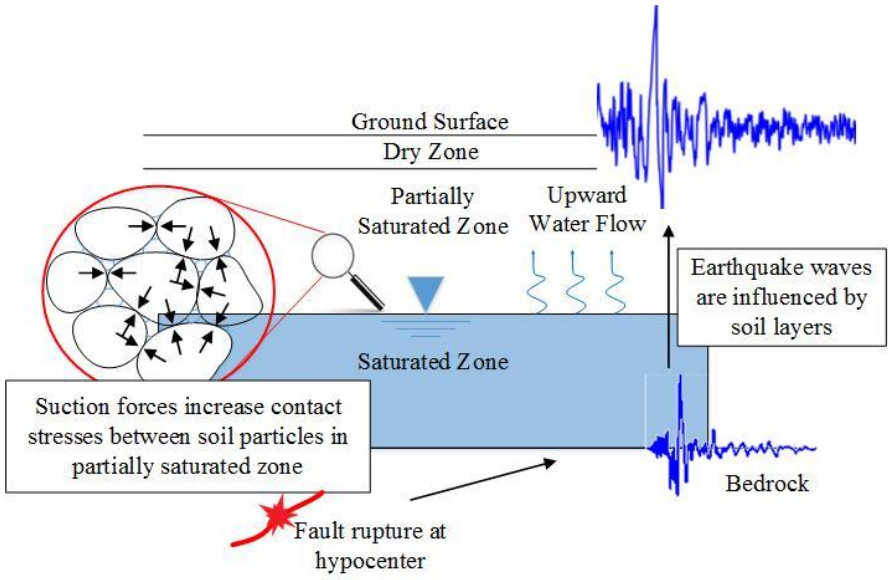

Figure 1-2. Schematic of wave propagation during earthquakes and inter-particle suction forces in three-phase soil

1.2. Research Objectives

This Ph.D. dissertation seeks the following objectives: (1) Study the effect of partial saturation on seismic site response; (2) Enhance the understanding of wave propagation mechanisms in partially saturated soils; (3) Develop simple and effective procedures to incorporate water saturation level in numerical models; (4) Provide practical recommendations for seismic design of unsaturated geosystems; (5) Evaluate the uncertainty associated with neglecting the effects of partial saturation and seasonal fluctuation of soil water content on site response.

1.3. The Scope of Research

This research addresses the mentioned objectives through the following major tasks: (1) preliminary numerical analysis, which simplistically studied the effect of partial saturation on seismic site response using DEEPSOIL software (Hashash et al. 2016); (2) Geotechnical centrifuge modeling where the effect of degree of saturation on site response was studied using steady state infiltration technique; (3) Sensitivity analysis to consider the effect of variations in different input parameters, associated with seasonal water table fluctuations, on the uncertainty in site response procedures.

1.4. Dissertation Structure

This dissertation provides a detailed background of the problem as well as the research tasks to address the above-mentioned objectives. The background of the research includes an overview of site response analysis, the influence of degree of saturation on soil dynamic properties and seismic site response, and different approaches of centrifuge physical modeling of unsaturated soils, which are all discussed in Chapter 2. Chapter 3 discusses the material selection and

characterization procedures. Chapter 4 explains the procedures and the results regarding the preliminary numerical site response analysis of unsaturated soils. Chapter 5 describes the renovated centrifuge facility at University of New Hampshire and its modification for physical modeling of partially saturated soils. Then, selection and calibration procedures of the instrumentations are discussed in Chapter 6. Chapter 7 presents the modeling procedure and the results of a necessary preliminary investigation on some of the hydraulic characteristics of unsaturated sands in the geotechnical centrifuge. The input motion selection and the procedures followed by calibration of the in-flight shaking table are discussed in Chapter 8. Chapter 9 presents the procedure and results of centrifuge physical modeling to assess site response of unsaturated soils. This is followed by Chapter 10, in which the performed parametric evaluation on the uncertainty in site response analysis, due to water table fluctuations, is presented. Finally, summary, conclusions, and recommendations for future works are discussed in Chapter 11.

CHAPTER II

BACKGROUND

2.1. Impact of Degree of Saturation on Dynamic Soil Properties

2.1.1. Dynamic Soil Properties

The behavior of soils in dynamic shear are characterized by two major parameters; shear modulus, representing the shear stiffness of soil, and damping, which quantifies the energy dissipated throughout dynamic events. Different parameters (e.g. strain level, loading pattern, and confining pressure) including water-saturation level might impact the dynamic soil properties (Seed and Idriss 1970, Kramer 1996). Conventionally, hysteresis loops are the outcomes of element-scale dynamic tests (e.g. cyclic triaxial or direct simple shear experiments) on soils through which the stress-strain path during cyclic loading of the material is illustrated (Figure 2-1, a). The dynamic stress-strain behavior of soils is often reflected through the backbone curve (Figure 2-1, b) where the strain-dependent variations of shear modulus are presented.

Shear modulus varies as a function of strain level in soils with its maximum at very low strain levels (i.e. less than 10^{-6}, Kramer 1996), denoted by G_0 or G_{max}. This modulus decreases as higher strain levels are induced in soil, conveniently denoted by G. Although, as per its definition, the shear modulus is the slope of the stress-strain curve and should be obtained as tangent shear modulus (G_{tan}) at each point, the strain-dependent shear modulus (G) is represented by secant shear modulus (G_{sec}) in dynamic soil testing due to its practicality (Figure 2-1). The decrease in shear modulus values is expressed by modulus reduction functions (Figure 2-2, a) which present the ratio of shear modulus at given strain levels to the maximum shear modulus (G/G_0). Unlike the dynamic shear modulus, damping increases as the induced shear strain rises since the frictional loss between soil particles damps out greater amount of energy. Typical damping variation over various strain levels is shown in Figure 2-2 (b).

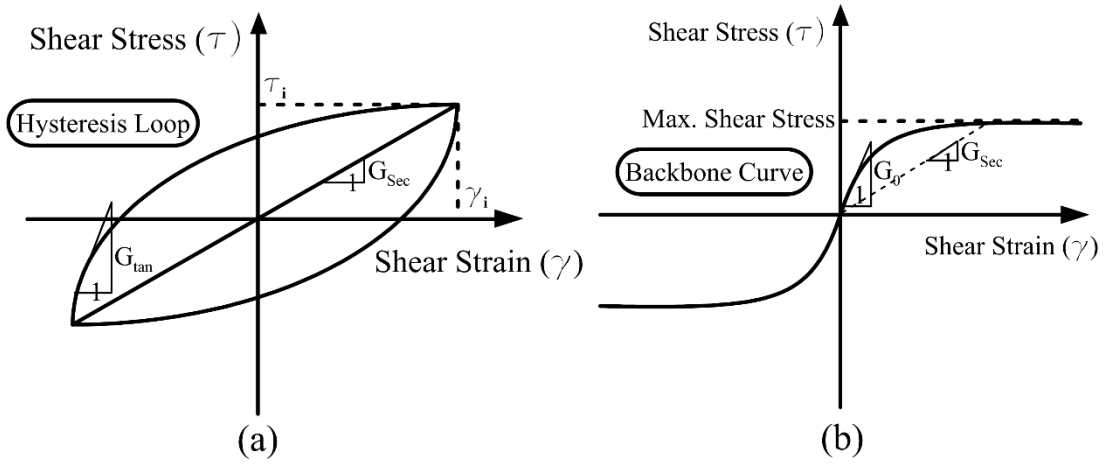

Figure 2-1 (a) Cyclic hysteresis stress-strain relationship; (b) Cyclic backbone curve

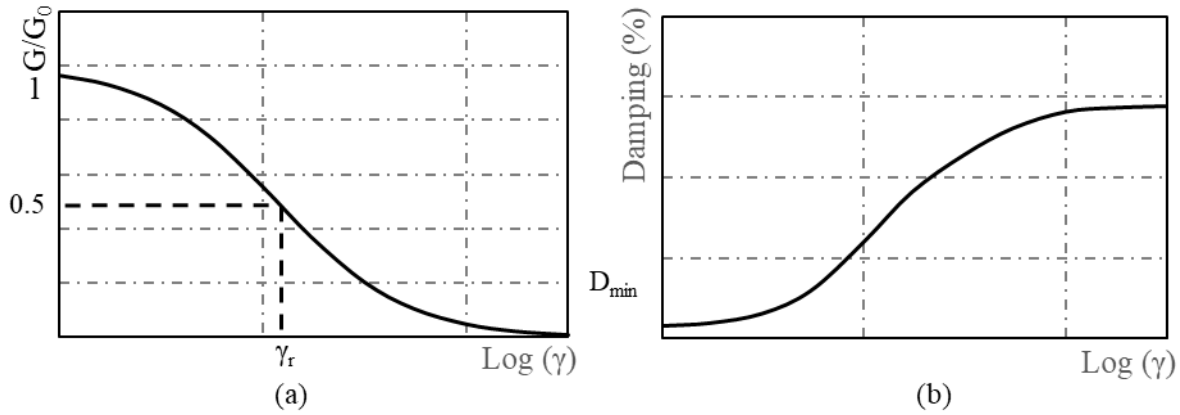

Figure 2-2 Typical (a) Modulus Reduction Curve (b) Strain-dependent Damping Curve

Small-strain shear modulus can be measured using different tools including resonant column and torsional shear apparatuses as well as bender element testing. According to previous studies (e.g. see Hardin & Black 1966, Seed & Idriss 1970, Iwasaki et al. 1978, Stokoe et al. 1995b, and Sawangsuriya et al. 2009, Gheibi and Hedayat 2018), small-strain shear modulus can vary as a function of void ratio (e), Over-Consolidation Ratio (OCR), and effective stress. The general format of empirical correlations of small-strain shear modulus can be expressed as:

$$G_0 = A(OCR)^K f(e) P_a^{1-n} \sigma'_m{}^n, \quad (2\text{-}1)$$

where P_a is the atmospheric pressure, σ'_m is the mean effective stress, and A, K, and n are fitting parameters. Using this general format, G_0 might be empirically formulated for different soils. For instance, Ghayoomi and McCartney (2011) obtained the G_0 for loose F-75 Ottawa sand through a set of bender element tests in geotechnical centrifuge and under steady-state infiltration as:

$$G_0 = 92.6\ (\sigma'_m/P_a)^{0.5}\ [\text{MPa}] \quad (2\text{-}2)$$

Darandeli (2001) modified the general format of the shear modulus reduction factor, initially proposed by Hardin and Drnevich (1972), as follows:

$$\frac{G}{G_0} = \frac{1}{(1+\frac{\gamma}{\gamma_r})^a} \quad (2\text{-}3)$$

where γ is the shear strain, γ_r is the reference shear strain corresponding to G/G_0 of 0.5 as illustrated in Figure 2-2 (a), and a is the power index proposed by Darandeli (2001). The values of γ_r and a were later empirically obtained from a set of torsional shear and resonant column experiments by Menq (2003):

$$\gamma_r = 0.12 \cdot C_u^{-0.6} \cdot \left(\frac{\sigma'_m}{P_a}\right)^{0.5 \cdot C_u^{-0.15}} \quad (2\text{-}4a)$$

$$a = 0.86 + 0.1 \cdot \log\left(\frac{\sigma'_m}{P_a}\right) \quad (2\text{-}4b)$$

where C_u is the coefficient of uniformity. Considering the proposed equations for small-strain shear modulus and shear modulus reduction functions, one can infer that the effective stress could significantly impact the dynamic soil modulus.

Another investigation by Zhang et al. (2005) used the following equation, proposed by Stokoe et al. (1995a) to define values of reference shear strain as a function of effective stress:

$$\gamma_r = \gamma_{r1} \cdot \left(\frac{\sigma'_m}{P_a}\right)^k \quad (2\text{-}5)$$

where γ_{r1} is the reference shear strain at a mean effective confining stress of 100 kPa and k is the stress correction factor. The values of γ_{r1}, k, and a (in Equation 2-3) were correlated with the Plasticity Index (PI) and the geologic age of soil deposits; shown in Figure 2-3 (a), (b), and (c) respectively (Zhang et al. 2005).

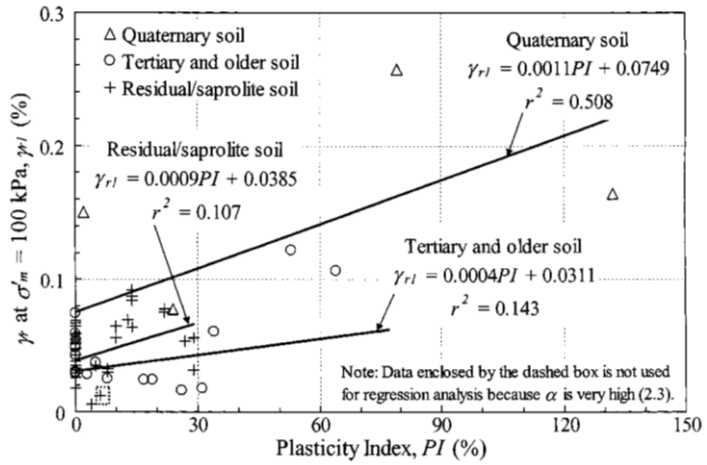

(a)

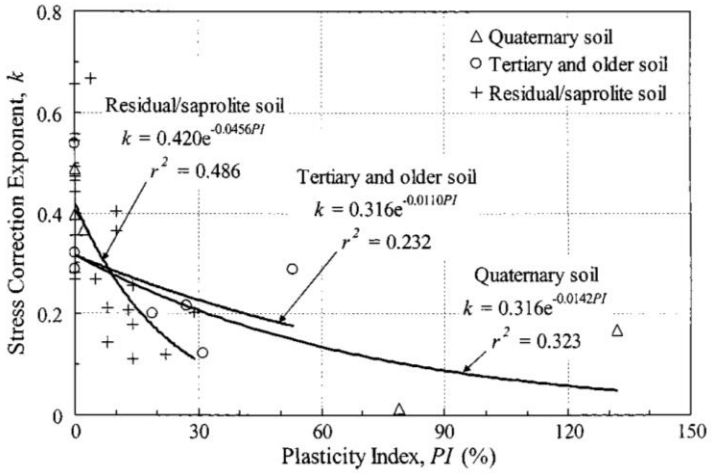

(b)

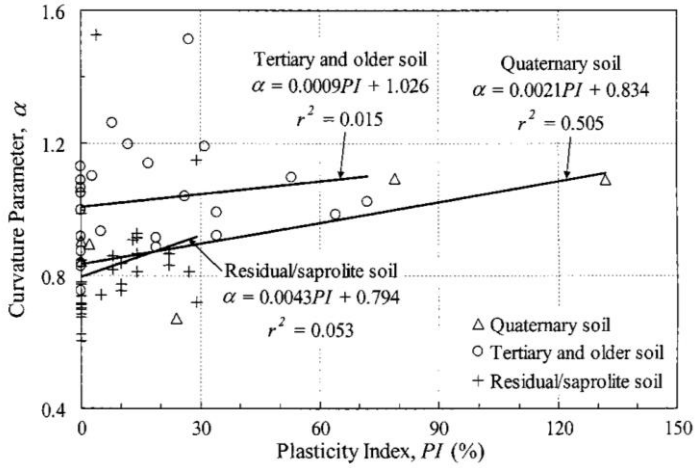

(c)

Figure 2-3. Correlations between plasticity index, geologic age, and different parameters of the generic equation for modulus reduction factor (a) γ_{r1} (b) k (c) a (Zhang et al. 2005)

Menq (2003) correlated the minimum damping value with C_u, D_{50}, and mean effective stress:

$$D_{s,min} = 0.55 \times C_u \times D_{50}^{-0.3} \left(\frac{\sigma'_m}{P_a}\right)^{-0.08} \quad (2\text{-}6)$$

Darendeli (2001) adjusted damping reduction equation by applying a scaling factor to "Masing" damping (Masing, 1926). This hyperbolic equation may be added to the small-strain damping proposed by Menq (2003) to obtain the strain-dependent damping:

$$D = b\left(\frac{G}{G_0}\right)^{0.1} . D_{Masing} + D_{s,min} \quad (2\text{-}7)$$

where D is the damping, b is a scaling coefficient that depends on the number of cycles (typically around 0.6), and D_{Masing} is the material damping determined from the Masing behavior. The prominent influence of effective stress on damping could be observed Menq's equations; i.e. in G/G_0 as well as $D_{s,\ min}$. Masing damping for a = 1 is determined using the following equation (Masing 1926):

$$D_{Masing}(\%) = \frac{100}{\pi}\left[4\frac{\gamma - \gamma_r \ln\left(\frac{\gamma+\gamma_r}{\gamma_r}\right)}{\frac{\gamma^2}{\gamma+\gamma_r}} - 2\right] \quad (2\text{-}8)$$

Later, Darandeli (2001) suggested an empirical equation to estimate the Masing damping for other values of a:

$$D_{Masing,Mod.} = c_1 D_{Masing} + c_2 {D_{Masing}}^2 + c_3 {D_{Masing}}^3 \quad (2\text{-}9)$$

where

$$c_1 = -1.1143\, a^2 + 1.8618\, a + 0.2523$$

$$c_2 = 0.0805\, a^2 - 0.0710\, a - 0.0095$$

$$c_3 = -0.0005\,a^2 + 0.0002\,a + 0.0003$$

Zhang et al. (2005) defined the small-strain damping using the following equation:

$$D_{min} = D_{min1}\left(\frac{\sigma'_m}{P_a}\right)^{-k/2} \quad (2\text{-}10)$$

where D_{min1} is a parameter correlated with the PI of the soil deposit independent of its geologic age:

$$D_{min1} = \text{a (PI)} + b \quad (2\text{-}11)$$

where a and b are fitting parameters, the values of which are equal to 0.008 and 0.82, respectively. Similar to the approach proposed by Menq (2003), they also formulated damping variations as a function of G/G_0 variations, although through a different equation:

$$D = 10.6\left(\frac{G}{G_0}\right)^2 - 31.6\left(\frac{G}{G_0}\right) + 21 + D_{min} \quad (2\text{-}12)$$

2.1.2. Effective Stress in Unsaturated Soils

Except regions with very high precipitation and shallow water table, surficial soil layers, above the ground water table, are mostly unsaturated. Due to different precipitation levels throughout the year, the water table level, and hence the height of vadose zone, varies seasonally. When the ground water level is not at the surface, water ascends due to capillarity forces and generates partially-saturated soils (Figure 1-2). The matric suction and degree of saturation profiles at equilibrium, without accounting for precipitation and/or evaporation, are illustrated in Figure 2-11. Although matric suction varies linearly above the ground water table, the degree of

saturation profile follows a nonlinear pattern, which is often referred as Soil Water Retention Curve (SWRC) in unsaturated soil mechanics.

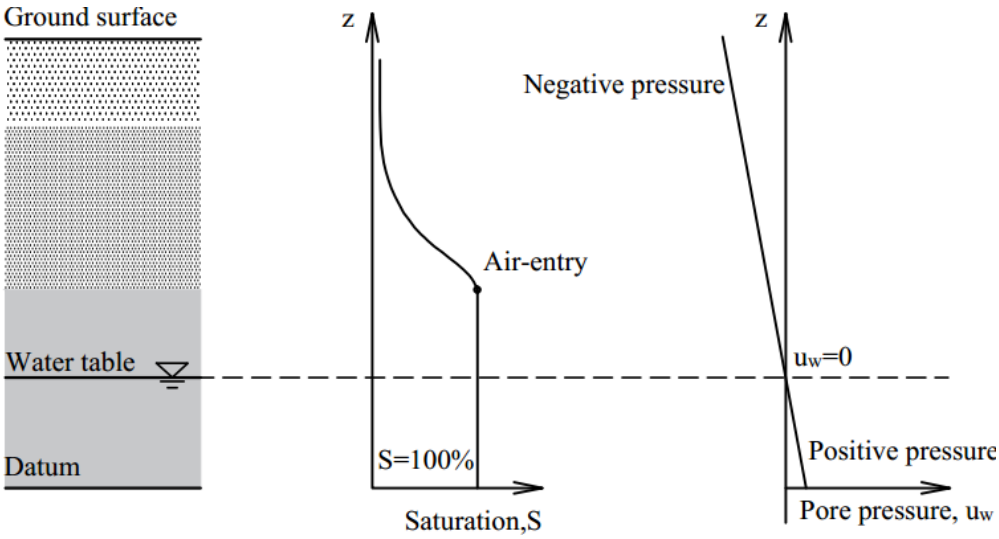

Figure 2-4. Equilibrated matric suction and degree of saturation profiles for unsaturated soil zone (Lu and Likos 2004)

The presence of suction in unsaturated soils increases the effective stress resulting in a stiffer soil (Lu and Likos 2006, Khosravi et al. 2016a, Jarast and Ghayoomi 2017, Jarast 2017) with different hydro-mechanical behavior (Ghayoomi and McCartney 2011, Hoyos et al. 2015, Khosravi et al. 2016b, Khosravi et al. 2017). Most studies on dynamic response of partially saturated soils have focused on the variations of small-strain shear modulus or damping as a function of matric suction or degree of saturation using bender elements (Marinho et al. 1995, Ng et al. 2009, Ghayoomi and McCartney 2011, Hoyos et al. 2015, Khosravi et al. 2016c) or resonant columns (Mancuso et al. 2002, Mendoza et al. 2005, Khosravi et al. 2010, Hoyos et al. 2015). Some studies also addressed the influence of partial saturation on strain-dependent shear modulus (Biglari et al. 2011 and Ghayoomi et al. 2017) using dynamic triaxial tests.

Small-strain shear modulus is, generally, proportional to the matric suction (i.e. inversely proportional to the degree of saturation). However, for sands, G_0 variations appeared to have a peak in middle range degrees of saturation (Khosravi et al. 2010, Ghayoomi and McCartney 2011). For instance, the bender element results from centrifuge experiments under steady state infiltration showed that shear wave velocity and small-strain shear modulus of unsaturated Ottawa sand were maximized around 40% degree of saturation (Figure 2-5) (Ghayoomi and McCartney 2011). Lu et al. (2010) discussed that it is the combined effect of matric suction and degree of saturation that influence the behavior of unsaturated soils. They synthesized experimental data from shear or tensile strength tests and proposed "suction stress" parameter that could be practically responsible for the mechanical behavior of unsaturated soils. The resulting effective stress equation was as follows:

$$\sigma' = (\sigma - u_a) + \sigma^s \tag{2-13a}$$

$$\sigma^s = \frac{S - S_r}{1 - S_r}(u_a - u_w) = \frac{u_a - u_w}{(1 + [\alpha (u_a - u_w)]^n)^{1-\frac{1}{n}}} \tag{2-13b}$$

$$S_e = \frac{S - S_r}{1 - S_r} \tag{2-13c}$$

where σ^s is the suction stress, u_a and u_w are pore air and pore water pressures, respectively, S is degree of saturation, S_e and S_r are the effective and residual degrees of saturation, respectively, and α and n are the parameters for the van Genuchten SWRC model (van Genuchten 1980), respectively. Similar to the concept of SWRC, Lu et al. (2010) introduced Suction Stress Characteristic Curve (SSCC), which could better correlate the mechanical properties of soils with the degree of saturation. Typical SWRC and SSCC for different soils are illustrated in

Figure 2-6. Although matric suction always increases when lowering the degree of saturation, the proposed term, suction stress, has a limit of zero at nearly-dry conditions for sands and silts.

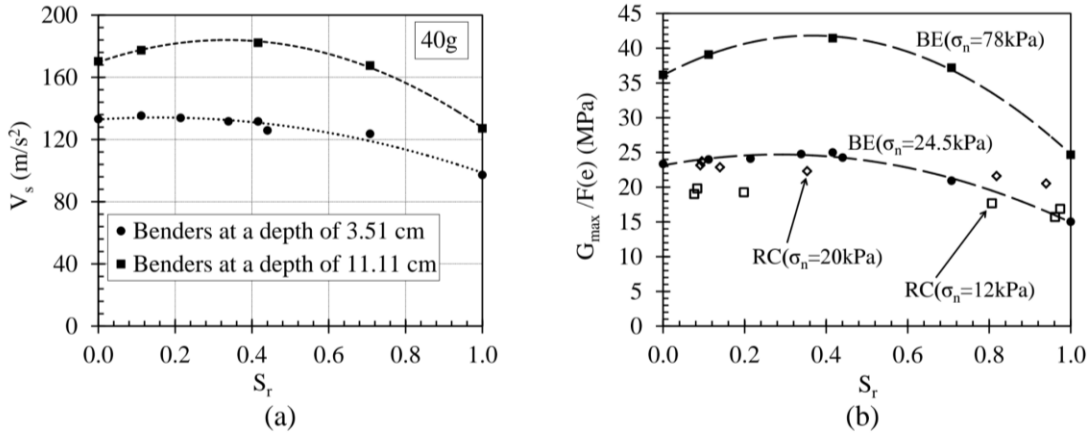

Figure 2-5. The effect of degree of saturation on (a) shear wave velocity and (b) normalized small-strain shear modulus (Ghayoomi and McCartney 2011)

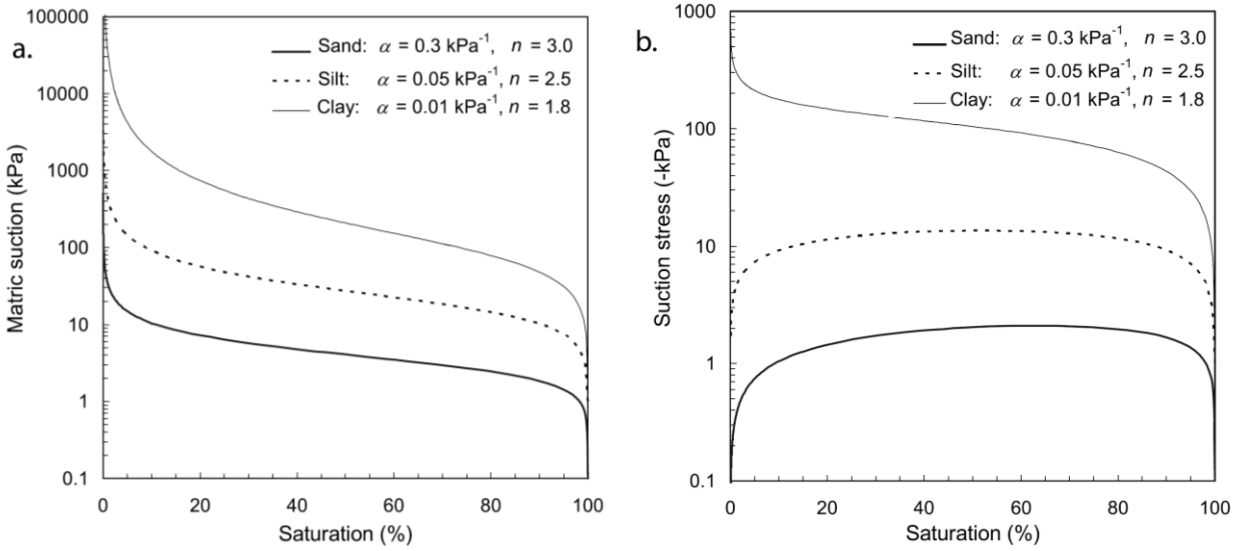

Figure 2-6. Typical alterations of (a) matric suction and (b) suction stress over degree of saturation for sand, silt, and clay (Lu and Likos 2010)

As an independent part of this research, the effect of matric suction (degree of saturation) on the strain-dependent shear modulus of partially-saturated sand was investigated through a set of dynamic triaxial tests (Suprunenko 2015, Ghayoomi et al. 2017). Strain- and stress-controlled

dynamic triaxial tests were performed on dry, saturated, and unsaturated sand specimens with different suction levels ranging from 2 kPa to 10 kPa. The results indicated that the shear modulus increased in unsaturated sand by increasing the suction level regardless of the induced strain level (e.g. see Figure 2-7).

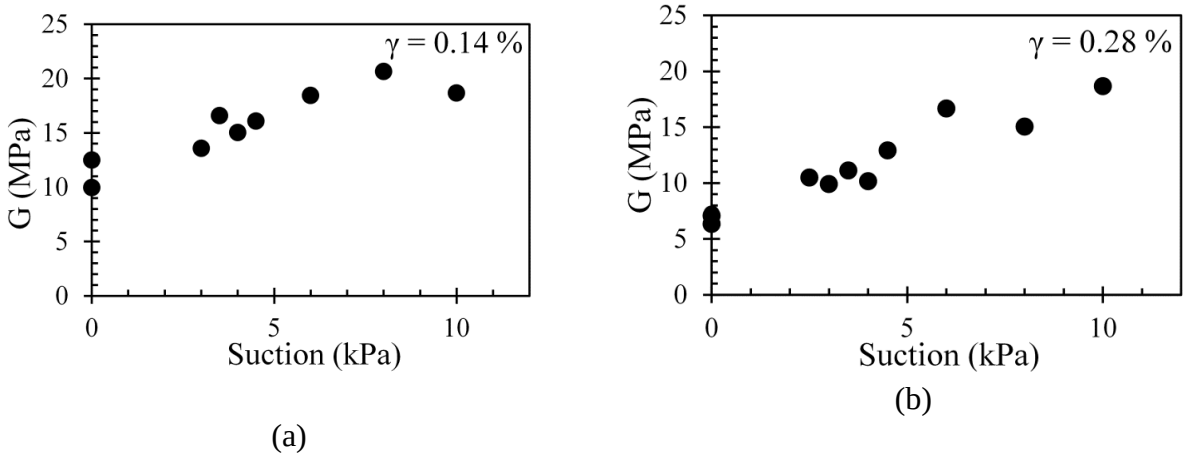

(a) (b)

Figure 2-7. Effect of suction on shear modulus of sand for different shear strain levels of (a) 0.14% and (b) 0.28% (Ghayoomi et al. 2017)

2.2. Overview of Site Response Analysis

Seismic waves generated by earthquakes often travel through soils with different mechanical and hydraulic characteristics where they can be dramatically altered in terms of intensity, frequency content, and duration (Figure 1-2). This transition is commonly evaluated using "Site Response Analysis", which is a crucial step toward seismic design of soil-structure systems. Applications of site response analysis include development of design response spectra for surface structures, estimating seismically induced stresses, strains, and settlements, and liquefaction assessment. Local site conditions such as soil density, plasticity index, stiffness, and damping can significantly affect seismic site response (Joyner et al. 1981, Vucetic and Dobry 1991, Borcherdt

1994, Midorikawa 1994, Choi and Stewart 2005). Thus, ignoring the effects of changes in the site conditions may lead to inaccurate assessment of the site response.

Parameters influencing the site response could be simplistically explored by inspecting the analytical solution to a linear Single Degree of Freedom (SDOF) system under cyclic motion representing a uniform soil layer overlying bedrock. The maximum acceleration amplification ratio in such a system would be approximated as follows (Roesset 1977):

$$\left(\frac{a_{surface}}{a_{bedrock}}\right)_{max} \approx \frac{1}{\left(\frac{\gamma_s V_s}{\gamma_r V_r}\right) + \left(\frac{\pi}{2}\right)\beta_S} \tag{2-14}$$

where:

β_S, γ_s, and V_s are the soil damping ratio, unit weight, and shear wave velocity, respectively, and γ_r and V_r are the unit weight and shear wave velocity of the rock, respectively. As the ratio of $\gamma_r/\ \gamma_s$ is between 1.1 and 1.4 for majority of sites (Dobry et al. 2000), the amplification ratio becomes a function of the shear wave velocity and damping where both are influenced by motion intensity and local site conditions. However, for sands, the shear wave velocity is mainly a function of local site conditions while the damping is predominantly affected by the motion intensity (Dobry et al. 2000). Despite the useful insights gained from the analytical solution to the dynamic response of the SDOF system, this simplified equation might not be used in real applications where soil becomes nonlinear under relatively intense earthquakes especially in layered grounds; e.g. Northridge region during the 1994 earthquake (Gibbs et al. 1996). Data obtained from different instrumented sites under strong ground motions (e.g. Stewart and Kwok 2008, Kaklamanos et al. 2015) as well as physical modeling experiments (e.g. Afacan et al. 2014, Hashash et al. 2015) are of interest to provide practical suggestions for site response assessment.

The role of local site condition and intensity of the rock motion in the site response were highlighted using fully monitored and instrumented sites during past earthquakes (Seed et al. 1976, Joyner et al. 1981, Idriss 1990, 1991, Borcherdt 1994, Stewart et al. 2003). Idriss (1990, 1991) investigated the influence of bedrock Peak Ground Acceleration (PGA) on the surface acceleration of sites with soft soil during 1985 Mexico City and 1989 Loma Prieta earthquakes. Increasing the intensity of rock motion led to lower amplification factors and even de-amplification in very intense rock motions; e.g. PGA higher than 0.4g (Figure 2-8). This could be attributed to the nonlinear stress-strain behavior of soils and higher damping values as a result of higher induced strain levels. The same general trend was observed in similar studies exploring the acceleration amplification factor as a function of bedrock PGA (e.g. Silva et al. 2000, Borcherdt 2002, Stewart et al. 2003, Choi and Stewart 2005). Joyner et al. (1981) correlated the site amplification factor and shear wave velocity through a simple seismological theory assuming the seismic energy preservation during wave propagation. They concluded that the amplification factor is inversely proportional to the square root of shear wave velocity, which was also confirmed by other researchers (Borcherdt 1994, Borcherdt and Glassmoyer 1994, Boore et al. 1994, Midorikawa et al. 1994).

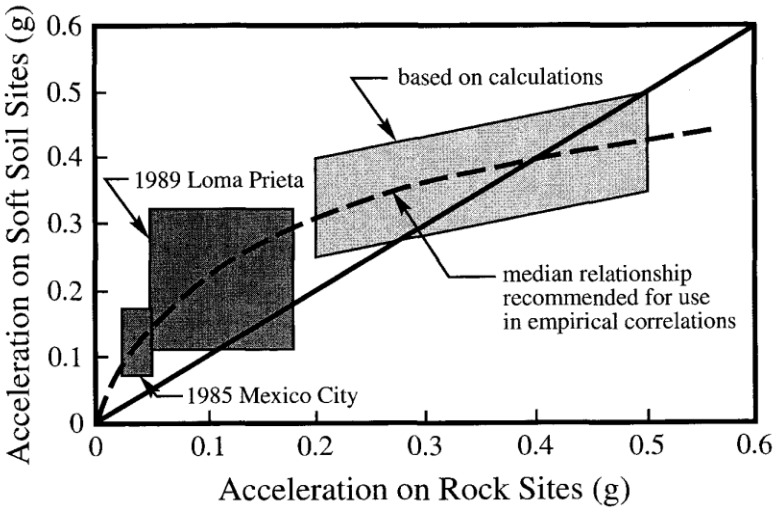

Figure 2-8. The effect of bedrock motion intensity on the acceleration amplification in soft soil sites (Idriss 1991)

Traditionally, different methods have been used to consider the effects of local site conditions and motion intensity on the surface motion evaluation; including simplified procedures regulated by seismic provisions to more complex site-specific ground response analysis for sensitive seismic designs. Current seismic design provisions (e.g. *NEHRP Recommended Provisions for Seismic Regulations for New Buildings and Other Structures 2009, ASCE/SEI 7-10 2010, International Building Code, and Minimum Design Loads for Buildings and Other Structures 2012*) regulate 5%-damped design spectrum to represent seismic events at ground surface. The parameters influencing design spectrum include the seismic hazard level on the bedrock, the effect of local site conditions, and the intensity of ground motion. The seismic hazard level for any region in the United States, if not due to man-made activities (e.g. see Garvey and Ozbay 2013, Rutqvist et al. 2013, Khademian et al. 2017, 2018a, and 2018b), is estimated using mapped spectral ordinates of the bedrock motion for short periods (S_s) and intermediate-periods (S_1). The other two parameters are taken into account using low-period and mid-period amplification factors (F_a and F_v) that are functions of local site conditions and intensity of bedrock motion

(Dobry et al. 2000). The local site condition is reflected through site classification systems. According to provisions after 1997, different sites could be categorized based on a harmonic average shear wave velocity of the top 30 m of the soil profile ($\bar{V}_s$), an average SPT blow-count number ($\bar{N}$), or a representative undrained shear strength ($\bar{S}_u$). Site classification system in the current seismic design codes is shown in Table 2-1. In addition, according to *NEHRP Provisions* for assessing liquefaction potential and soil strength loss, mapped PGA values should be multiplied by PGA amplification factors (F_{PGA}) to obtain the PGA associated with the design Maximum Considered Earthquake (MCE). The same values of F_a are used as F_{PGA} coefficients in *NEHRP Provisions*.

Table 2-1. Site classification (after NEHRP Provisions 2009)

NEHRP Category	**Description**	$\bar{V}_s$	$\bar{N}_{SPT}$	$\bar{S}_u$
A	Hard rock	> 1500 m/s	N/A	N/A
B	Firm to hard rock	760 - 1500 m/s	N/A	N/A
C	Dense soil, soft rock	360 - 760 m/s	> 50	> 100 kPa
D	Stiff soil	180 - 760 m/s	15 - 50	50 – 100 kPa
E	Soft clays	< 180 m/s	< 15	< 50 kPa
F	Special study soils, e.g. liquefiable soils, sensitive clays, organic soils, soft clays>36 m thick			

According to *NEHRP Provisions*, site-specific ground response analysis shall be performed for structures on site class F. However, this procedure is often performed for sensitive structures on other site classes as well. The site-specific ground response is numerically evaluated considering the soil nonlinearity through equivalent or nonlinear stress-strain relationships. Different numerical Finite Element or Finite Difference codes have been developed for site-specific response analysis considering equivalent linear (e.g. SHAKE91, Idriss and Sun 1992; DEEPSOIL, Hashash et al. 2016) or nonlinear (e.g. DEEPSOIL; DESRA, Lee and Finn 1978;

DMOD, Matasovic 1993,;FLAC, Itasca 2005; OpenSees, Mazzoni et al. 2006) constitutive models. Seismic response of a Multi-Degree of Freedom (MDOF) system to a one-dimensional propagating input motion is analyzed in majority of these numerical procedures. Equivalent linear models are used to find the seismic response of a MDOF system in frequency domain assuming equivalent shear modulus and damping values for soil layers. However, in order to account for soil nonlinearity, the equation of motion could be directly solved in time-domain in nonlinear models.

In spite of substantial advances in numerical codes, to date, the influence of partial saturation could not be directly assessed in site response analysis using commercial programs. In order to evaluate the site response analysis in unsaturated soils and to validate potential improvement to site response numerical codes, data from physical modeling experiments simulating the seismic response of unsaturated soil layers would be imperative.

2.3. The Influence of Partial Saturation on Seismic Site Response

Degree of water saturation is among the parameters that influence the seismic response of soil layers (Ghayoomi et al. 2013). Inter-particle suction in partially saturated soils increases the effective stresses on the grain skeleton (Lu and Likos 2006) which, in turn, yields to different soil dynamic properties as discussed previously (Mancuso et al. 2002, Ghayoomi and McCartney 2011). As a result, seismic wave propagation mechanisms may vary in partially saturated soil layers (Yang and Sato 2000) that would lead to a different seismic site response (Yang 2006, D'Onza et al. 2008, Ghayoomi et al. 2013, Mirshekari and Ghayoomi 2015, 2017). Soils, in dry or fully saturated conditions, have been believed to result in more conservative solutions because matric suction in unsaturated soils increases the ground stiffness. Therefore, partial saturation has

not been directly considered in the state-of-the-practice site response analysis. However, recent investigations on the site response in unsaturated soils showed that this assumption might not be always reasonable (Ghayoomi and McCartney 2012, Ghayoomi and Mirshekari 2014, Mirshekari and Ghayoomi 2015, 2017). Further, the influence of the degree of saturation on seismic response analysis is often considered by incorporating the in-situ measured shear wave velocity of shallow unsaturated soil layers. However, the extent of this influence might be beyond the suction-dependency of the dynamic soil properties where the wave propagation mechanisms may vary (Yang 2006). In addition, soil properties may differ between the time of the construction and prior to the earthquake due to the seasonal fluctuation of water table. Thus, recognizing this difference would be essential in assessing the uncertainty in projected site response.

Yang (2006) analytically studied the frequency-dependent amplification of inclined vertically propagated shear waves (SV waves) in soil layers overlying bedrock. The results indicated that a slight decrease in the degree of saturation of fully-saturated soil layers causes a significant difference in vertical amplification of the SV waves. Specifically, for earthquake frequencies between 1 to 10 Hz, unsaturated soils may lead to a higher vertical amplification than saturated soil layers (Figure 2-9, a). D'Onza et al. (2008) implemented the small-strain modulus and damping obtained from suction-controlled resonant column tests in a series of numerical site response analyses. Suction was found to significantly affect the natural frequency and PGA amplification factor in clayey silt and silty sand layers. According to their numerical study, the natural frequency of the soil layers increased in higher suction values whereas PGA amplification factor was reduced. Ghayoomi et al. (2013) studied seismically induced settlements in partially saturated sand by applying sinusoidal cyclic loads to sand layers in a set

of suction-controlled centrifuge tests using steady-state infiltration technique (Ghayoomi et al. 2011). The least amount of surface settlement occurred in middle range degrees of saturation due to the increase in shear modulus. Moreover, they observed a maximum 20% increase in PGA amplification factor in unsaturated sand with respect to the one in dry condition (Figure 2-9, b) (Ghayoomi and McCartney 2012).

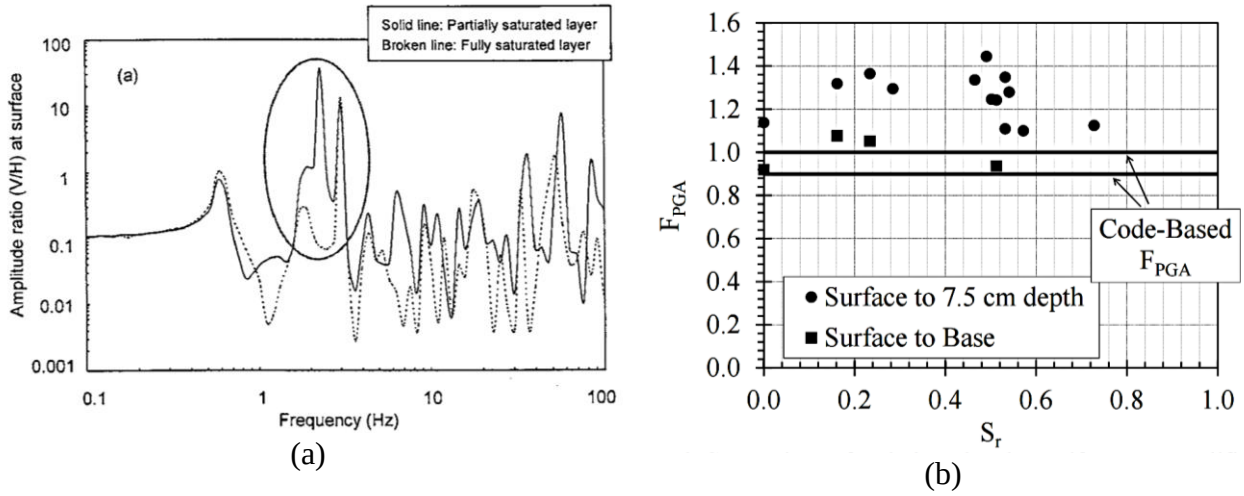

(a) (b)

Figure 2-9. (a) Frequency-dependent amplitude ratios at surface for propagated waves from a saturated bedrock (Yang 2006) (b) PGA amplification factor versus degree of saturation (Ghayoomi and McCartney 2012)

Despite the proven influence of the degree of saturation on the dynamic soil properties and the site response, comprehensive data sets from physical and numerical modeling of seismic response of partially saturated soils are still required. Centrifuge physical modeling of free-field seismic ground response using a "degree of saturation-controlled" system is of a great value to validate this effect and to calibrate future numerical and analytical predictive models.

2.4. Centrifuge Modeling of Unsaturated Soils

Centrifuge modeling is an experimental technique in geotechnical engineering where a small-scale model of a prototype phenomenon is loaded onto one end of a centrifuge, spun up so that a target gravity level on the specimen is achieved, and then the testing program is performed in

higher g-levels. Geotechnical centrifuge testing has been increasingly used for scaled modeling of earthen systems where prototype values can be determined from the scaled results. Preserving the stress scaling factor as unity is the key in centrifuge modeling, which requires other prototype parameters to be scaled, accordingly; proportional to the centripetal acceleration of N_g (e.g. the length is scaled by 1/N). Scaling factors for different parameters in centrifuge modeling have been investigated and addressed in previous studies (e.g. Ko 1988, Garnier et al. 2007). Some of the scaling laws in centrifuge modeling are listed in Table 2-2. Small-scale models enable researchers and engineers with relatively inexpensive testing programs to simulate highly destructive events such as earthquakes and to significantly reduce the duration of diffusion experiments.

Table 2-2. Scaling factors for centrifuge modeling (after Ko 1988)

Quantity	**Prototype**	**Model**
Length	1	1/n
Velocity	1	1
Acceleration	1	n
Mass	1	$1/n^3$
Force	1	$1/n^2$
Energy	1	$1/n^3$
Stress	1	1
Strain	1	1
Mass Density	1	1
Energy Density	1	1
Dynamic Time	1	1/n
Diffusion Time	1	$1/n^2$
Creep Time	1	1

Centrifuge testing of partially saturated soils has been promisingly implemented in different applications such as measurements of hydraulic characteristics of fine materials (Nimmo and Akstin 1988, McCartney and Zornberg 2010, Reis et al. 2011), understanding pollutant behavior

in soils (Knight and Mitchell 1997, Esposito 2000), simulating scaled earth dams and slope stability problems (Deshpande and Muraleetharan 1998, Caicedo and Thorel 2014), climatic studies of soil-atmosphere interaction (Tristancho et al. 2011), research on thermomechanical response of energy foundations (Stewart and McCartney 2013), measurements of unsaturated dynamic properties of soils (Ghayoomi and McCartney 2011), and understanding the seismic behavior of unsaturated soil layers (Ghayoomi et al. 2011, Mirshekari and Ghayoomi 2017). These studies, in general, fall into three major categories: experiments that included an unsaturated flow (e.g. see Nimmo et al. 1987, Esposito 2000, McCartney and Zornberg 2010, Parks et al. 2011, Mirshekari and Ghayoomi 2017), tests on fine soils where they were mixed and compacted with a certain moisture content (Deshpande and Muraleetharan 1998), or those where capillary rise occurred from a constant water level (e.g. see Cooke and Mitchell 1991, Crancon et al. 2000, Depounits et al. 2001).

Unsaturated soil testing in geotechnical centrifuge has involved experimental challenges such as how to generate unsaturated conditions, control the degree of saturation, maintain the pre-determined water level, and importantly how to back-calculate moisture content or matric suction using the prototype soil-water retention relations. Specifically, mapping the results of scaled models of different testing scenarios in partially saturated soils to full-scale prototype situations requires accurate assessment of the model-to-prototype conversion of suction, water-content, and their relation.

2.4.1. Capillary Rise in a Geotechnical Centrifuge

Capillary rise in unsaturated soils could be studied using the “bundle of capillaries” theory where the unsaturated soil pores are simplistically modeled by equivalent cylindrical tubes (Figure

2-10, a) (Lord 1999, Rezzoug et al. 2000). After capillary rise has reached equilibrium in a tube, the velocity- and acceleration-related forces become negligible and the only opposite force acting against surface tension is the weight of water. Capillary height at equilibrium might be expressed as a function of water column weight, tube diameter (pore sizes in soils), and surface soil/water tensions:

$$h = \frac{2T\cos\delta}{a\rho g} \tag{2-15}$$

where h is capillary rise, T is surface water/soil tensions, δ is the contact angle between tube (soil granules) and water, a is the effective capillary diameter, ρ is the water density, and g is the applied gravity acceleration. The capillary rise in reality occurs in a more complex pattern where pore water ascends along different paths (fingers) with different heights depending on the pore diameters in various locations of soil layers (Lu and Likos 2004). In unsaturated soils, the height below the air-entry suction head is often named as "capillary fringe height" while the height corresponding to residual water content is called "capillary rise height" (Lu and Likos 2004). A detailed overview of the scaling laws of capillary rise was obtained by dimensional analysis (Arulanandan et al. 1988) where a non-dimensional group for capillary effects was formed as a function of surface tensions, fluid density, pore sizes, and g-level. Regardless of the analysis type, by assuming independency of surface tension from the g-level and using the same material in prototype and model, the capillary rise in model becomes inversely proportional to the gravity level (Arulanandan et al. 1988, Lord 1999, Rezzoug et al. 2000). The surface tension, however, might be a function of g-level as a result of water menisci distortion in higher gravities (Schubert 1982).

Previous studies have shed light on how the capillary rise is scaled in capillarity-governed problems through analytical methods (Arulanandan et al. 1988, Lord 1999, Rezzoug et al. 2000) and, to some extent, experimental procedures (Esposito 2000, Crançon et al. 2000, Knight et al. 2000, Depountis et al. 2001, Rezzoug et al. 2004). These investigations showed that the capillary height is reduced with the length scaling factor during centrifugation. However, the experimental programs that were used to validate this conclusion involved some uncertainties and require further scrutiny.

Capillary rise scaling factor was investigated by controlling the water level in an adjacent tank and estimating the capillary ascension (wetting experiments) by either monitoring the wet front of soil using optical measurements (Depountis et al. 2001, Rezzoug et al. 2004) or measuring the VWC profile (Crançon et al. 2000). The scaling law was, also, studied by draining an initially-saturated specimen to a certain water level (drying experiments) where the moisture profile was measured by weighing soil samples during the centrifuge stoppage times (Cooke and Mitchell 1991, Esposito 2000). Although the capillary height was measured in both testing methods, the lack of matric suction measurements left a gap in interpretation of the results. As a part of NECER (Network of European Centrifuges for Environmental Geotechnical Research) project, capillary rise was estimated in four geotechnical centrifuges using video cameras to distinguish the unsaturated and dry soils through the contrast between dark and light zones (Figure 2-10, b) (Depountis et al. 2001, Rezzoug et al. 2004). This measurement technique only estimated the boundary location between dry and wet areas and did not provide model profiles of degree of saturation. Moreover, using an optical distinction between wet and dry soils to estimate the capillary rise is questionable where water, even in very high suction values, cannot be

extracted from the soils beyond the residual degree of saturation. In one of the network facilities (Burkhart et al. 2000), tensiometers were used in addition to the optical cameras to measure matric suction. The capillary rise heights measured by optical method were almost twice the heights obtained from tensiometers readings. According to the results from the tensiometers, the capillary rise scaling factor was slightly lower than 1/N in higher gravities which could be related to the effect of higher gravity on the shape of water menisci and capillary pressure. The effect of water menisci distortion on capillary ascending in higher gravities could not be verified due to the short span of g-level variations in those tests (i.e. g-level changed from 1 to 11). In addition, since the VWC was not measured alongside suction readings, the model SWRC could not be achieved.

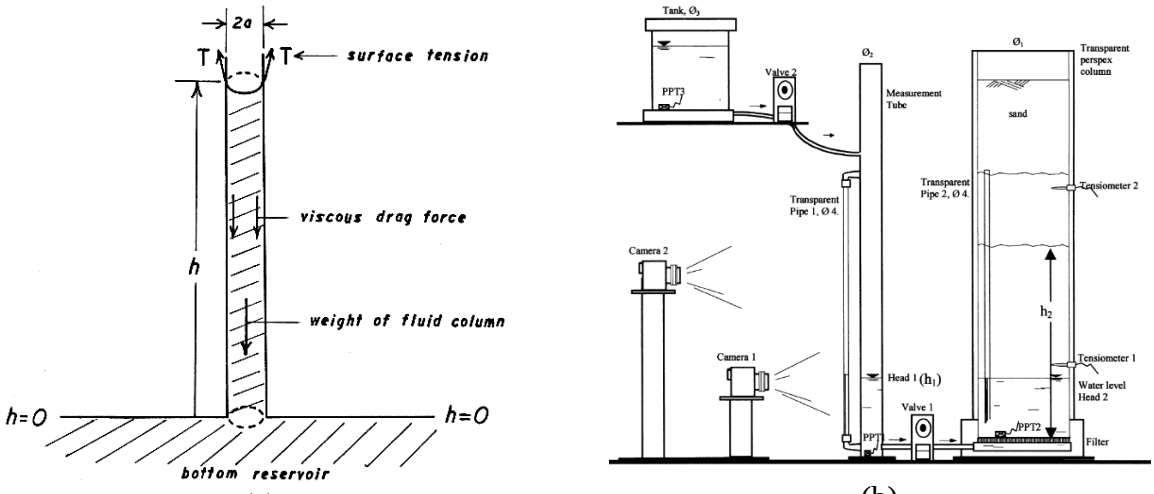

(a) (b)

Figure 2-10. (a) Capillary rise in a tube (Lord 1999) (b) A schematic of the setup for optical measurements of capillary rise (Depountis et al. 2001)

Crancon et al. (2000) used four Time Domain Reflectometry (TDR) sensors in a container with an established water level and estimated the rise height by fitting a van Genuchten curve to the sensor measurements. However, this procedure was based on the assumption of g-level-independency of the constitutive model between matric potential and volumetric water content.

Esposito (2000) and Knight et al. (2000) studied the capillary rise scaling during drainage experiments as a preliminary component of their research on pollutant release in unsaturated soil layers. Both studies consisted of draining water from an initial saturated condition for a certain period followed by stopping the centrifuge operation, oven-drying small soil samples from different locations of their specimens, and measuring moisture content along their soil profile. Even though, in both studies, the centrifuge stoppage was reportedly abrupt, the measured moisture contents at stoppage times were not a precise representative of those values at high-g. Furthermore, the location of soil sampling involves uncertainties, especially when length scaling factor is incorporated.

Small centrifuges were used historically for quicker SWRC measurements, as per ASTM D6836 (ASTM 2001), especially for higher suction levels; i.e. within finer materials (Briggs and Mclane 1907, Gardner 1937, Russell and Richards 1939, Hassler and Brunner 1945). Knowing that the matric suction is a stress-type variable and given the stress scaling factor of unity, one could utilize the same scaling value for suction measurements in unsaturated testing. However, since the shape of water menisci might be distorted in higher gravities (Schubert 1982) the Soil Water Retention Curve (SWRC) could differ in higher centrifugal fields. Thus, different soil-water retention behavior might be observed in the prototype system versus the scaled model.

SWRC measurement in fine-grained soils by means of commercial centrifuges was more recently studied and compared with other methods (Khanzode et al. 2002, Reatto et al. 2008, Reis et al. 2011, Malengier et al. 2015). The common procedure (Khanzode et al. 2002, Reatto et al. 2008, Reis et al. 2011, also discussed in ASTM D6836) comprised of locating small specimens (e.g. 50 mm in diameter and 20 mm in height in Reis et al. 2011) on a ceramic disk

and draining water freely during the centrifuge flights. Then, different suction values were obtained upon reaching equilibrium depending on angular velocity and thickness of the disks (location of the specimens). Due to the lack of any in-flight instrumentation, the VWC was measured by weighing soil specimens successively at stoppage times during the tests and matric suction was estimated using the equation initially proposed by Gardner (1937). Even though, in those studies, the centrifuge stoppage was reportedly abrupt, the measured moisture contents at stoppage times were not a precise representative of those values at high-g. Lately, Malengier et al. (2015) proposed an innovative approach using bench-scale centrifuge testing whereby the van Genuchten's parameters, and consequently SWRC, can be estimated through in-flight measurements of changes in weights of outflow and the entire sample. The SWRC, then, is obtained indirectly by solving the Richard's equation for unsaturated flow. Regardless of the selected approach, continuous in-flight measurements of matric suction and VWC can significantly enhance the insight towards the dependency of SWRC on higher gravity levels.

2.4.2. Steady State Infiltration Technique

Background

The steady state infiltration approach was devised from centrifuge permeameters (Nimmo et al. 1987, 1992, Conca and Wright 1990, Dell'Avanzi 2004, McCartney and Zornberg 2010), mainly used to streamline measurements of hydraulic parameters in unsaturated soils. This technique was implemented in different soils such as gravels (Conca and Wright 1990), sands (Nimmo et al. 1987), and clayey materials (Zornberg and McCartney 2010). Controlling the matric suction along the relatively short height of their specimens (e.g. 38 mm in Nimmo et al. 1987) provided means to verify validity of Darcy's law in increased gravitational field (Nimmo et al. 1987),

study the influence of different compaction levels on hydraulic conductivity of sandy soils (Nimmo and Akstin 1988), determine diffusion coefficients of angular gravels (Conca and Wright 1990), and study the effect of centrifugation on clay hydraulic characteristics (McCartney and Zornberg 2010).

Recently, the steady state infiltration has also been incorporated into more complex geotechnical systems in larger centrifuges to generate suction-controlled fields (Ghayoomi et al. 2011, Ghayoomi and McCartney 2011, Mirshekari and Ghayoomi 2017). The applications of a suction-controlled field in geotechnical centrifuges have comprised of studying seismically induced settlements of partially saturated sands (Ghayoomi et al. 2011), measurements of small-strain shear modulus in partially saturated sands (Ghayoomi and McCartney 2011), and understanding the seismic site response of partially saturated soils (Mirshekari and Ghayoomi 2017).

McCartney and Zornberg (2010) studied hydraulic characteristics of a low-plasticity unsaturated clay including SWRC and hydraulic conductivity function using steady state infiltration in a centrifuge permeameter. The VWC (θ), matric suction (ψ), and discharge velocity (v_m) were measured in consecutive drying and wetting paths where the degree of saturation was changed by altering both g-level and discharge velocity in different patterns. Negligible hysteresis was observed through all the drying and wetting cycles, which was speculated to happen due to: starting the tests from a degree of saturation of almost 90% and passing along scanning curves; conducting the experiments on a relatively narrow range of VWC that prevented air pores from being entrapped between soil particles; and/or applying a continuous steady state infiltration throughout the tests during which water may have flowed along the same pore paths in the drying and wetting processes. In addition, the effect of g-level on the SWRC of clay was

examined by comparing suction and VWC measurements of consecutive drying tests under different centripetal accelerations. The comparison, however, was not able to demonstrate a distinct influence of acceleration level on the SWRC since the data was scattered as a result of successive rewetting of the specimens. Comparisons between prototype SWRC (i.e. using hanging column and pressure chamber tests) and those obtained from centrifuge permeameter showed the same α- and N-van Genuchten fitting parameters (1980) for different tests although different residual VWC (θ_r) and saturated VWC (θ_s) were estimated due to the difference in the porosity of tested specimens. Parks et al. (2011) employed an in-flight permeameter and continuously measured θ and ψ within a layer of Ottawa sand to study hydraulic characteristics of sands during steady-state infiltration experiments. After a wet-compacted specimen was completely drained to θ_r, at different g-levels, they applied infiltration onto the specimen awaiting the steady-state condition at each g-level. However, the obtained matric suction profiles were not uniform in any of the g-levels, which was likely due to the impact of outflow boundary conditions. Although only one discharge rate was used in the mentioned study, due to the non-uniform θ and ψ profiles, for each g-level, several θ-ψ data points during drying and infiltration parts were obtained. Aside from the significant scatter in the results, a clear influence of g-level on SWRC was not concluded and different water entry suction values from 1-g and high-g measurements were reported. This was hypothesized to be due to different wetting mechanisms in infiltration experiments.

Scaling parameters of unsaturated flow were addressed by either using dimensional analysis (Goodings 1982, Cargill and Ko 1983, Arulanandan et al. 1988, Cooke and Mitchell 1991, Butterfield 1999, Barry et al. 2001) or comparing the governing equations in prototype and

scaled systems (Goforth et al. 1991, Lord 1999, Dell'Avanzi et al. 2004). The dimensional analyses of unsaturated flow used the dimensionless "capillary effect" number, which led to the same scaling parameters as in saturated laminar flow problems. However, different scaling factors were obtained from those of saturated flow considering Poiseuille's equation for capillary-governed flow (Lord 1999). Dell'Avanzi et al. (2004) provided a consistent framework to offer formulation for suction profiles and addressed the scaling issues where Richards' equation for unsaturated flow (Richards 1931) was analytically solved. In case of a large-enough centrifuge (i.e. ratio of centrifuge arm to the length of specimen higher than 10) the acceleration field would be approximately uniform in the specimen and the prototype/model scaling factors of 1, 1/N, N, and N^2 would be obtained for matric suction, discharge velocity, flow rate, and time for N-g centrifuge test, respectively.

Theoretical Formulation

The fluid potential in a control volume of soil under higher gravitational field could be expressed by Bernoulli's equation:

$$\Phi = -\frac{1}{2}\omega^2(r_0 - z)^2 + \frac{1}{2}(\frac{v}{n})^2 - \frac{\psi}{\rho_w} \quad (2\text{-}16)$$

where Φ is the fluid potential, ω is the angular velocity of the rotation, r_0 is the radial distance of the rotation axis and bottom of the specimen, z is the distance of the control volume to the bottom of the specimen, v is the discharge velocity, n is the soil porosity, and ρ_w is the fluid density. Comparing with the gravity and suction terms in Bernoulli's equation the second term indicating the velocity component of fluid's energy can be omitted as the seepage velocity in unsaturated flow is negligible. The discharge velocity of the flow may be related to the fluid

potential and hydraulic conductivity using Darcy's law. Then, it can be introduced in the principle of continuity equation that results in Richards' equation for unsaturated flow (Richards 1931) assuming material isotropy and constant control volume during the experiments:

$$\frac{\partial}{\partial z}\left[k(\psi)\left(\frac{\omega^2}{g}(r_0 - z) - \frac{1}{\rho_w g}\frac{\partial \psi}{\partial z}\right)\right] = 0 \tag{2-17}$$

where k(ψ) is the unsaturated hydraulic conductivity as a function of matric suction, and g is the earth gravity. Solving Richards' equation yields to the following generic equation for suction profile during steady state infiltration in higher gravities:

$$\psi = \rho_w z \omega^2 \left(r_0 - \frac{z}{2}\right) + \rho_w g v K(z) + \psi_0 \tag{2-18}$$

where K(z) is the integration of inverse hydraulic conductivity along the depth of the specimen and ψ_0 is suction at the bottom of the specimen defining the boundary conditions. For the real unsaturated flows, Richard's equation is more convenient to be solved numerically (Bear et al. 1984, Šimůnek and Nimmo 2005). Dell'Avanzi et al. (2004) assumed Gardner's exponential hydraulic conductivity function (Gardner 1958) for unsaturated soils to analytically obtain the K (z) (Equation 2-19), and solved Richards' equation for steady state flow under higher gravitational field estimating suction profile along the depth of the specimen (Equations 2-20(a) and 2-20(b)).

$$K(z) = \frac{1}{a\rho_w g v}\left[a(\psi - \psi_0) + \ln\frac{\left|\frac{v}{N_r k_{sat}} + e^{-a\psi}\right|}{\left|\frac{v}{N_r k_{sat}} + e^{-a\psi_0}\right|}\right] \tag{2-19}$$

$$\psi = -\frac{1}{a} ln\left[e^{\left(ln\left|\frac{v_m}{N_r k_{sat}} + e^{-a\psi_0}\right| - a\rho_w z_m \omega^2 (r_0 - \frac{z}{2})\right)} - \frac{v_m}{N_r k_{sat}}\right] \; if \; \left(\frac{v_m}{N_r k_{sat}} + e^{-a\psi_0}\right) > 0 \tag{2-20(a)}$$

$$\psi = -\frac{1}{a} ln \left[-e^{\left(ln\left|\frac{v_m}{N_r k_{sat}} + e^{-a\psi_0}\right| - a\rho_w z_m \omega^2 (r_0 - \frac{z}{2})\right)} - \frac{v}{N_r k_{sat}} \right] \; if \; \left(\frac{v_m}{N_r k_{sat}} + e^{-a\psi_0}\right) < 0 \quad \text{2-20(b)}$$

where a is the Gardner's hydraulic conductivity parameter in kPa^{-1} (Gardner 1958), e is the natural base of logarithms, N_r is the g-level depending on z parameter, and k_{sat} is the soil saturated hydraulic conductivity. The suction profiles could be affected by the centripetal acceleration and discharge velocity, the extent of which are shown in Figure 2-11 for a 0.25-m long specimen in a 1-m radius centrifuge with a saturated boundary condition. As illustrated through the analytical solution, to change the suction in 40 g, it requires an order of magnitude change in discharge velocity. The impacts of g-level and discharge velocity on the steady state suction and VWC profiles were demonstrated experimentally in an in-flight permeameter (McCartney and Zornberg 2010) where the effect of discharge velocity was found to be lower than g-level variations.

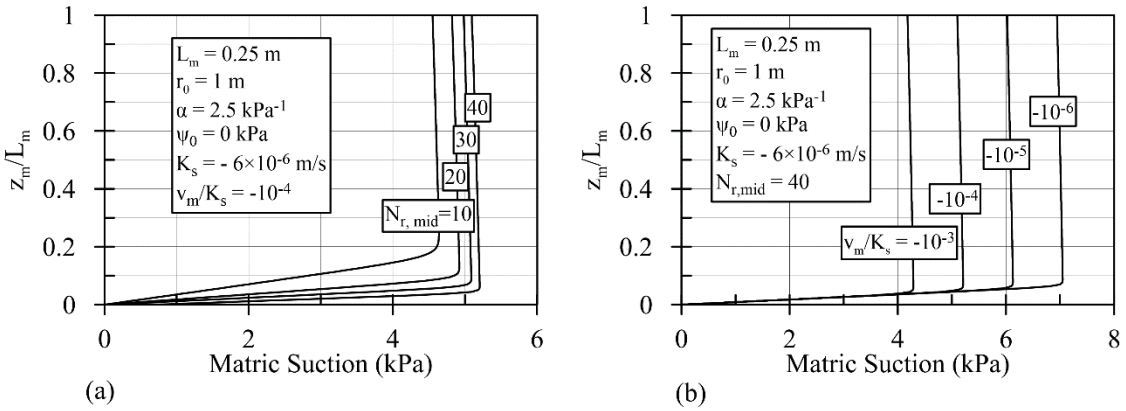

Figure 2-11. Suction Profiles during Steady-state Infiltration from Dell'Avanzi's Analytical Solution (a) for different g-levels and (b) for different discharge velocities.

Further, Dell'Avanzi et al. (2004) compared the suction profiles in prototype and model defining prototype/model suction and discharge velocity scaling factors during the steady-state infiltration as follow:

$$\alpha_{\psi} = \frac{\alpha_z \frac{z}{k(\psi)} - \alpha_z K(z)}{N_r \chi \frac{z}{k(\psi)} - N_r K(z)} \quad \text{2-21 (a)}$$

$$\alpha_{v} = \frac{\rho_w g - \frac{\alpha_{\psi}}{\alpha_z}\frac{\partial \psi}{\partial z}}{\rho_w g N_r - \frac{\partial \psi}{\partial z}} \quad \text{2-21 (b)}$$

Where α_z, α_v, and α_Ψ are the geometry, discharge velocity and suction scaling factors, respectively, and χ is the uniformity factor defined as follows:

$$\chi = 1 + \frac{z/r_0}{2(1 - z/r_0)} \quad \text{(2-22)}$$

Since the length scaling factor varies throughout the depth of the specimen and equals the inverse of the g-level, the suction scaling equation could be reduced to:

$$\alpha_{\psi} = \frac{\frac{z}{k(\psi)} - K(z)}{\chi \frac{z}{k(\psi)} - K(z)} \quad \text{(2-23)}$$

Uniformity and suction scaling factors are shown in Figure 2-12 (a) versus r_0/L_m (the ratio of centrifuge arm's length to the length of specimen) for the bottom, middle, and top of a soil specimen under centripetal acceleration of 40 g. The uniformity parameter and suction scaling factor become approximately 1 where r_0/L_m is greater than 10. This might be the case for some of the in-flight permeameters or large centrifuges (Ghayoomi et al. 2011; Ng et al. 2014). However, in situations where the steady state infiltration technique was used in some in-flight permeameters as well as smaller geotechnical centrifuges (Zornberg and McCartney 2010; Mirshekari and Ghayoomi 2017), this ratio may become less than 10 signifying the importance of suction scaling values. Further parametric study on Equation 2-23 shows the insensitivity of

the suction scaling factor to K(z) and, in turn, to the g-level. The range of K(z) values for typical applications is negligible comparing with the inverse of typical unsaturated hydraulic conductivity for sands, silts, or clays. This parametric study simplifies the suction scaling factor equation and suggests a scaling factor that is only a function of specimen height and centrifuge arm's length:

$$\alpha_{\psi} = \frac{1}{\chi} \tag{2-24}$$

The validity of this reduced-form equation could be verified by inspecting the values of uniformity and suction scaling factors in Figure 2-12 (a). It should be noted that Equation 2-24 expresses the dependency between uniformity of the suction profile and uniformity of the acceleration field where, suction in upper portion of the profile becomes lower in non-uniform acceleration fields. This phenomenon is shown in Figure 2-12 (b) for a 0.25-m long specimen under the same centripetal acceleration of 40 g with different centrifuge arm's lengths. This scaling factor is only valid when comparing the suction (or degree of saturation) profiles of prototype and model in infiltration problems where the length and discharge velocity are modeled accordingly. The scaling factor of $1/\chi$ should not be applied to measured matric suctions or when back calculating matric suction from degree of saturation. Rather, the stress scaling factor of 1 is used in the case of projecting measured matric suctions to prototype values. Moreover, the feasibility of back-calculation of the matric suction from the high-g degree of saturation values has to be solely evaluated by studying the effect of g-level on SWRC and is not a suction scaling problem. Therefore, verification of this suction scaling factor was not sought in this study, and the measured matric suctions were considered the same as their prototype values.

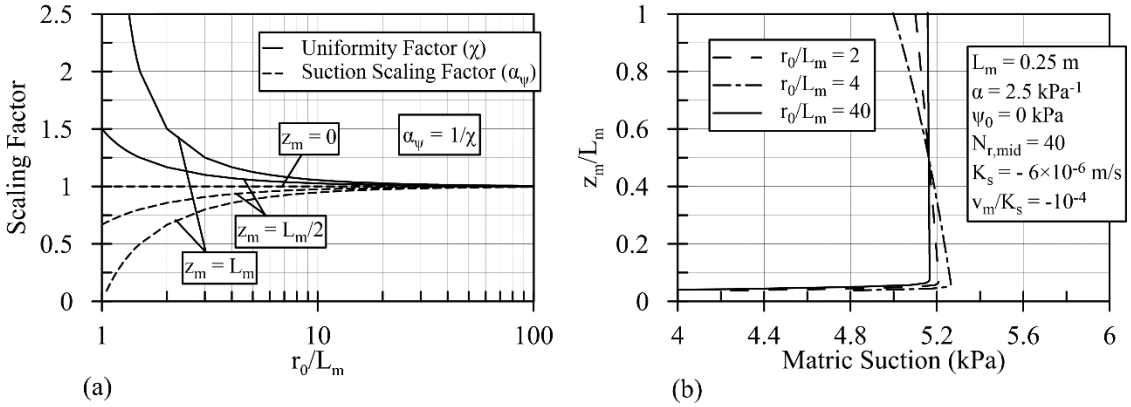

Figure 2-12. (a) Uniformity and suction scaling factor over r_0/L_m (b) Suction profiles for different r_0/L_m

2.5. Summary and Conclusions

A thorough literature review on different aspects of this research was presented in this chapter. Initially, a general background on dynamic soil properties was given, and the effect of partial saturation on different dynamic properties (including small-strain and strain-dependent shear modulus and damping) was discussed. Then, an overview of site response analysis and its dependency on local site conditions as well as motion intensity were discussed. Further, the available data in the literature on the influence of partial saturation on seismic site response were presented, and the reasons behind hypothesizing degree-of-saturation-dependency of site response were explained. At the end, different centrifuge modeling processes to generate and control partially saturated field, including capillary rise from water table and steady state infiltration technique, were reviewed. The next chapter will discuss the material selection and characterization procedures and will present the geotechnical and hydraulic properties of the materials used in this study.

CHAPTER III

MATERIAL SELECTION AND CHARACTERIZATION

3.1. Material Selection

Among the mentioned approaches of centrifuge testing on unsaturated soils, the steady state infiltration and capillary rise procedures can be employed in experiments with granular materials (i.e. sands and gravels). For granular soil layers, the centrifugation along with free drainage leads to very low degrees of saturation due to their relatively higher permeability values. For fine soils (i.e. clays and silts), although all the mentioned approaches are applicable, the low permeability of fine-grained soils requires a significantly longer period of infiltration experiments as well as a considerably lower discharge velocity. These will add to the difficulties of the infiltration experiments in fine-grained soils where the steady state infiltration would be practically impossible to achieve when using a spraying system for the inflow water.

F-75 Ottawa sand was used in the infiltration experiments because while the corresponding suction at residual water content might reach to 10 kPa, yet it is permeable enough to permit the steady state infiltration occurrence within the discharge range of the experiments. Furthermore,

using finer materials would require longer time to reach the steady state condition, which was not applicable due to the limitations in supplying enough water from the inflow tank. To be consistent with the infiltration tests, the same sand was used for capillary tests since it allowed to capture degree of saturation profiles with acceptable resolution in its transition zone (before the residual degree of saturation) for most of the g-levels. Moreover, the grain size distribution and hydraulic properties of Ottawa sand are practical representatives of some site conditions in real field.

In addition to Ottawa sand, Bonny silt was used in preliminary numerical analysis to be representative of finer soils with higher suction levels. In order to evaluate the effect of soil type (i.e. grain size distribution and induced level of suction stress) on the uncertainty in site response due to water table fluctuation, typical hydraulic characteristics of two materials (i.e. Bonny silt and a fine well-graded sand) were assumed.

3.2. Material Characterization

3.2.1. Geotechnical Properties

The grain size distribution of the F-75 Ottawa sand, classified as SP according to USCS system, is illustrated in Figure 3-1. The drained friction angle of the sand was obtained through a set of static traixial tests (Suprunenko 2015) resulting in a friction angle of 40 degrees. Some of the Geotechnical properties of this sand are listed in Table 3-1. In addition, Geotechnical properties of Bonny silt, used in the preliminary numerical analysis, are listed in Table 3-2 as reported in Khosravi and McCartney (2011).

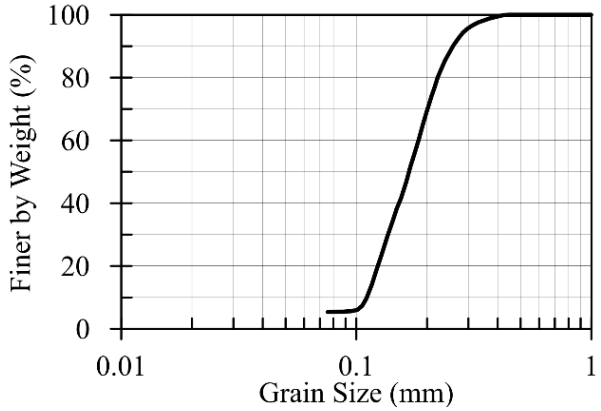

Figure 3-1. Grain size distribution of F-75 Ottawa sand

Table 3-1. Geotechnical properties of F-75 Ottawa sand

Parameter	**Ottawa Sand**
Mineralogy	Quartz, 99.8% SiO_2
Grain shape	Rounded
Coefficient of curvature, C_c	1.71
Coefficient of uniformity, C_u	1.01
Specific gravity, G_s	2.65
D_{50} (mm)	0.182
Dry density limits, $\rho_{d\text{-}min}$, $\rho_{d\text{-}max}$ (kg/m^3)	1469, 1781
Void ratio limits, e_{min}, e_{max}	0.49, 0.80
Friction angle, ϕ (deg)	40
Poisson's ratio, υ	0.38
Saturated Hydraulic Conductivity, k_s (m/s)	6×10^{-6}

Table 3-2. Geotechnical properties of Bonny silt (after Khosravi and McCartney 2011)

Parameter	**Bonny Silt**
USCS Symbol	ML
Dry unit weight, Υ_d (kN/m^3)	16.5
Specific gravity, G_s	2.6
Uniformity coefficient, C_u	29.17
Curvature coefficient, C_c	8.59
Friction angle, ϕ (deg)	29
Hydraulic conductivity, K_s (m/s)	2.74×10^{-8}

3.2.2. Hydraulic Properties

SWRC of Ottawa sand was measured using hanging column test as well as axis translation/tensiometric technique using traixial setup (Ghayoomi et al. 2017) and Direct Simple Shear (DSS) apparatus (Le and Ghayoomi 2017). The hanging column setup consists of three major parts; a specimen chamber, an outflow burette, and a vacuum support system. Matric suction is kept constant along a specimen during different stages of the test by means of having a saturated High Air Entry Value (HAEV) disk underlying the soil sample, which is connected to a burette using a bubble-free water tube (Figure 3-2). The burette is connected to the vacuum supplying system, which applies suction to the inside air. Since a long thin tube is located inside water in the burette, the difference between the air pressure inside the burette and the outside air pressure forms a bubbling point at the tip of the thin tube. This bubbling point creates a reference pressure inside the burette so that the applied suction to the specimen can be calculated by measuring the elevation difference between the bubbling point and the center of the specimen. In this system, the suction increments are generated by altering the height of specimen chamber. The volume of effluent water can be monitored using the burette and the VWC of the specimen can be obtained accordingly. Since the change in elevation of the specimen chamber is limited, this test is specifically suitable for coarse-grained materials with lower suction levels at residual water content.

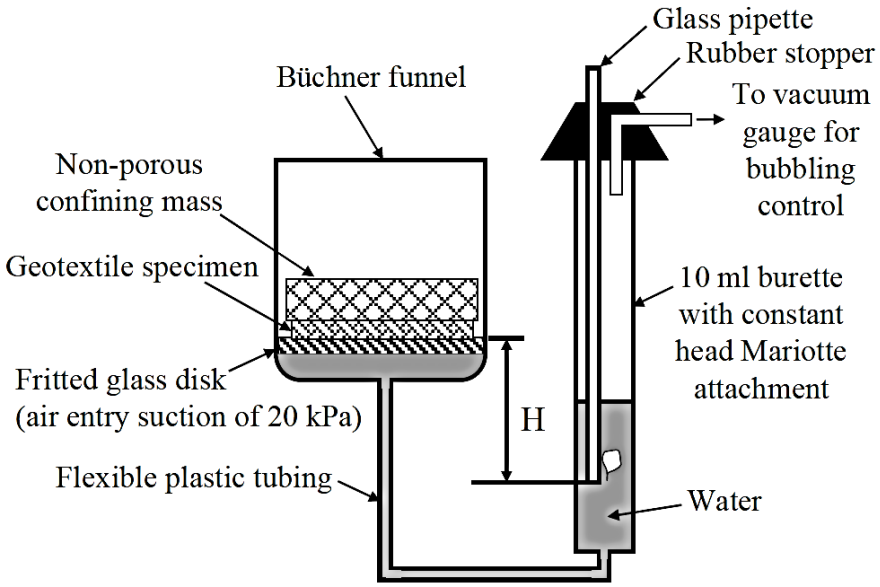

Figure 3-2. Schematic of hanging column apparatus (McCartney 2007)

Axis translation and tensiometeric techniques follow the same concept of having a soil specimen atop an HAEV disk to keep the air and water interfaces separated (Figure 3-3). Water from an initially-saturated specimen can be extracted by increasing the difference between air and water pressure; i.e. u_a-u_w. Increasing the term u_a-u_w can be accomplished by either increasing the air pressure from top of the specimen (axis translation technique) or decreasing the water pressure from the bottom of the specimen (tensiometeric technique). In this study, water was sucked out of both triaxial and DSS systems using a flow pump through the HAEV disk, which is also capable of high-resolution measurements of effluent water volume. The measured SWRC using both methods, i.e. hanging column and tensiometeric technique, along drying and wetting paths are shown in Figure 3-4, which demonstrated a good agreement amongst the different methods (Mirshekari and Ghayoomi 2015, Ghayoomi et al. 2017, Le and Ghayoomi 2017). The resulting van Genuchten fitting parameters are listed in Table 3-3.

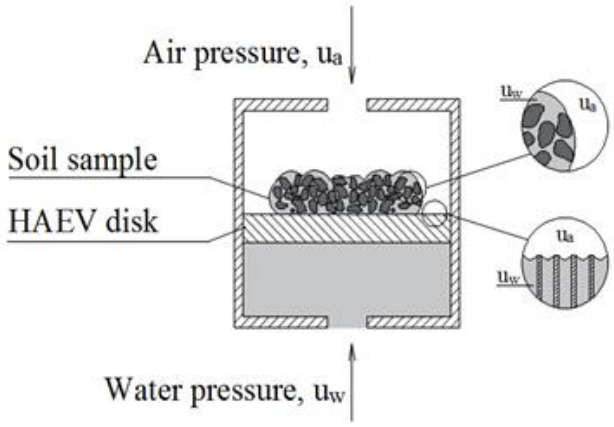

Figure 3-3. Typical schematic for an axis translation/tensiometeric setup (Lu and Likos 2004)

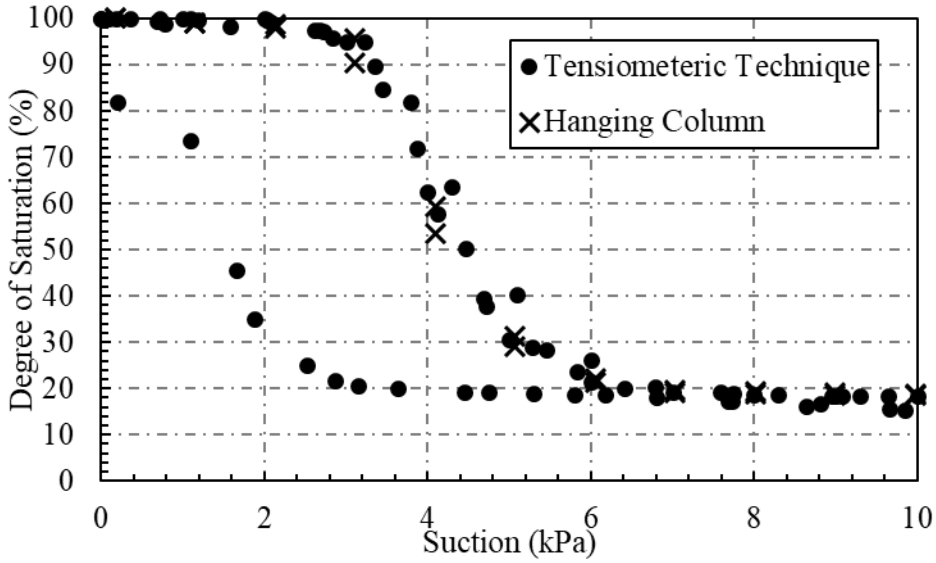

Figure 3-4. The obtained SWRC of F-75 Ottawa sand

Table 3-3. van Genuchten fitting parameters obtained for F-75 Ottawa sand

Parameter	**Value**
a_{vG} for Drying Path (kPa^{-1})	0.25
N_{vG} for Drying Path	9
θ_r for Drying Path	0.07
θ_s for Drying Path	0.392
a_{vG} for Wetting Path (kPa^{-1})	0.7
N_{vG} for Wetting Path	5
θ_r for Wetting Path	0.07
θ_s for Wetting Path	0.322

Van Genuchten SWRC parameters of Bonny silt, used in the preliminary numerical modeling, were derived from the data reported by Khosravi and McCartney (2011) for 100 kPa net normal stress (Figure 3-5). It should be noted that due to water occlusion, which occurred at higher matric suctions (i.e. higher than 70 kPa), only the top portion of SWRC of Bonny silt was captured in that study.

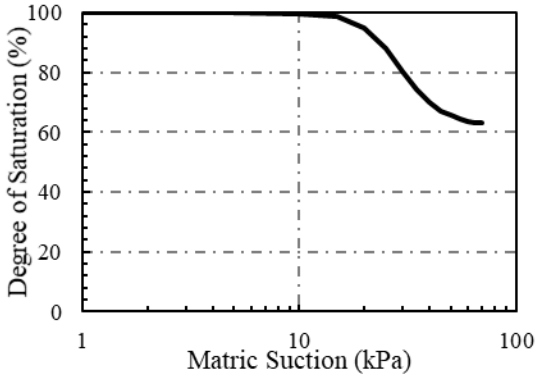

Figure 3-5. SWRC of Bonny silt (after Khosravi and McCartney 2011)

For the parametric analysis, presented in the last chapter of this dissertation, hydraulic properties of a fine well-graded sand and Bonny silt were used, which are illustrated in Figure 3-6 (a) and (b), respectively. The SWRC of Bonny silt was assumed as that reported in Lu et al. (2014), which was thoroughly captured until the residual degree of saturation at matric suctions about 10^5 kPa. Van Genuchten fitting parameters for both Bonny silt (obtained from the data in Khosravi and McCartney 2011 as well as those in Lu et al. 2014) and the fine well-graded sand are listed in Table 3-4.

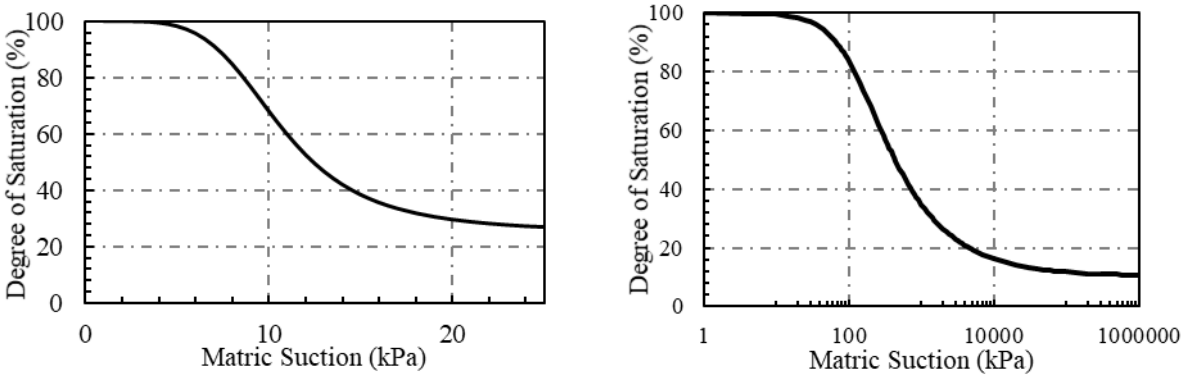

Figure 3-6. SWRCs used in parametric analysis for (a) fine well-graded sand and (b) Bonny silt (after Lu et al. 2014)

Table 3-4. Van Genuchten fitting parameters for the materials in the preliminary numerical analysis as well as the parametric study

Parameter	**Bonny Silt (Khosravi and McCartney 2012)**	**Bonny Silt (Lu et al. 2014)**	**Fine Well-Graded Sand**
a_{vG} for Drying Path (kPa^{-1})	0.036	0.008	0.1
N_{vG} for Drying Path	5	1.62	5
θ_s for Drying Path	0.435	0.435	0.4
θ_r for Drying Path	0.27*	0.045	0.1

* Occluded water content

3.3. Summary and Conclusions

In this chapter, selection and characterization of the materials used in this study were discussed. The materials used in this research include F-75 Ottawa sand, for the experimental program and preliminary numerical analysis, Bonny silt, for the preliminary numerical analysis and the parametric study, and a typical fine well-graded sand, for the parametric study. Geotechnical and hydraulic properties of the selected materials, obtained from the experiments in this study or from the literature, were presented. The next chapter will present the results of preliminary numerical modeling, which served to shed light on the effect of partial saturation on seismic site response and to help in planning an appropriate experimental program.

CHAPTER IV

PRELIMINARY NUMERICAL SITE RESPONSE ANALYSIS OF PARTIALLY SATURATED SOIL LAYERS

4.1. Introduction

In order to understand the seismic behavior of unsaturated soils and schedule a reasonable experimental program, the seismic response of partially saturated sand and silt layers was numerically studied as a preliminary stage of this project using DEEPSOIL software. In the absence of any available numerical procedure to account for partial saturation, this influence was investigated by adjusting the soil unit weight and effective stress for any given degree of saturation. Changes of the effective stress in unsaturated soils, in turn, altered soil dynamic properties including small-strain and strain-dependent shear modulus and damping. Accordingly, partial saturation in the soil layers appeared to considerably influence the site response, where the extent of this effect was a function of soil type as well as induced motion characteristics.

4.2. Numerical Modeling Procedure

In the numerical analyses, 10-m sand and silt layers as well as 30-m sand layers were modeled in DEEPSOIL program. The 30-m and 10-m depths were selected in harmony with seismic provisions recommendations for site classification procedure and the approximate depth of centrifuge seismic experiments, respectively. The study on 30-m sand layers was performed using equivalent linear analysis while both equivalent linear and nonlinear analyses were employed in the case of 10-m sand and silt layers. The equation of motion is solved in frequency domain using an iterative procedure through equivalent linear analysis where the values of shear modulus and damping are modified in each step. However, to more accurately analyze seismic response of soil layers, the equation of motion could be solved in time domain where the shear modulus and damping values change throughout the loading duration.

The 10-m and 30-m soil layers were divided to 13 and 23 sub-layers, respectively, for the sake of computational accuracy and efficiency. Dynamic properties of soil were assumed to be constant within each layer and calculated for the center of the layers. Thickness of layers increase gradually in depth ranging between 0.25 to 1 m and 0.25 to 2 m for the 10-m and 30-m soil layers, respectively. Ottawa sand (for both analyses) and Bonny silt (for the 10-m soil layer) were selected as the earthen materials to be representative of soils with relatively low (i.e. up to 10 kPa) and higher (i.e. up to 70 kPa) matric suction levels, respectively.

In this preliminary step, the degree of saturation was assumed to be constant within the depth to enable the parametric evaluation of the effect of partial saturation. In addition, this condition was similar to the target centrifuge tests that employed steady state infiltration resulting in a uniform degree of saturation profile in the physical experiments. Dry and partially saturated conditions

were numerically modeled in both 10-m and 30-m analyses. However, saturated condition was not considered in the analyses where the response will be different due to the occurrence of liquefaction in saturated sand layers. The soil layers in partially saturated condition were assumed to have 4 different degrees of saturation for the 30-m sand layer (i.e. 20, 40, 60, and 80%), while the unsaturated condition was only represented by 1 degree of saturation in the 10-m analyses (i.e. 91% and 80% for Ottawa sand and Bonny silt, respectively). The selected degrees of saturation in the 10-m analyses are the ones that correspond to the maximum suction stress (Equation 2-13b) to provide a more significant difference between the dry and unsaturated cases. The suction stress variations over degree of saturation for Ottawa sand and Bonny silty are shown in Figure 4-1. Suction stress versus effective degree of saturation (a) Ottawa sand (b) Bonny silt.

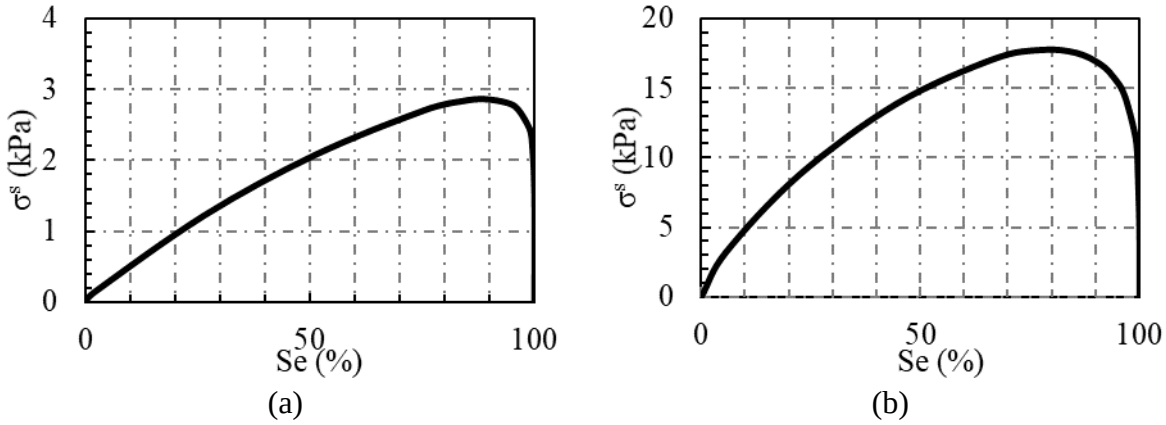

Figure 4-1. Suction stress versus effective degree of saturation (a) Ottawa sand (b) Bonny silt

The effective stress formula proposed by Lu et al. (2010) was employed, to account for partial saturation by linking the effective stress, net normal stress, and matric suction (Equations 2-13a and 2-13b). Further, the modified effective stress values were used to find dynamic soil properties (i.e. shear modulus, G, and damping, D). The equation proposed by Ghayoomi and McCartney (2011) was used to define small-strain shear modulus of Ottawa sand, which was

shown to be valid for F-75 Ottawa sand with 40% relative density (Equation 2-2). The generic equation proposed by Sawangsuriya et al. (2009) with specific fitting parameters obtained from the experimental data of Khosravi and McCartney (2011) was employed to calculate the small-strain shear modulus of Bonny silt:

$$G_0 = A.f(e)\,\sigma'_m{}^{n} \tag{4-1}$$

where A and n are fitting parameters and f (e) is used to account for void ratio which is expressed as $1/(0.3 + 0.7\,e^2)$. In order to take the strain-dependency of the shear modulus into account, the modulus reduction formulation proposed by Menq (2003) was considered for both soils (Equations 2-3, 2-4a, and 2-4b). The strain-dependent damping values were calculated as a function of effective stress (degree of saturation) using the equation by Darendeli and Stokoe (2001), which adds to the small-strain damping (from Menq. 2003) resulting in the total damping value (Equation 2-7).

1-D scaled 1994 Northridge earthquake motions, recorded at WPI station, with PGAs of 0.1g, 0.3g, and 0.6g, were selected as the input motions in this step to study the effect of different earthquake intensities on the site response of unsaturated soils. Different characteristics of the input motions, including acceleration time histories, 5% damped spectral acceleration, and Arias Intensity time histories are illustrated in Figure 4-2. Frequency domain, Equivalent Linear (EL), and time domain, nonlinear (NL), analyses were performed on soil columns of both materials. Fully saturated soils layers were not evaluated as they have different response because of seismically induced excess pore water pressure and potential liquefaction event.

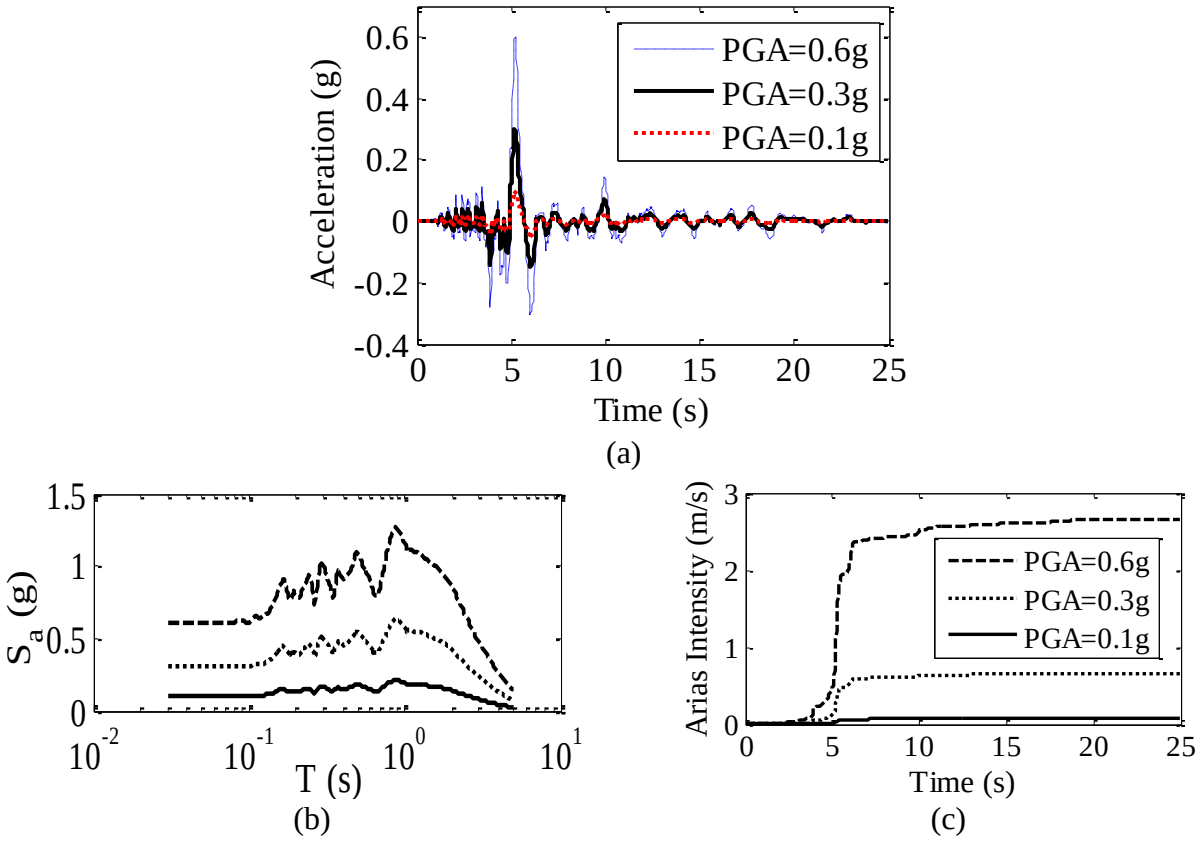

Figure 4-2. Characteristics of scaled Northridge earthquake motions (inputs of preliminary numerical analyses); (a) Acceleration time histories; (b) 5% damped spectral accelerations (S_a) over spectral period (T); (c) Arias Intensity time histories.

4.3. Results

4.3.1. The Results for 30-m Sand Layers

The results of numerical analyses of 30-m deep ground layers with different degrees of situation (i.e. 0, 20, 40, 60, and 80%) are presented herein. The soil profiles were shaken under bedrock motions with PGA of 0.1, 0.3, and 0.6 g. The presented results include PGA amplification factor profiles, Arias intensity time histories, 5% damped pseudo-spectral acceleration graphs, and lateral deformation profiles.

Peak Ground Acceleration (PGA) reflects the maximum absolute acceleration value of the motion. The acceleration amplitudes and frequency content of the motion changes as it

propagates from the bedrock to the soil surface. Accordingly, the PGA of the motion alters from the bedrock to the soil surface. PGA amplification factor (F_{PGA}) representing the ratio of the PGA of the motion in depth to the PGA of the bedrock motion is commonly used for practical site response analysis, $F_{PGA}=PGA_m/PGA_b$. The F_{PGA} variations of the ground motion with depth for different degrees of saturation under bedrock PGA of 0.1, 0.3, and 0.6 g are shown in Figure 4-3 (a), (b), and (c), respectively.

The F_{PGA} in shallow ground under low intensity earthquakes, i.e. $PGA_b=0.1g$, decreases as the degree of saturation changes from 0.8 to 0 (Figure 4-3 a). This is attributed to the interaction between different parameters in partially saturated soils including shear modulus, damping, unit weight, and the induced level of strain. For higher matric suction values, shear modulus increases while material damping decreases. These variations, in turn, will lead to lower and higher acceleration amplification, respectively. It should be noted that the values of shear modulus and damping are highly dependent on the strain level induced in soil layers, which also changes as a function of partial saturation. Besides, the higher water content leads to higher inertial stresses during a seismic event that affects the response of unsaturated soil layers. The impact of degree of saturation on F_{PGA} in deeper ground is almost zero mostly due to minimal effects of suction and water content on the effective stress and soil properties. Further, the abovementioned trends became insignificant in higher intensity motions, i.e. $PGA_b=0.3g$, due to the more dominant effect of large-strain modulus and damping (Figure 4-3 b) where these two are less sensitive to suction comparing with small-strain modulus and damping. The irregular amplification pattern observed in Figure 4-3 (c) indicates that the equivalent linear analysis is not accurately predicting the site response under high intensity shaking, i.e. $PGA_b=0.6g$.

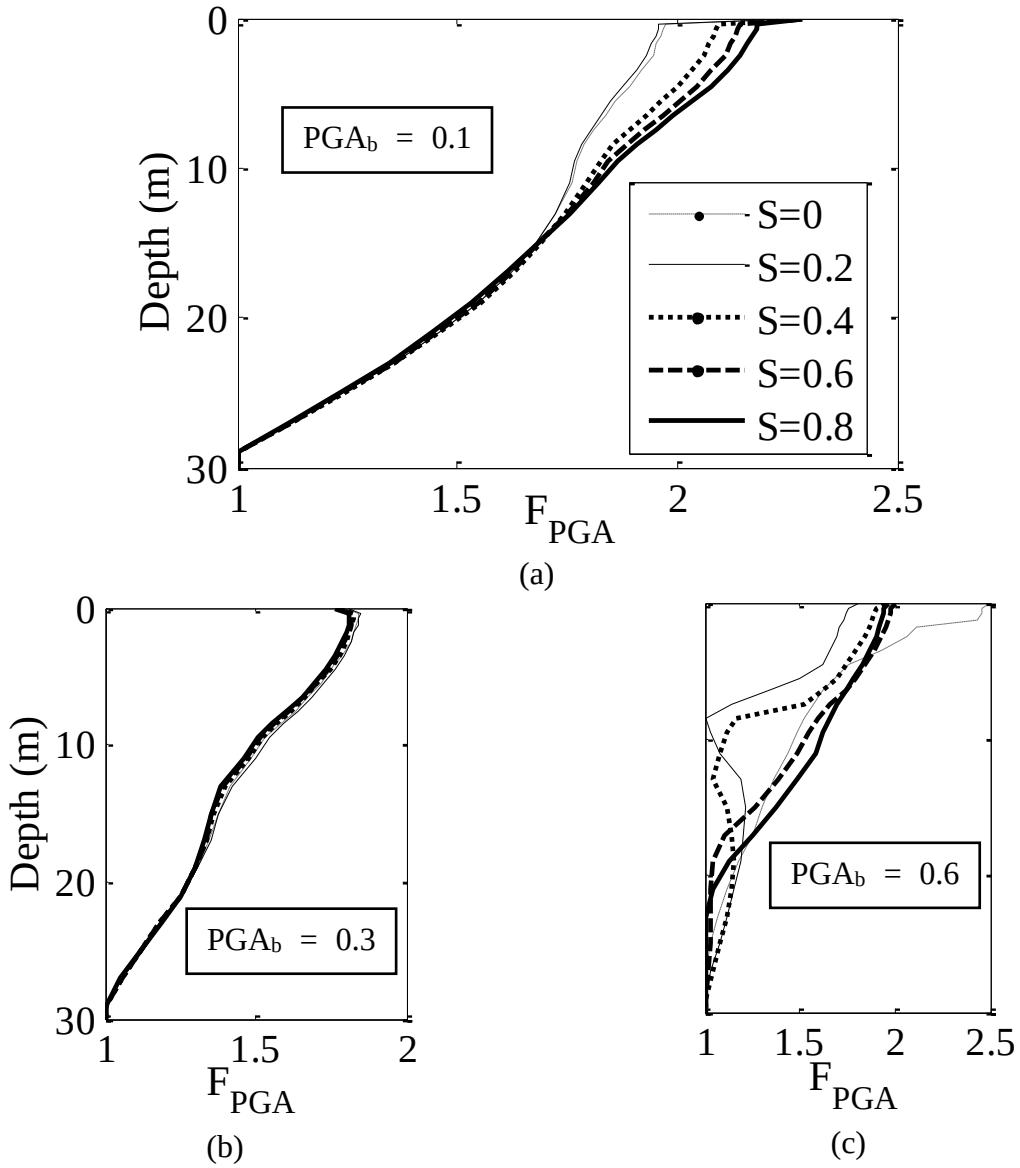

Figure 4-3. PGA Amplification Factor (F_{PGA}) profiles in the 30-m deep sand layer for different degrees of saturation under the earthquake motion with (a) PGA_b=0.1g; (b) PGA_b=0.3g, (c) PGA_b=0.6g.

Arias intensity (Arias 1970), a well-known cumulative intensity characteristic denoted by I_a, was selected to represent the accumulated energy buildup during a shaking event in dry and unsaturated sites, which is calculated using the following equation:

$$I_a(t) = \frac{\pi}{2g}\int_0^t a^2(t)dt \tag{4-2}$$

where a (t) is the acceleration time history and g is the earth gravitational acceleration. The Arias Intensity time histories of the top layer at the soil surface for different degrees of saturation follow a similar trend as in F_{PGA}, as shown in Figure 4-4. This demonstrates that not only PGA of the motion increased as a result of partial saturation, but overall, the acceleration values in unsaturated ground were higher than those in dry soil.

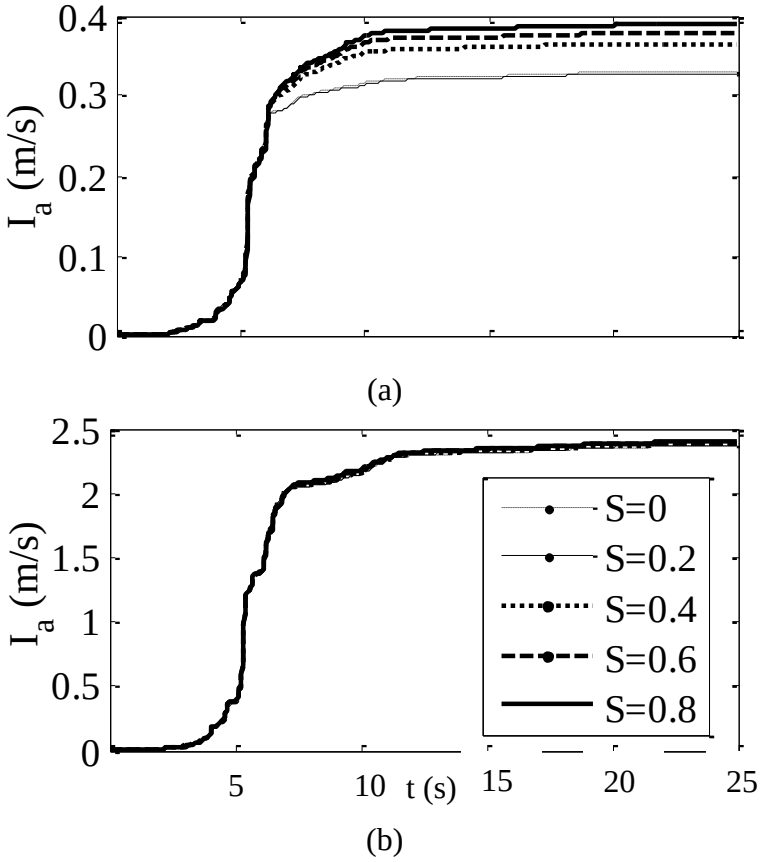

Figure 4-4. Arias Intensity time histories of surface motions in 30-m deep soil profiles with different degrees of saturation under the earthquake motions with (a) PGA_b=0.1g; (b) PGA_b=0.3g.

Previous studies revealed that more holistic ground motion indices should be implemented in any seismic soil response assessment that include different characteristics of an earthquake motion, i.e. intensity, frequency content, and duration (Ghayoomi and Dashti 2015). As a result, considering the frequency content of the motion and its variability from the bedrock to the soil

surface is inevitable. The 5%-damped spectral acceleration of the surface motion in soil profiles with different degrees of saturation is shown in Figure 4-5. The trend is similar to what was observed in Figure 4-3 and Figure 4-4 in the dominant natural period, while the differences are not significant in other periods. This pattern can be seen in Figure 4-6, which focuses on a narrower range of periods.

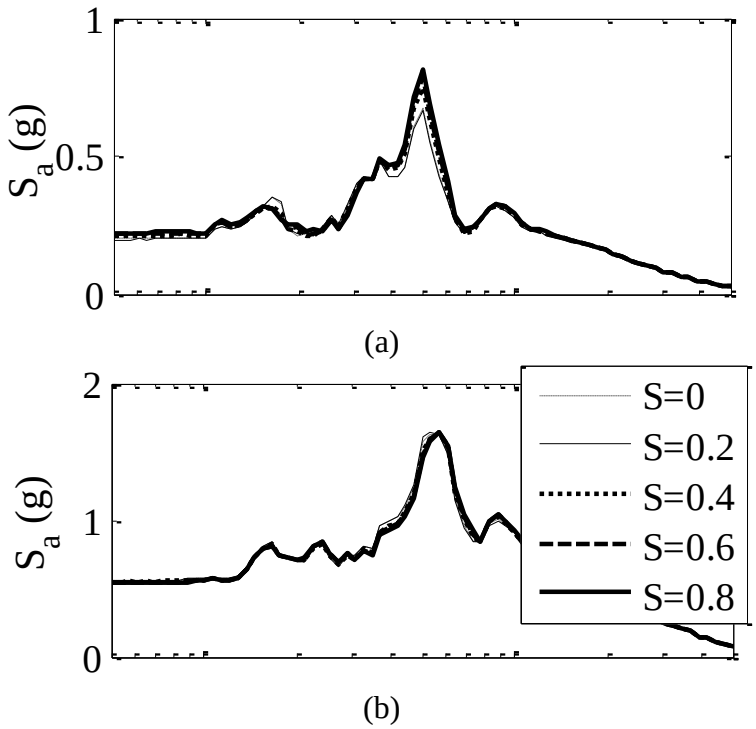

Figure 4-5. 5% damped spectral acceleration of surface motions in 30-m deep soil profiles with different degrees of saturation under the earthquake motion with (a) PGA_b=0.1g; (b) PGA_b=0.3g.

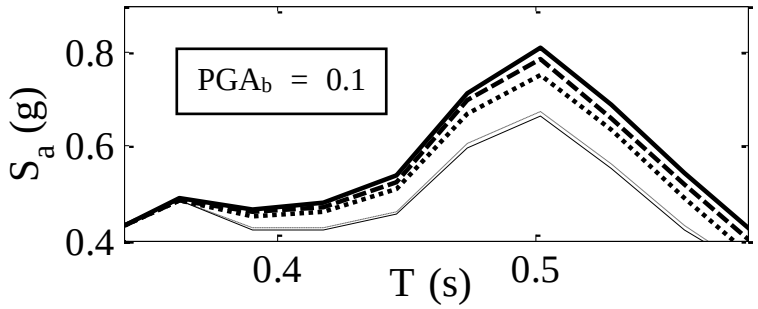

Figure 4-6. 5% damped spectral acceleration of surface motions in 30-m deep soil profiles with different degrees of saturation under the earthquake motion with PGA_b=0.1g.

Soil lateral deformation is directly related to the lateral stiffness and strength. The lateral deformation profiles for different degrees of saturation are shown in Figure 4-7. These profiles increased as the degree of saturation increased indicating a softer response in higher moisture content.

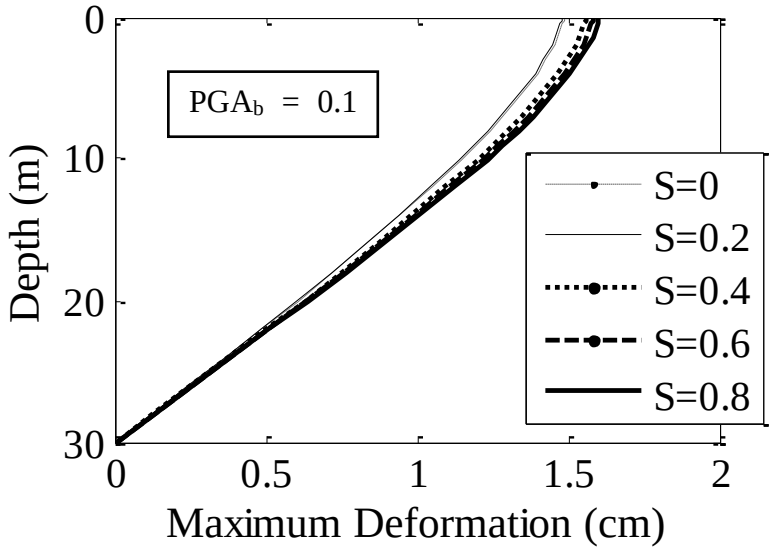

Figure 4-7. Lateral deformation profiles of 30-m deep soil layers with different degrees of saturation under the earthquake motion with PGA_b=0.1g.

4.3.2. The Results for 10-m Sand and Silt Layers

The results of analyzing 10-m deep sand and silt layers included PGA, Arias intensity, 5% damped spectral acceleration, and soil lateral deformations, all of which were calculated for the center of each layer. F_{PGA} profiles of dry and unsaturated 10-m soil layers, obtained from both EL and NL analyses, under the base PGA of 0.3g are shown in Figure 4-8. F_{PGA} values in dry Ottawa sand was less than those in partially saturated condition in both EL and NL analyses. In Bonny silt, however, more inconsistency in amplification factor was observed with depth. Dry Bonny silt experienced higher amplification in shallower depth, but this trend changed in depth,

which was similarly observed under other motion intensities with much severe irregularities. In addition, there was a substantial difference between the results of EL analyses and those of NL with EL analysis leading to much higher amplification factors in both materials. This indicates that PGA is not always the best representative of the motion (Ghayoomi and Dashti 2015).

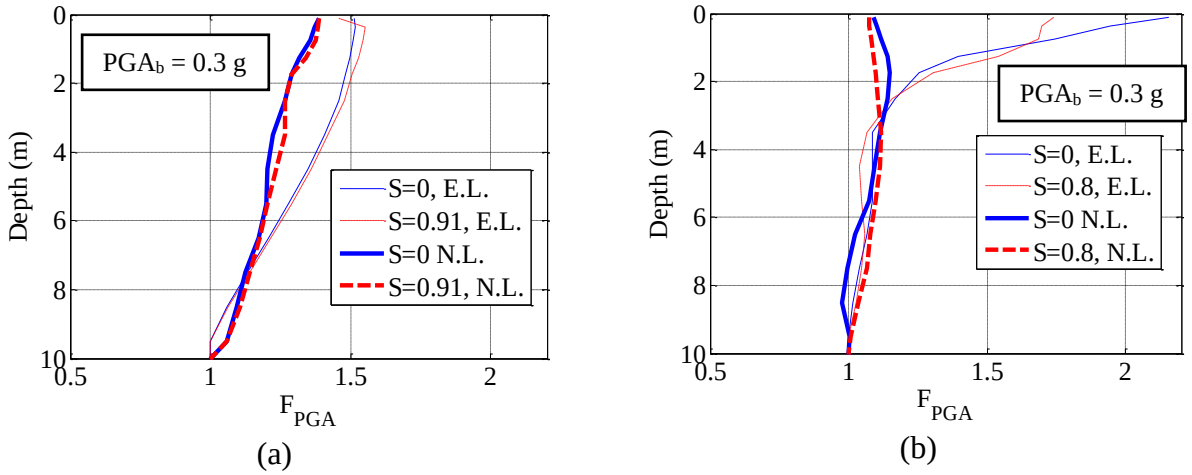

Figure 4-8. PGA Amplification Factors (F_{PGA}) variation in depth for dry and unsaturated 10-m soil layers under the earthquake motion with PGA_b= 0.3g for (a) Ottawa sand and (b) Bonny silt

Arias intensity time histories of 10-m sand and silt layers under the excitation PGA of 0.3g are shown in Figure 4-9 for EL and NL analyses. The analyses results showed higher Arias intensities for unsaturated Ottawa sand and dry Bonny silt, which was visible in most cases. Arias intensity and F_{PGA}, mostly, followed the same variation trend for the silt and sand layers. The higher values of Arias intensity resulting from EL analysis than NL models was similarly observed.

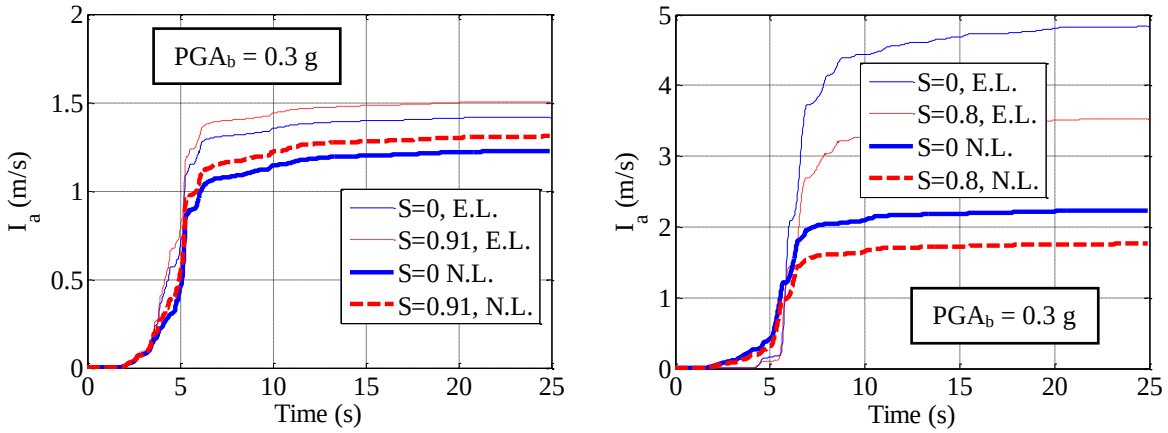

Figure 4-9. Arias Intensity time histories of surface motions in 10-m dry and unsaturated soil columns under the earthquake motion with PGA$_b$= 0.3g for (a) Ottawa sand and (b) Bonny silt

The graphs of 5% damped spectral acceleration of the surface motions under the bedrock PGA of 0.3g, for 10-m layers of Ottawa sand and Bonny silt, are shown in Figure 4-10. The surface spectral accelerations calculated for Ottawa sand were very similar in all cases. Spectral accelerations of dry Bonny silt, however, were consistently higher than those of unsaturated silt, which shows a good agreement with the PGA amplification factor and Arias intensity variations.

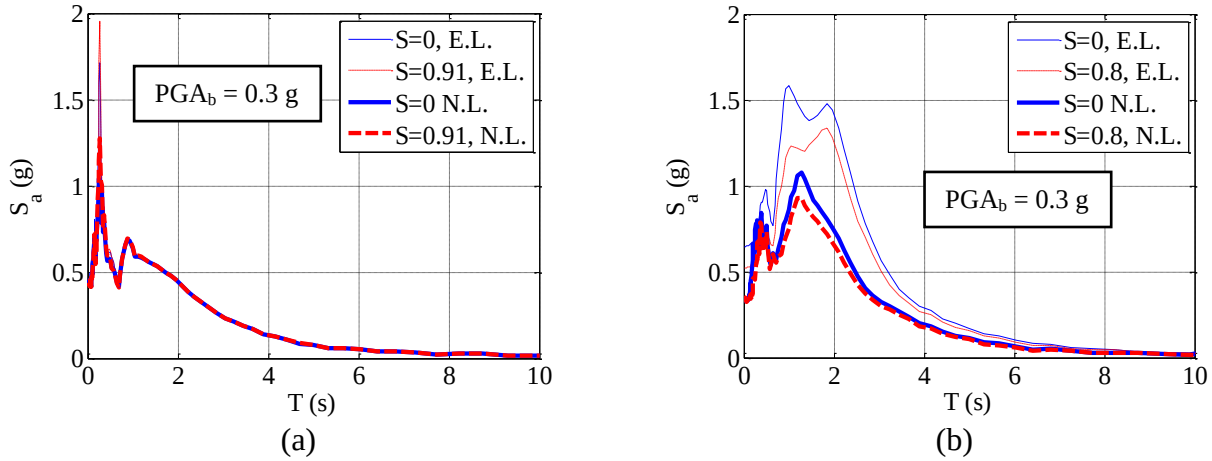

Figure 4-10. 5% damped spectral acceleration of surface motions in dry and unsaturated soils under the earthquake motion with PGA$_b$= 0.3g for (a) Ottawa sand and (b) Bonny silt

Lateral deformation profile reflects the stiffness of the soil layer and the intensity of induced motion. The lateral deformation profiles of the target soils under PGA$_b$=0.3g are shown in Figure

4-11. Almost for all the graphs, deformations were higher in unsaturated Ottawa sand, indicating the most consistent results among all the motion characteristics. For the Bonny silt, however, analyses led to opposite results as dry soils experienced higher deformation. These results demonstrated a good agreement with intensity amplification and spectral acceleration results. As a summary, Ottawa sand and Bonny silt showed higher intensity amplification for unsaturated and dry cases, respectively, which led to higher deformation of soil deposits.

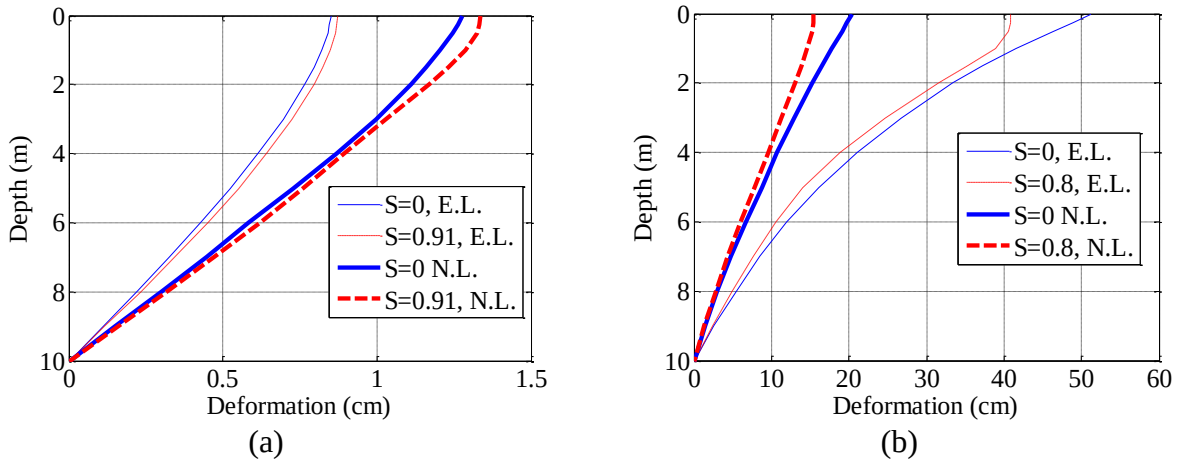

Figure 4-11. Lateral deformation profiles of dry and unsaturated soil layers under the earthquake motion with PGA_b=0.3g for (a) Ottawa sand and (b) Bonny silt

4.4. Summary and Conclusion

The modeling procedures and results of a set of equivalent linear and nonlinear site response analyses for partially saturated sand and silt layers with uniform suction profiles were presented in this chapter. The intensity amplification, spectral acceleration, and lateral deformation were monitored from the base to the soil surface. The results of this preliminary study clearly indicated the influence of degree of saturation on the seismic site response. The trends associated with this influence depended on the degree of saturation (matric suction), induced motion,

analysis approach, and most importantly the selection of dynamic material properties. For soils with low suction levels (e.g. Ottawa sand) intensity amplification, spectral acceleration, and deformations were higher for unsaturated situation as opposed to those in the soils with higher suction levels (e.g. Bonny silt). The results of this preliminary study were partly in contrast with the previously believed assumption of lower intensity amplification and lateral deformations for unsaturated soils.

This numerical investigation shed light on different parameters influencing the site response of unsaturated soils demonstrating the need for further physical modeling of this problem. However, the numerical modeling was simplified through several assumptions including: (1) considering the effect of partially saturated conditions through an indirect influence on dynamic soil properties and not studying the wave propagation mechanisms in unsaturated soils; (2) simplifying suction variations in depth as uniform profiles which does not occur in nature; (3) employing the effective-stress based formulations, which were empirically developed from the experiments on dry and saturated soils, to account for variations of dynamic soil properties in unsaturated soils. However, the degree of saturation or matric suction might have a separate influence (aside from the effective stress dependency) on the dynamic properties of unsaturated soils (e.g. as discussed in Dong et al. 2016 or Ghayoomi et al. 2017). Additional DEEPSOIL numerical analyses of unsaturated soil layers are performed as a part of the study to assess uncertainty of site response analysis due to the seasonal water table fluctuations, which will be presented in Chapter 10.

CHAPTER V

CENTRIFUGE PHYSICAL MODELING EXPERIMENT DEVELOPMENT

5.1. Introduction

The renovated 5 g-ton centrifuge at the University of New Hampshire (UNH) was originally constructed in the early 70s at the California Institute of Technology (Figure 5-1). It was relocated to UNH in 2013 and was employed to study the seismic response of unsaturated soils as its first major project. Since this research was the first study that implemented the centrifuge facility at UNH after its relocation, some renovation steps were also identified as preliminary tasks within the scope of this research. In addition, other modifications were required to incorporate the infiltration technique for unsaturated testing, which were performed during the early stages of the project. These tasks will be discussed in this chapter.

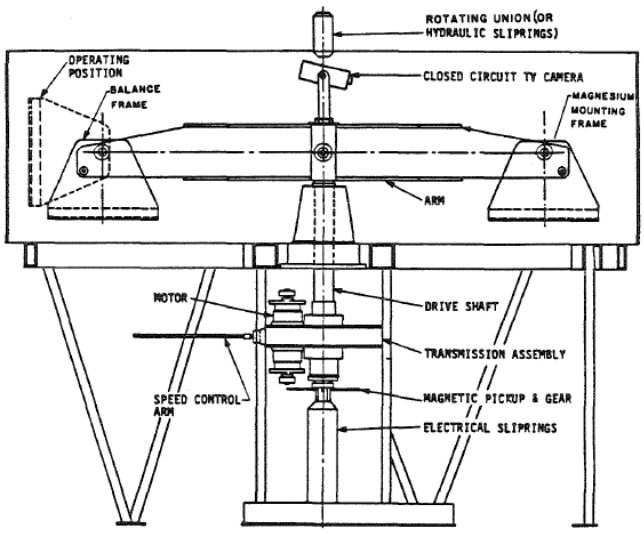

Figure 5-1. Schematic of the original centrifuge at California Institute of Technology (Hushmand et al. 1984)

5.2. Centrifuge Renovation

The UNH centrifuge has an arm radius of 1 m from the center of rotation to the platform in its fully extended position. The nominal payload capacity of the centrifuge is 5 g-ton being able to carry a 100 kg or 30 kg payload up to 50g or 175g respectively. The centrifuge was received at UNH in separate pieces and was reassembled in house. Upon completion of the assembly process the maximum safely achievable g-level was defined to be 75 and 60 without and with the container, respectively. The centrifuge is enclosed in a protective chamber to avoid direct contact of the user and in-flight loads (Figure 5-2, a). An emergency stop is also deployed, which shuts down the power in case of large movements of the enclosing chamber (i.e. larger than 1/8 inch). The centrifuge and operation room are separated using a brick wall, which was constructed after the assembly process was completed. External and internal views of the centrifuge are shown in Figure 5-2 (a) and (b), respectively.

The centrifuge is equipped with an in-flight shaking table (shown in Figure 5-2, c) that is capable of imposing harmonic or seismic displacement time histories. A hydraulic servo valve, controlled by brand-new National Instruments system, operates the table. Due to servo valve limitations, the current system has an analog displacement threshold of 10-mm. The data is transferred through a SCXI 1531 input module, which is located in a NI SCXI-1000 chassis. The Data Acquisition System (DAQ) of the centrifuge is shown in Figure 5-3. The centrifuge offers two slip-rings; the obsolete one at the top, which was initially used for data collection purposes, and one at the bottom responsible for transferring hydraulic fluid. Nowadays, the captured data is easier transferred through the onboard Wi-Fi leaving the top slip-ring responsible only for electrical power of the system. The bottom slip-ring was replaced with a new one with four fluid supply lines, two devoted to the hydraulic fluid and two to the infiltrating water for the purpose of this research project as shown in Figure 5-4.

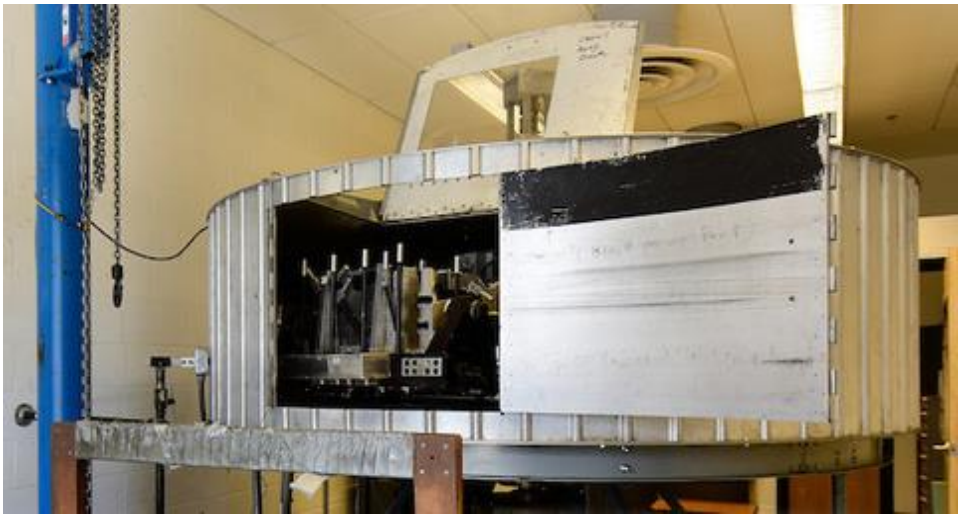

(a)

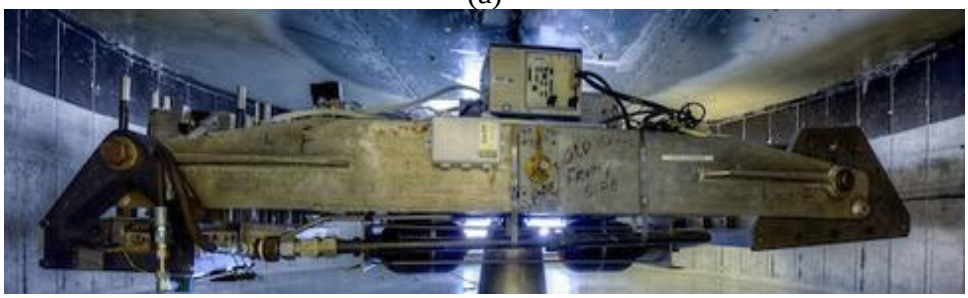

(b)

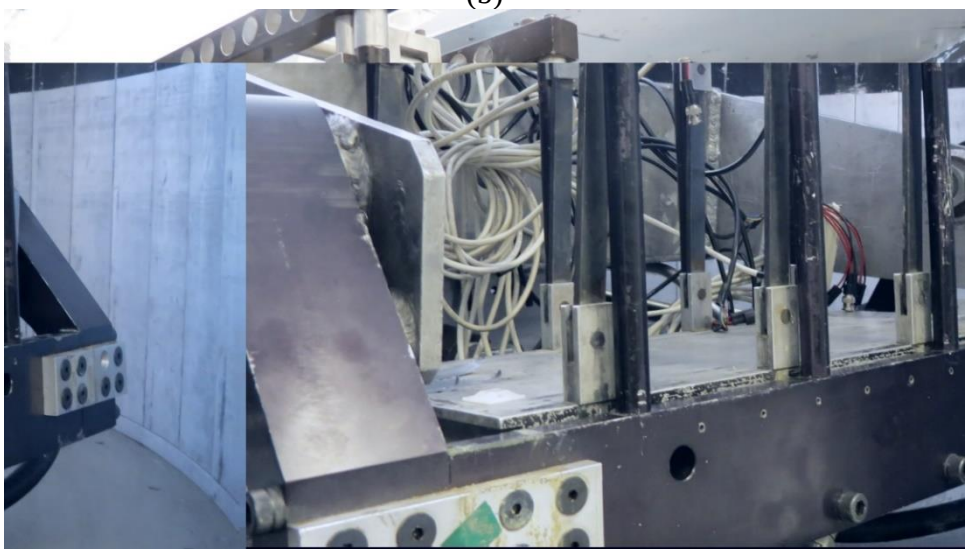

(c)

Figure 5-2. The Centrifuge Facility at University of New Hampshire (a) the enclosing chamber (b) the internal view of the arms (c) the shaking table side

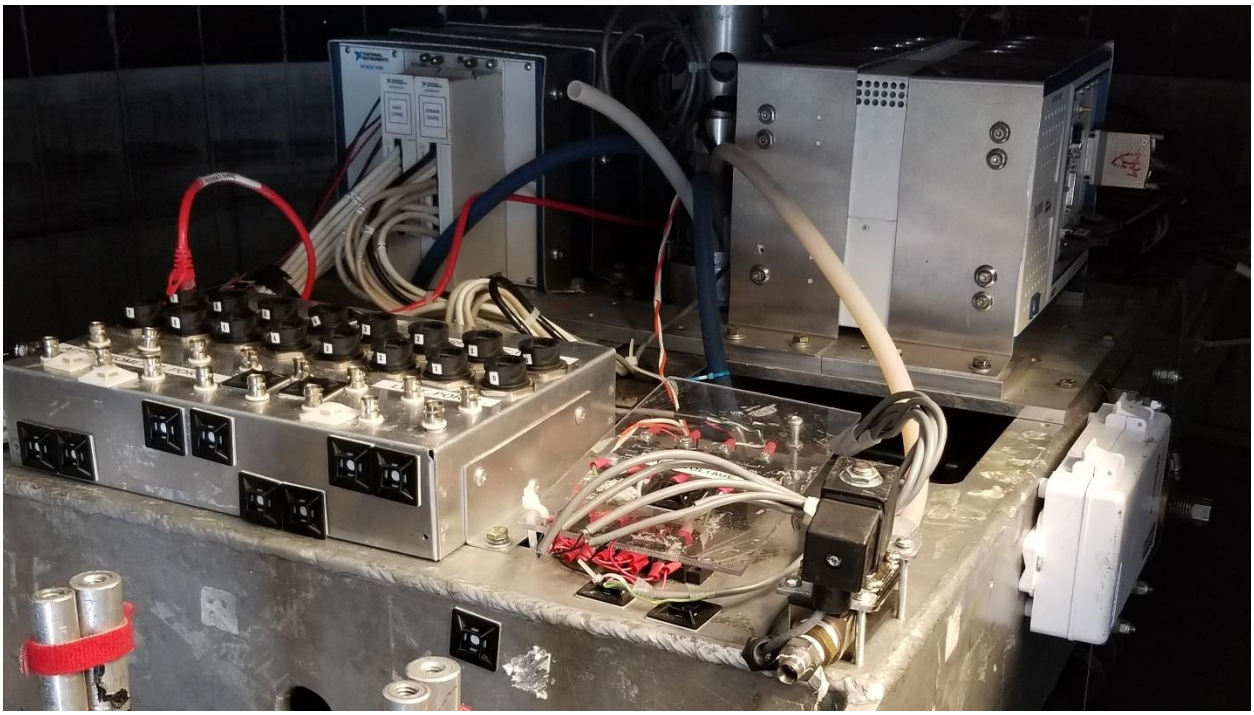

Figure 5-3. The Data Acquisition system (DAQ) of the centrifuge facility at University of New Hampshire

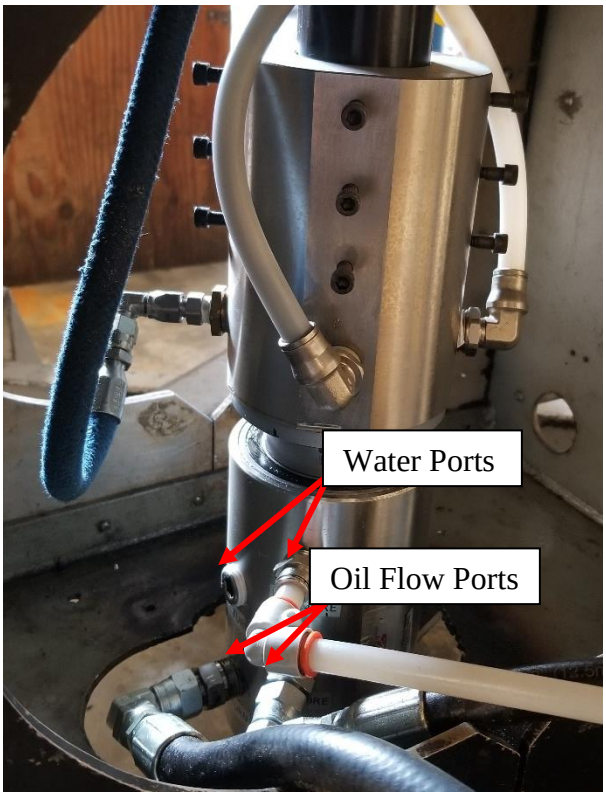

Figure 5-4. The slip ring modified for additional water lines

5.3. Laminar Container

The influences of boundary restraints on the site response were investigated in the past studies (e.g. see Whitman and Lambe 1986). Stacked-ring assembly (Whitman et al. 1981, Lambe and Whitman 1982, Heidari and James 1982, and Arulanandan et al. 1983), laminar container (Hushmand et al. 1988), and hinged-plate model container (Afacan et al. 2014) were used to minimize the box effects. A laminar container, initially built by Hushmand et al. (1988), was used herein to avoid adverse boundary effects on the shear wave propagation (Whitman and Lambe 1986). The container consists of 19 rectangular aluminum laminates, each 12.7 mm thick, which are separated using cylindrical bearing with negligible frictional resistance (Hushmand et al. 1988); shown in Figure 5-5 (a). The inner dimensions of the box are 355.6 mm in length, 177.8 mm in width, and 254 mm in height with the ratio of length to width as 2. In order to allow for free drainage of water, the container base plate was replaced with an outflow control aluminum plate with 14 drainage ports on its side. The outflow was routed to the side drainage ports through a network of holes inside the plate as shown in Figure 5-5 (b). The outflow plate was designed and built in-house and was anodized to avoid long-term corrosion. A plastic membrane was glued to the bottom drainage plate to prevent movement of water and sand particles into the gaps between laminates which is shown in Figure 5-6 (a) and (b).

(a)

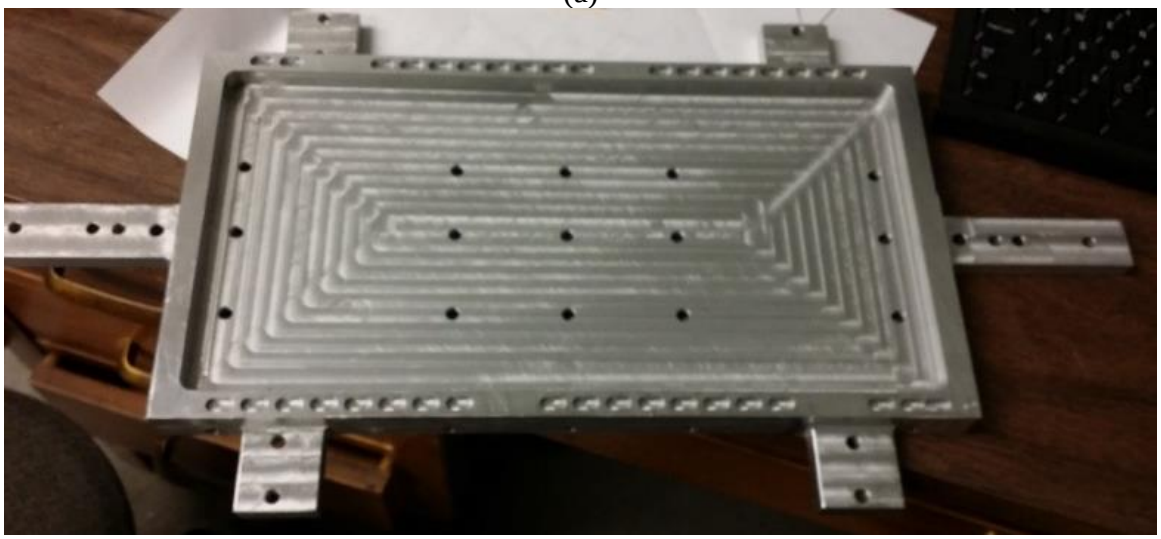

(b)

Figure 5-5. The laminar container used in this study originally designed and built by Hushmand et al. (1988) (b) the modified outflow base plate

(a)

(b)

Figure 5-6. Plastic membrane inside the container (a) gluing process (b) glued to the container

5.4. Infiltration Setup

The basic procedure to apply steady-state infiltration inside the laminar container in this study is similar to Ghayoomi et al. (2011). A schematic of the employed setup is illustrated in Figure 5-7. Inflow water was supplied from an 80-gallons air-pressurized tank, rated for 150 psi, located outside the centrifuge. An inlet slip-ring port was deployed to route the water to 8 fog-spray nozzles through a network of plastic tubing. Three sets of BETE nozzles were utilized in this investigation to obtain various discharge rate and, therefore, different degree of saturation profiles. 1/8 PJ10, 1/8 PJ20, and 1/8 PJ40 nozzles were used for degrees of saturation lower than 45%, between 45% and 60%, and higher than 60% in 50g, respectively. The nozzles spray water with a 90-degree cone-shape pattern and were arranged to cause minimal overlap and inconsistency between the sprayed areas. A set of 8 nozzles with their tubing network mounted on racks, ready to be used in an experiment is shown in Figure 5-8.

In order to control the inflow rate, a solenoid valve was employed in conjunction with an ultra-precision needle valve ahead of the nozzles. The solenoid valve was used to open the water flow during the centrifugation while the needle valve was in charge of controlling the inflow rate. Drainage was conducted through four outflow ports opened by miniature solenoid valves. The outflow water was guided to four drainage tanks mounted on the front, back, and bottom of centrifuge platform. Initially, the effluent water was planned to be drawn out through the slip ring while the test was in progress. However, based on the observations during pilot experiments, it appeared to be practically impossible to drag water inward in high g-levels. To overcome this issue, the outflow tanks were designed large enough to contain the effluent water during one seismic experiment and, on the other hand, small enough so they will not collide with the

enclosing chamber during the flight. More than 12 pilot experiments were performed prior to conducting the main experiments, to verify and assure the proper performance of the infiltration system. Different components of the infiltration setup, including the pressurized water tank, a typical BETE nozzle, the employed solenoid and needle valves, and an outflow water tank are shown in Figure 5-9.

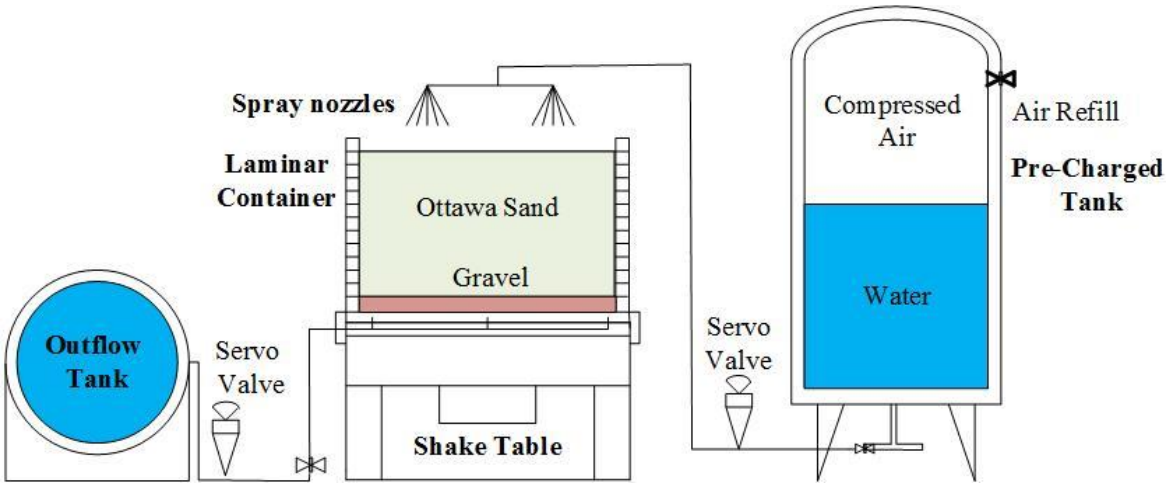

Figure 5-7. Schematic of the setup used to implement infiltration inside a laminar container

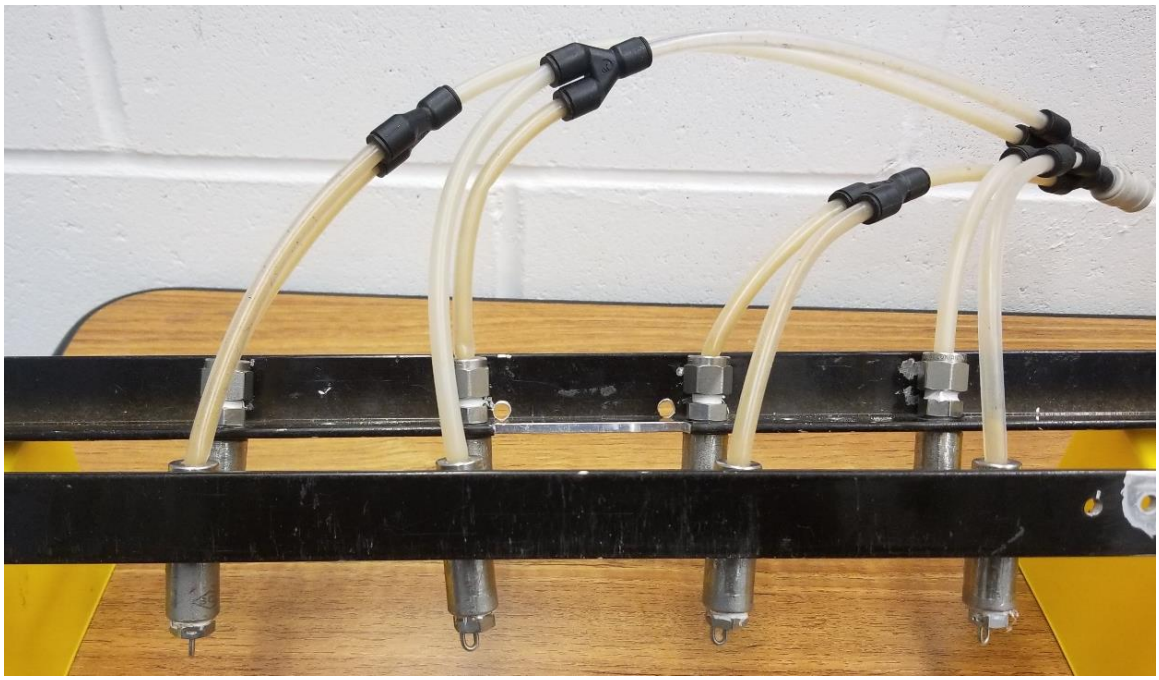

Figure 5-8. A set of nozzles along with plastic tubing mounted on the top racks

(a)

(b)

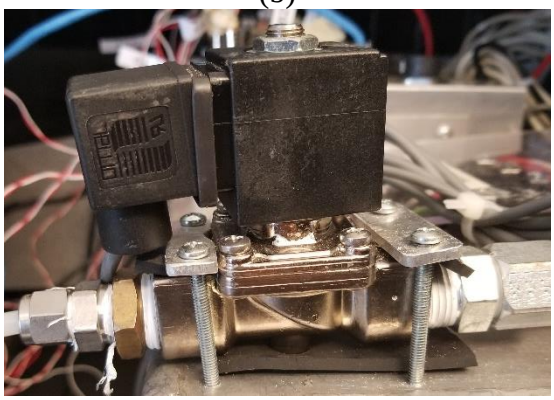

(c)

(d)

(e)

(f)

Figure 5-9. Different components of the infiltration setup (a) air-pressurized water tank (b) a typical BETE nozzle (c) the inflow solenoid valve for opening the flow (d) one outflow solenoid valve (e) the ultra-precision needle valve (f) a side outflow tank

5.5. Summary and Conclusions

This chapter explained the accomplished steps to renovate the centrifuge, modify the laminar container, and implement the infiltration setup for partially-saturated testing in the centrifuge facility at UNH. Centrifuge renovation and reoperation was partly performed as some preliminary steps in this project. In addition, some modifications were required to adjust the testing system for infiltration purposes (e.g. adding hydraulic ports to the bottom slip ring). The laminar container was modified for free drainage of water by replacing its base plate with an outflow control aluminum plate. Further, different components of the infiltration system (e.g. air-pressurized tank, small effluent tanks, inflow and outflow solenoid valves, tubing and spraying nozzles, etc.) were illustrated, and the procedure of steady state infiltration in higher gravities was explained. As another essential task prior to the target experiments, proper instrumentations for this study were selected and calibrated, which will be discussed in the next chapter.

CHAPTER VI

SELECTION AND CALIBRATION OF SENSORS

6.1. Introduction

All the instrumentations used in this research, including seismic experiments as well as hydraulic characteristics studies, are listed in Table 6-1 and shown in Figure 6-1. The instrumentations in this study comprised of dielectric sensors, miniature tensiometers, miniature pore water pressure transducers, accelerometers, and Linearly Variable Deformation Transducers (LVDT) to measure volumetric water content, both matric suction and pore pressure, pore water pressure, acceleration, and displacement, respectively. Although the sensors were provided with initial calibration sheets (except the obsolete Druck pore pressure transducers), most of the sensors needed additional calibrations to reach higher precision. Therefore, among the deployed sensors in this study, only accelerometers were not calibrated in-house prior to the experiments. The measured data using all the instrumentations except dielectric sensors, which offered their own logging system, was transferred through a SCXI 1531 input module which was located in a NI

SCXI-1000 chassis. The preparation and calibration steps for all the sensors are discussed in this chapter.

Table 6-1. The instrumentations used in this study

Instrumentation	Brand	Type	Measured Parameter	Additional Calibration
Dielectric sensors	Decagon Devices	EC-5 5TM	Volumetric Water Content	Yes
Miniature Tensiometers	Measurement Specialties	EPB-PW	Pore Pressure and Matric Suction	Yes
Miniature Pore Pressure Transducers	Druck	PDCR 81	Pore Pressure	Yes
LVDTs	Measurement Specialties	MHR 250, MHR 500	Displacement	Yes
Accelerometers	PCB	353B17	Acceleration	No

(a)

(b)

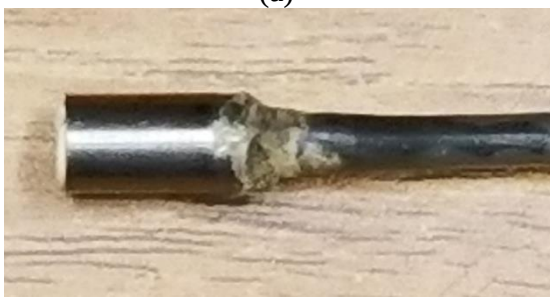
(c)

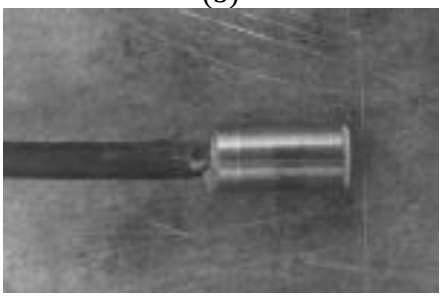
(d)


(e)

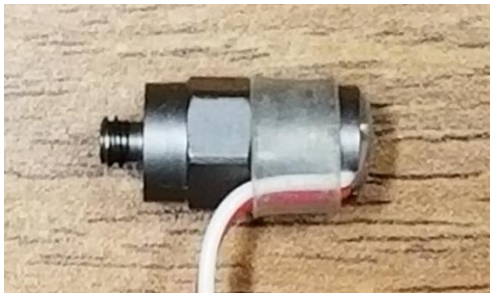
(f)

Figure 6-1. The instrumentations used in this study (a) EC-5 dielectric sensor (b) 5TM dielectric sensor (c) miniature pore pressure transducer (d) miniature tensiometer (e) LVDT (f) accelerometer

6.2. Dielectric Sensors

EC-5 dielectric sensors (from Decagon Devices in Pullman, WA) were used, which converted the dielectric permittivity of soils to the VWC (Kizito et al. 2008). In addition, one 5TM dielectric sensor (from the same brand) was used in selected tests, which is capable of recording temperature as well as the VWC. The data from the dielectric sensors were monitored through an EM50 Decagon data logger installed on the arm of centrifuge (shown in Figure 6-2) and recorded manually when desired during the tests. Since the resistivity of soils are also a function of mineralogy, texture, and salinity of the material, it is generally recommended to calibrate the sensors in the same testing conditions (i.e. the same soil type, used water, temperature, and sensors' alignment) to increase the measurement accuracy (Cobos and Chambers 2010). To that end, specific calibration program was carried out in the lab temperature in several molds filled with Ottawa sand, which was mixed with the water supplied from the same tank used in the target centrifuge tests.

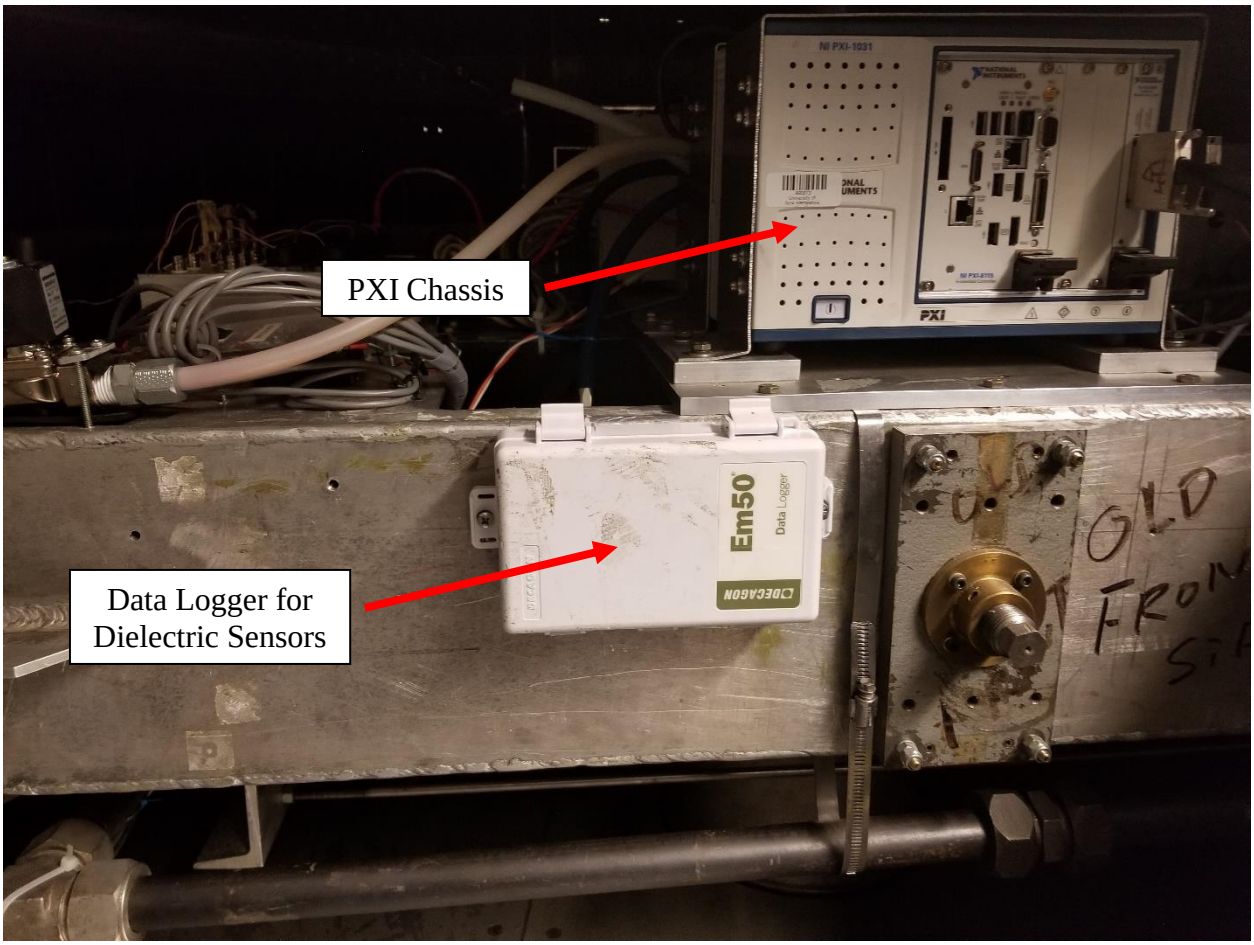

Figure 6-2. EM50 data logger mounted on the centrifuge arm

The calibration, initially, included mixing oven-dried sand with different amounts of water and keeping the wet sand in a sealed plastic bag for 24 hours to allow for moisture homogenization throughout the soil. The wet soil was compacted in three lifts in a container and the sensors were vertically inserted to the specimen. Thereafter, an average moisture content of the specimen was found by obtaining and oven-drying several small samples of wet soil from different locations of the container. The obtained moisture content was used to find VWC using the total weight of wet soil and the volume of container, which, then, was correlated with the recorded VWC data using the moisture probes. This procedure was repeated for different VWCs and for each sensor, where linear calibration for each sensor was obtained. An example calibration graph for an EC-5 sensor

is shown in Figure 6-3. The absolute mean error, of random type, in VWC measurements was found to be between 0.74% and 1.62% for different sensors. The values of coefficient of determination and absolute mean error for the dielectric sensors employed in this study are listed in Table 6-2.

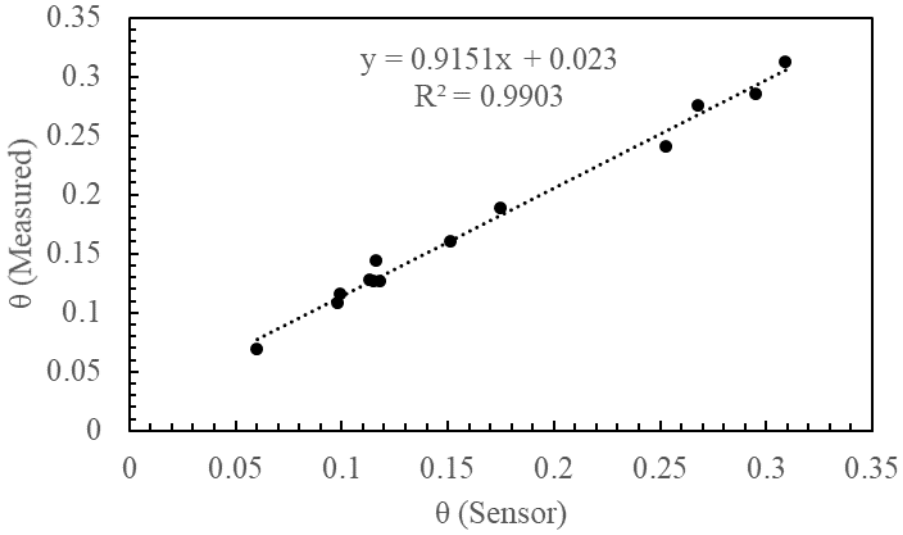

Figure 6-3. An example calibration of the capacitance sensors

Table 6-2. Range of R^2 and error values for dielectric sensors employed in this study

Sensor	R^2	Absolute Mean Error (%)
Dielectric EC-5-1	0.96	1.3
Dielectric EC-5-2	0.99	0.7
Dielectric EC-5-3	0.98	1
Dielectric EC-5-4	0.99	0.7
Dielectric EC-5-5	0.96	1.6
Dielectric 5TM	0.98	1.1

Since the sensors would be located horizontally inside the specimens in centrifuge tests (despite vertical alignment in their conventional applications), the same procedure was repeated with horizontally-aligned sensors to study the influence of sensors' alignment on the measured data. Accordingly, the calibration data from horizontal and vertical alignments of the sensors were compared through which the alignment was demonstrated to have a negligible impact on the

measured values. The calibration was accomplished in several molds (i.e. one compaction mold, one plastic mold, and one Plexiglass mold with the diameters of 10 cm, 11 cm and 20 cm, respectively) to assure the insignificant influence of boundaries on the sensors' performance. It should be noted that the dielectric sensors provided a lower accuracy in degrees of saturation close to fully saturated condition especially in centrifuge testing, where the water head increased in higher gravities. To overcome this issue, the calibration was solely based on the data in unsaturated condition and the results were presented in terms of degree of saturation.

6.3. Pore Water Pressure Transducers and Miniature Tensiometers

Measurement of matric suction in centrifuge modeling has been a main challenge in small-scale simulation of systems with unsaturated soils. The need for capturing instant variations of matric suction requires small water reservoir between the porous stone and diaphragm of sensors, which is provided in miniature tensiometers. In addition, the effect of increased self-weight of sensors in high-g demands miniature tensiometers to avoid soil disturbance. Among the centrifuge studies on hydraulic characterization of unsaturated soils, only a few provided in-flight measurements of matric suction (i.e. Burkhart et al. 2000, McCartney and Zornberg 2010) where the tensiometers had a relatively long response period; e.g. 30 minutes in case of a major change in suction for the ones used in McCartney and Zornberg (2010). The slow response of the tensiometers was in harmony with the experiment context where they measured high suction values of clay during a long period of testing (McCartney and Zornberg 2010) or had the liberty to await the equilibration (Burkhart et al. 2000). However, in the current study capturing prompt changes of matric suction was of interest in both seismic tests as well as study on hydraulic characteristics of unsaturated soils. The reasons for requiring miniature transducers in the

experimental program include rapid changes of matric suction within sand layers, constrained testing time due to the limited water supply during the infiltration tests, causing less non-uniform sand densification due to their self-weight, and measurement of dynamic variations of matric suction during seismic tests. Hence, miniature transducers were selected to be used for matric suction measurements in this study.

Although the obsolete PDCR81 Druck pore pressure transducers were originally intended to measure positive pore water pressure, they were previously modified by applying a non-corrosive glue to the porous stone perimeter, to allow for matric suction measurements (Muraleetharan and Granger 1999). However, as it was noticed during that investigation, the modification still may not thoroughly seal the circumference of the porous stones when steady measurement is needed. Given the prior experiments on unsaturated soils using the Druck sensors and due to their availability, as the first step, the performance of Druck sensors in matric suction measurements was evaluated. In order to examine the proper functionality of four available Druck sensors in matric suction measurements, the sensors were initially located inside a wet compacted specimen along with dielectric sensors. The results showed that three of the sensors are capable of some short-term matric suction measurements. Some of the matric suction measurements in this step along with VWC data are shown in Figure 6-4.

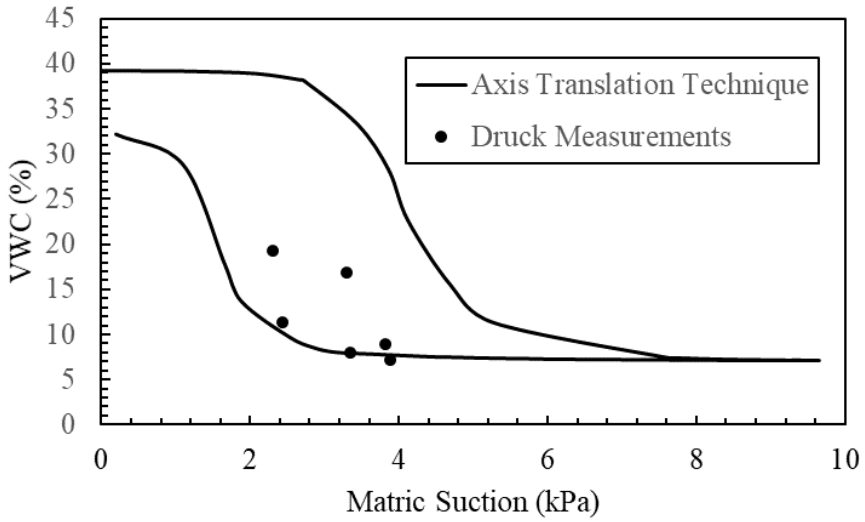

Figure 6-4. Druck 81 measurements inside wet compacted soil alongside VWC data

The second step consisted of dry pluviation of sand inside two containers (a triaxial cell with 25.4 cm diameter and 58.4 cm height and a PVC container with 14.6 cm diameter and 35.6 height, both having drainage ports at the bottom), locating the Druck and dielectric sensors at specified elevations, and saturating the specimen from the bottom. In order to avoid desaturation of sensors, water was locally sprayed on the sand around the sensors as the pluviation continued. Thereafter, the specimen was desaturated by free drainage of water from the bottom as well as applying suction to the bottom of the specimen through a vacuum pump. As a result of this test, only one of the sensors was evaluated to keep measuring suction during a longer time. This was likely because the transducers were incapable of staying saturated throughout the testing period. It should be noted that the performance of Druck sensors was also evaluated in some preliminary centrifuge infiltration tests where, similarly, only one sensor could measure, even short-term, reasonable matric suction values.

As the next step, in order to seal the porous stone circumference of Druck sensors, a very thin layer of Dow 3151 sealant was applied to the perimeter between the porous stone and housing of

a sensor. Schematic of a Druck pore pressure transducer, modified for suction measurements, is illustrated in Figure 6-5. Thereafter, the same steps were repeated to examine the performance of the modified sensor in suction measurements. Although the sensor was capable of reasonable suction measurements in a wet-compacted sand, it could not steadily measure suction variations during the drying experiments (as shown in Figure 6-6). This was also observed during centrifuge experiments, which was similarly reported by Muraleetharan and Granger (1999).

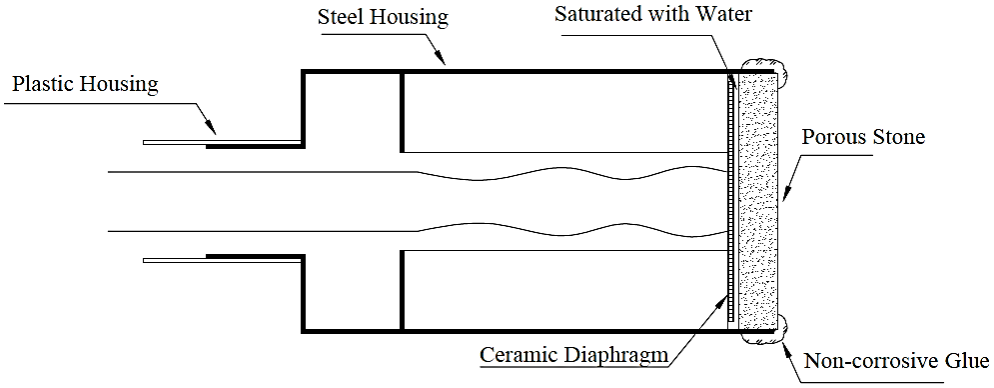

Figure 6-5. A schematic of a Druck81 pore pressure transducer modified for suction measurements

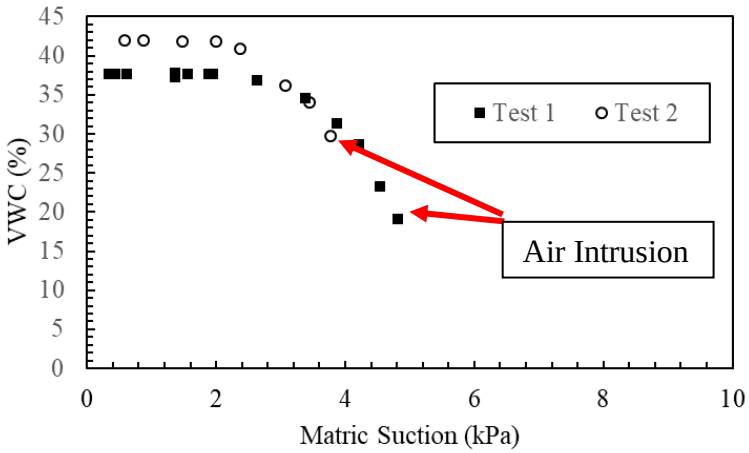

Figure 6-6. Measurements of modified Druck81 sensors in drying experiments

Upon ensuring the incapability of Druck sensors in steady matric suction measurements, three EPB-PW miniature tensiometers (Take and Bolton 2003), from Measurement Specialties, were used in this study to measure matric suction. Two of the employed miniature tensiometers have

porous stones with 50-kPa air entry value whereas the other one has a 100-kPa porous stone. One sensor, with 50-kPa porous stone, was asked to be manufactured with a thicker housing to monitor the effect of large soil weight on the measurement performance. Two PDCR81 sensors were also used in capillary tests within the saturated zone to measure positive pore water pressure and identify the depth of water level. Hereafter, the miniature tensiometers and pore pressure transducers are called EPB tensiometers and Druck PPTs, respectively.

In order to acquire a higher precision in pressure/suction measurements, both Druck and EPB sensors have to be fully saturated. The method introduced by Take and Bolton (2003) was used herein to saturate the sensors in a Plexiglas cylindrical setup with pressure and vacuum ports (shown in Figure 6-7, a). The sensors were passed through cord grip fittings to assure that the cell was sealed against air leakage while the wires were not pinched as well. In addition to using cord grip fittings, to avoid pinched wires, heat shrink tubing was applied to part of the wire of each sensor. The saturation procedure consisted of applying vacuum for 90 minutes to the sensors in air, then, raising water level in the cell so the sensors were soaked in water; followed by applying vacuum to the cell for another 12 hours and ultimately, opening the cell to the atmospheric pressure. The complete setup used for calibration of Druck and EPB sensors is shown in Figure 6-7 (b).

The sensors were calibrated using a burette connected to the sealed Plexiglas cell where the water was lowered gradually inside the burette and the pressure acting on diaphragm was obtained as a function of the distance between water head in burette and the diaphragm elevation. Negative pressure was generated at the level of diaphragm by setting the water level in burette lower than the diaphragm elevation (shown in Figure 6-8) which led to the same calibration

results as obtained in positive pressure (i.e. the same calibration slope and intercept). An example of calibration graphs in positive and negative pressures is illustrated in Figure 6-9. Then, the calibration cell was filled with soil and the sensors' performance, while embedded in soil, was verified against a column of water connected to the cell. Moreover, deploying the EPB sensors along with a T5 Decagon lab tensiometer in a compaction mold demonstrated precise performance of miniature sensors where the difference between the two measurements was less than 0.5 kPa for all the sensors.

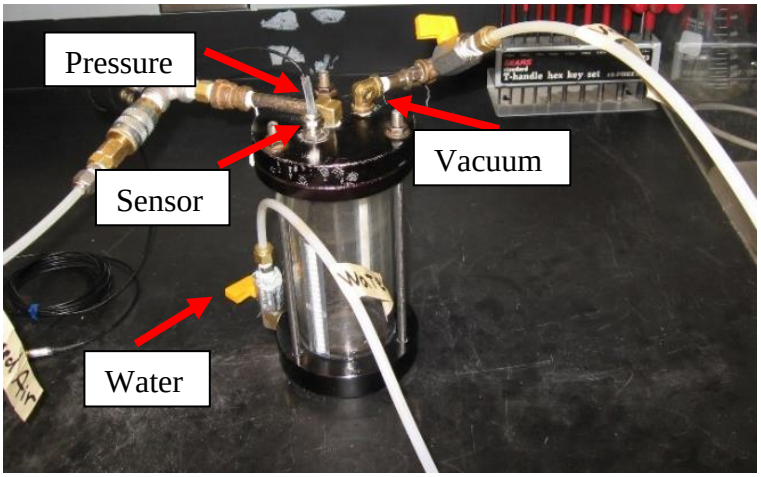

(a)

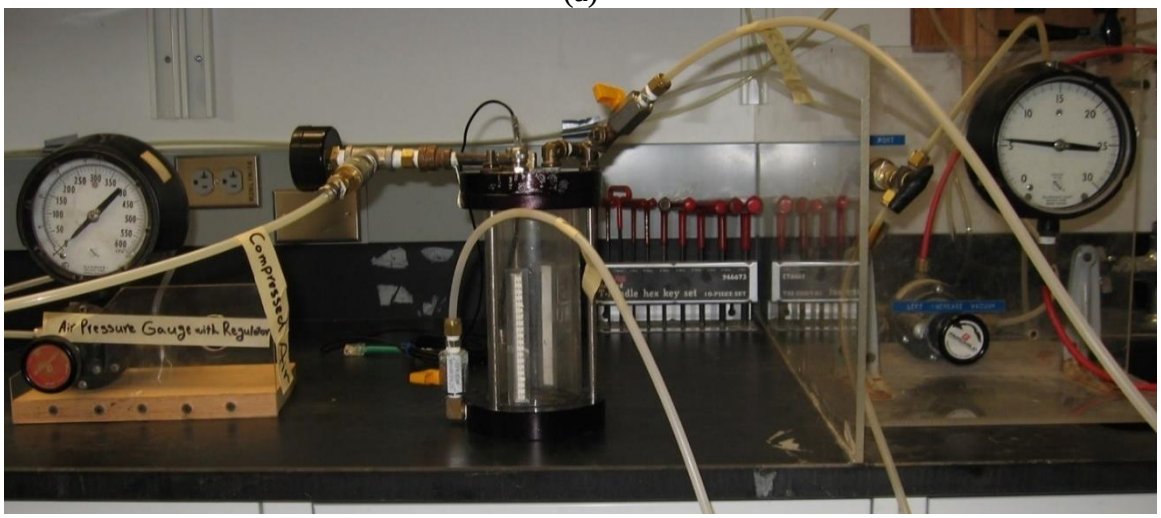

(b)

Figure 6-7. (a) The plexiglass cell used for de-airing and calibration procedures (b) The employed setup for calibration of Druck and EPB sensors

The saturation and calibration steps were repeated for both EPB and Druck sensors prior to each test to obtain the shortest response duration and the maximum accuracy of measurement, respectively. The absolute mean errors of EPB and Druck measurements were found to be between 0.01 to 0.28 kPa and 0.1 to 0.5 kPa, respectively, varying among different calibration charts. The values of coefficient of determination and absolute mean errors of the EPB and Druck sensors used in this study are listed in Table 6-3. The Druck transducers offer a lower level of accuracy, which was in harmony with their intended application of measuring the depth of water table. However, the EPB sensors were used for obtaining SWRC which required higher level of precision. Since the EPB miniature tensiometers were obtained after the seismic centrifuge tests had been conducted, they were only employed in the experiments on hydraulic characteristics of unsaturated sand. The Druck pore pressure transducers were employed within the saturated zone to measure the depth of water table in experiments involving capillary rise approach. The data from both EPB tensiometers and Druck PPTs were recorded continuously with a sampling frequency of 10 Hz using an onboard Data Acquisition (DAQ) system.

Table 6-3. Range of R2 and error values for miniature tensiometers and pressure transducer

Sensor	**R^2**	**Absolute Mean Error (kPa)**
EPB 1	0.9899-1	0.014 - 0.28
EPB 2	0.9963-1	0.01 - 0.2
EPB 3	0.997-1	0.017 - 0.16
Druck 1	0.9724-0.9988	0.1-0.5
Druck 2	0.9754-0.9969	0.167-0.5

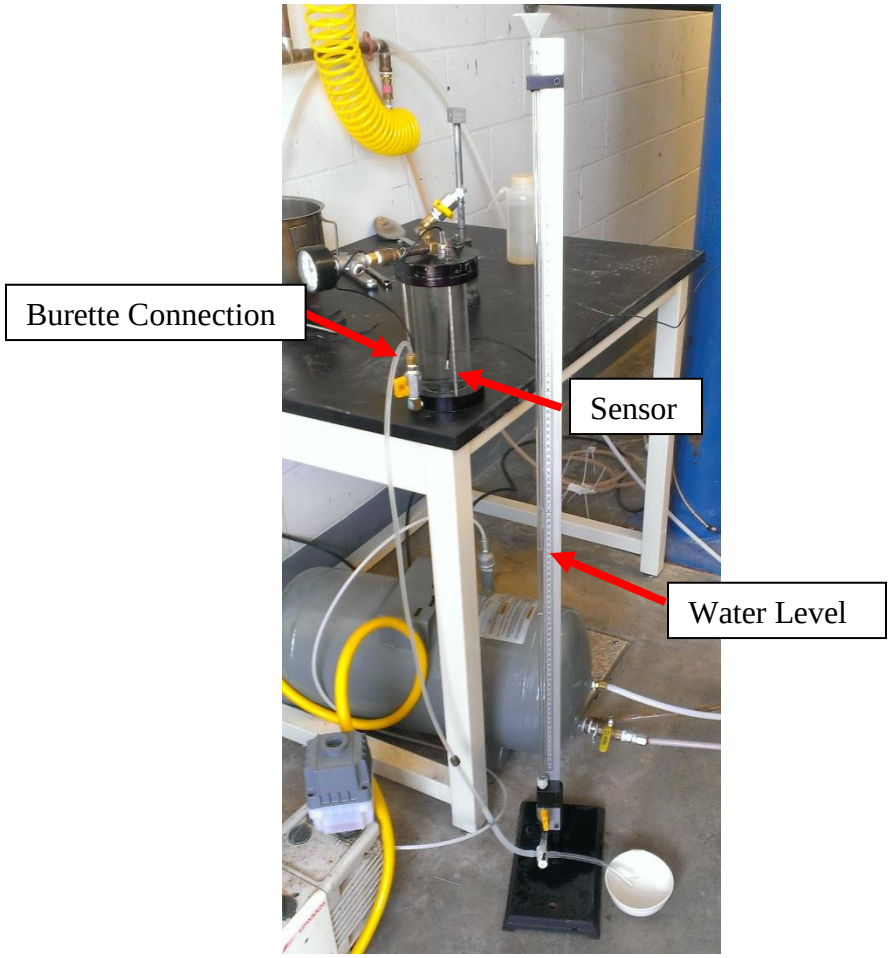

Figure 6-8. Generating Negative Water Pressure at the Diaphragm of the Sensor by Setting the Water Level in Burette Lower than the Sensor Diaphragm Elevation

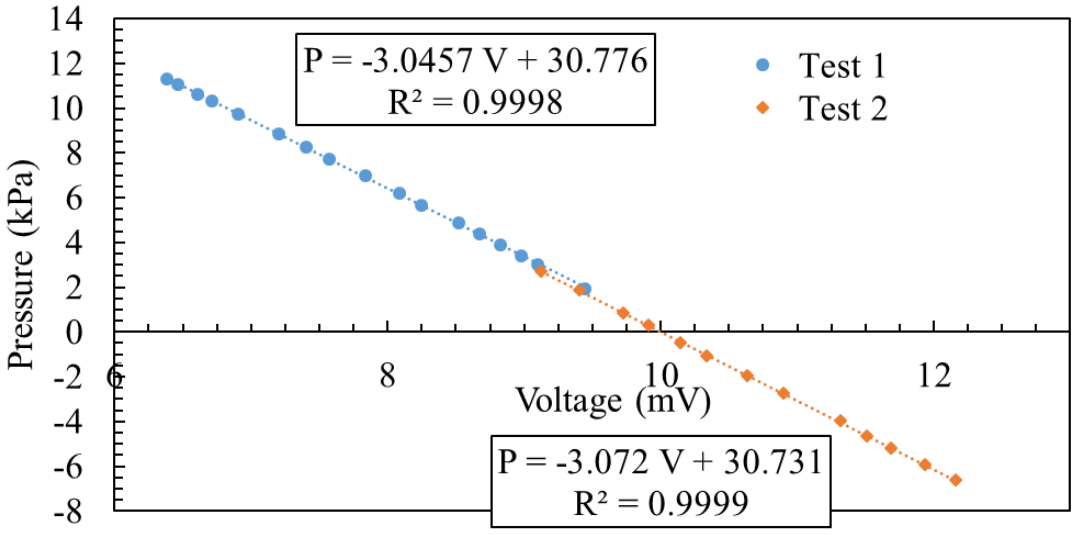

Figure 6-9. An example of a calibration graph for an EPB miniature tensiometer

6.4. Linearly Variable Deformation Transducers

LVDTs were used to measure displacements in the experimental program. The employed LVDTs included MHR 250 and MHR 500 ASSY models (from Measurement Specialties), which were capable of measuring 1.27 and 2.54 cm, respectively. In order to increase precision of the displacement measurements, each LVDT, along with its own brass core, was calibrated using a GCTS device with a resolution of 0.001 mm (Figure 6-10).

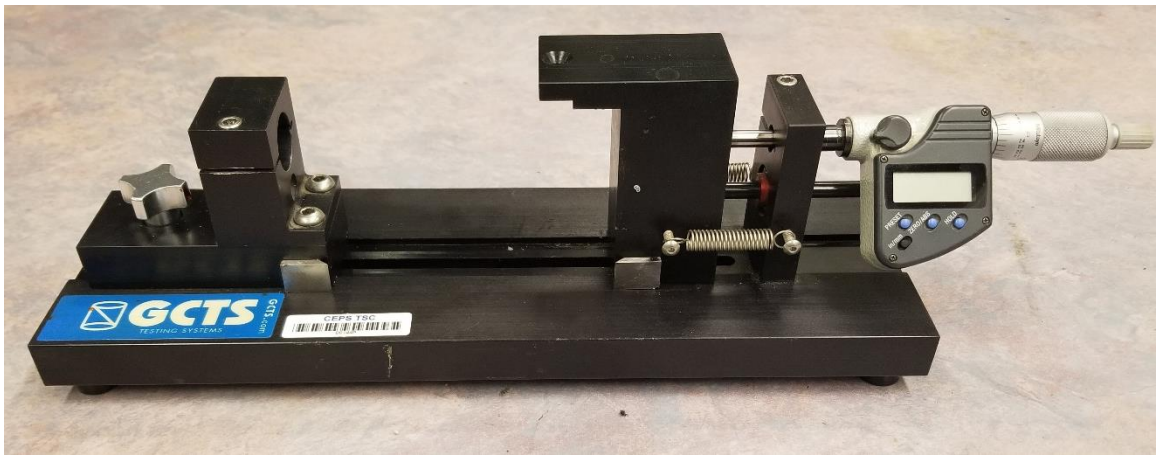

Figure 6-10. The LVDT calibration device

6.5. Accelerometers

Several quartz shear Integrated Circuit Piezoelectric (ICP) accelerometers (from PCB Piezoelectronics, Inc. of Depew, NY) were used to record acceleration time histories in seismic experiments. Since the accelerometers provide acceptable measurement accuracy they were not calibrated prior to the experiments. However, the accuracy of the accelerometer measurements was verified against double derivative of the displacement time histories obtained from Linear Positioning Sensor (LPS) of the shaking table as well as external LVDTs. Although the verifications demonstrated an accurate measurement of the accelerometers, the captured acceleration time histories were polluted with noise with an amplitude of almost +/- 0.25g.

In order to investigate the source of this noise and eliminate it, first, the performance of the accelerometers was verified in another laboratory using a NI 9234 module. The noise level of measured accelerations through NI 9234 module appeared to be significantly lower and in an acceptable range (i.e. +/- 0.01g), which demonstrated the acceptable performance of accelerometers in a different environment. Different tasks, including different LabView configurations, grounding the sensors, removing other modules from the chassis, and locating the module in different slots, were carried out to troubleshoot this issue. Accordingly, the source of the noise was found to be the power supply inside the chassis which produced high-frequency signals. Although using the current system the noise is inevitable, since the level of noise does not change in higher gravities, its amplitude will be reduced when the signal is scaled down to prototype values.

6.6. Summary and Conclusions

In this chapter, the selection of instrumentations in this study and their calibration processes were discussed. The sensors used in this study included dielectric sensors, miniature tensiometers, miniature pore water pressure transducers, accelerometers, and LVDTs. The dielectric sensors were calibrated in the same soil type and room temperature supplying water from the same tank as it was used in the target experiments. The effect of sensors' alignment (i.e. horizontal or vertical) and boundary conditions (i.e. the container size) were demonstrated to be insignificant on their measurements. The Druck pore pressure transducers were modified in this study by applying a glue to their housing perimeter to make steady suction measurements. However, the Druck sensors were not able to make steady-enough suction measurements and were only used to measure pore water pressure in the centrifuge tests. EPB miniature tensiometers were used in this

study to record continuous measurements of matric suction in higher gravities. The saturation, calibration, and measurement verification procedures for these sensors were discussed in this chapter. In addition, coefficient of determination and mean errors for the dielectric sensors, pore water pressure transducers, and miniature tensiometers were obtained from their calibration sheets and presented herein. Finally, the calibration of LVDTs and verification of accelerometer measurements were discussed. The experimental program and the results of the preliminary study on soil-water retention characteristics in higher gravities will be presented in the next chapter.

CHAPTER VII

SOIL-WATER RETENTION SCALING IN CENTRIFUGE MODELING OF UNSATURATED SANDS

7.1. Introduction

As it was discussed in Chapter 2, conversion of the scaled model results, in the experimental programs involving partially saturated soils, to their corresponding prototype values need an appropriate evaluation of model/prototype mapping of matric suction, volumetric water content, and their relation. To that end, a thorough investigation was performed to address the questions on scaling laws of unsaturated soils and high-g SWRC measurements. The results of prototype and scaled models of unsaturated sand layers were compared while simulated using two different approaches: (1) where capillary rise occurs from an identified water table during drainage experiments and (2) when water infiltrates through an unsaturated soil layer; specifically, during steady state flow. Ottawa sand was selected in harmony with the steady state infiltration procedure in this study, which also, provided long-enough capillary ascending in the tests with determined water tables. By providing continuous in-flight measurements of VWC and matric suction the scaling factor associated with capillary rise, suction, and hydrostatic water pressure

distribution in high gravitational acceleration fields are verified. In addition, the SWRC in single gravity and higher gravities are examined during both unsaturated soil modeling processes.

7.2. Experimental Programs

7.2.1. Sample Preparation

The sand was dry pluviated to obtain loose specimens with an approximate relative density of 45% reaching the final height of 22.9 cm in model scale for all the tests. A gravel layer with a thickness of 1.3 cm was placed at the bottom of the container to generate a saturated boundary condition in steady state infiltration tests, which was separated from the drainage plate and overlying sand using two layers of fabric filter. The fabric layer and placement of gravel layer are shown in Figure 7-1 (a) and (b), respectively. The gravel layer was, also, used in capillary tests to prevent local sand-washing during the saturation process.

During the sand pluviation, the sensors were located at different depths of the specimen depending on the system layout in different tests. Schematics of the layout of the employed instrumentations in tests following capillary rise and infiltration approaches are shown in Figure 7-2 (a) and (b), respectively.

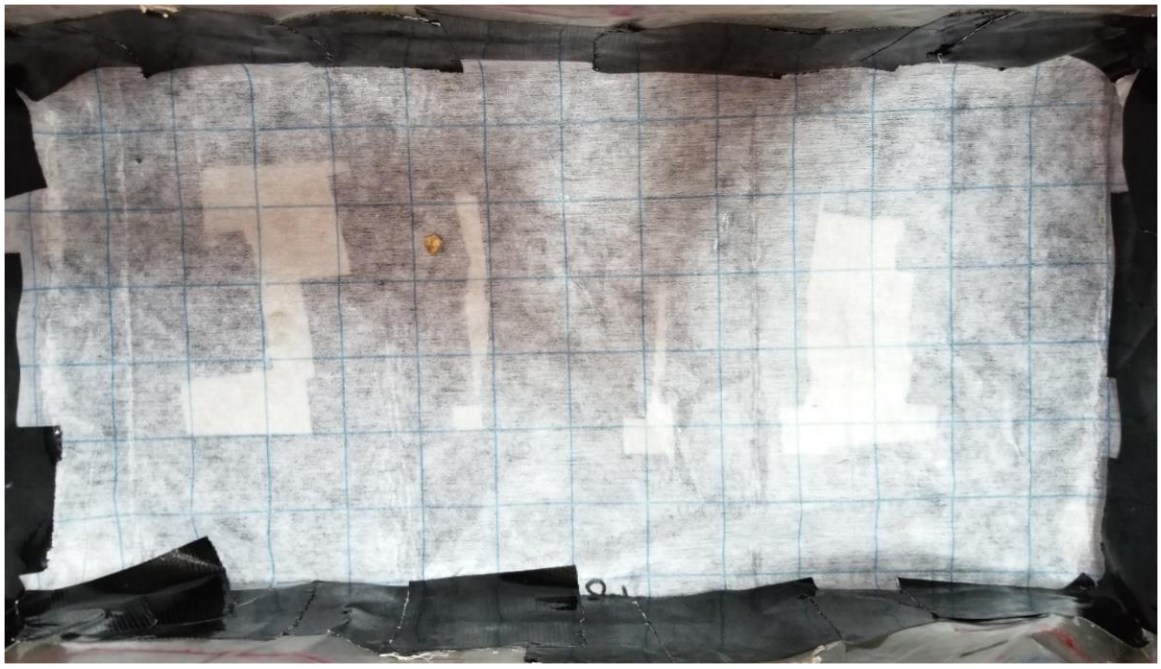

(a)

(b)

Figure 7-1. (a) Fabric layer between the gravel layer and drainage plate (b) leveling the gravel layer

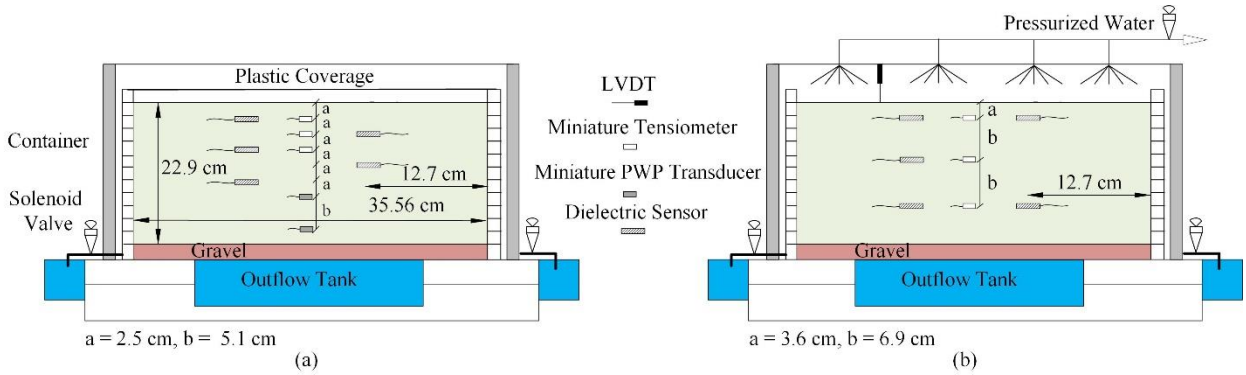

Figure 7-2. The deployed instrumentations in (a) Capillary rise tests and (b) Steady state infiltration tests

Upon placing the pore pressure transducers and miniature tensiometers on soil layer, the soil around sensors were locally wetted to avoid desaturation of the sensors prior to saturating the specimen. Dry pluviation of sand and locating dielectric sensors as well as miniature tensiometers/pore pressure transducers are shown in Figure 7-3 and Figure 7-4, respectively.

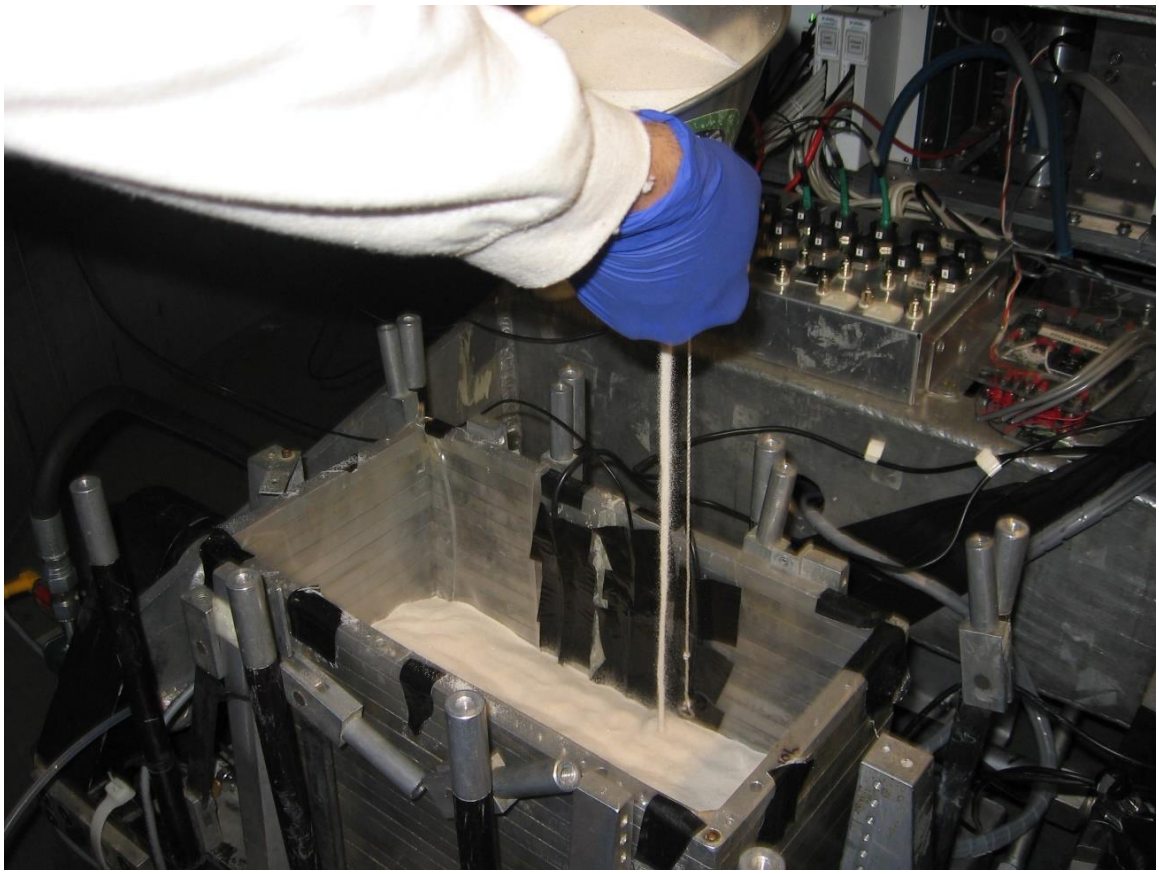

Figure 7-3. Dry pluviation of the specimen

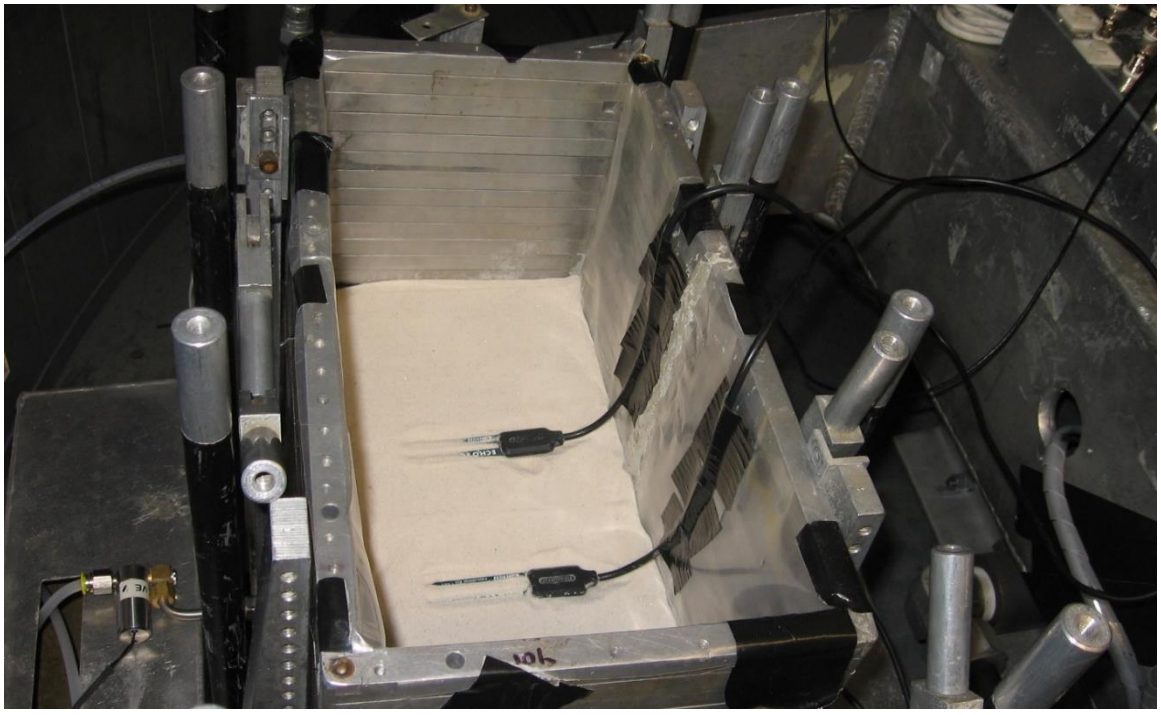

(a)

(b)

Figure 7-4. (a) Locating dielectric sensors (b) local wetting of the sand around miniature tensiometers

Upon completion of the pluviation and instrumentation, the specimen was saturated from the bottom by passing water through the drainage ports on the base plate until no air bubble was appeared on the surface and a thin film of water formed above the sand layer. The saturation

setup and a fully-instrumented and saturated specimen are shown in Figure 7-5 and Figure 7-6, respectively. Then, the specimen was spun up to the target g-level measured at the middle of the soil layer. The geostatic stress in high gravity would ensure full saturation by dissolving possibly-trapped small air bubbles. Hydrostatic water pressure measurements from PPTs and EPBs confirmed the saturation success.

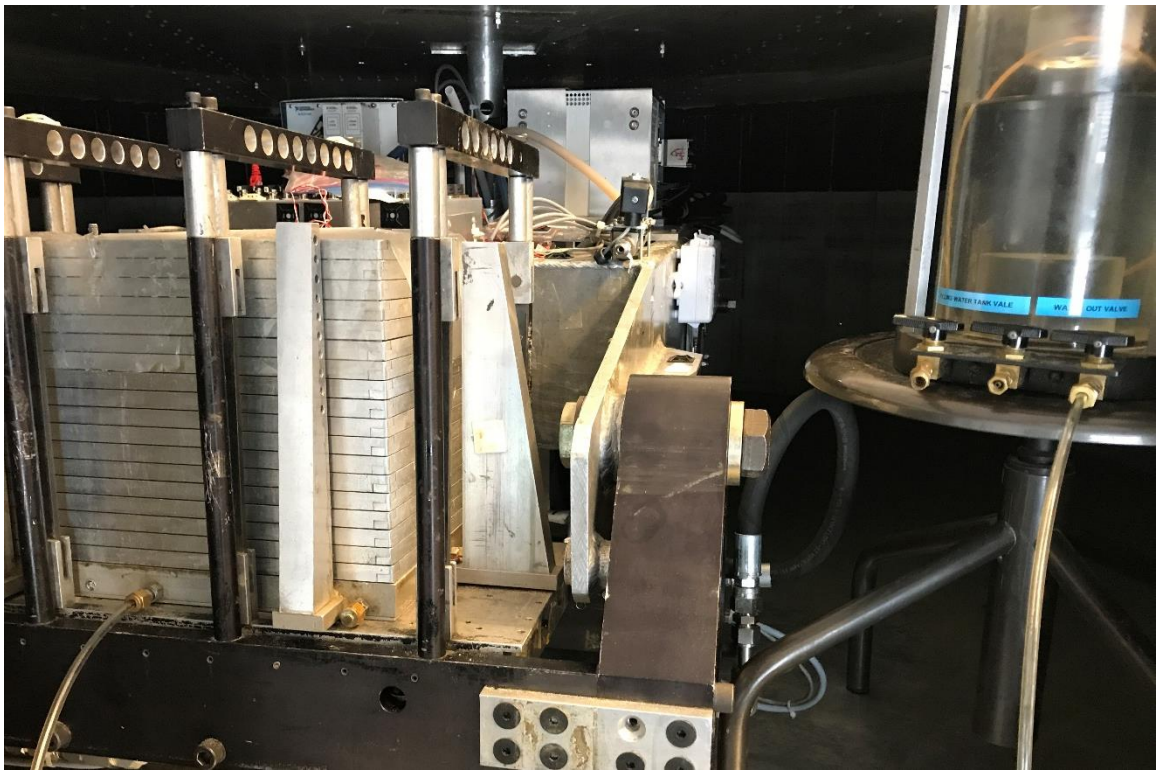

Figure 7-5. The saturation setup

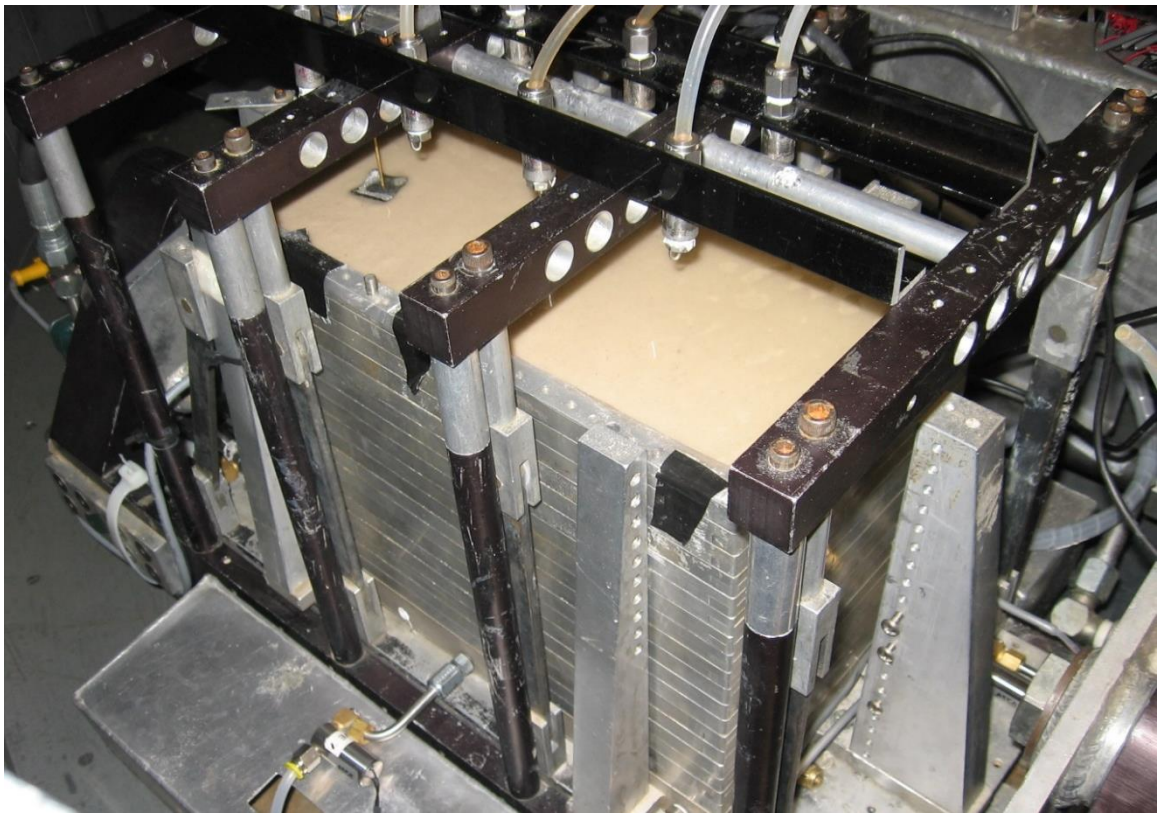

(a)

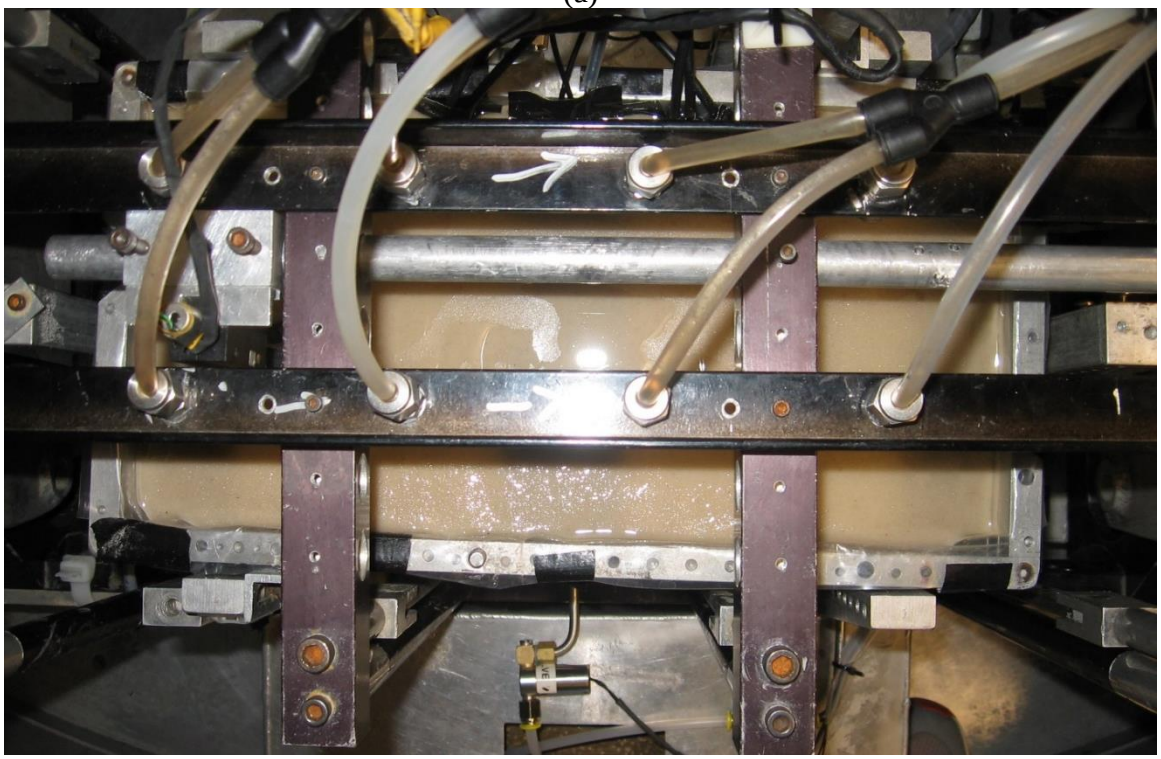

(b)

Figure 7-6. A saturated specimen (a) side view (b) top view

7.2.2. Capillary Rise Tests

In order to study the capillary rise modeling, associated scaling laws, and in-flight SWRC measurements, water level in the soil layer was lowered gradually from the soil surface in different g-levels (i.e. 5, 10, 15, 20, 30, and 40 g) using a miniature outflow solenoid valve. The specimen was spun up to 50 g prior to reaching the target g-level in each test, so that potential sand packing due to centrifugation would occur in advance, minimizing the change in relative density among different tests. The experiment started at 40 g where the water level was lowered gradually. VWC and matric suction were continuously monitored at each step until no further change was observed for at least 3 minutes, significantly longer the combined time required for water level stabilization and equilibration of sensors' measurements; i.e. less than 20 s. The pore water pressure/matric suction data from EPB and Druck measurements after a water level variation at 40g are shown in Figure 7-7 where the equilibration period could be observed as almost 20 s. After the drying steps for the test at 40g were finished, the centrifuge was stopped, and the specimen was re-saturated. Thereafter, the test at 30 g was conducted and the same procedure was repeated until the test at the last g-level (i.e. 5 g). Schematics of the expected hydrostatic pressure/suction and degree of saturation profiles during tests at each g-level are shown in Figure 7-8 (a) and (b), respectively.

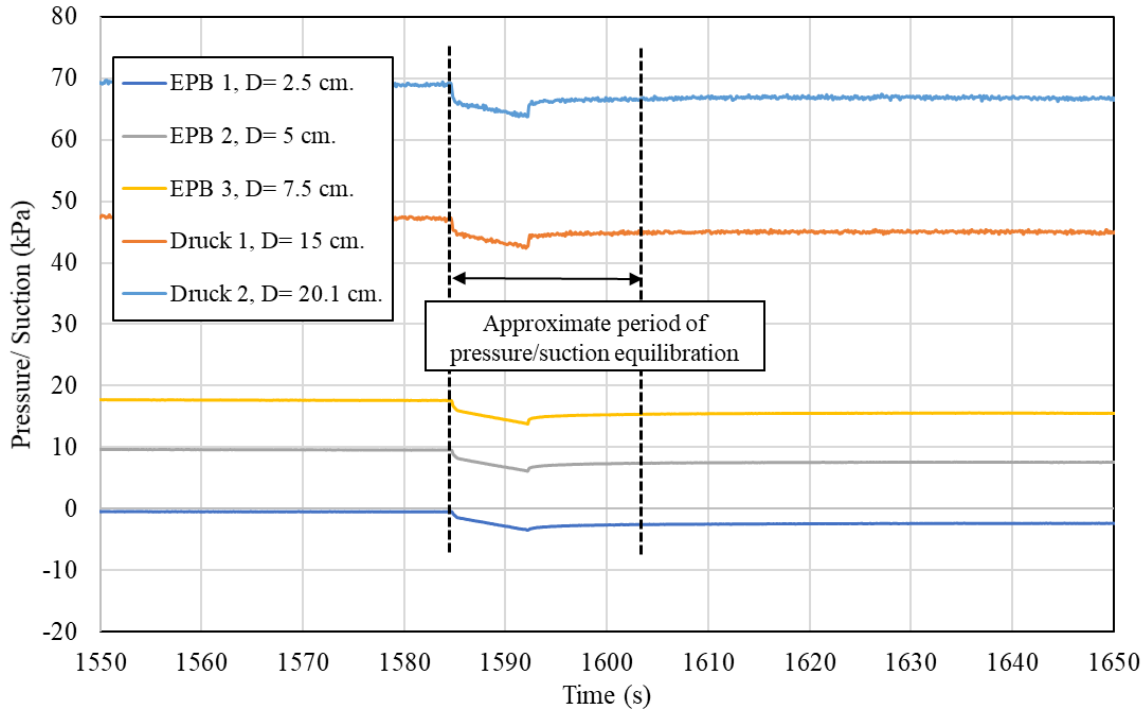

Figure 7-7. Pressure/suction equilibration after water level variation during the capillary rise experiment at 40g

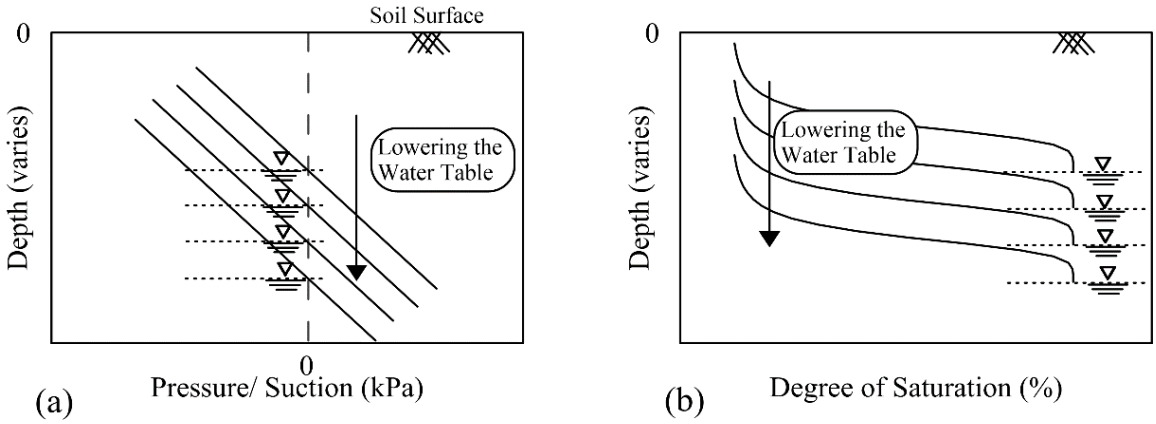

Figure 7-8. Schematic of variations in (a) hydrostatic pressure/suction and (b) degree of saturation profiles during capillary tests at each g-level

During the capillary experiments, the container was covered with a plastic sheet appropriately prior to each test so that no significant evaporation occurred. Albeit no settlement was recorded during this test, according to the pilot tests and similar experiments a negligible settlement would occur due to the saturation and spin up of a loose sand specimen leading to a minimal change in

relative density of the specimen. The moisture probes were located relatively close to each other in capillary tests to better capture VWC profiles in higher g-levels. Since the moisture probes were heavier than other sensors (i.e. mass of 20 grams for each EC-5 dielectric sensor), they were not positioned in a vertical array to distribute the load and avoid adverse effects of sensors' self-weights in high-g.

According to the Decagon sensor manuals, the influence zones of EC-5 and 5TM dielectric sensors are 25 mm and 50 mm, respectively. The distance between moisture probes in a vertical array was 5 cm or more during both capillary rise tests as well as steady state infiltration experiments (Figure 7-2). In addition to EC-5 sensors, only one 5TM sensor was located as the bottommost sensor in the capillary experiments. Therefore, neither EC-5 nor 5TM sensors were located inside the influence zone of the other sensors, as per the manual's recommendation. However, the influence zones of the 5TM sensor and the EC-5 sensor above it were overlapping in the capillary tests. In order to study the extent of this possible influence, an additional pilot test in a container was performed where an EC-5 sensor and the 5TM sensor were injected 5 cm apart each other inside wet-compacted soil. Then, the readings were compared when the adjacent sensor was plugged to the data logger (overlapping the influence zones) or unplugged (vice versa), which showed a 2% difference in terms of VWC. This percentage is negligible comparing to the accuracy of EC-5 or 5TM sensors (2% and 3%, respectively) as per Decagon's manuals or those absolute mean errors obtained in this study (Table 6-2). The EPB miniature tensiometers were deployed at the same level with the top three moisture probes so that SWRC would be obtained at those levels. The Druck PPTs were placed in saturated zone to identify the water level in each step.

7.2.3. Steady State Infiltration Tests

During the steady state infiltration tests, the degree of saturation was controlled by varying the discharge velocity as well as g-level. Experiments with various discharge velocities were conducted during which the specimen experienced drying and wetting successively. The tests were performed under a total number of 7 discharges (D1 to D7) with D1 and D7 indicating the lowest and highest discharges, respectively. The applied discharge in each test was changed by either varying the opening of needle valve or using a different set of nozzles. 1/8 PJ10, 1/8 PJ20, and 1/8 PJ40 nozzles (from BETE brand) were deployed to apply different discharges in the D1 and D2, D3 to D6, and D7 experiments, respectively. In each test, the initially saturated specimen was spun up to 50 g and the water infiltration was applied until a steady state condition with a relatively uniform degree of saturation profile was achieved. Upon reaching a steady state condition at 50 g, while the spraying continued, the g-level was changed. Then, the steady state was again achieved for g-levels of 40, 30, 20, 10, and 5, consecutively. The steady state condition was verified by monitoring the VWC and matric suction until constant measurements were reached for at least 3 minutes where longer time span was needed to reach equilibrium as the g-level decreased. Following this procedure, the VWC-suction data points shifted along the drying path in steady state condition at 50 g, which then was rewetted along hysteresis paths as the g-level decreased (as schematically shown in Figure 7-9, a). During the D7 experiment, the drainage valve stopped functioning at 20 g followed by an increase in the degree of saturation, especially in the lower portion of the specimen. The valve was fixed after the centrifuge was stopped, and the test was continued starting from 20 g. The alterations of average VWC, in three instrumented locations, at different g-levels and under each discharge are shown in Figure 7-9 (b).

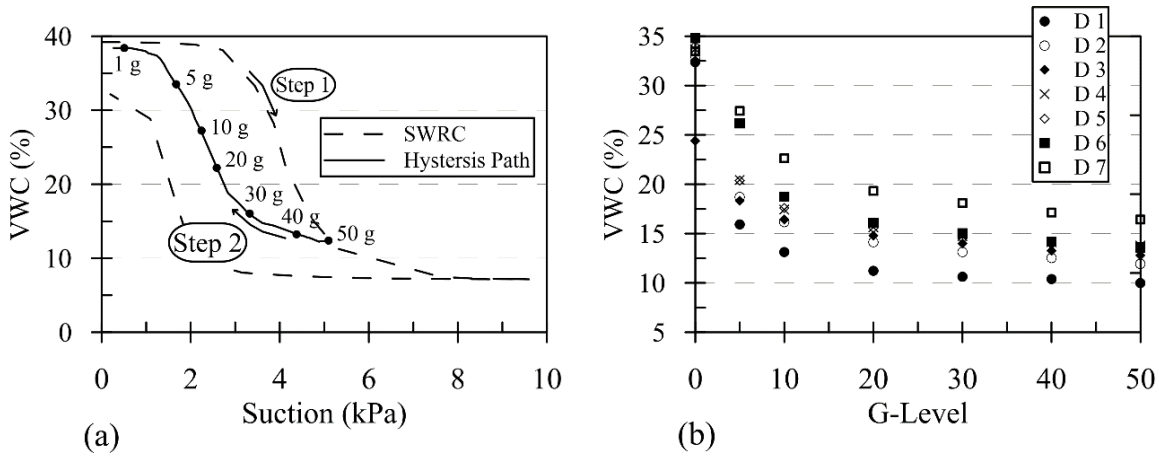

Figure 7-9. (a) The experienced water retention path during each infiltration test (b) VWC variations during tests with different discharge velocities

7.3. Results and Discussions

7.3.1. Capillary rise tests

The capillary rise tests were performed in six g-levels where at each level the depth of water table was lowered in a sequence (ranging from 9 to 22 interval steps in different tests). In order to verify the performance of Druck PPTs and EPB miniature tensiometers, the data from the initial spin up of the saturated specimen were collected, shown in Figure 7-10 in prototype scale. The slope of hydrostatic pressure is nearly equal to the unit weight of water for all the g-levels, demonstrating an accurate performance of the sensors. The slight variation of the slope from the unit weight of water was similarly reported by (Allmond and Wilson 2012) where they used pore water pressure transducers of several brands. This difference could be a result of a small error (with the extent of few millimeters) in locating the sensors at specified heights. In addition, the intercepts of the lines slightly shifted down as the g-level increased which was due to the permeation of the extra film of water atop the specimen (with the approximate height of 3 mm) into the soil as the g-level increased.

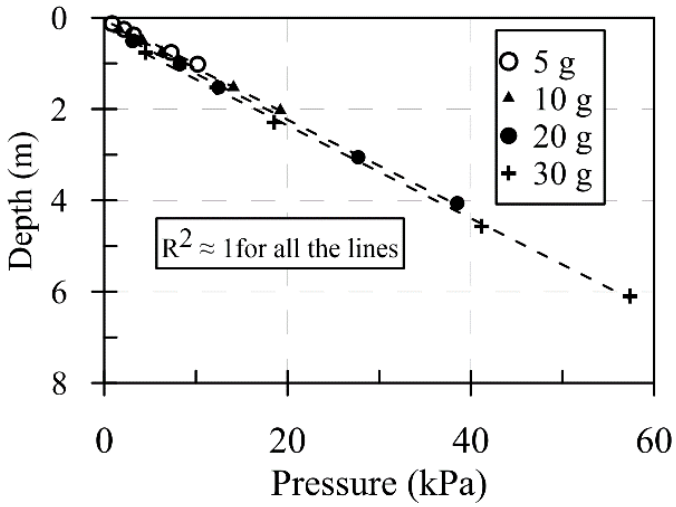

Figure 7-10. Hydrostatic pressure during the initial spin up in capillary rise tests

The measured time histories of VWC and pore water pressure/suction alongside the recorded temperature during the test in 40 g are shown in Figure 7-11. When interpreting the time series, it should be noted that the two bottommost dielectric sensors were not located at the same level with the Druck PPTs. The Druck PPTs were intentionally kept saturated during the tests while all the dielectric sensors experienced the unsaturated condition to have a better resolution of the capillary ascending in different tests. Since the data from the EPB and Druck sensors were automatically recorded through the DAQ, they started from the beginning of each test while the VWC data were monitored at the desired times and, hence, did not start from the time zero. It is, also, noticeable that the measurements of EPB miniature tensiometers were capped at suction levels around 7 to 15 kPa depending on the g-level and position of the instrumentations. This might have happened because of the specific shape of water menisci in the porous stone/sand interface region in degrees of saturation near the residual water content. The VWC data did not start from the same saturated value at the beginning of the test due to the previously mentioned insufficient accuracy of the dielectric sensors in saturated conditions. To avoid the

misinterpretation of the results, the VWC was converted to degree of saturation by dividing all the recorded value of each sensor by its own saturated VWC.

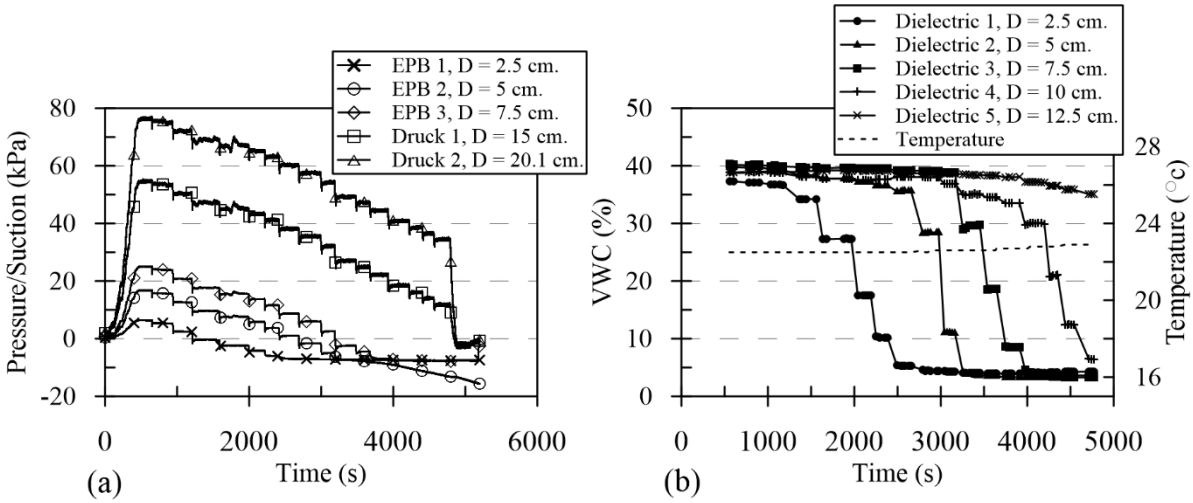

Figure 7-11. Time histories of (a) pore water pressure/suction and (b) volumetric water content during the 40-g capillary test

The hydrostatic pressure/suction as well as the degree of saturation profiles for four water table heights in each experiment (g-level), all converted to prototype scale, are shown in Figure 7-12 (a) and (b), respectively. The measured matric suctions followed hydrostatic linear profiles for the suction levels lower than corresponding values of residual water content (i.e. around 7 to 15 kPa as mentioned earlier). The depth of water level, at each step, was identified using the obtained water pressure distribution from the Druck PPTs. Then, degree of saturation profiles with curves similar to the SWRC proposed by van Genuchten (1980) were fitted to the data sets in depth starting from the acquired water table level; shown in Figure 7-12 (b). The capillary fringe heights in each case (i.e. each g-level and water level) were obtained as the capillary ascending associated with the air entry value, shown in Figure 7-13.

A practically close match, with the coefficient of determination (R^2) of 0.965, was observed between the curve representing 1/N scaling factor and the obtained data points. The slight

inconsistency between the estimated values and the expected curve might be associated with the capillary finger phenomenon (Lu and Likos 2004) as well as the dielectric sensors performance. The dielectric sensors provide measurements with a slight, yet not negligible, error; the extent of which was discussed earlier. According to the capillary finger concept (Lu and Likos 2004), capillary ascending does not occur uniformly in real cases where unsaturated soil can be conceptualized as "bundled tubes". Therefore, it is possible that water ascended in different paths especially in some interval depths, which might be averagely represented by SWRC with an acceptable precision. Furthermore, although the dielectric sensors were located relatively close to capture a high-resolution VWC profile, the majority of data points in higher g-levels (i.e. 30 and 40 g) fall on regions of SWRC with either saturated or residual water content. This provides less data points to fit to the van Genuchten curve leading to relatively less accurate estimations of capillary ascending in higher g-levels. It should be noted that van Genuchten curves, measured from 1-g tensiometeric technique experiments, also matched closely with almost all the recorded data showing the validity of 1/N as the scaling factor of capillary rise and capillary fringe heights. For instance, the degree of saturation profiles for the drying experiment at 15 g alongside the 1-g SWRCs starting from the acquired water table are illustrated in Figure 7-14.

The relationship between the degree of saturation and matric suction in higher gravitational fields was examined through the SWRC in each g-level. Three SWRCs were obtained (each at the locations of EPB miniature tensiometers shown in Figure 7-2, a) at each g-level, which are illustrated in Figure 7-12 (c). The cap in the measurements of EPB tensiometers in higher suction values was observed in the SWRCs where the suction readings did not increase after reaching a certain limit. The values of the degree of saturation, measured using the top sensors, prior the air

entry were less than 100% in lower g-levels. This was due to the re-saturation of an unsaturated soil in new g-levels that led to the air-entrapment in top portion of the specimen. The experimental program was initiated with the test at 40 g and the g-level was reduced to 5 g as the tests continued. Therefore, the initial degree of saturation for the top sensor shifted away from fully saturated condition as the g-level decreased because of the hysteresis effect.

The SWRCs for all the g-levels were obtained at depths of 2.5 (top), 5.1 (middle), and 7.6 cm (bottom) in the model and are shown in Figure 7-15 (a), (b), and (c), respectively. van Genuchten (1980) SWRC model was fitted to the obtained data points at each location using the least-squares regression method. The variations of data from the fitted van Genuchten curves can be estimated from the values of absolute mean error, which were 8.8, 3.3, and 3.9% in terms of degree of saturation for the measurements at depths of 2.5, 5.1, and 7.6 cm, respectively. The higher variation of the data obtained from the top sensors is an indicative of the hysteresis effects at the top of the specimen, for the latter tests with lower g-levels. The mean errors at the other two locations were only slightly higher than the error of deployed moisture probes. The lower and upper bounds of van Genuchten curves, shown in Figure 7-15, were obtained as curves with a distance of absolute mean error from the main curve.

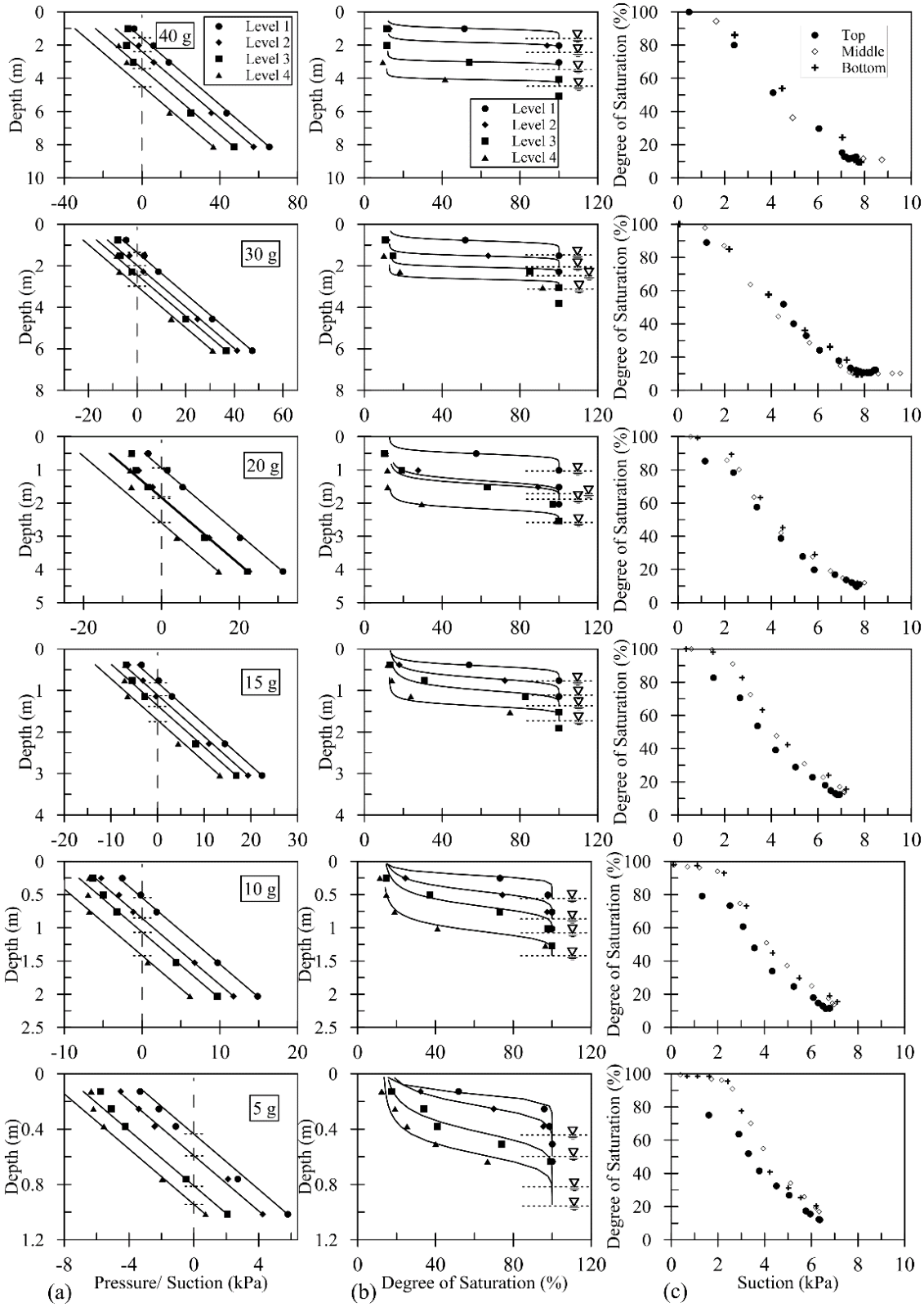

Figure 7-12. Profiles of (a) pore water pressure/suction and (b) degree of saturation as well as (c) obtained SWRCs at the different heights during the capillary rise tests

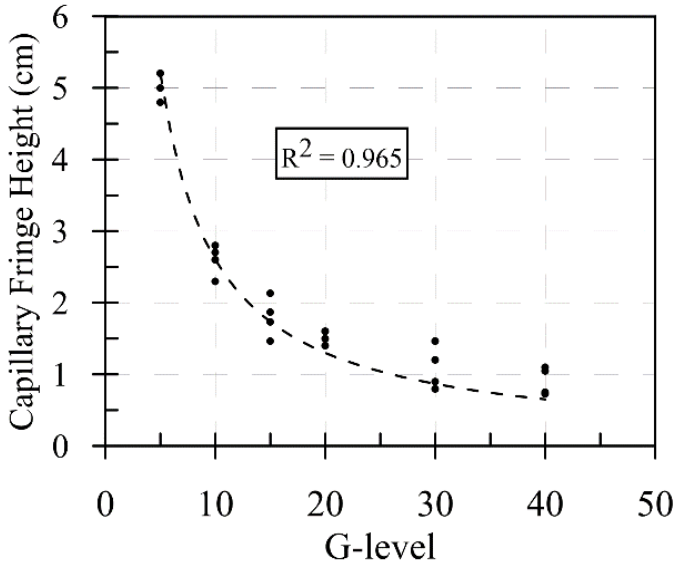

Figure 7-13. Capillary fringe height in model scale for tests under different g-levels

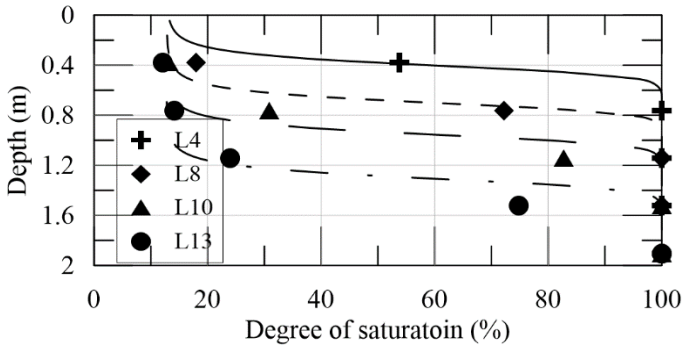

Figure 7-14. Degree of saturation profiles obtained in drying experiment at 15 g alongside 1-g SWRC curves for each water table

Only a slight change occurred in the residual degree of saturation and the slope of the SWRC among the g-levels. However, the air entry value slightly varied among different tests (between 1.8 and 2.4 kPa); i.e. decreasing as the g-level increased. This might have occurred since the tests with higher g-levels had been conducted at the beginning of experimental program and the relative density of sand had increased slightly as the tests continued due to the self-weight effect in several spin ups and downs of the centrifuge. The change in density, however, was kept minimal by spinning the centrifuge up to 50 g prior to the beginning of the experiments. The

higher relative density, in turn, led to a slight increase in air entry value in tests with lower g-levels.

Based on the available data set from hanging column and axis translation tests, as discussed previously, a 1-g SWRC band was proposed for comparison in Figure 7-15. Although the 1-g and high-g SWRCs demonstrated a good agreement, the air entry value and slope of high-g SWRCs were different from the 1-g band leading to lower degrees of saturation for the interval values. The variations of both air entry value and slope of SWRCs from the 1-g measurements were partly due to small hysteresis that occurred at the beginning of each sequence of lowering water table. According to Figure 7-11, when water level was lowered spikes can be distinguished in pore water pressure or matric suction after which matric suction abruptly reached the equilibrium. However, since the data from moisture probes were monitored less frequently, these peaks were not reflected in the VWC time histories. The abrupt changes of VWC and matric suction at the beginning of each sequence led to small hysteresis effects that accumulated as the test, at each g-level, proceeded. The accumulated hysteresis effects for the test at 15 g are shown in Figure 7-16. These small hysteresis loops, in turn, led the unsaturated sand to take paths in θ-ψ coordinate with slightly different air entry value and slope in high-g. In addition, albeit the possible influence of g-level on the shape of water menisci (Schubert 1982) was hard to be tracked in an experimental study, this phenomenon could have an impact on the final SWRC as well as capillary ascending in higher gravities.

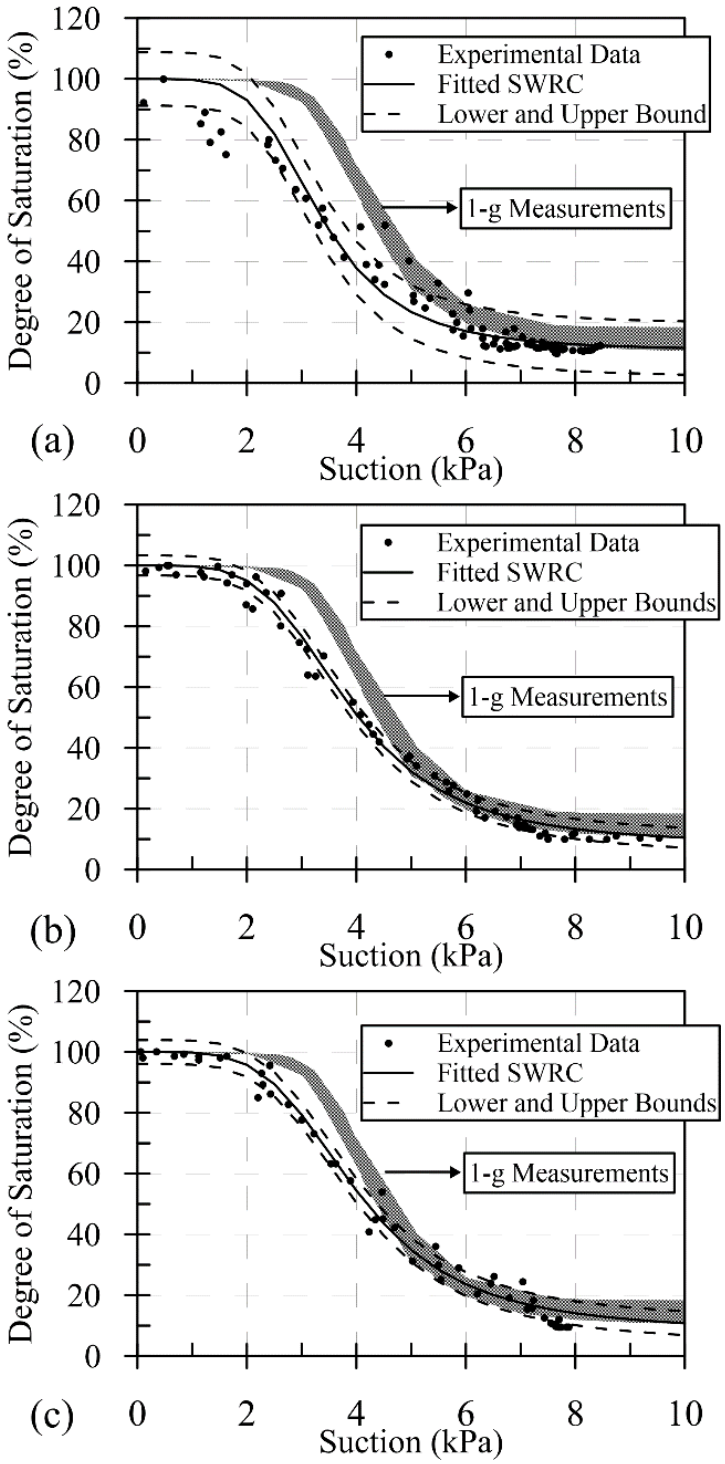

Figure 7-15. SWRCs obtained in six g-levels at three (a) top (D = 2.5 cm) (b) middle (D = 5 cm) and (c) bottom (D = 7.5 cm) instrumented locations of the specimen

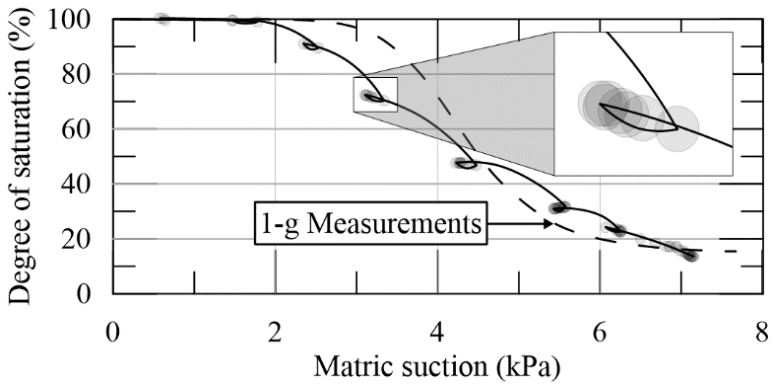

Figure 7-16. Small hysteresis effects accumulated during the experiment at 15 g

7.3.2. Steady state infiltration tests

The tests consisted of a drying stage where the steady state condition was initially obtained at 50g from the saturated state, and a wetting stage where the g-level was lowered with a constant discharge and the VWC increased as the g-level decreased. Therefore, the matric suction-VWC graph for each test started from a data point on the drying path of the SWRC and continued along a scanning hysteresis path.

The steady state infiltration tests were carried out using seven spraying discharges, and during each test, the steady state condition was obtained in 7 g-levels (i.e. 50, 40, 30, 20, 10, 5, and 1). The time histories of VWC and pore water pressure/matric suction during D1 test, with g-level varying from 50g to 1g, at the bottommost instrumented location are illustrated in Figure 7-17 (a) and (b), respectively. The time histories consist of two major parts of centrifuge spin up and steady state infiltration establishment at the target g-level. In order to highlight the changes of monitored parameters under different discharges in one experiment, the variations of matric suction and VWC at different instrumented locations, during the periods with established steady state condition in D1 experiment are illustrated in Figure 7-18 (a) and (b), respectively. The time

histories initiated from the time of 1000 s after the test was started, which is slightly after the beginning of infiltration in 50 g.

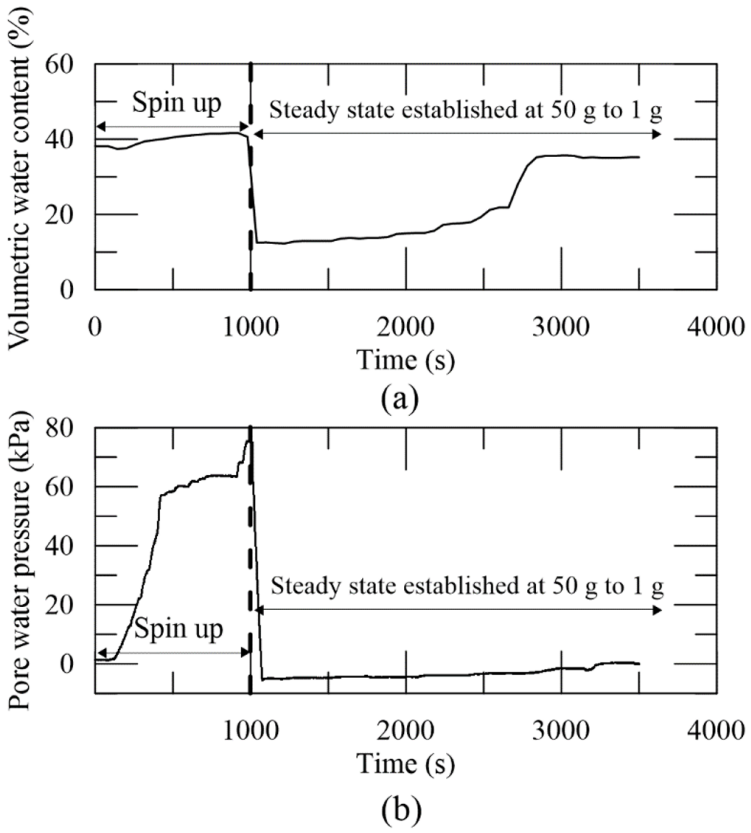

Figure 7-17. Sample time histories during steady state infiltration experiments for (a) VWC and (b) Pore water pressure/suction

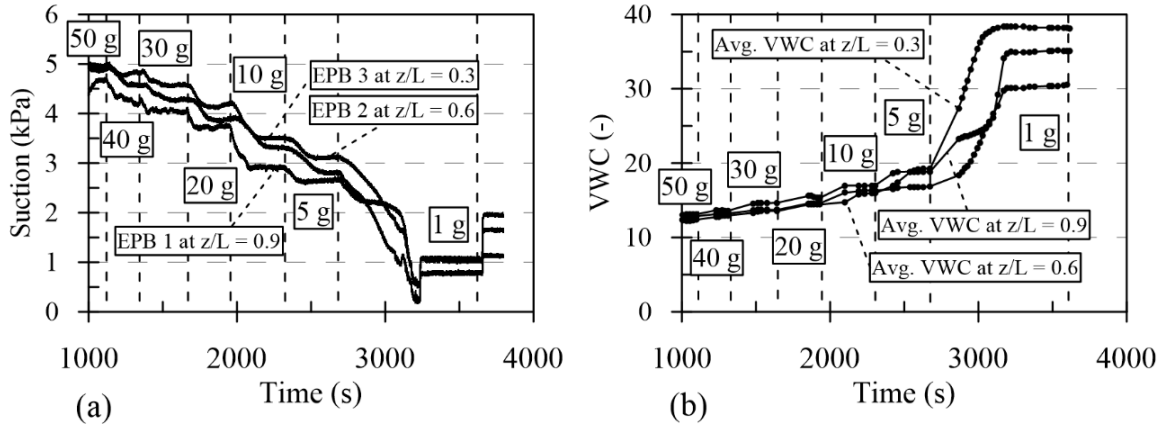

Figure 7-18. Variations of (a) matric suction and (b) volumetric water content during the steady state infiltration experiment, D1

The achieved matric suction and degree of saturation profiles at steady state condition under different discharges and g-levels are shown in Figure 7-19 (a) and (b), respectively. The steady state condition, initially, was established at 50 g for all the tests, which corresponds to the lowest degree of saturation (highest matric suction) and as the test proceeded to lower g-levels, degree of saturation increased. The tests with lowest and highest discharge velocities (i.e. D1 and D7, respectively) encountered the highest uncertainty, which was due to the performance of nozzles in very high or low discharges. Moreover, for very low discharges of water, the air turbulence on top of the specimen might have influenced the spraying pattern resulting in a less-uniform degree of saturation profile.

The obtained SWRCs at the instrumented locations under each discharge are shown in Figure 7-19 (c). The continuous measurement of VWC and matric suction allowed data acquisition even before reaching the steady state at g-level; shown in Figure 7-19 (c) in grey color. Although these data cannot be referred as the values of VWC or matric suction in steady state condition, they might be used to show the transition paths. They reasonably matched with the steady state condition results and could be used for the illustration purposes in the SWRC curves. The tests consisted of a drying stage where the steady state condition was initially obtained at 50 g from the saturated state, and a wetting stage where the g-level was lowered with a constant discharge and the VWC increased as the g-level decreased. Therefore, the matric suction-VWC graph for each test started from a data point on the drying path of the SWRC and continued along a scanning hysteresis path. It should be noted that since the discharge rates were different in the experiments, the starting point was not the same for all the discharges. However, as discharge variations had a relatively low impact on the degree of saturation in 50 g, the difference in VWC

and matric suction of the starting points was not significant except for D1 and D7 with the lowest and highest discharges, respectively. The scatter in the results of D7 test was partly due to the increase in the degree of saturation at 20 g, which occurred as the drainage valve stopped functioning. As the degree of saturation increased, the specimen underwent an additional hysteresis leading to a higher scatter in the results.

In order to evaluate the influence of g-level on the SWRC, the average values of measured VWC and matric suction in three depths, under established steady state infiltration, are illustrated at each g-level (Figure 7-20). The results from the D7 test with g-level lower than 20 were removed in this graph as they had experienced an extra hysteresis. The change in the g-level led to a more significant variation in terms of degree of saturation than altering the discharge, which was similarly reported in McCartney and Zornberg (2010). Therefore, it was practically impossible to capture a complete hysteresis path for each g-level by varying the discharge velocity and only a portion of the SWRC was obtained for each g-level. The coherence between the obtained SWRCs at each g-level clearly demonstrated that the g-level did not influence the SWRC of sand. The observed scatter in the results was mainly due to the fact that the tests did not start from the same point on the drying curve of the SWRC.

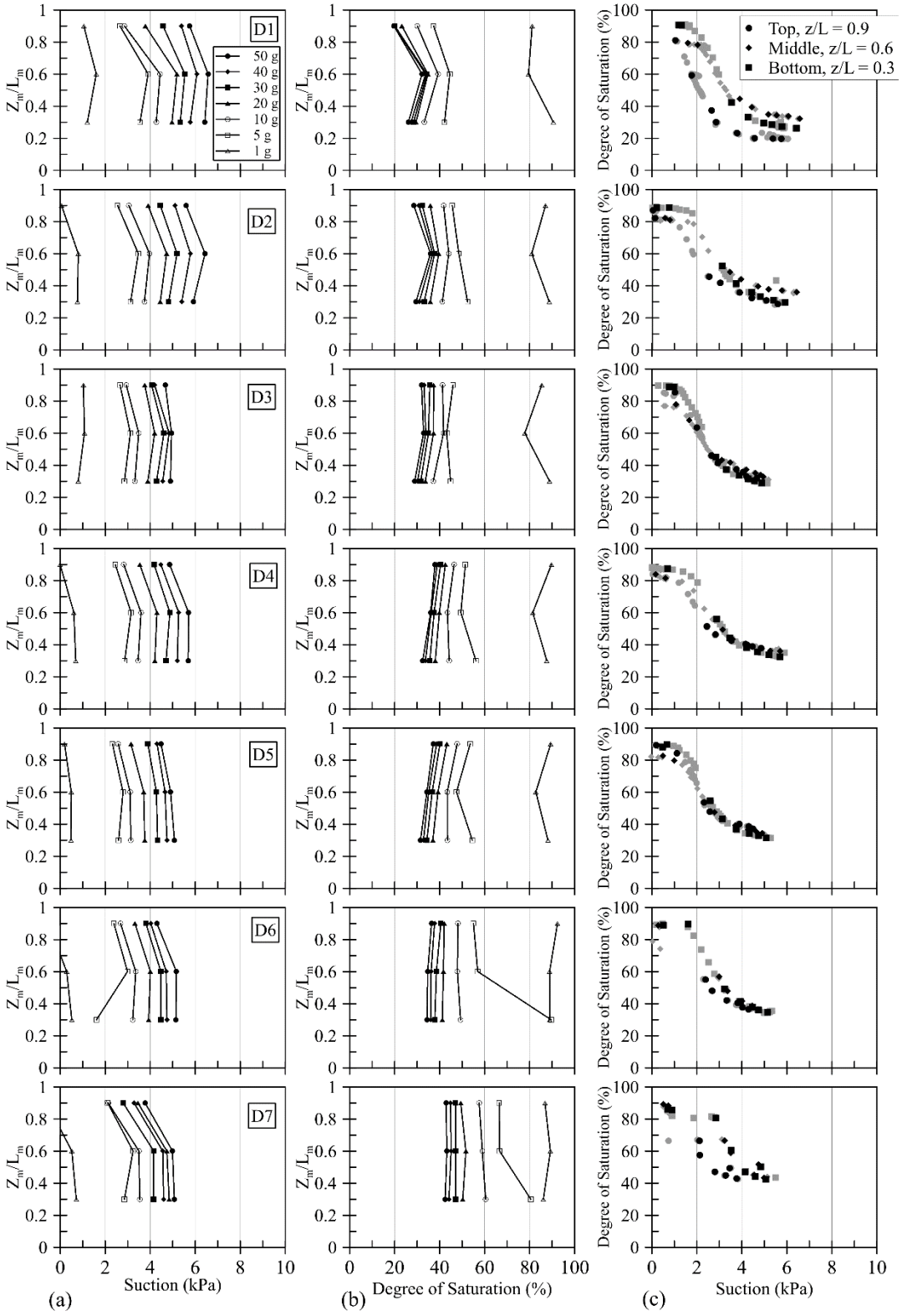

Figure 7-19. The achieved profiles of (a) matric suction and (b) volumetric water content versus normalized depth (Z_m/L_m) as well as (c) SWRCs during steady state infiltration experiments under different discharges (the grey color indicates the data before equilibrium)

In order to evaluate the high-g SWRCs under steady state infiltration, the SWRC at 1 g along a hysteresis path is plotted. The 1-g SWRC test started from the saturated state and moved along the drying path until reaching to a VWC similar to the VWC values at 50 g during the infiltration tests. Thereafter, the specimen was rewetted to obtain a scanning path starting approximately from the same point as of those in high-g tests. In addition to this scanning curve, the measured SWRC drying band is shown in Figure 7-20. The adequacy of the centrifuge results is verified by the good agreement between the high-g and 1-g measured SWRCs especially in higher ranges of matric suction. For the lower matric suctions, the change in the initial point of hysteresis curve led to a higher difference in terms of degree of saturation.

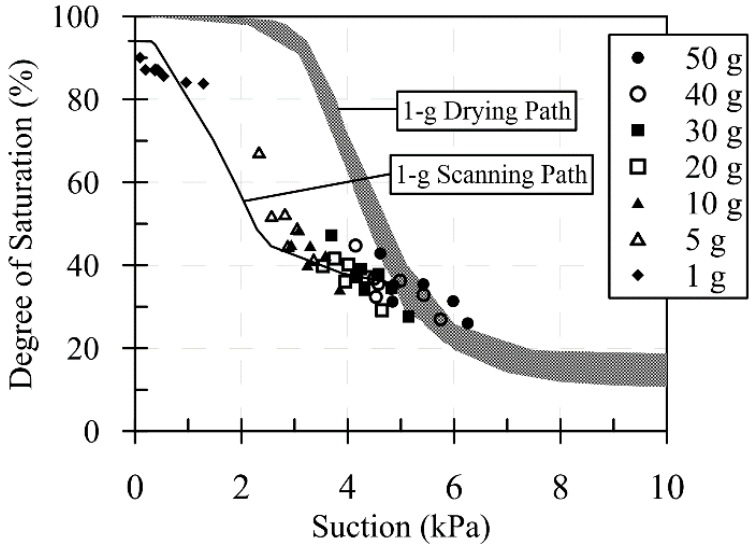

Figure 7-20. Average degree of saturation-suction variations throughout the specimen at steady state conditions in different g-levels

7.4. Summary and Conclusions

The experimental program and the results of centrifuge tests following drying as well as steady state infiltration procedures were presented in this chapter. The drying experiments were performed in six different g-levels (i.e. 5, 10, 15, 20, 30, and 40 g), where in each g-level water

level was lowered gradually and the corresponding matric suction and VWC were measured at different instrumented locations in the specimen. The infiltration tests were carried out with seven different discharges, and under each discharge, g-level was consecutively lowered from 50 to 5 g. As a result, profiles of volumetric water content and matric suction were obtained for different discharge velocities and in various g-levels. Further, the high-g SWRC in infiltration tests, averaged from the measurements in three instrumented locations, was obtained.

The comparisons between the SWRCs measured at 1 g and higher gravities as well as hydrostatic variation of pore water pressure in higher gravities demonstrated the successful measurements of different sensors (i.e. miniature tensiometers and dielectric sensors) in centrifugal fields. The capillary fringe ascending, in different g-levels, was determined as the height corresponding to the air entry value in SWRCs obtained from the measurements of dielectric sensors. The results demonstrated the g-level independency of the SWRC, and also validated the length scaling factor of 1/N to be used for capillary ascending scaling. Small hysteresis effects were observed when water table was lowered gradually at each g-level, which resulted in a small divergence between the high-g and 1-g measured SWRCs.

The steady state infiltration tests comprised of tests under several discharges where in each experiment the steady state condition was established in different g-levels. A significant hysteresis was observed during the infiltration tests under each discharge velocity when the steady state infiltration was established while lowering the g-level. An average SWRC, along the mentioned hysteresis path, was obtained from θ-ψ measurements in different g-levels and under different discharges. A good agreement was observed between the SWRC measured during high-g steady state infiltration and that obtained using tensiometeric technique in 1-g condition

showing the g-independency of the SWRC in infiltration experiments. The next chapter will discuss the calibration procedure for the in-flight shaking table as another preliminary step prior to the target seismic tests.

CHAPTER VIII

CALIBRATION OF THE IN-FLIGHT SHAKING TABLE AND INPUT MOTION SELECTION

8.1. Introduction

Since the dynamic time in centrifuge models is scaled with a factor of 1/N, model seismic motions encompass a much wider frequency range (e.g. the scaled Northridge motion in this study covers frequencies up to 500 Hz). The high frequency content of the applied motions requires very large fluid flow rate through the servo valve as well as a very high oil pressure in the system. Therefore, the in-flight shaking tables are incapable of imposing the same command motion to the specimen. As a common practice, in-flight shaking tables are calibrated for a specific earthquake motion by matching the "target" and the "achieved" motion on the shaking table (Ketcham et al. 1991, Mason et al. 2010). The performed steps for calibrating the in-flight shaking table and the characteristics of the selected input motions are discussed in this chapter. In this chapter, all the presented results are in model scale, unless otherwise stated.

8.2. Input motion selection

Two seismic input motions were selected in this study to shed light on the effects of partial saturation on site response under different motions. Scaled motions of 1994 Northridge and 1995 Kobe earthquakes, recorded at WPI and Takatori stations, respectively, were selected as the desired motions in this investigation. The initial attempts to calibrate the shaking table for the original recorded Northridge and Kobe motions failed due to the shaking table analog limits (i.e. the maximum input displacement of 10 mm). Therefore, the PGA of Northridge and Kobe desired motions were scaled from 0.42g and 0.67g to 0.3g and 0.2g in prototype scale, respectively. Different characteristics of the input motions, including acceleration time series, Arias intensities, magnitude of FFTs, and spectral accelerations are illustrated in Figure 8-6, at the end of this chapter. All the motions encompass a wide range of frequency content where the influence of degree of saturation on site response can be observed at different frequencies. Kobe motion was selected since it has a significantly higher accumulated energy (demonstrated with the magnitude of Arias intensity) than Northridge motion (even with a lower PGA).

8.3. Calibration of the in-flight shaking table

The method introduced by Mason et al. (2010) was used in this study whereby the "command" motion sent to the shaking table was iteratively modified using a set of frequency response analysis, so the "achieved" motion became approximately similar to the "target" motion. In order to calibrate the motions, the "desired" scaled motions were modified to reach the "target" motions by filtering unwanted frequency ranges (i.e. herein, frequencies higher than 8 Hz, in prototype scale, were filtered from both scaled Northridge and Kobe motions). To start the calibration process, as the first trial, the first "command" motion was defined as the exact same

"target" motion, and the "achieved" motion at the shaking table was captured. The acceleration time histories and the magnitude of Fast Fourier Transforms (FFT) for the first command (target) and the first achieved motions of the Northridge scaled event are shown in Figure 8-1 (a) and (b), respectively. A poor agreement was observed between the first achieved and target motions, which was aimed to be improved in the subsequent steps.

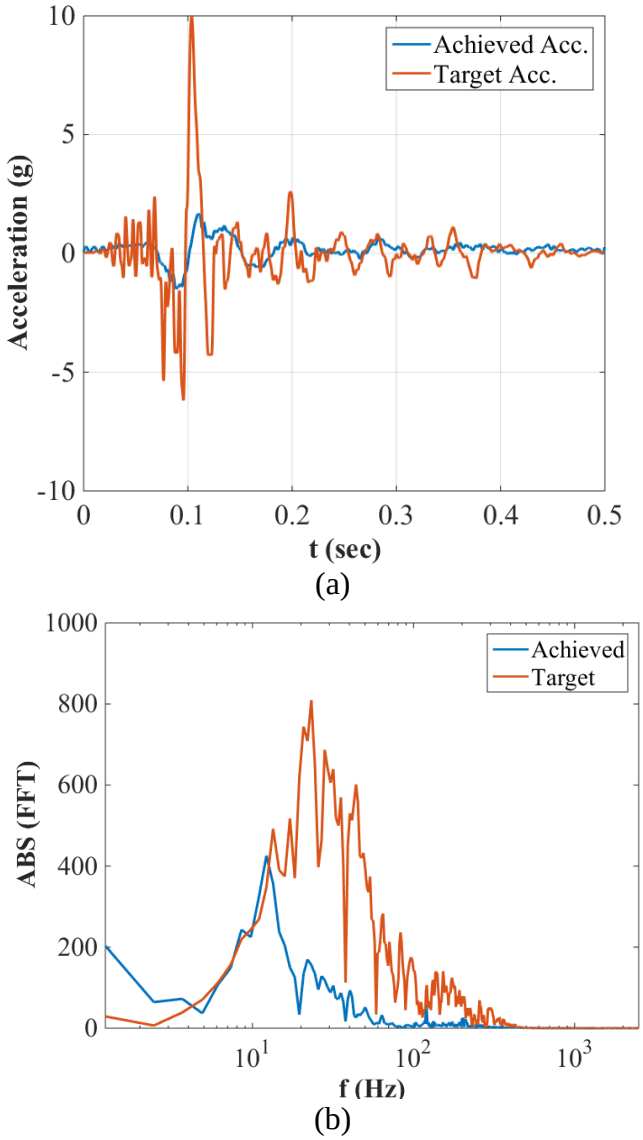

Figure 8-1. The first command (target) and first achieved motions for the scaled Northridge earthquake in terms of (a) acceleration time history and (b) magnitude of FFT

In order to find the second "command" motion, a transfer function was defined using either the ratios of the FFTs of the achieved and command motions or the corresponding transmissibility function between these two motions (Figure 8-2, b):

$$TF^1 = \frac{FFT\ (Achieved\ Motion^1)}{FFT\ (Command\ Motion^1)} = \frac{FFT\ (Achieved\ Motion^1)}{FFT\ (Target\ Motion)} \quad (8\text{-}1a)$$

$$TF^1 = T_{xy}(f) = \frac{P_{xy}\ (f)}{P_{xx}\ (f)} \quad (8\text{-}1b)$$

where P_{xy} and P_{xx} are the cross power spectral density and power spectral density functions, respectively. Thereafter, the second command motion, in frequency domain, was achieved by dividing the last command motion (i.e. target motion for this trial) by the obtained transfer functions (Figure 8-2, c):

$$FFT\ (Command\ Motion^2) = \frac{FFT\ (Command\ Motion^1)}{TF^1} = \frac{FFT\ (Target\ Motion)}{TF^1} \quad (8\text{-}2)$$

The acceleration time history of the second command motion, then, was obtained using the inverse FFT function (Figure 8-2, d). Since the values of transfer function for this trial were relatively low, especially at mid-range frequencies between 10 and 100 Hz, magnitude of the calculated acceleration time history for the second command motion was significantly higher than that of the target motion (i.e. higher than 150 g). It should be noted that according to the original procedure explained by Mason et al. (2010) the transfer function is obtained as the ratio of the command motion over the achieved motion, and then is multiplied by the last command motion to obtain the new command motion. However, in this study both approaches were practiced, where employing the Equations 8-1 and 8-2 led to more efficient results.

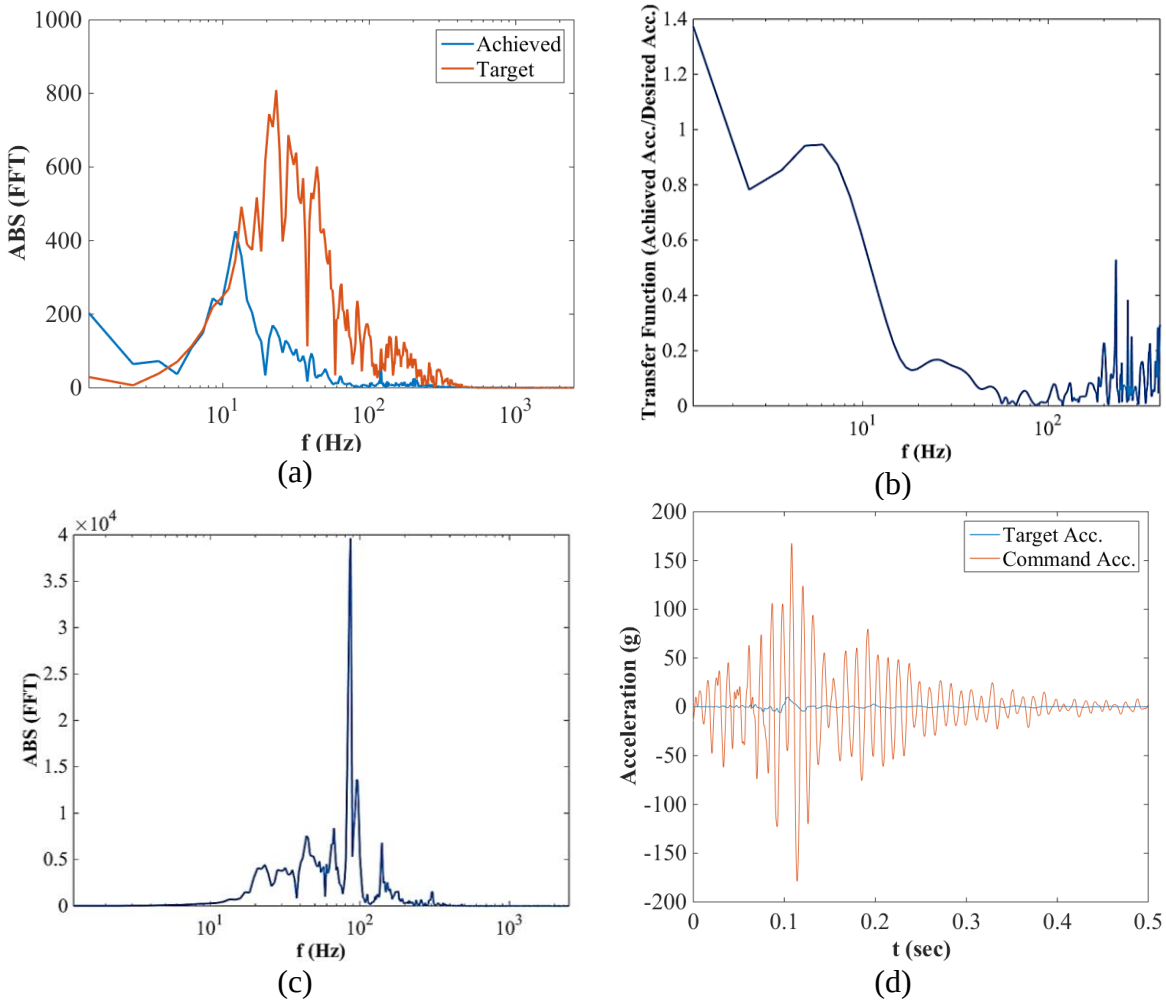

Figure 8-2. Obtaining the second command motion for the Northridge earthquake (a)FFTs of the first command and achieved motions (b)the obtained transfer function (c)FFT of the second command motion (d)acceleration time series of the first and second command motions

Since the shaking table operated with input displacement time series, the acceleration time histories, were double integrated and baseline corrected using a polynomial function to obtain the corresponding displacement values at each trial (Figure 8-3). As two transfer functions were employed in each step (the FFT and transmissibility transfer functions), two displacement time histories were obtained as the new command motions in each step.

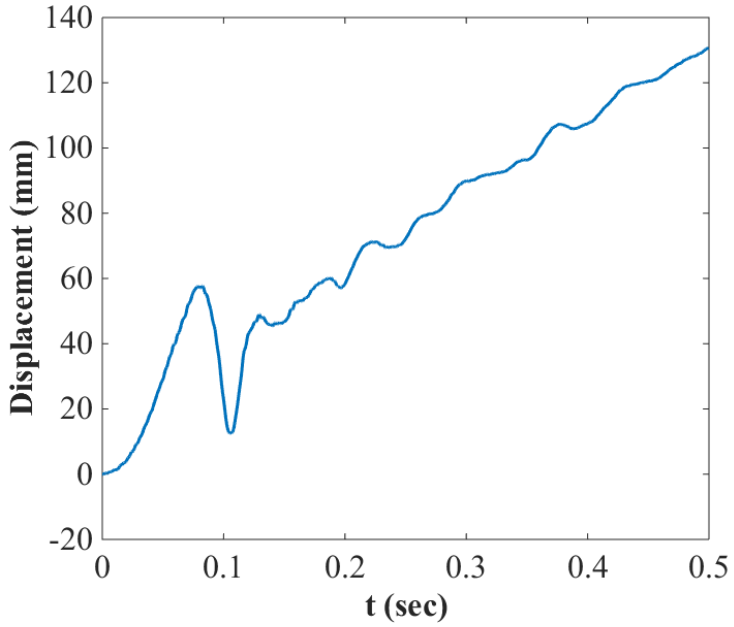

(a)

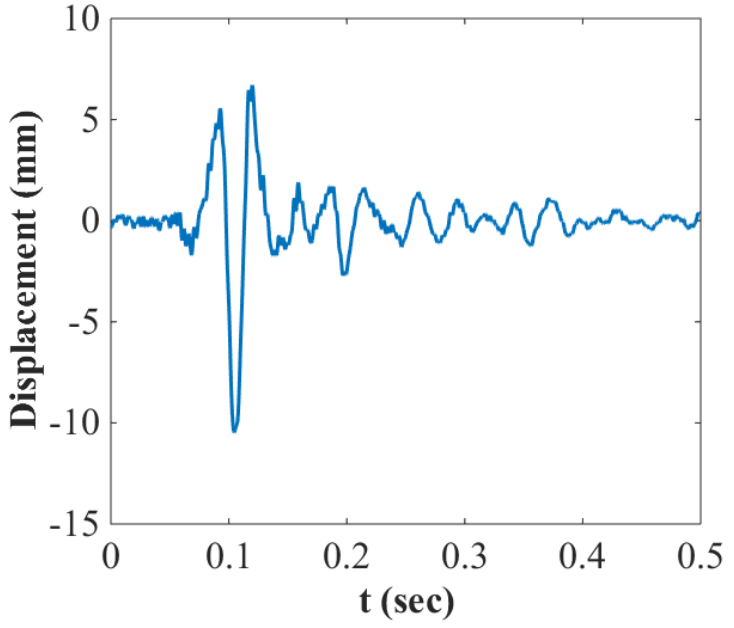

(b)

Figure 8-3. Displacement time history of the second command motion for the scaled Northridge motion earthquake (a) before and (b) after baseline correction

As the next step, both displacement time histories of the second command motion were applied to the specimen, and the achieved motions were recorded. Then, the achieved motion closer to the target motion was selected and the discussed steps were repeated to obtain displacement time

histories of the next command motion. After applying the command motion to the specimen, in each step, the achieved motions were compared with the target motion in terms of different motion characteristics (i.e. acceleration time history, magnitude of FFT, 5% damped spectral acceleration, and Arias intensity). The trial-and-error process was continued until the achieved motion was sufficiently similar to the target motion in terms of the mentioned motion characteristics. The acceleration time histories of the achieved and target motions for the Northridge earthquake, recorded in several trials, are shown in Figure 8-4.

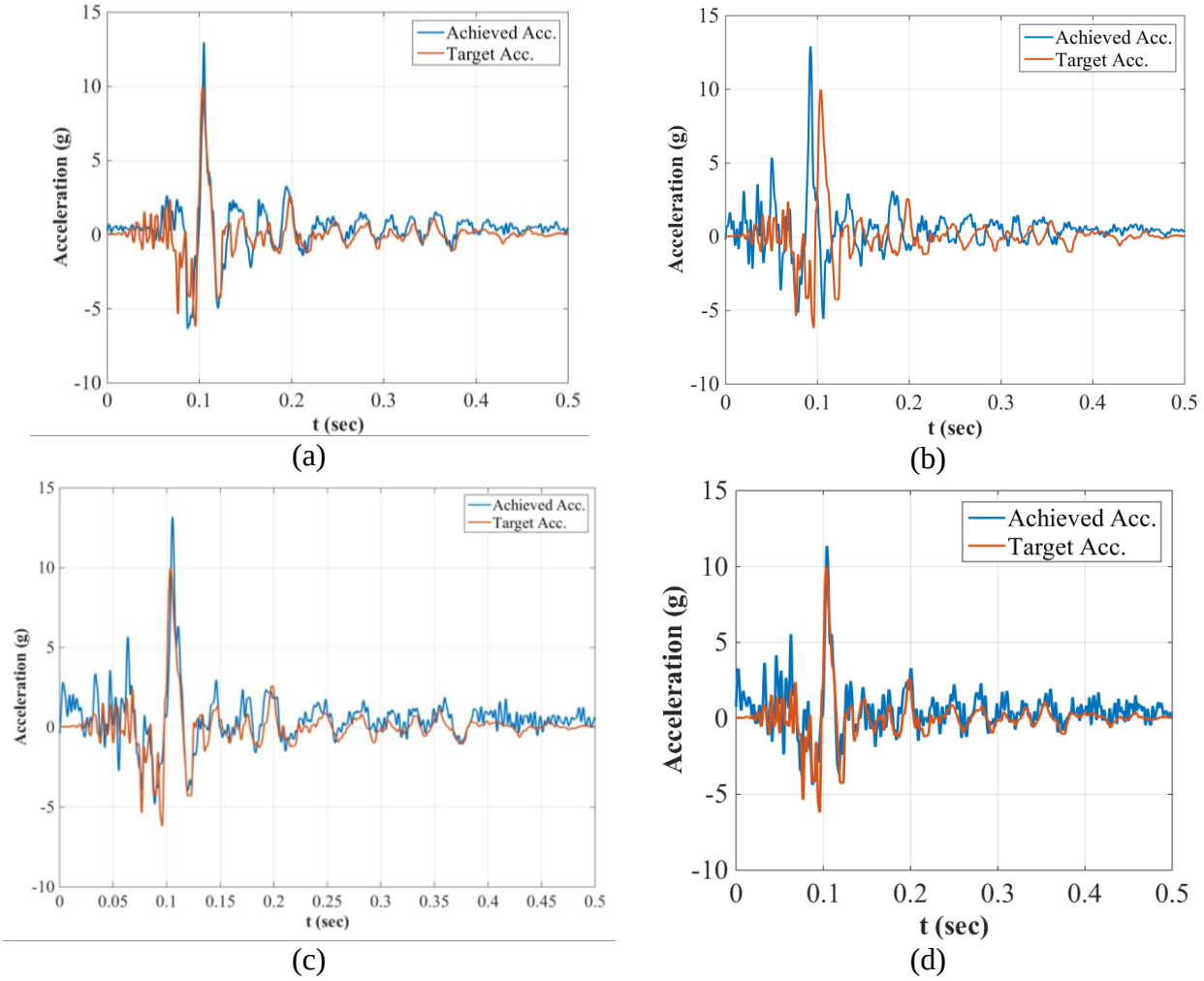

Figure 8-4. Some of the achieved acceleration time histories for the scaled Northridge motion (a) second trial (b) third trial (c) seventh trial and (d) final attempt

The acceleration time history and frequency content of the final achieved motion for the scaled Northridge event are shown in Figure 8-5 (a) and (b), respectively. Although eight trials were performed where the achieved motion became sufficiently close to the target motion, some slight differences between the final achieved and target motions could still be observed. Specifically, the difference in terms of magnitude of FFTs at high and very low frequencies (i.e. slightly higher than 100 Hz and less than 10 Hz, respectively) resulted in slightly different acceleration time history for the achieved motion than that of the target motion.

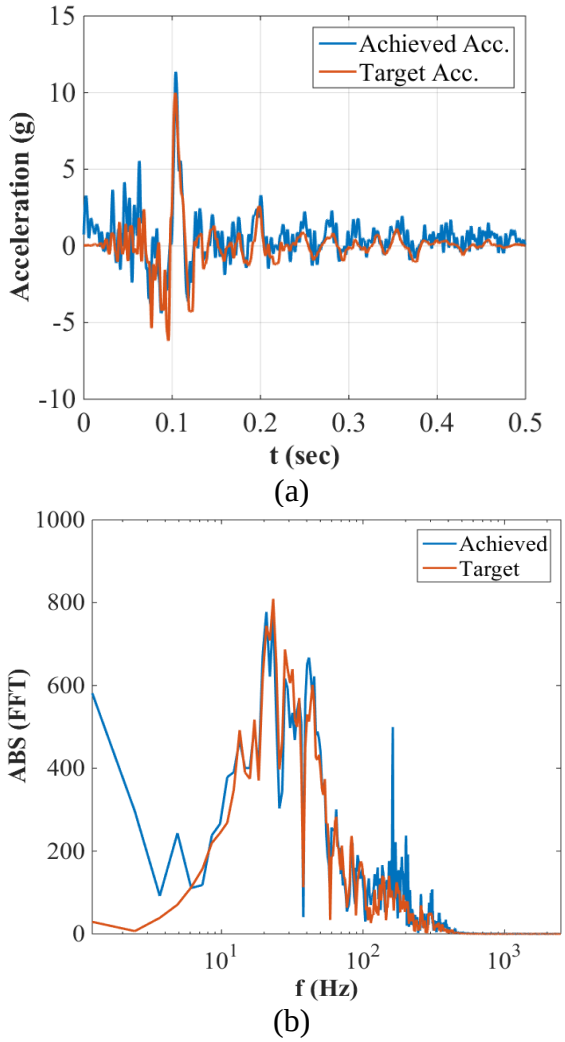

Figure 8-5. Comparison between the target and final achieved motions in terms of (a) acceleration time history and (b) magnitude of FFT

Eight and five trials were performed to calibrate the shaking table for the Northridge 0.3g and Kobe 0.2g motions, respectively. However, considering the efforts to find the maximum reachable acceleration level using the current system, more than 30 tests were performed in this regard. The final achieved Northridge and Kobe motions in terms of different motion characteristics, including acceleration time history, Arias intensity, Fourier amplitude, and 5% damped spectral acceleration, all in prototype scale, are illustrated in Figure 8-6. During the target seismic tests, although the same command motion was imposed to all the specimens with different degrees of saturation, the input motions recorded at the shaking table level were slightly different. This could be due to different specimen weights and the nonlinearities involved with the performance of in-flight shaking tables.

8.4. Summary and Conclusions

The input motion selection and the steps to calibrate the in-flight shaking table were discussed in this chapter. Scaled 1994 Northridge and 1995 Kobe motions were selected as the input motions in this study, which had the PGA of 0.3 and 0.2 g, respectively. Different characteristics of both input motions, including acceleration time histories, Arias intensity time series, FFT amplitude, and spectral acceleration graphs were presented. In order to calibrate the in-flight shaking table, the method introduced by Mason et al. (2010) was used where the command motion was adjusted through an iterative procedure so that a good agreement between the achieved and target motions was obtained. The target centrifuge seismic tests on unsaturated sand specimens were performed under both calibrated input motions, which will be discussed in the next chapter.

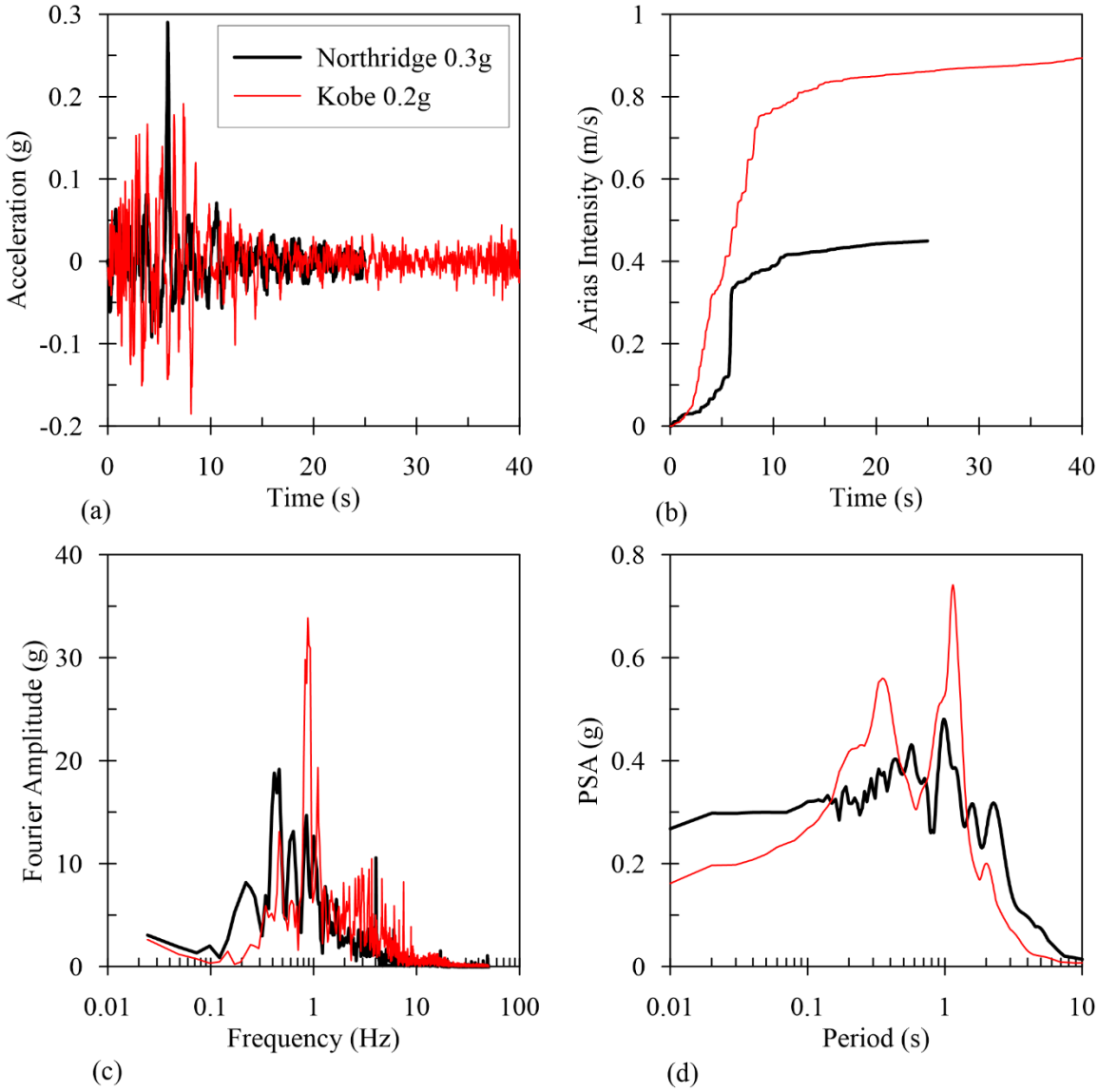

Figure 8-6. Obtained scaled Northridge and Kobe motion characteristics (in prototype scale) (a) Acceleration time histories; (b) Arias intensities; (c) Fourier amplitudes; (d) 5% damped spectral accelerations

CHAPTER IX

CENTRIFUGE TESTS TO ASSESS SEISMIC SITE RESPONSE OF PARTIALLY SATURATED SOILS

9.1. Introduction

In order to assess the effect of partial saturation on seismic site response of sand layers, a set of dry, unsaturated, and saturated centrifuge experiments were conducted under the scaled Northridge and Kobe earthquake motions. Table 9-1 summarizes the performed tests under each input motion. Steady state infiltration, using a spraying system, was implemented to control and provide uniform degrees of saturation profiles in depth. Upon reaching a uniform degree of saturation profile in depth, the calibrated motions were applied to the base of specimens and the seismic response was captured. The experimental procedures and the results of physical modeling are presented in this section.

Table 9-1. Number of seismic tests for each input motion

Input Motion	Number of Tests			
	Dry	Unsaturated	Saturated	Total
Northridge 0.3g	3	11	1	15
Kobe 0.2g	1	3	-	4

9.2. Experimental Procedures

For the seismic experiments, loose specimens with an approximate relative density of 45% and final height of 22.9 cm (in model scale) were prepared using dry pluviation technique. In addition, a gravel layer was placed at the bottom of the sand specimen to provide a saturated boundary condition, separated from the sand layer using geotextile filters. Accelerometers and dielectric sensors were placed at different depths of the soil layer when needed (Figure 9-1). Upon completing the pluviation, spray nozzles and vertical LVDTs were mounted on the sensor racks atop the container sitting on the in-flight shaking table. Moreover, horizontal LVDTs were placed on a side frame measuring the displacements of the laminates. The specimen was, then, saturated (for saturated and unsaturated tests) by passing de-aired water through two drainage ports on the base plate. A completely prepared and mounted specimen is shown in Figure 9-2. A slight negligible change in the relative density was measured due to the saturation and centrifugation.

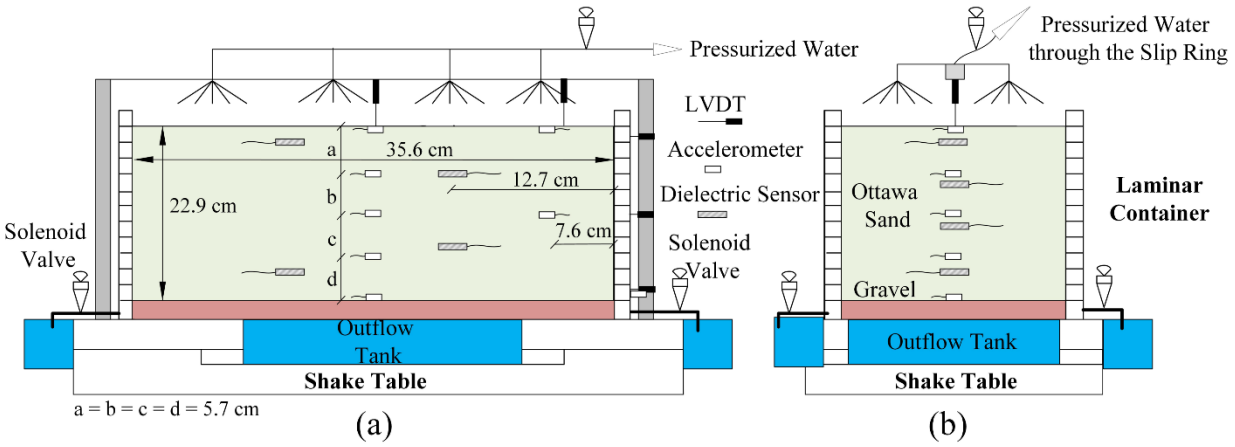

Figure 9-1. Instrumentation in the laminar container modified for steady-state infiltration: (a) Side-view Schematic (b) Front-view Schematic.

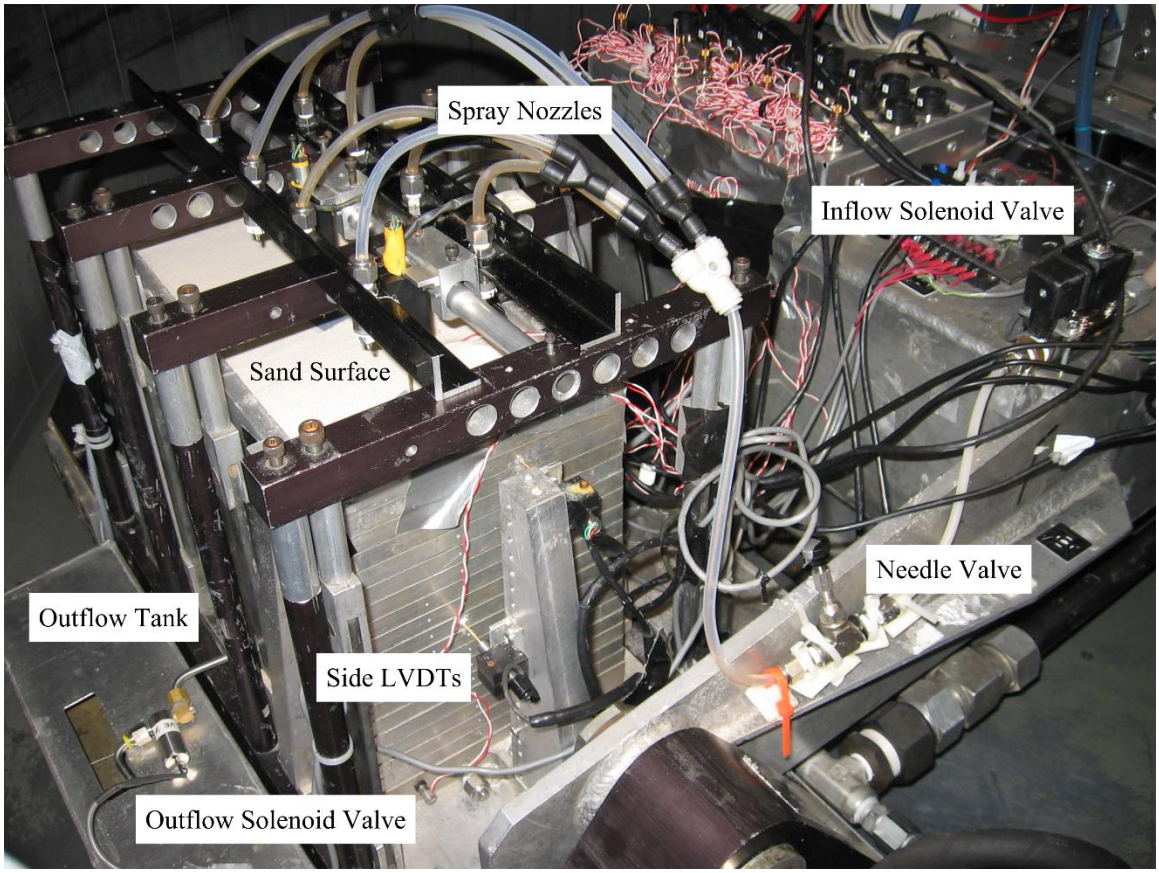

Figure 9-2. Fully assembled experimental setup.

The centrifuge was spun up to 50-g acceleration measured at the middle of the soil layer. Upon reaching the target g-level, the inflow and outflow solenoid valves were opened to generate a steady-state infiltration within the specimen. Different discharge rates were obtained in this study

by varying the types of nozzles and opening of the needle valve (i.e. v_m/k_{sat} between $1.5x10^{-4}$ to $2.4\ x10^{-3}$). Consequently, various uniform degree of saturation profiles were obtained ranging from 32% to 68% (corresponding to matric suctions from 3.9 to 4.9 kPa) within a short time span after starting the infiltration (e.g. about 1 minute for all the specimens). Some of the achieved degrees of saturation and their corresponding discharge velocities are shown in Figure 9-3 along with the corresponding analytical solutions (Equation 2-20). Although a somewhat uniform degree of saturation profile was reached across the height of the specimen, the bottommost section (about 5% in length) still had a transient degree of saturation varying from the fully saturated boundary condition to the target degree of saturation. This length was aimed to become minimal by increasing the g-level (Figure 2-11). The transition zone has to be considered when interpreting and applying the results of this study.

After a constant degree of saturation was achieved throughout the specimen, the input earthquake motions (i.e. the scaled Northridge and Kobe motions) were applied to the sand layer and the response was captured. Conventionally, a more viscous pore fluid with similar mechanical properties with water has been implemented to address the time scaling conflicts between dynamic and diffusion problems in the centrifuge (Dewoolkar et al. 1999). However, the mechanisms of dynamic suction variations mainly rely on distortions of water menisci during seismic events and differ from those of excess pore water pressure generation and dissipation. The unsaturated tests in this study were performed in degrees of water saturation much lower than one (for fully saturated) to avoid the time scaling conflict for dynamic problems in the centrifuge models. In addition, the steady state infiltration technique leverages the accelerated

flow of the water in the soil in high g-level, which would not be the case for higher viscosity fluids.

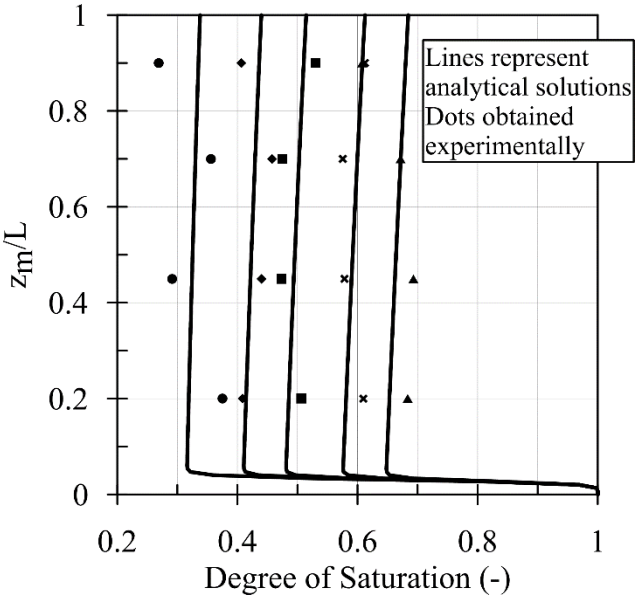

Figure 9-3. Experimentally developed profiles of degree of saturation along with the analytical solutions (after Dell'Avanzi et al. 2004).

9.3. Results and Discussion

The centrifuge experiments under scaled Northridge motion were performed on three dry specimens (D1, D2, and D3), eleven unsaturated specimens (specified with the letter U followed by the degree of saturation) with degrees of saturation varying between 32% and 68%, and one saturated (S) specimen. In addition, one dry and three unsaturated tests were carried out under the scaled Kobe motion (Table 9-1). The captured acceleration and displacement time histories were post-processed to obtain various motion characteristics. Then, the influence of the degree of saturation on the seismic response was investigated in terms of different motion parameters including PGA, frequency-dependent motion amplification, cumulative intensity amplification, lateral deformation, and seismic settlement. The following results are all presented in prototype scale unless specified.

9.3.1. Peak Ground Acceleration Amplification

PGA amplification factor (F_{PGA}) was calculated at different depths using the following equation:

$$F_{PGA} = \frac{PGA}{PGA_{base}} \tag{9-1}$$

where PGA and PGA_{base} are the maximum accelerations at a given depth and at the bottom of the specimen (considered as bedrock motion herein), respectively. In addition to the F_{PGA}, frequency-dependent amplification factors (i.e. F_a and F_v) were considered in this study, which are presented later in this chapter. Arrays of normalized acceleration time histories for selected experiments (i.e. D3, U38, and U66) are shown in Figure 9-4. Consistent with the results of simplified numerical analysis (Mirshekari and Ghayoomi 2015), the time histories indicate a higher acceleration amplification at the ground surface for unsaturated tests comparing with the dry one. The amplification ratio was higher for the test with lower degree of saturation (higher matric suction), U38, than the one in U66. In addition, the amplification ratio was lower within unsaturated sand layers than that in the dry specimen at other levels showing a depth-dependent influence of partial saturation on site response.

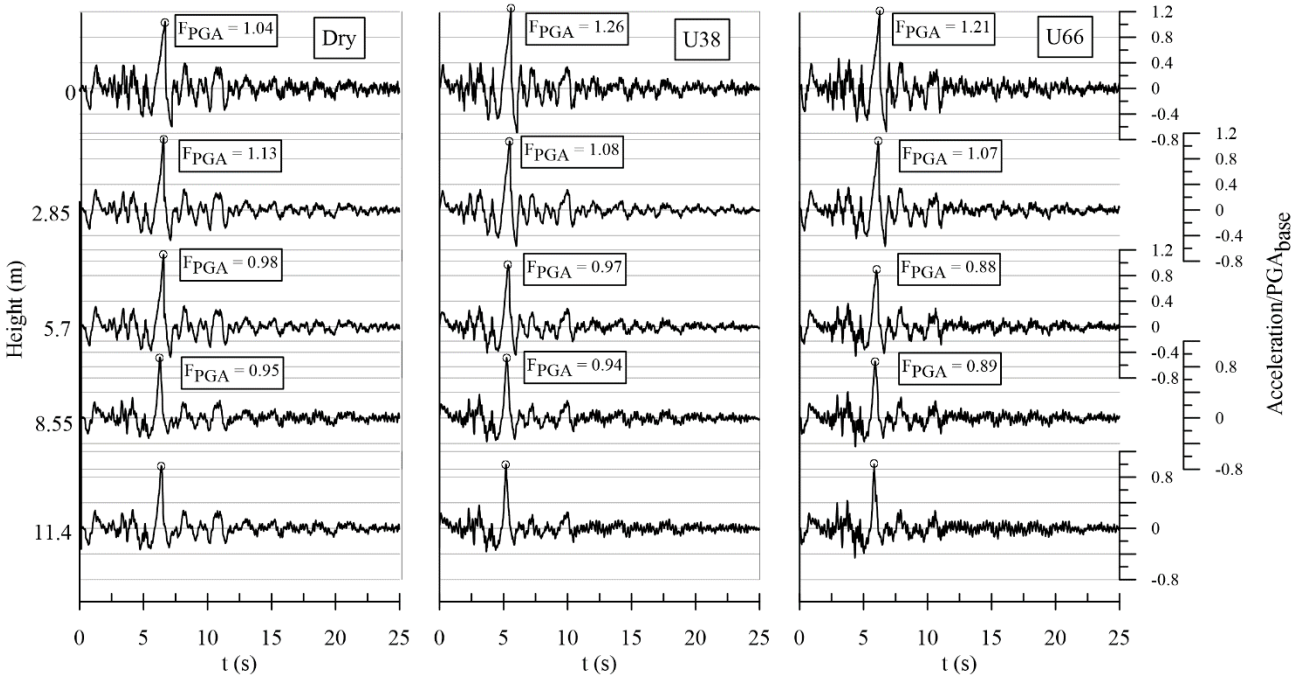

Figure 9-4. Selected arrays of acceleration time histories

As mentioned earlier, PGA_{base} slightly varied among different tests that, in turn, caused an additional influence on the F_{PGA} values. In order to eliminate this effect, a relationship was formulated to normalize the PGA of base motions to a reference value. To find such a correlation, F_{PGA} values were graphed over PGA_{base} for tests with approximately similar degrees of saturation; e.g. D1, D2, and D3 and U48, U49, and U50; shown in Figure 9-5. Knowing the expected trend from previous studies (Idriss 1990, 1991, Silva et al. 2000, Borcherdt 2002, Stewart et al. 2003, Choi and Stewart 2005), F_{PGA} was set inversely proportional to PGA_{base} for the given limited range of acceleration. The following linear correlation was developed where the slope of the line was similar for dry and partially saturated cases:

$$F_{PGA} = -5.75 * PGA_{base} + d \quad (9\text{-}2)$$

where the parameter d indicates the influence of degree of saturation. The F_{PGA} values were modified by moving along the same slope such that a reference base PGA of 0.3 g was achieved for all the tests based on the abovementioned linear relationship:

$$F_{PGA,Mod.} = F_{PGA} - 5.75 * (0.3 - PGA_{base}) \quad (9\text{-}3)$$

This modification could increase or decrease the F_{PGA} depending on the values of PGA_{base} (e.g. for the test U66 with PGA_{base} of 0.2828 the F_{PGA} was modified from 1.212 to 1.1131).

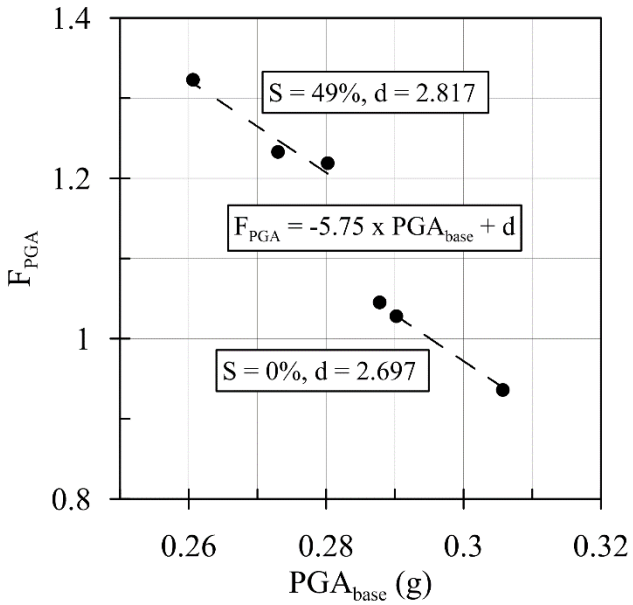

Figure 9-5. Correlation of PGA amplification factor (F_{PGA}) and base peak ground acceleration (PGA_{base})

Modified surface F_{PGA} values for different degrees of saturation are shown in Figure 9-6 (a). While the amplification factors for dry tests were approximately one, the unsaturated soil condition led to higher amplification factors at surface especially at lower degrees of saturation (with an average increase of 16%). The amplification factor for the case of fully saturated sand layer was expectedly lower than the ones in dry and unsaturated sand layers due to the de-amplification of motion in possibly fully- or partially-liquefied ground (the liquefaction occurrence was not assured due to the absence of pore water pressure transducers). Therefore,

the focus of this study has been mainly on comparing the response of dry and unsaturated sand layers.

The amplification factor at the soil surface was shown to be inversely proportional to the degree of saturation with a nonlinear pattern. The amplification factor is somewhat constant for mid-level degrees of saturation where the change in suction is almost negligible (i.e. between 45% and 70% degrees of saturation). In addition, the code-based (*NEHRP 2009, ASCE/SEI 7-10 2010*) amplification factor is demonstrated in Figure 9-6 (a) where the weighted-average shear wave velocity, $\overline{V_s}$, was calculated using the following formula:

$$\overline{V_s} = \frac{H}{\int_0^H \frac{1}{v_s}\, dz} \tag{9-4}$$

where H is the soil layer thickness, z is the depth, and v_s is the depth-dependent shear wave velocity resulted from small-strain shear modulus values at each depth. The site class, thereafter, was estimated using Table 2-1 where regardless of the choice of the small-strain modulus formula (i.e. Ghayoomi and McCartney 2011, Seed and Idriss 1970, Hardin 1978), a Class D was assigned. Also, estimating an average shear wave velocity for 30-m soil layer as suggested by the code or for 11.43-m soil layer in this study would yield to the same site class. Although partial saturation increased the PGA amplification, the code-suggested F_{PGA} value for this case is conservatively higher than nearly all the experimental values. The values suggested by seismic provisions were developed based upon a large number of recorded data from the past earthquakes in different site conditions (Dobry et al. 2000) while this study limited the testing conditions (e.g. uniform degree of saturation profiles; one type of sand, and one earthquake motion) to evaluate the effect of partial saturation.

The observed higher amplification in unsaturated sand layer in comparison with the one in the dry condition is consistent with the ones from simplified numerical site response analysis (Ghayoomi and Mirshekari 2014, Mirshekari and Ghayoomi 2015) and centrifuge physical modeling under cyclic loads with equivalent PGA of 0.55 g and 0.65 g (Ghayoomi and McCartney 2011). However, Ghayoomi and McCartney (2011) found the code-based amplification factors to be lower than the measured F_{PGA} values. This difference could be either a result of simulating seismic motions using cyclic loads in Ghayoomi and McCartney (2011) or different suction-dependent site response mechanisms in very strong ground motions such as continuous full cycles of dynamic loads.

Further inspecting Equation 2-14, both parameters affecting the SDOF response (i.e. shear wave velocity and damping) are found to be a function of the degree of saturation. Shear wave velocity or small-strain shear modulus are increased in partially saturated soils as a function of matric suction (Khosravi et al. 2010, Ghayoomi and McCartney 2011, Dong et al. 2016). On the contrary, damping decreases while matric suction increases (Hoyos et al. 2015). Given the inversely proportional relations between the amplification factor and both shear modulus and damping in Equation 2-14, the increase in shear wave velocity of unsaturated soils yields to lower amplification whereas the decrease in damping leads to higher amplification. As a result, the influence of partial saturation on the site response should be holistically explored considering the interaction between the change in shear modulus and damping.

Shear modulus and damping are functions of their small-strain values and induced level of strain in soils. Small-strain shear modulus is proportional to the square root of effective stress in dry or saturated soils (Seed and Idriss 1970, Hardin 1978) while small-strain damping is correlated to

the effective stress raised to a much lower power (e.g. -0.08 according to Menq 2003). Therefore, the influence of the effective stress is more pronounced on shear wave velocity in comparison with damping, resulting in a general trend of lower amplification factors for stiffer sites (*NEHRP Recommended Seismic Provisions for New Buildings and Other Structures 2009*). The presence of suction in unsaturated soils increases the effective stress, however, the variations of small-strain dynamic properties for different degrees of saturation might not only depend on the effective stress (Dong et al. 2016). Dong et al. (2016) discussed that water can soften the soil matrix in unsaturated soils by reducing the inter-particle friction that contradicts the added stiffness caused by the matric suction. Hence, the influence of damping and shear modulus on the site response may become comparable. Also, the extent of the influence of partial saturation on the site response could vary in depth depending on the dominance of variations in either damping or shear modulus.

Further, the seismically induced strain level in soil layers plays an important role in interpreting the acceleration amplification factors. Basically, higher intensity earthquake motion leads to higher strain-dependent damping and lower strain-dependent shear modulus. Then, the amplification factor decreases (Idriss 1990, 1991) as a result of the interaction of these two parameters. In unsaturated soil conditions, however, the induced shear strains are affected not only by the intensity of the motion but also by the soil stiffening and lower damping. Depending on the induced level of shear strain, the mobilized shear modulus and damping in soil layers may vary and, consequently, alter the amplification factor.

Since matric suction increases the contact effective stresses in unsaturated soils, more insights might be gained by illustrating F_{PGA} versus matric suction, shown in Figure 9-6 (b). In addition,

Lu et al. (2010) discussed that “suction stress”, the combined effect of matric suction and degree of saturation, is responsible for mechanical behavior of unsaturated soils (Equation 2-13, b). F_{PGA} values are shown versus suction stress in Figure 9-6 (c). Although the performed tests cover a wide range of degree of saturation, only a slight variation occurred in terms of matric suction (i.e. from 3.9 to 4.9 kPa) while the suction stress expands the range from 0.8 to 2.3 kPa. The suction stress might be a better predictor of seismic soil behavior while the amplification factor was not coherently linked to the change in matric suction. Overall, unsaturated specimens showed a higher amplification factor at surface, however, F_{PGA} decreases as suction stress increases.

In order to understand the variations of amplification factor along the depth, F_{PGA} profiles are shown over the height of the sand layer for different degrees of saturation in Figure 9-7 (only for the tests with five accelerometers in the middle array); where an average F_{PGA} is presented for the tests with similar degrees of saturation. The degree of saturation imposed a depth-dependent influence on PGA amplification factor. Despite the observed trend at the soil surface, shown in Figure 9-6, F_{PGA} values in depth of unsaturated sand layers are mostly (except for the lowest degree of saturation) lower than the ones of dry sand. This difference can be associated with the coupled effects of depth-, strain-, and suction-dependent damping and shear modulus on motion amplification pattern. For example, the suction stress results in a higher increase in the effective stress in shallow soils where total stresses are low. Further, the inconsistent amplification profiles in unsaturated soil layers would imply more complex wave propagation mechanisms in unsaturated soils (Yang 2006).

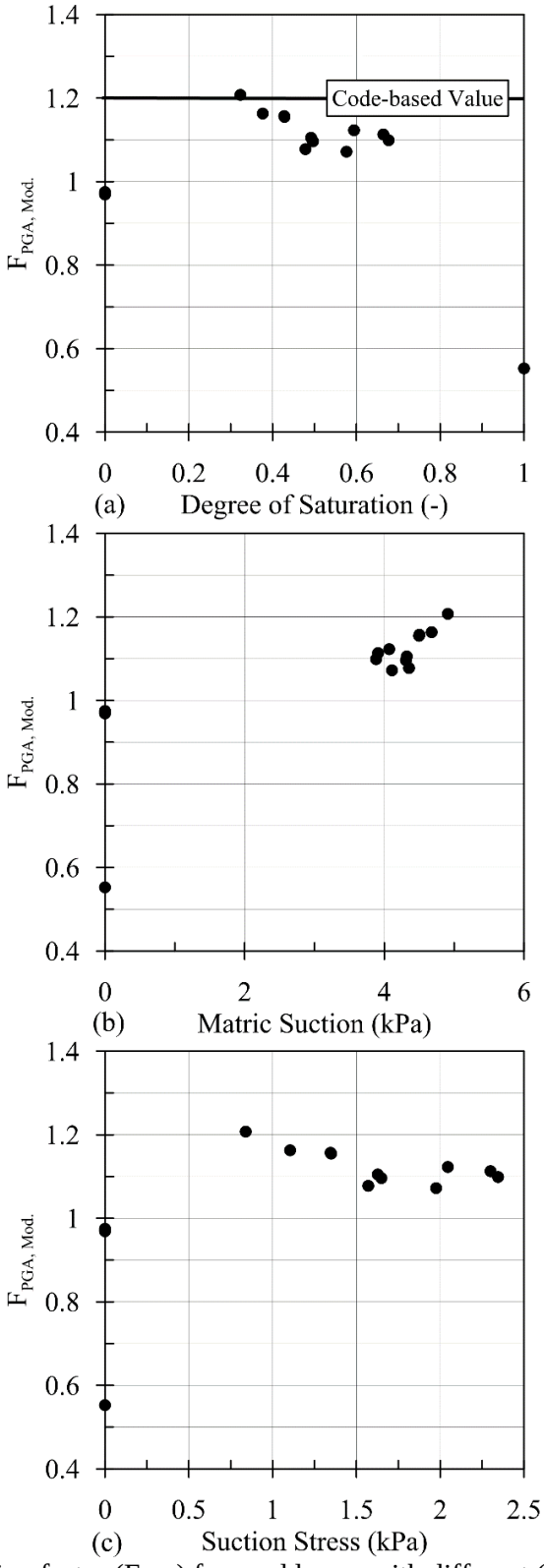

Figure 9-6. PGA amplification factor (F_{PGA}) for sand layers with different (a) degrees of saturation; (b) matric suction; and (c) suction stress.

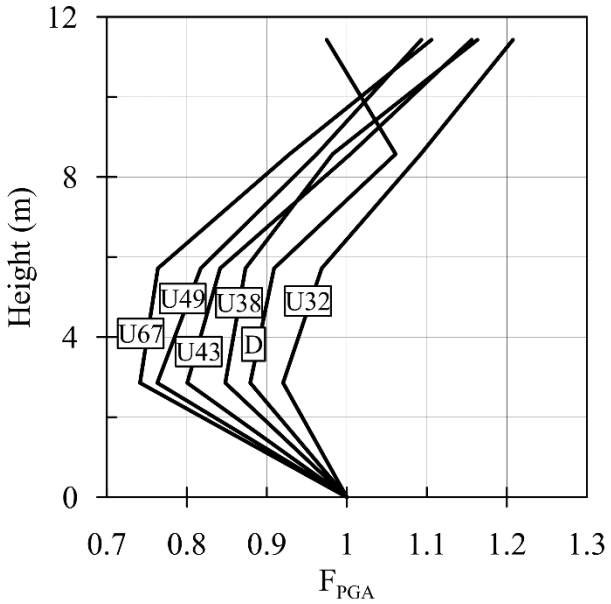

Figure 9-7. Profiles of PGA amplification factors (F_{PGA}) for sand layers with different degrees of saturation

9.3.2. Frequency-dependent Motion Amplification

In order to assess the effect of partial saturation on frequency content of the motion, FFT amplitude of the recorded surface motion was obtained and those for selected tests (i.e. D3, U38, and U66) are shown in Figure 9-8. Although the degree of saturation changes significantly between the tests, the corresponding matric suction variation is not substantial for this sand. This causes a minimal change in the effective stress due to partial saturation, which explains the negligible observed difference in terms of frequency content between the tests.

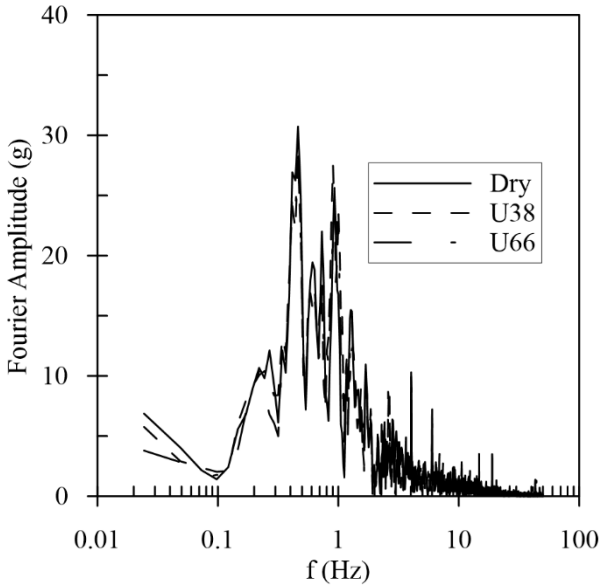

Figure 9-8. FFT amplitude of surface motions in selected tests

In addition, surface to bedrock amplification of response spectra or Fourier spectra could be used to investigate the frequency-dependent amplification of seismic motions. Low-period and mid-period amplification factors (F_a and F_v, respectively) are commonly evaluated as average values of Ratio of Response Spectra (RRS) or the ratio of Fourier spectra within a period or frequency range; e.g. between 0.1 to 0.5s and between 0.4 to 2s for F_a and F_v for the recorded data of Loma Prieta earthquake 1989, respectively (Borcherdt 1994). An average value of RRS between 0.1 to 0.5s and 0.6 to 2s were used herein to calculate F_a and F_v, respectively, since for the specific case of this study the values of RRS at 0.4s do not represent amplification at mid-term periods; as shown in Figure 9-9.

F_a and F_v variations for different degrees of saturation and suction stresses are shown in Figure 9-10. Both amplification factors were higher at soil surface in partially saturated specimens than the ones in dry condition. This clarifies that unsaturated condition yields to higher amplification at surface regardless of the period range. An average increase of 19% and 6% were observed in

F_a and F_v values of unsaturated specimens than dry ones, respectively. This indicates a higher influence of unsaturated condition on motion amplification at low-period range. Since no strong correlation between the F_a and F_v and PGA_{base} was found for the tests with similar degree of saturation, the frequency-dependent amplification factors were not modified with respect to the base motion. This explains the reason that the data is more scattered in terms of F_a and F_v in comparison with the F_{PGA}. In order to better compare the response of dry and unsaturated sand layers in terms of frequency-dependent amplification, 5% damped smoothed surface-to-base RRS graphs for selected tests are shown in Figure 9-11. The general higher motion amplification in unsaturated soil, more substantial in low period range, is discernable.

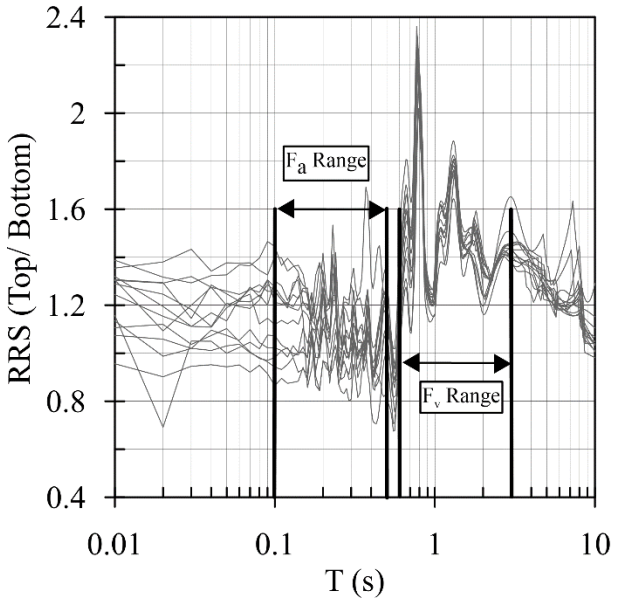

Figure 9-9. Period range selection procedure for low- and mid-period amplification factors

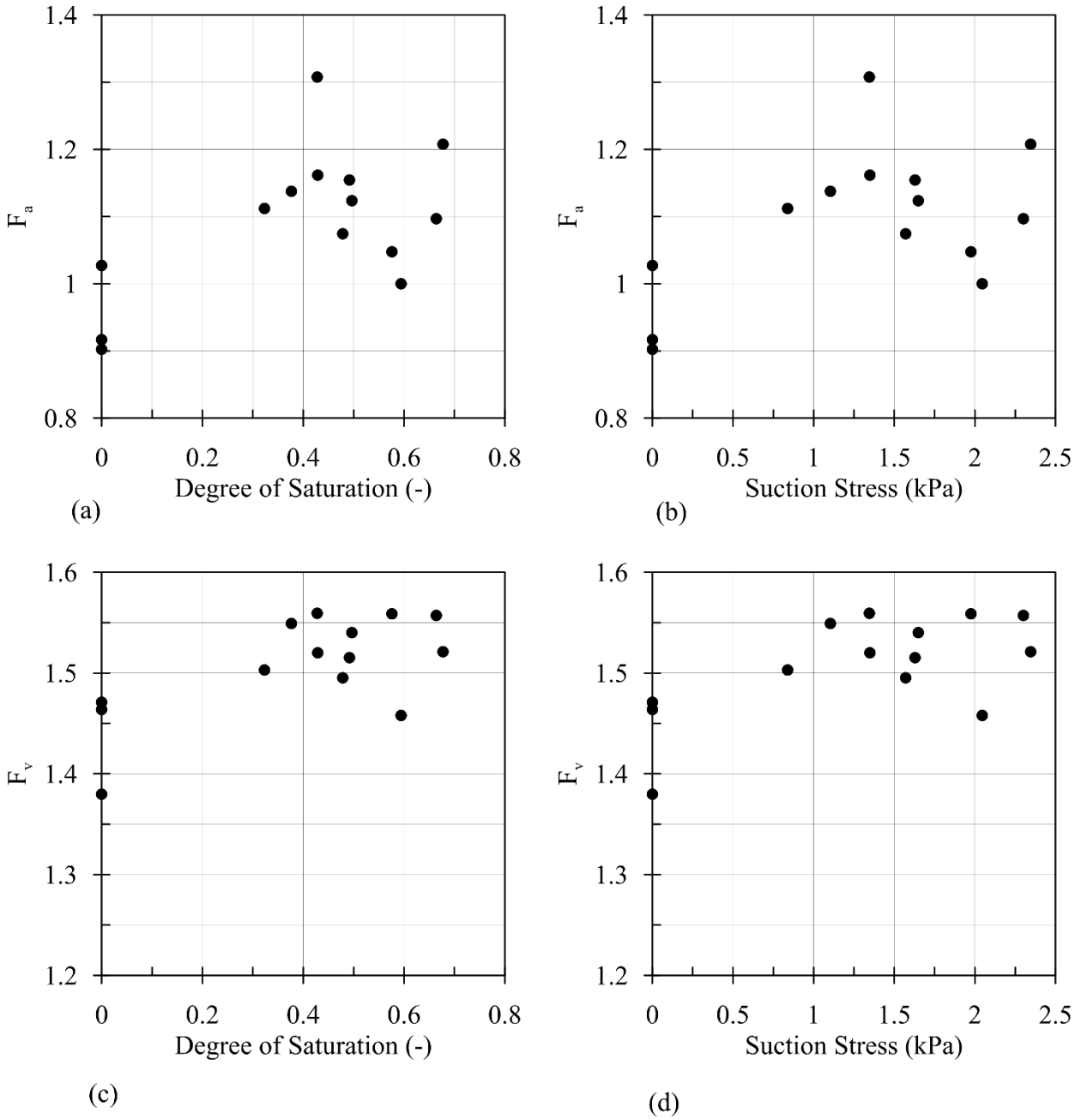

Figure 9-10. Low-period amplification factors (F_a) for different: (a) degrees of saturation; and (b) suction stress. Mid-period amplification factors (F_v) for different: (c) degrees of saturation; and (d) suction stress

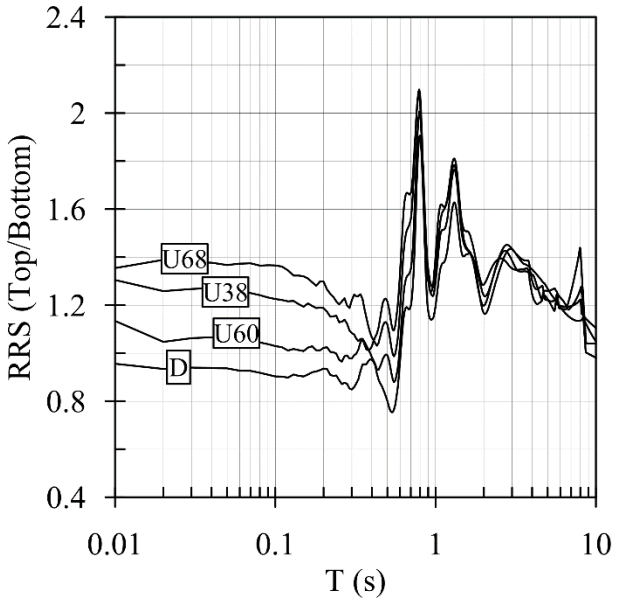

Figure 9-11. Ratio of Reponses Spectra (RSS) for selected tests for sand layers with different degrees of saturation.

9.3.3. Cumulative Intensity Amplification

Arias intensity (Arias 1970), a well-known cumulative intensity characteristic, was selected to represent the accumulated energy buildup during a shaking event in sites with different degrees of saturation. Arias intensity time histories of the selected tests (i.e. D3, U38, and U66) are shown in Figure 9-12 demonstrating a higher energy level in unsaturated condition than the dry test. Moreover, ratio of the maximum Arias intensity at the soil surface over the maximum Arias intensity at the base was used to quantify the change in energy level of the motions. The variation of Arias Intensity ratio with the degree of saturation is shown in Figure 9-13, enabling a comparison between the response of dry and unsaturated sand layers. To avoid misinterpretation of the results only the tests with bedrock Arias intensity within a ±5% offset from the reference dry motion were shown. The presented results show an overall 6% increase in Arias Intensity amplification for unsaturated specimens where the acceleration was amplified differently in different frequency ranges.

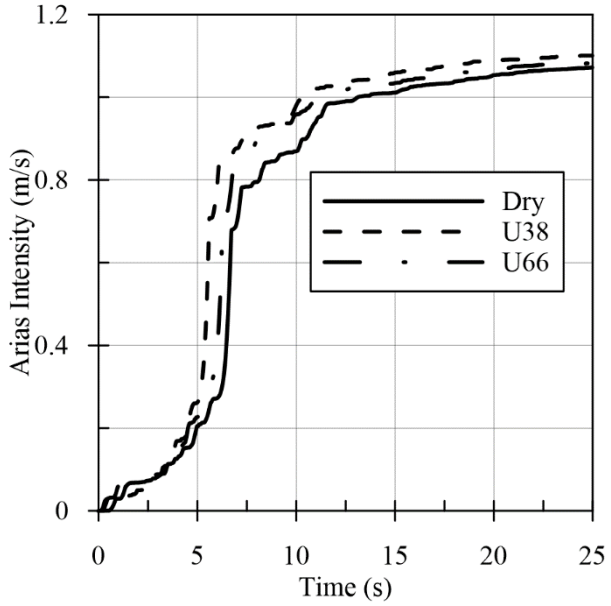

Figure 9-12. Arias intensity time histories of surface motions for selected tests

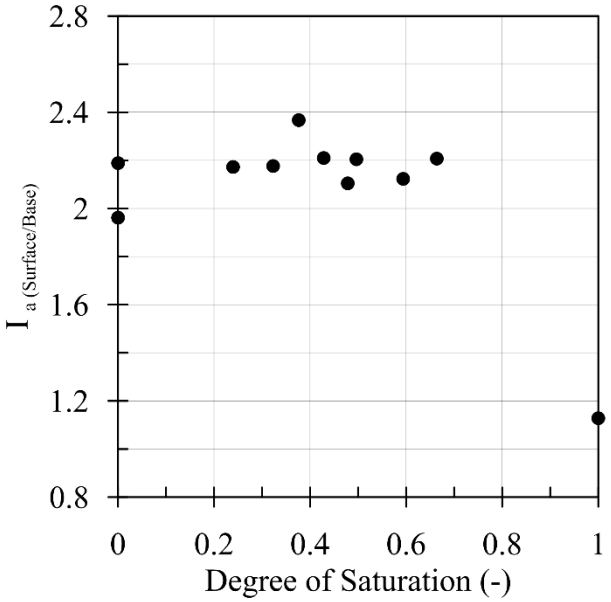

Figure 9-13. Surface-to-base ratio of Arias intensity for sand layers with different degrees of saturation.

9.3.4. Lateral Deformation

Lateral deformations were obtained using direct measurements of the side LVDTs as well as double integration of acceleration time histories followed by baseline correction of the obtained displacement time histories (Zeghal et al. 1995). Maximum lateral deformation profiles of

selected tests based on accelerometer and LVDT measurements are shown in Figure 9-14 (a) and (b), respectively. Maximum lateral deformation at the soil surface measured by both methods are illustrated against degree of saturation in Figure 9-14 (c). Overall, the lateral deformation of unsaturated soils obtained from both LVDTs and accelerometers are lower than that of dry soils by the ratio of 10% and 8% for LVDT and accelerometer measurements, respectively. This can be attributed to the higher shear modulus and stiffness in unsaturated sand resulted in lower induced shear strain and lateral deformations. The acceleration-based lateral deformation values were lower than those of LVDT measurements that could be due to the double integration process that involved base line correction. This difference in deformations obtained from the two methods is consistent with previous work by Hashash et al. (2015).

9.3.5. Seismic Settlement

Seismic settlement time histories of selected tests (i.e. D3, U38, and U66), measured by the middle LVDT, are shown in Figure 9-15. In spite of the observed trend of higher acceleration amplification in unsaturated sand, seismic settlement decreased as a result of higher shear modulus in unsaturated conditions. To illustrate the changes of seismically induced settlements versus degree of saturation, the settlement values were estimated by an average value of the middle and side LVDT's measurements after shaking and shown in Figure 9-16. Seismic settlements were generally lower for partially saturated sand layers as a result of stiffer response of unsaturated sand. A minimum settlement at a middle range degree of saturation, e.g. at about 38% in this case, is consistent with Ghayoomi et al. (2013) for seismically induced settlements under cyclic loads. Ghayoomi et al. (2013) attributed this trend to the collective effects of seismic compression and post shaking consolidation.

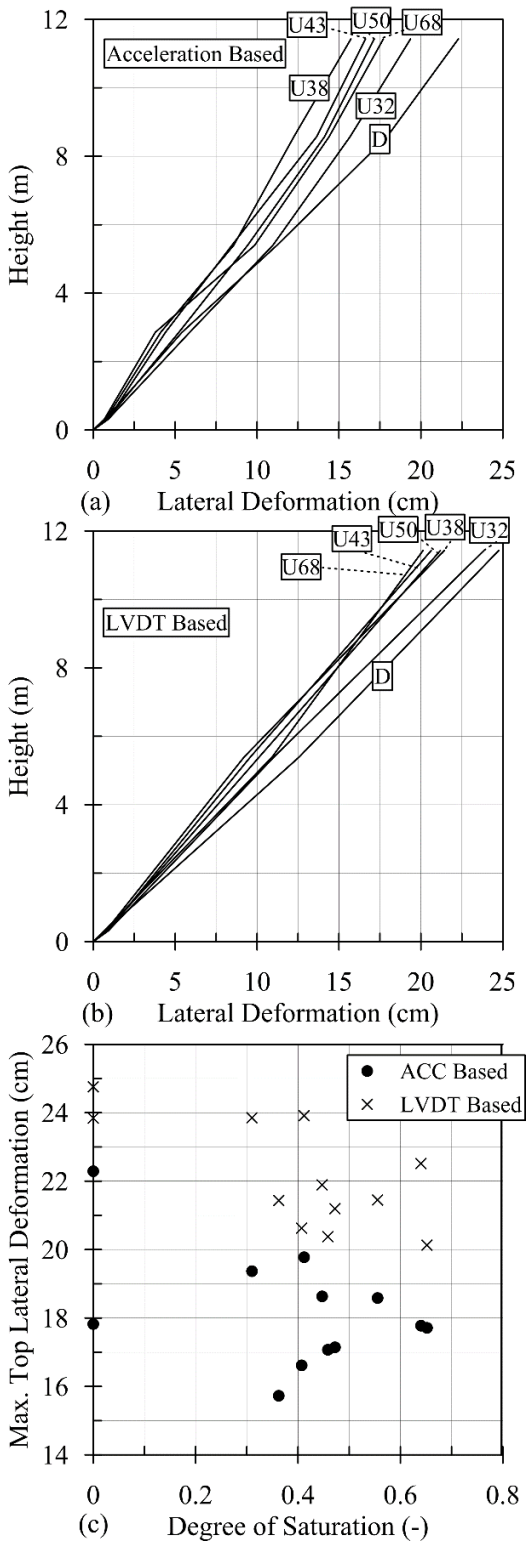

Figure 9-14. Maximum lateral deformation profiles for selected tests with different degrees of saturation based on (a) LVDT measurements; and (b) accelerometer measurements. (c) Maximum surface deformation of sand layers with different degrees of saturation.

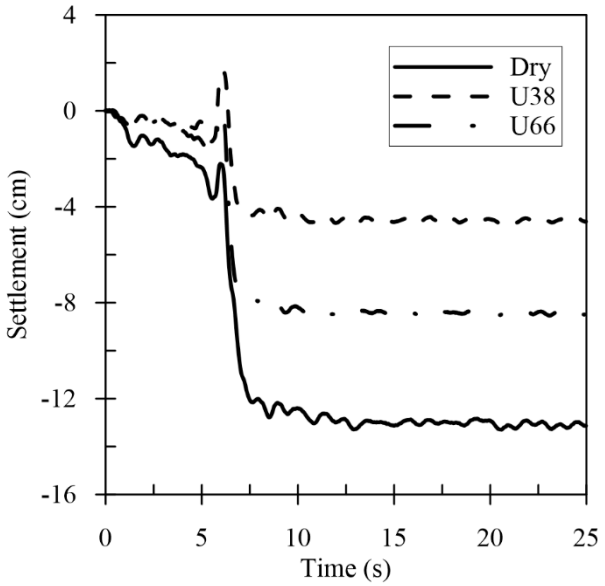

Figure 9-15. Surface settlement time histories for selected tests

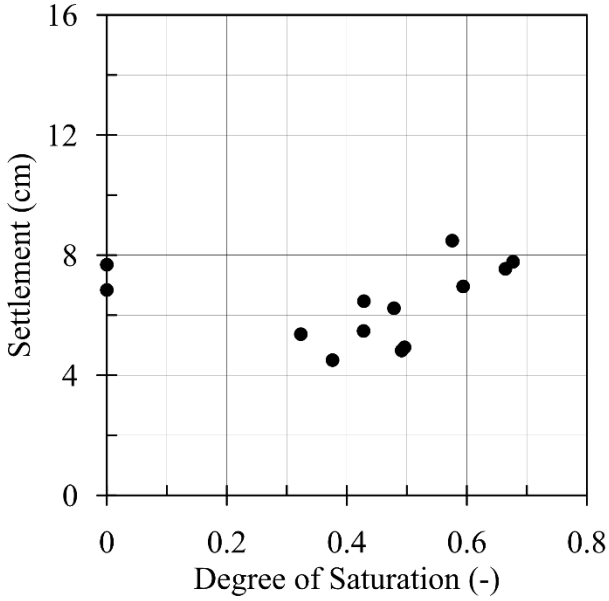

Figure 9-16. Seismic surface settlement of sand layers with different degrees of saturation

9.3.6. The effect of partial saturation on seismic site response under different input motions

In order to evaluate the effect of different input motions on the site response of unsaturated soil layers, the results of one dry and two unsaturated tests under Northridge 0.3g and Kobe 0.2g seismic motions are presented herein. The values of degree of saturation for each input motion

are listed in Table 9-2. The seismic response is compared under the two input motions in terms of different motion characteristics including Peak Ground Acceleration amplification factor (F_{PGA}), Arias intensity, top-to-bottom Ratio of Response Spectra (RRS), and surface settlements.

Table 9-2. Average degree of saturation in the experiments

Base Motions	**Degree of Saturation (%)**		
Northridge 0.3g	0	57%	66%
Kobe 0.2g	0	54%	66%

The surface/base F_{PGA} values for the soil layers under both motions are shown in Figure 9-17 (a). Further inspection of the results reveals that, as discussed earlier, since the PGA of base motion slightly changes in different tests, the intensity of base motion might also affect the resulted amplification factors. The small changes in input motion characteristics are commonly due to the nonlinearities involved with in-flight shaking table performance. The variations of F_{PGA} over the range of PGA_{base} in the presented experiments are illustrated in Figure 9-17 (b). The presented variations of amplification factors in both Figure 9-17 (a) and (b) are a function of PGA_{base} as well as the alterations in terms of degree of saturation.

In order to eliminate the dependency of the amplification factors on PGA_{base}, the values of F_{PGA} were modified using Equation 9-3 so that the base PGA is consistently 0.3g and 0.2g for Northridge and Kobe earthquake motions, respectively. The modified amplification factors are shown in Figure 9-17 (c). Although the results of Figure 9-17 (a) do not show a clear trend over the tested range of degree of saturation, after eliminating the influence of base PGA on the amplification factors, the results yielded to a consistent trend where the F_{PGA} values increased for higher degrees of saturation. This is likely due to the interaction of the variations in key parameters of sand layers including shear wave velocity, shear modulus reduction factor, damping, induced level of strain, and unit weight. The higher amplification factors in unsaturated

Ottawa sand layers were also obtained through simplified numerical procedures (Mirshekari and Ghayoomi 2015) as well as centrifuge tests under cyclic loads (Ghayoomi and McCartney 2011). Consistent with the trend of lower amplification factors for more intense motions (e.g. in Idirss 1991, Silva et al. 2000, and Stewart et al. 2003), the F_{PGA} values of the same degree of saturation were observed to be higher for Kobe motion than the ones captured under Northridge event.

The frequency/period-dependency of the amplification factors in dry and unsaturated sand was studied by calculating the RRS values for the tests under both input motions. The RRS graphs for dry and unsaturated sand layers shaken with Kobe and Northridge motions are shown in Figure 9-18 (a) and (b), respectively. The common trend, observed for both earthquakes, consists of a higher increase in acceleration amplification in unsaturated sand layers than the dry ones in lower period ranges (high frequencies), which is reduced as the period increases. For the higher periods (i.e. > 2 s), the dry soil resulted in higher acceleration amplification for both motions.

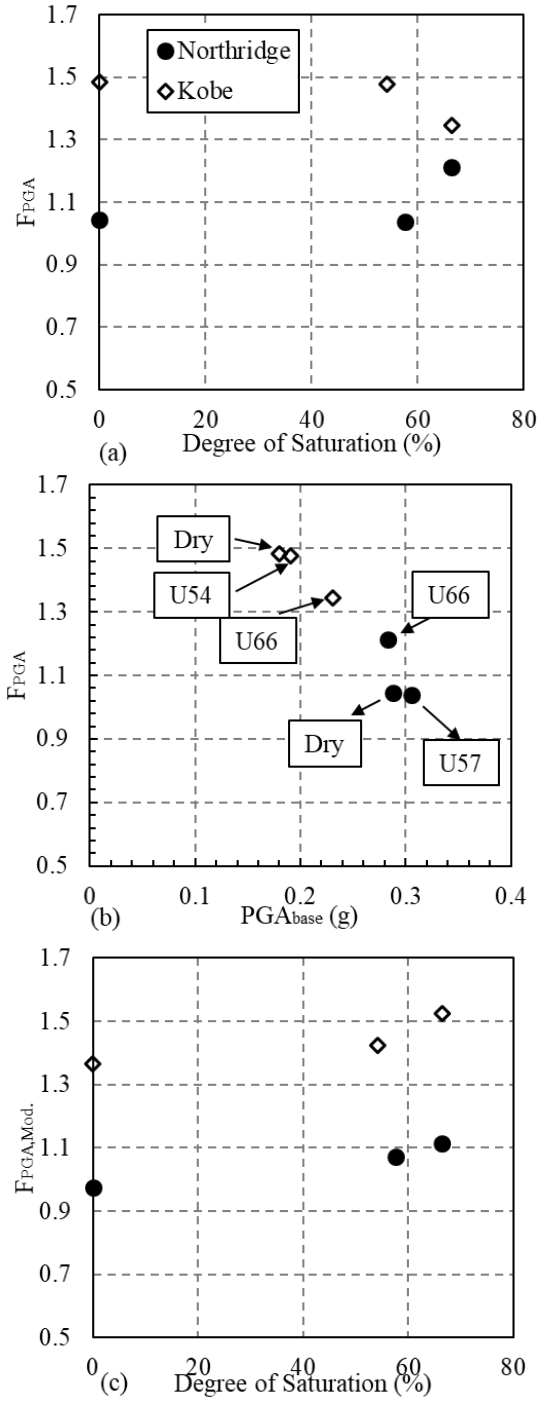

Figure 9-17. (a) PGA amplification factor versus degree of saturation (b) Variations of PGA amplification factor for different base PGA (c) Modified PGA amplification factor versus degree of saturation

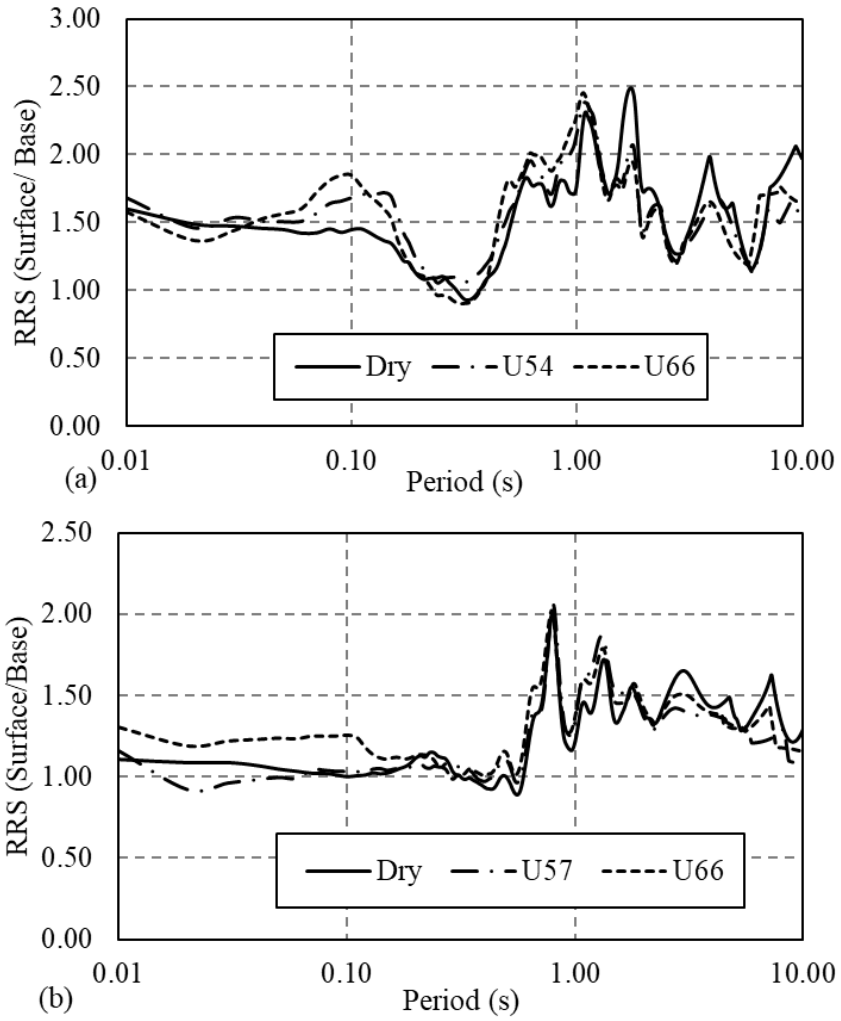

Figure 9-18. Ratio of response spectra for (a) Kobe and (b) Northridge motions

In order to assess the variations of the energy build-up during the seismic events in dry and partially saturated soils, time histories of Arias intensity were obtained for all the captured motions. The time histories of Arias intensity for captured surface motions, normalized by dividing by the maximum Arias intensity of the base motion, are shown in Figure 9-19. The unsaturated sand layers showed higher energy amplifications for both Kobe and Northridge motions. For the case of Kobe motion, the unsaturated soil layer with 54% degree of saturation showed a considerably higher energy amplification during the seismic event.

The higher values of Arias intensity for the unsaturated soils demonstrate that, given the variations of amplification factors over different periods, partial saturation led to an overall higher intensity amplification than the similar dry soil. Although the Arias intensity time histories were normalized with respect to the energy level of the base motion, it should be noted that the energy amplification during different input motions could be a function of the base motion intensity, similar to the dependency of F_{PGA} on PGA_{base}. This extra effect, however, has not been separated from the influence of partial saturation on the Arias intensity, and therefore is embedded in the observed trend in Figure 9-19.

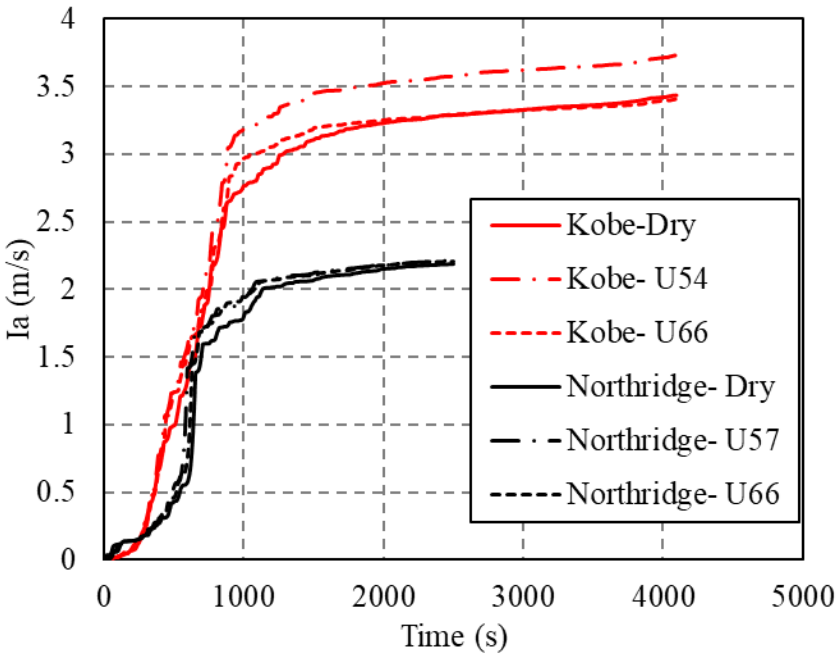

Figure 9-19. Arias intensity time histories of dry and unsaturated sand layers under Kobe and Northridge motions

Variations of seismic settlement over degree of saturation of sand layers are illustrated in Figure 9-20. The settlement of unsaturated sand layers appeared to be consistently lower than the ones in dry condition, which was similarly observed by Ghayoomi et al. (2011) and is likely due to the increased stiffness of the unsaturated medium. The settlements caused by Kobe motion were

higher than the ones observed during Northridge motion, which was due to its longer duration and higher intensity.

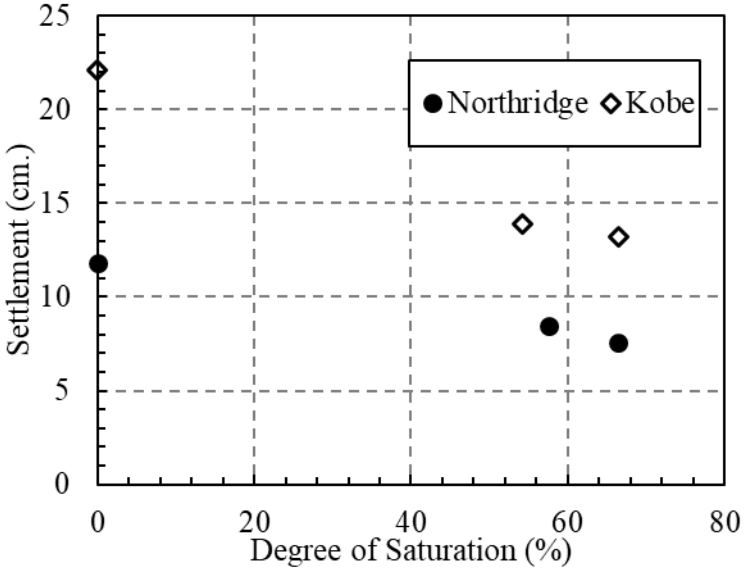

Figure 9-20. Seismically-induced settlements, resulted from Kobe and Northridge motions, versus degree of saturation

9.4. Summary and Conclusions

The results of centrifuge seismic experiments on dry, partially-saturated, and saturated specimens under scaled Northridge and Kobe motions were presented in this chapter. Steady-state infiltration technique was used to generate a uniform degree of saturation field and different degrees of saturation were obtained by changing the inflow discharge velocity. The results of seismic modeling were presented in terms of normalized acceleration, settlement, and Arias intensity time histories as well as PGA amplification factor, FFT amplitude, RRS, and lateral deformation profiles for different specimens.

In contrast with the previously-believed assumption, surface-to-base PGA amplification factor was found to be higher for unsaturated conditions especially for the test with lower degree of

saturation. The observed trend for PGA amplification factors was a function of depth where F_{PGA} values were mostly lower in unsaturated soils within the deeper instrumented levels. The acceleration amplification was frequency-dependent showing higher amplification within short-period ranges. Similar to the observed trend for F_{PGA}, the surface-to-base amplification ratio of accumulated energy was higher within the unsaturated sand layers during the earthquake. However, lower seismic settlement and lateral deformation were captured for the unsaturated sands due to their increased stiffness. The change in frequency content due to partial saturation was negligible as a result of low matric suction limit of the tested sand. Acceleration amplification factor was a function of motion intensity where higher F_{PGA} values were obtained under Kobe motion as a result of its lower PGA. Seismically induced settlements were higher for sand layers triggered by Kobe motion due its higher energy level. In addition to assessing the effect of partial saturation on seismic site response, this research project aimed to evaluate the uncertainty introduced in site response analysis as a result of seasonal water table fluctuations. To that end, the results of numerical modeling, that considered the effect of water table fluctuations into the site response analysis, will be presented in the next chapter.

CHAPTER X

PARAMETERIC ANALYSIS ON THE UNCERTAINTY IN SITE RESPONSE DUE TO WATER TABLE FLUCTUATIONS

10.1. Introduction

This chapter discusses the effect of water table fluctuations and the uncertainty in seismic site response analysis. The difference between degree of saturation of soils at the time when the shear wave velocity is measured and the time that an earthquake happens leads to different soil properties at the time of seismic event from those considered in common site response analysis. This difference in soil properties introduces an uncertainty in site response analysis, which is a crucial step towards geotechnical and structural seismic design.

In this chapter, numerical analyses were performed using the DEEPSOIL program considering an equivalent-linear approach. Data from surface-downhole station pairs, as part of the Kiban-Kyoshin network (KiK-net) database, were used as a baseline ground motion data for validation and parametric evaluation. The depth of water table was changed from the baseline depth

(inferred from the compression wave velocity profile at the site) and the influence of different parameters (i.e. small-strain shear modulus, damping, modulus reduction factor, unit weight, and soil type) was evaluated. The effect of varying each parameter, as a result of water table fluctuation, was investigated through inspecting the changes in different surface-to-base amplification characteristics including Ratio of Response Spectra (RRS), Fast Fourier Transform Transfer Function (TF), and their residual values. This parametric study can be used as the first step towards a statistical analysis of the uncertainty in SSRA due to water table fluctuations. In addition, motion characteristics considering variation in all soil properties are presented where the uncertainty induced in SSRA as a result of water table fluctuation in a single case is demonstrated.

10.2. Methods

10.2.1. Site Selection

An instrumented site was selected from the suite of KiK-net sites, which is suitable for 1-D site response analysis (Kaklamanos et al. 2015). NMRH04 site was selected in this study since it contains sandy soil as the surficial layers, which allows the partial saturation to have a more profound influence on the site response as higher matric suction values can cause a more considerable effect on dynamic soil properties. Further, NMRH04 is a soft soil site, categorized by NEHRP site class of E, where studying seismic site response is of interest. In addition, the depth of water table was estimated to be at 8 m for this site, which was deeper comparing with the other sites. This can lead to higher matric suction values (considering a linear suction profile) and intensify the effect of water table fluctuation on the site response. Station NMRH04 is located in Nemuro subprefecture on eastern Hokkaido Island in Japan (Figure 10-1). The site can

be classified as site class E, according to *NEHRP provisions* (FEMA, 2009), consisting 185 m layer of Quaternary soil over layers of sandstone and siltstone. The profiles of shear and compression wave velocities are shown in Figure 10-2. In addition, selected information on the monitored site is listed Table 10-1.

Although the site mainly consists of sand layers, to evaluate the effect of material type on the uncertainty in site response due to water table fluctuation, hydraulic characteristics of Bonny silt were also used in the analyses. The employed SWRCs and van Genuchten fitting parameters, for a typical fine well-graded sand as well as Bonny silt, were previously presented in Chapter 3. It should be noted that since the input parameters of the baseline model were estimated using the empirical correlations with shear and compression wave velocities, the input parameters for soil profiles with fluctuated water table were solely assessed using the assumed SWRCs for the materials. The procedure for estimating those input parameters will be discussed in the next sections.

Table 10-1. Selected information on the Kik-net station used in this study

Parameter	**Value**
Latitude (deg)	43.3953
Longitude (deg)	145.1264
$\overline{V}_{s,30}$ (m/s)	168
NEHRP Site Class	E
Depth to bedrock (m)	185
Depth of downhole seismometer (m)	216
Natural frequency (Hz)	0.40
Geologic age	Quaternary

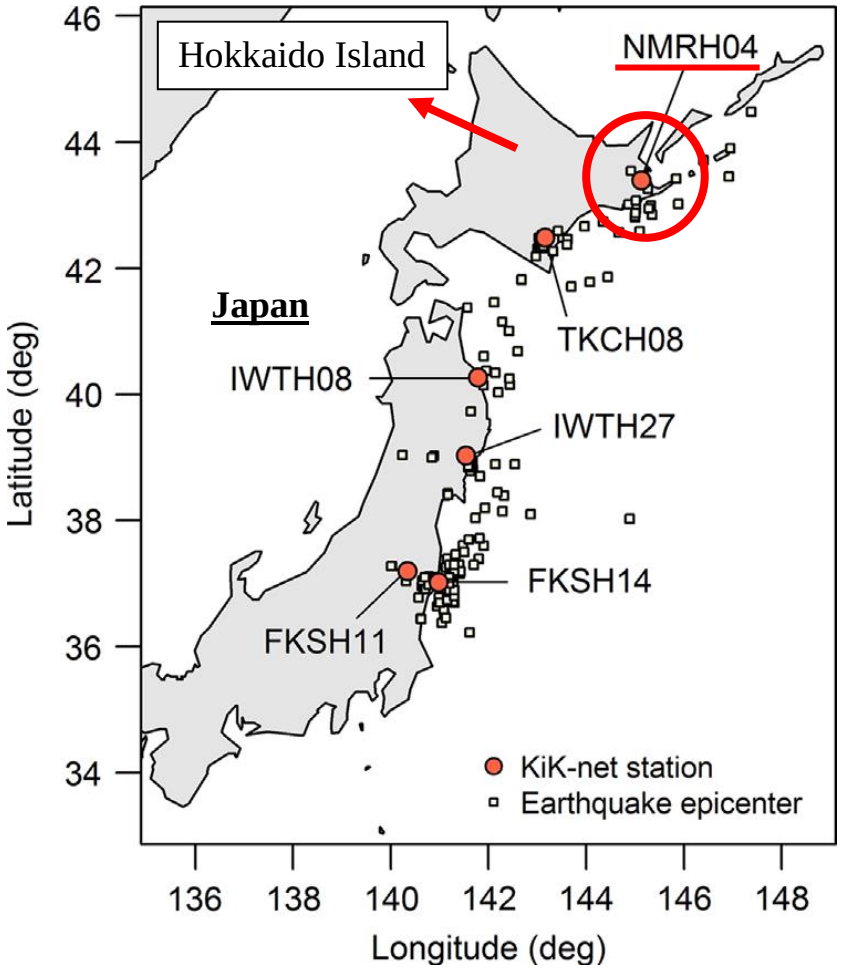

Figure 10-1. The location of station NMRH04 (after Kaklamanos et al. 2015)

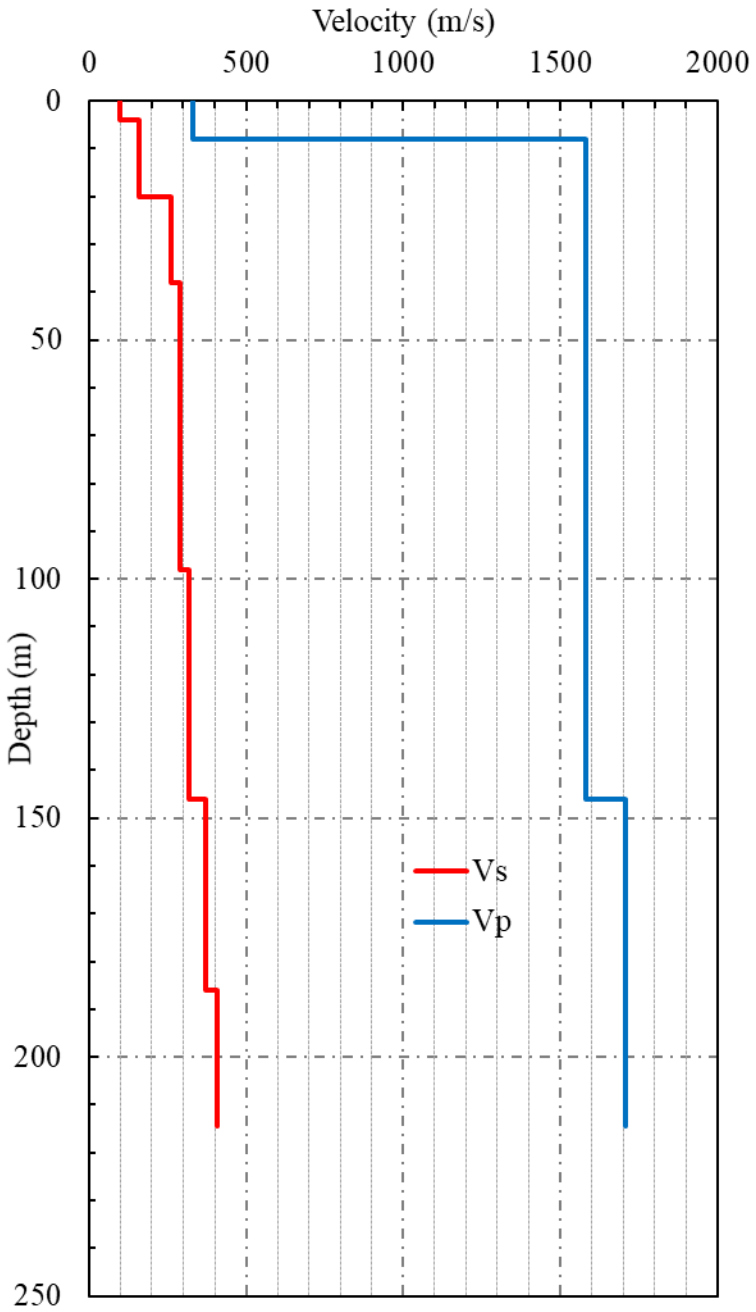

Figure 10-2. Shear and compression wave velocity profiles at NMHR04 site

10.2.2. Equivalent Linear Site Response Models

Equivalent-linear analysis was performed for this study as it could produce sufficiently accurate response for PGA_{base} less than 0.2g (Assimaki et al. 2008) or strain levels less than 0.3% (Kim and Hashash 2013), where the equation of motion for a multi-degree-of-freedom system is solved in frequency domain. The values of shear modulus and damping are iteratively modified in this method to the effective level of shear strain (i.e. 0.65 times maximum shear strain) in different soil layers at each step. The empirical equations proposed by Boore (2016) were used to estimate the unit weight of soil layers based on the measured profiles of shear and compression wave velocities. The shear wave velocities were input to the program, and the small-strain shear moduli for different soil layers were calculated in DEEPSOIL using the following generic equation:

$$G_0 = \rho V_s^2 \qquad 10\text{-}1$$

where G_0 is the small-strain shear modulus, ρ is the density of the soil layers, and V_s is the shear wave velocity.

The modulus reduction as well as damping curves were generated using the empirical framework proposed by Zhang et al. (2005) (Equations 2-3 and 2-12) since it takes geologic age of soil deposits into consideration, which leads to a better performance comparing to Darandeli's equation when using the KiK-net database (Kaklamanos et al. 2015). The formulations proposed by Zhang et al. (2005) require mean effective stress, PI, and geologic age of soil deposits as their inputs. Herein, the effective stress in partially saturated zone was calculated considering suction stress equation proposed by Lu et al. (2010), i.e. Equations 2-13a and 2-13b. In order to find

suction stresses in soil layers, typical hydraulic characteristics of sand and silt were used. In addition, hydrostatic matric suction variations with no precipitation/evaporation was assumed when calculating the values of matric suction and degree of saturation above water table. The PI value was assumed to be zero for the site as it consisted of sandy soil. The geologic age of soil deposits was found from the descriptions provided in the observation logs. Since the saturated layers are known to have compression wave velocities of 1000 to 2000 m/s (Hasselstroem 1969, Haeni 1986, Grelle and Guadagno 2009), depth of water table was estimated as the corresponding depth where compression wave velocity reached 1500 m/s.

10.2.3. Incorporating Water Table Fluctuation in Numerical Site Response Analysis

The water table level was altered to two extreme levels: at the ground surface and 16 m below the ground surface, resulting in different soil properties including shear wave velocity, unit weight, shear modulus reduction curves, and damping. Variations of each parameter, aligned with the fluctuation of water table, was determined using the baseline values in the soil profile with 8 m depth of water table as a reference (i.e. the original estimated water table). The following equations were used to link between the unit weight of soil layers with different water table levels:

$$\gamma_t = \gamma_d(1 + \omega) \tag{10-2}$$

$$\frac{\gamma_{t1}}{\gamma_{t2}} = \frac{(1 + \omega_1)}{(1 + \omega_2)} \tag{10-3}$$

where γ_t is the total unit weight of wet soil, γ_d is the dry unit weight, and ω is the moisture content of soil layers. Given the values of moisture content at different levels, unit weight of soil layers with 8 m depth of water table, and using the above equations, total unit weight of soil layers with different groundwater levels could be inferred. The values of moisture content were estimated using the following equation, assuming 0.65 and 2.65 as the void ratio and specific gravity, respectively:

$$\omega = \frac{S.e}{G_s} \tag{10-4}$$

where S is degree of saturation, e is the void ratio, and G_s is the specific gravity. The values of degree of saturation were derived from the approximated SWRC based on the material type (i.e. either sand or silt). The unit weight profiles, obtained using the explained procedure, for sand and silt layers with different levels of water table are shown in Figure 10-3 (a) and (b), respectively. The difference between the unit weight profiles of sand and silt layers is reflective of the SWRC of the materials. Since the moisture content of the reference profile, in the sand layers, significantly decreased within a short distance above its water table, a sharp increase in the estimated unit weight profiles with water table at and 16 m below the ground surface is observed at those depths. Likewise, because of the steep decrease in moisture content of the profile with water table at 16 m below the ground surface, unit weight values of that profile are substantially decreased within a range of 2 m above its water table.

The unified equation for estimating small-strain shear modulus in dry, unsaturated, and saturated conditions, proposed by Dong et al. (2016), was employed to estimate the divergence of G_0 values in soil layers with fluctuated water table from those of the soil layer with water table at 8 m:

$$G_0 = G_0^{Sat}\left(\frac{1}{S_e}\right)^{9.6.n^{-6}}\left(\frac{\sigma'}{P_{atm}}+1\right)^{\gamma_0} \quad (10\text{-}5)$$

where G_0^{sat} is the small-strain shear modulus of saturated soil without confinement, S_e is the effective degree of saturation (Equation 2-13, c), n is the van Genuchten fitting parameter, and γ_0 is an empirical fitting parameter, which was assumed as 0.5 in this study. Since the value of G_0^{sat} is constant for soils with different degrees of saturation, the shear wave velocity for soil layers with fluctuated water table was obtained with respect to those values measured for the profile with water table at 8 m below ground using the following ratio:

$$\frac{G_{01}}{G_{02}} = \left(\frac{S_{e2}}{S_{e1}}\right)^{9.6n^{-6}}\left(\frac{\left(\frac{\sigma'_1}{P_{atm}}+1\right)}{\left(\frac{\sigma'_2}{P_{atm}}+1\right)}\right)^{\gamma_0} \quad (10\text{-}6)$$

The shear wave velocity profiles, obtained using the above ratio, for sand and silt layers with different levels of water table are shown in Figure 10-4 (a) and (b), respectively. The difference between the shear wave velocity profiles in the unsaturated zones of sand and silt layers is because of the different SWRC of the materials, which led to different effective degrees of saturation as well as different power "n". However, within the saturated zones, since the effective degree of saturation is one, the difference between V_s profiles is only a reflective of the change in effective stress due to the water head variations.

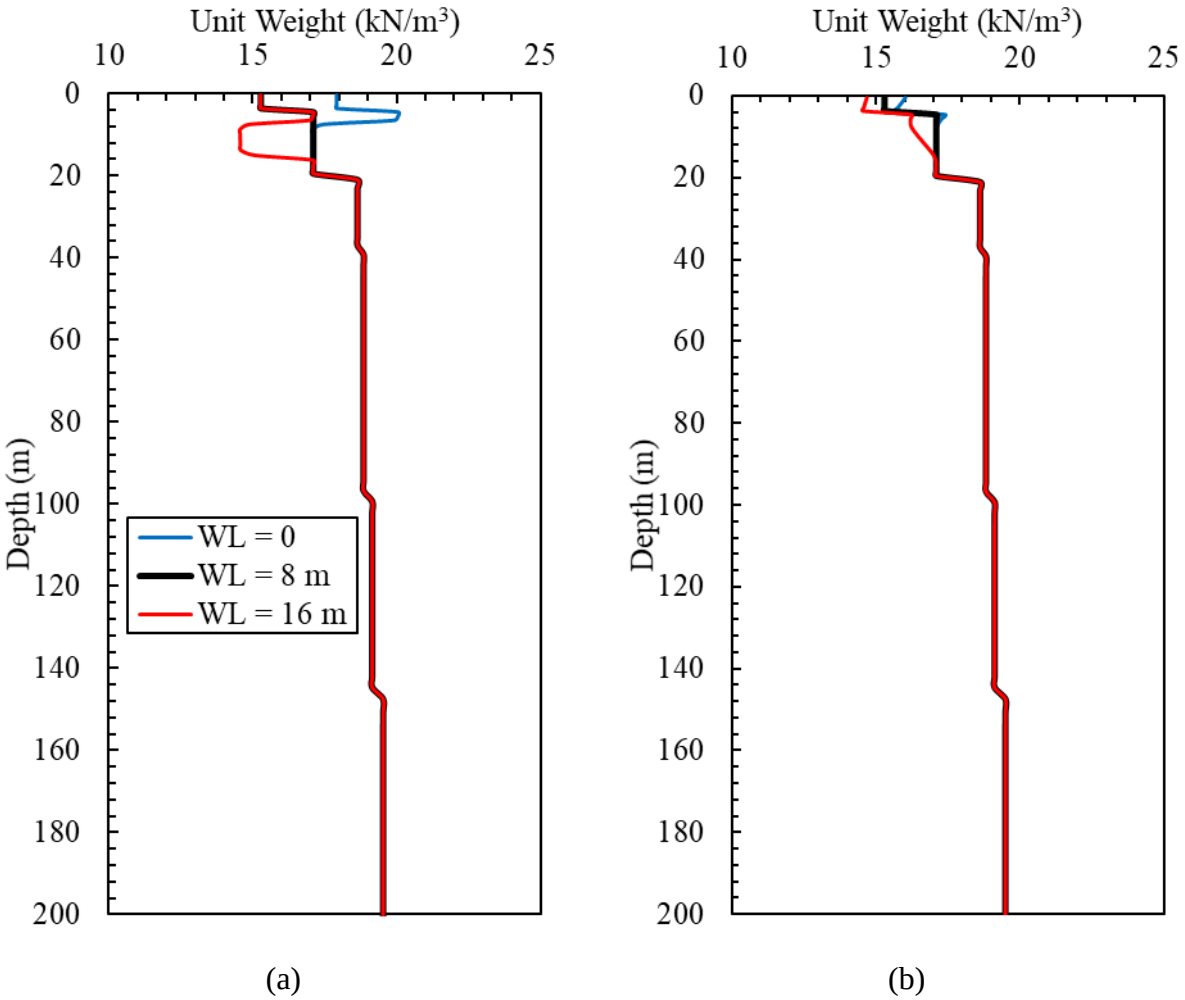

(a) (b)

Figure 10-3. Unit weight variations due to water table fluctuations assuming (a) fine sand and (b) silt layers

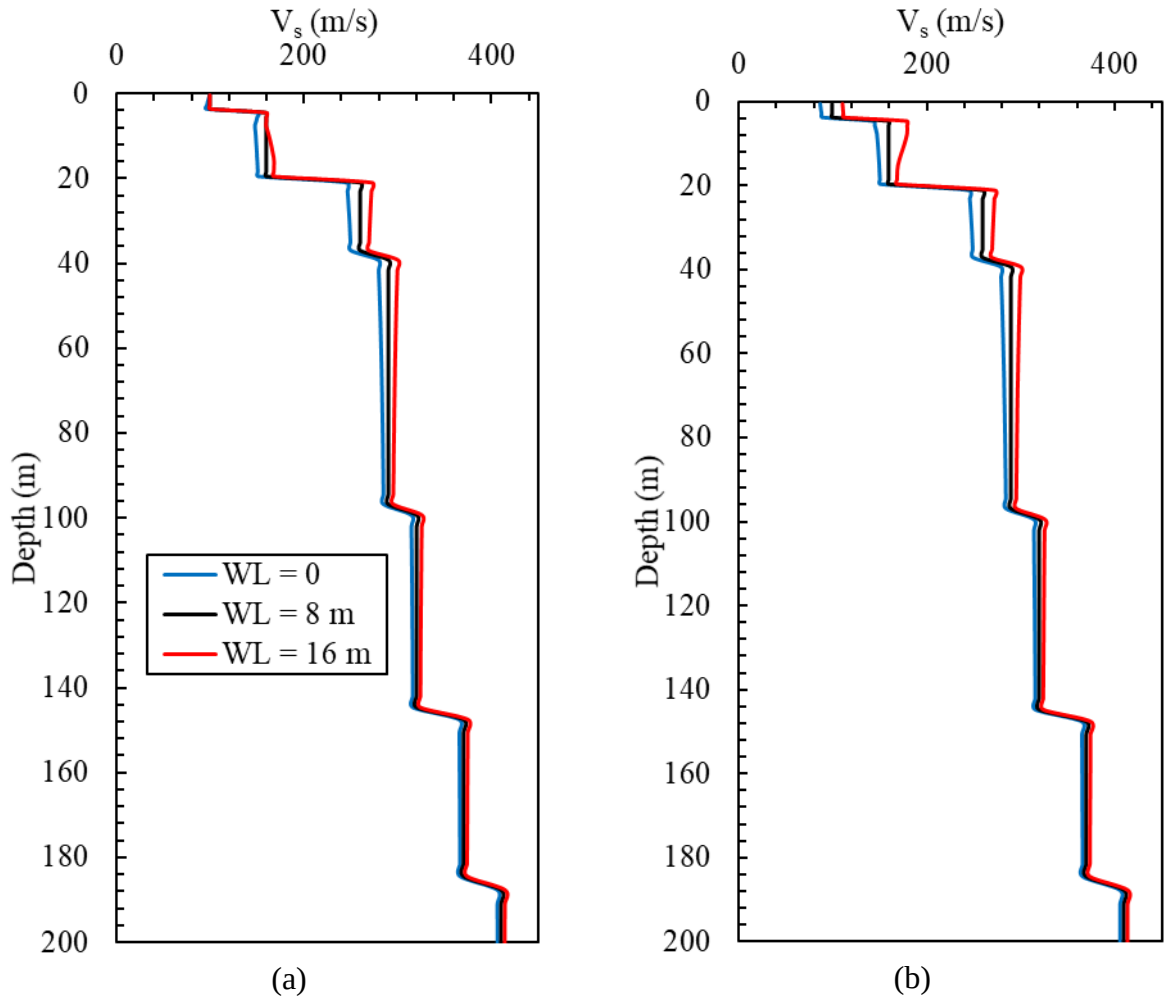

Figure 10-4. Shear wave velocity variations due to water table fluctuations assuming (a) fine sand and (b) silt layers

Damping curves were obtained using empirical equations proposed by Zhang et al. (2005), as a function of effective stress within the soil layers. The effective stress in different soil layers was estimated considering the suction stresses caused by partial saturation, which varied depending the water table level. As discussed in Chapter 2, suction stress is a function of both degree of saturation as well as matric suction (Equation 2-13b), where both parameters vary within the soil layers as a function of depth of water table. Damping curves for six selected depths in sand and silt layers are shown in Figure 10-5 and Figure 10-6, respectively.

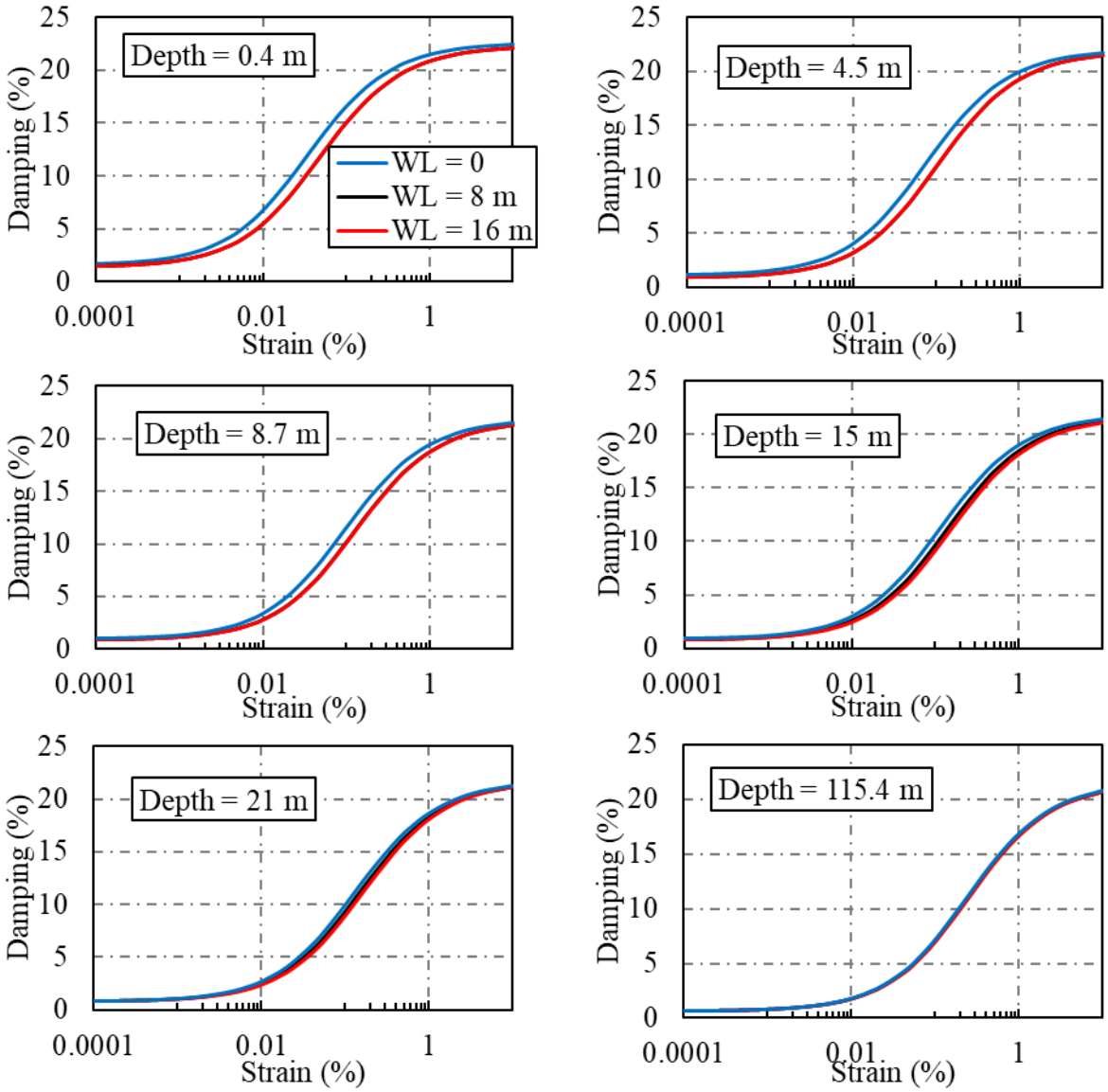

Figure 10-5. Damping variations due to water table fluctuations at different depths assuming a fine sand layer

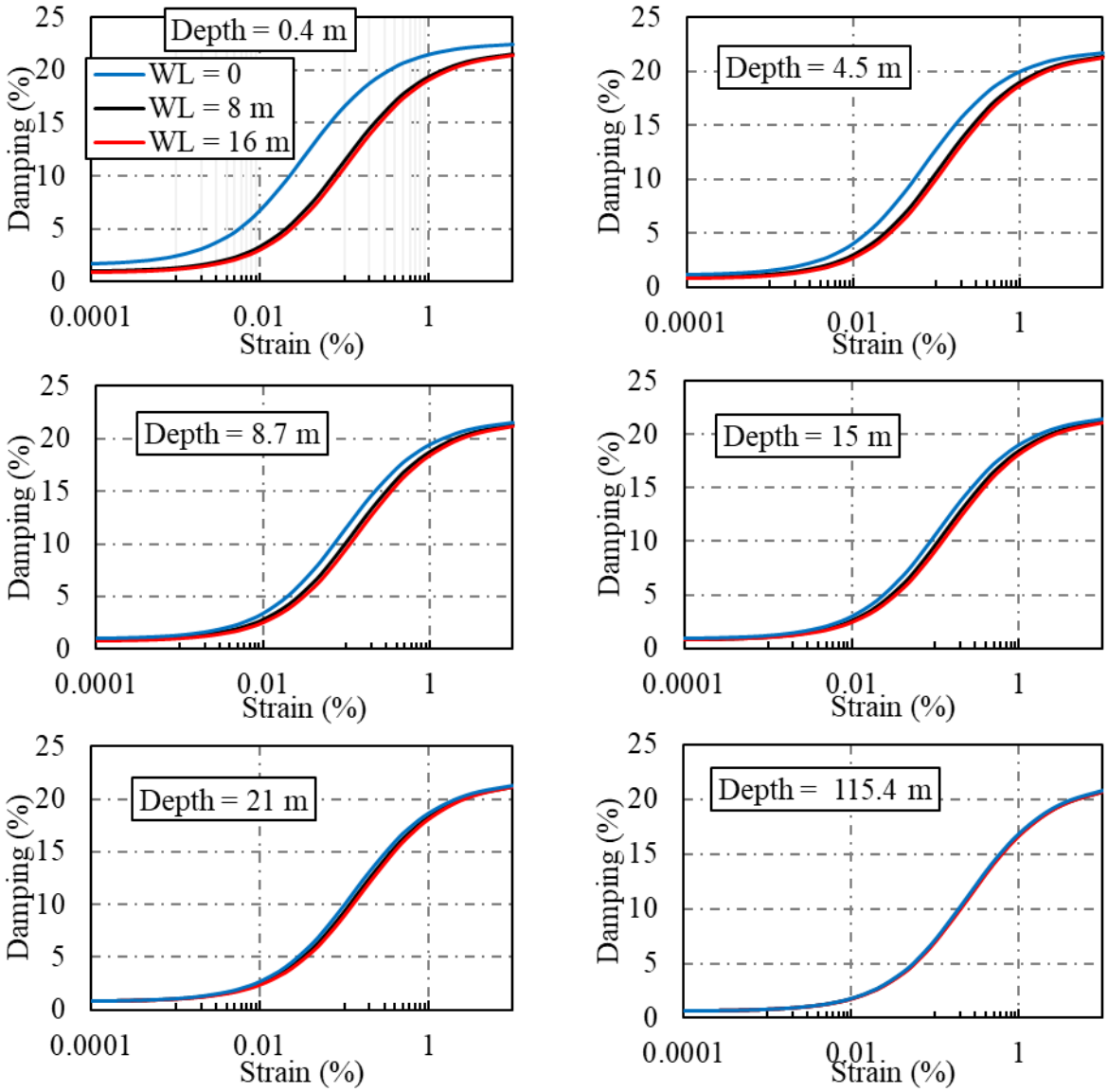

Figure 10-6. Damping variations due to water table fluctuations at different depths assuming a silt layer

Similar to damping, shear modulus reduction curves were also obtained using empirical equations proposed by Zhang et al. (2005), where partial saturation influenced the effective stress values. Shear modulus reduction curves for six selected depths in sand and silt layers are shown in Figure 10-7 and Figure 10-8, respectively.

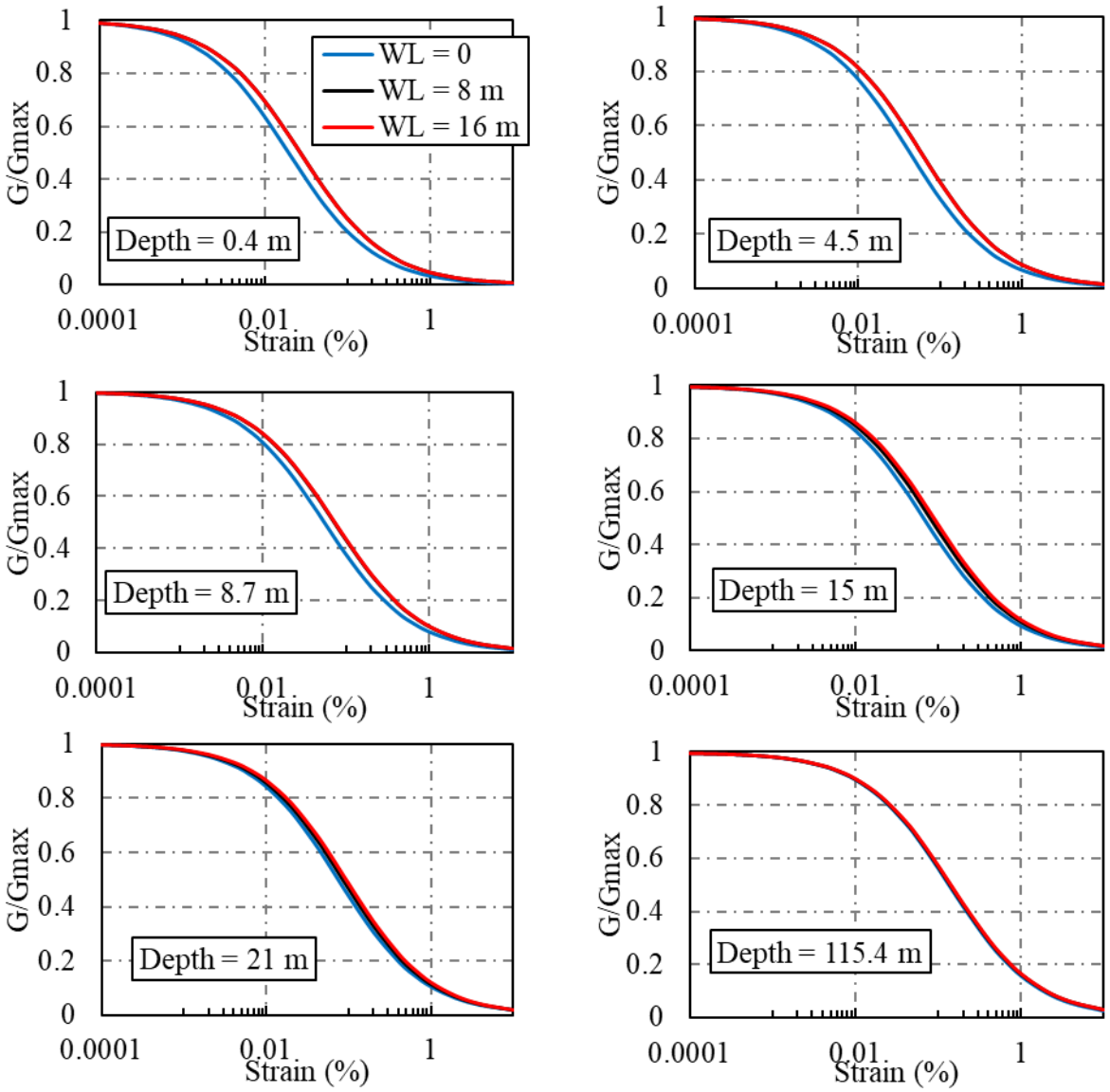

Figure 10-7. Variations of modulus reduction curve due to water table fluctuations at different depths assuming a fine sand layer

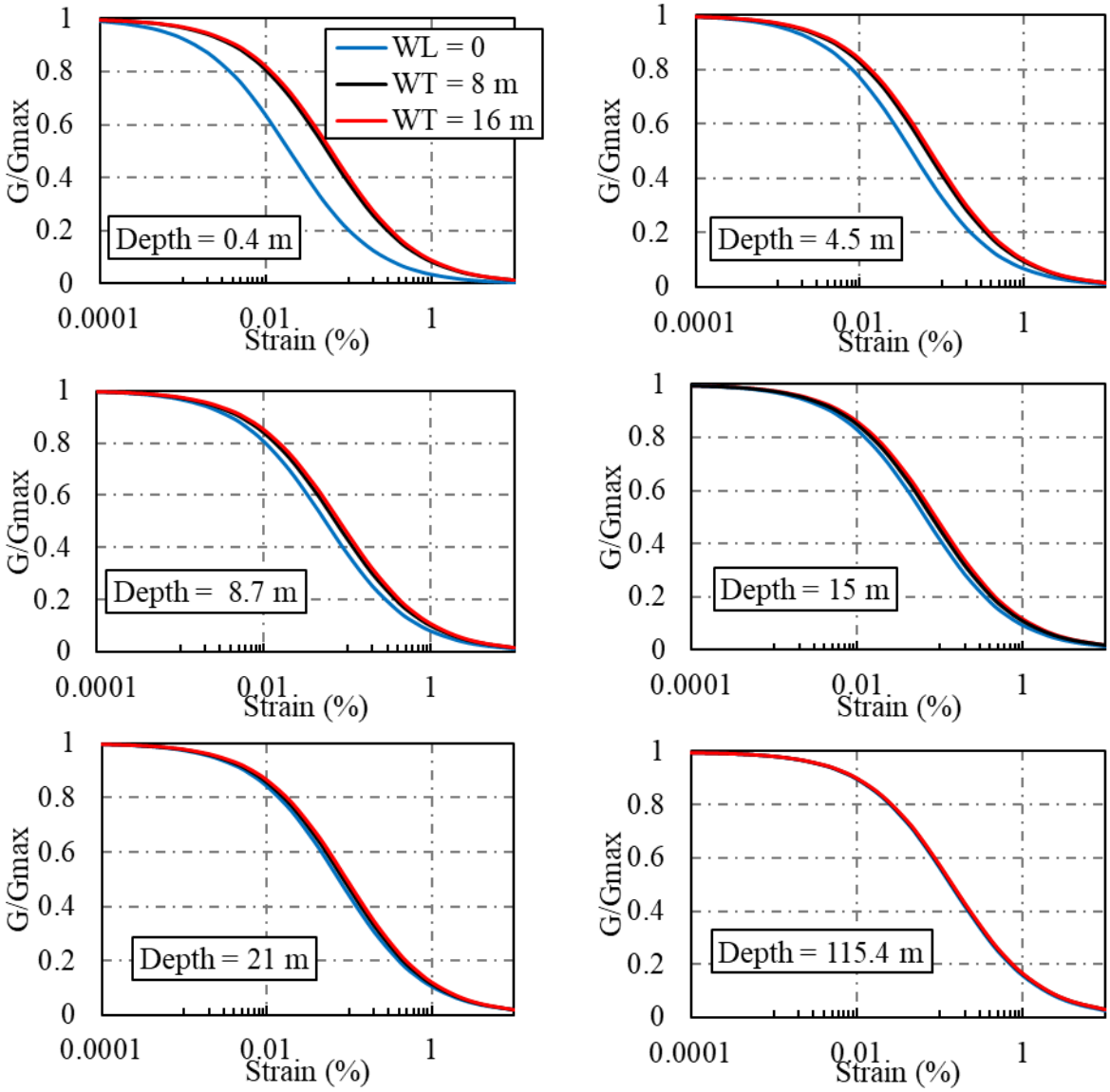

Figure 10-8. Variations of modulus reduction curve due to water table fluctuations at different depths assuming a silt layer

10.2.4. Input Motion Characteristics

The KiK-net database provides the acceleration time series of 23 seismic events at the location of NMRH04 site, recorded at the ground surface and bedrock level, in North-South (NS) and East-West (EW) directions. The number of motions with the corresponding $PGA_{bedrock}$ range is listed in Table 10-2. The motion selected in this study, with $PGA_{bedrock}$ of 0.018 g, is among the motions with low intensity; the characteristics of which in EW and NS directions are illustrated in Figure 10-9 and Figure 10-10, respectively. The selected motion encompasses a wide range of frequencies (i.e. from 0.01 Hz to 10 Hz) where the effect of partial saturation or water table fluctuations could be observed within different frequency ranges.

Table 10-2. Number of recorded motions, at the location of NMRH04 site, with different PGA levels

Number of Motions	**$PGA_{Bedrock}$ Range**	**Intensity**
2	PGA > 0.1 g	High
41	0. 01 g < PGA< 0.1 g	Medium
7	PGA < 0.01 g	Low

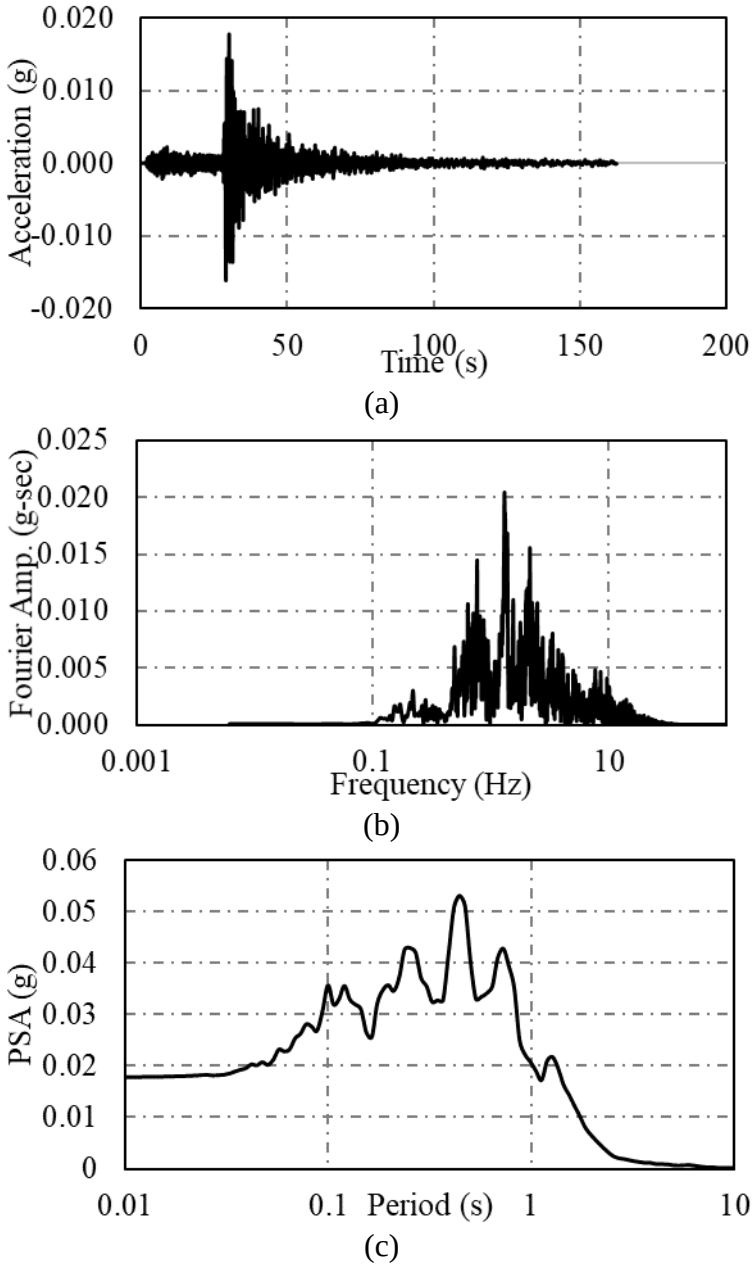

Figure 10-9.Input motion characteristics in EW direction; (a) acceleration time history (b) Fourier amplitude (c) 5% damped pseudo-spectral acceleration

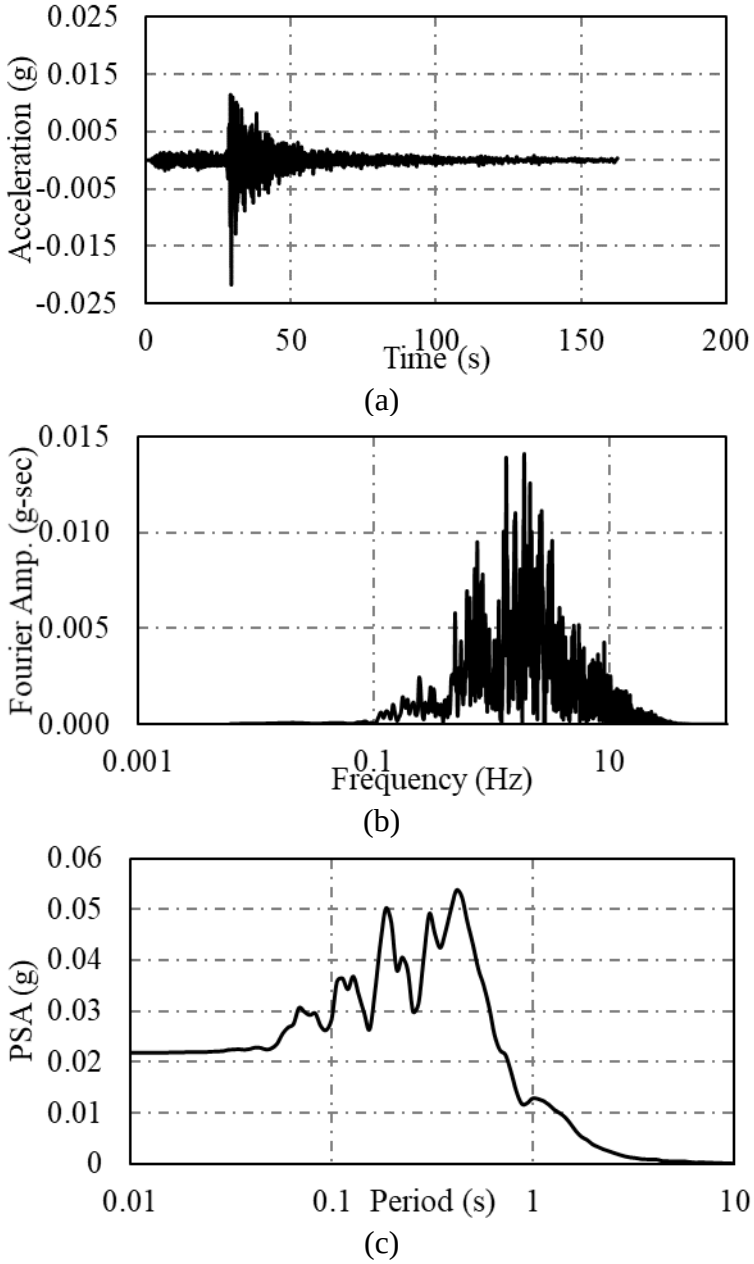

Figure 10-10. Input motion characteristics in NS direction; (a) acceleration time history (b) Fourier amplitude (c) 5% damped pseudo-spectral acceleration

10.3. Verification of Numerical Modeling

The numerical analysis in this study was verified against another Equivalent-Linear (EL) analysis, using SHAKE2000 (Ordonez 2000), as well as Nonlinear (NL) analysis, using DEEPSOIL, for the same site reported by Kaklamanos et al. (2015). The soil profile in NMRH04 location was numerically shaken under both EW and NS input motions through an equivalent linear analysis in DEEPSOIL. Similar to the conventional site response procedures, the soil above the water table was assumed to be completely dry, and the effect of partial saturation was not considered in this step. The resulting pseudo-spectral acceleration graphs were plotted against those recorded using the accelerograms at the ground surface (observed motions) as well as the results of Kaklamanos et al. (2015); shown in Figure 10-11.

Although the equivalent linear analysis in Kaklamanos et al. (2015) was performed using a different program, both equivalent linear models, in SHAKE and DEEPSOIL, led to very similar spectral acceleration values at the surface. This is attributed to the similar identified layers in the programs, soil properties, and analysis type. Although the monitored values are different from those obtained numerically, especially under NS motion, this variance is a result of a number of uncertainties in site response analysis including the estimated soil properties, modeling a 3D motion using a simplified 1D analysis, and potentially the depth of groundwater table at the time of seismic event. Overall, the observed trends validate the procedure of the numerical modeling in this study.

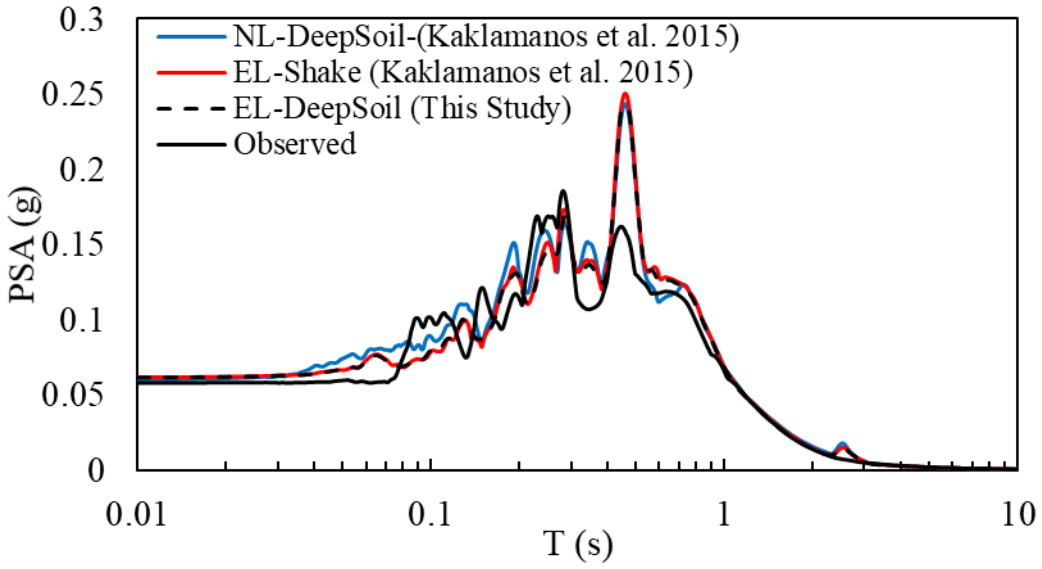

(a)

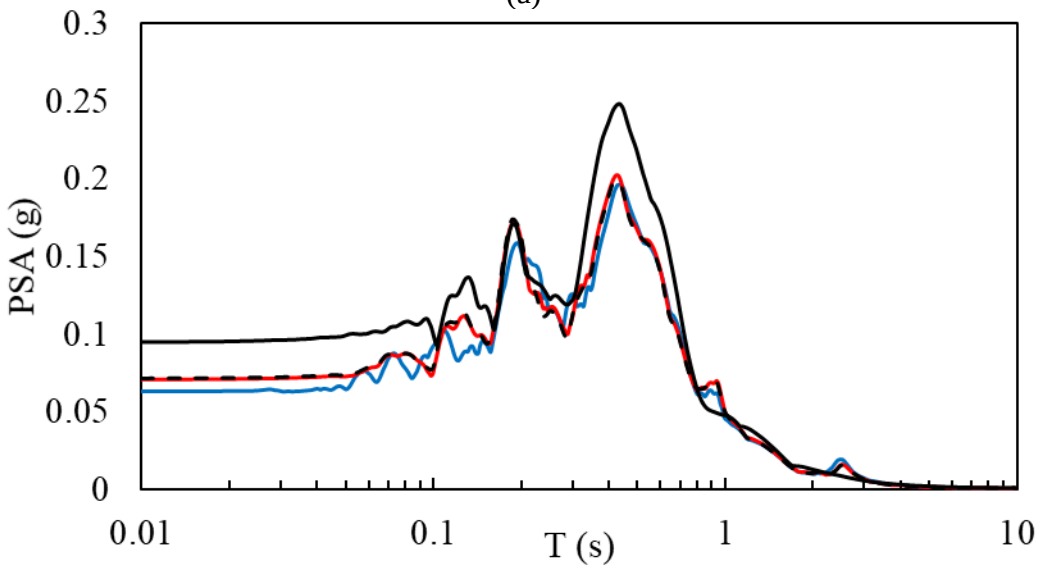

(b)

Figure 10-11. Verification of DEEPSOIL models against the models from Kaklamanos et al. (2015) under the input motions in (a) EW direction and (b) NS direction

10.4. Sensitivity analysis of the effect of variations in different parameters due to water table fluctuations on site response analysis

In order to assess the extent of influence of variations in each soil parameter as a result of water table fluctuations, soil profiles with water tables at the ground surface (representing fully saturated soil layer) and water tables at 8 and 16 m below the ground surface were numerically

analyzed under the same input motion. For assessing the sensitivity of the analysis to each parameter, only one parameter was changed at a time for soil profiles with different water table levels. The surface motion for each analysis was calculated as the geometric mean of EW and NS ground motions. This combined result of each analysis was then post-processed to obtain different motion characteristics including surface-to-base Ratio of Response Spectra (RRS) as well as surface-to-base FFT transfer functions (TF). To evaluate the divergence of each parameter from the observed curves, residual curves for both RRS and FFT transfer functions were obtained using the following equations:

$$RRS_{Residual}(T) = ln\big(RRS_{Observed}(T)\big) - ln\big(RRS_{Predicted}(T)\big) \quad \text{10-7(a)}$$

$$TF_{Residual}(f) = ln\big(TF_{Observed}(f)\big) - ln\big(TF_{Predicted}(f)\big) \quad \text{10-7(b)}$$

In addition, normalized difference between the observed and predicted values were used to quantify the change in each analysis with respect to those observed at the ground motion:

$$RRS_{Ratio}(T) = [RRS_{Observed}(T) - RRS_{Predicted}(T)]/RRS_{Observed}(T) \quad \text{10-8(a)}$$

$$TF_{Ratio}(f) = [TF_{Observed}(f) - TF_{Predicted}(f)]/TF_{Observed}(f) \quad \text{10-8(b)}$$

Herein, residuals and normalized difference ratio for the analyses when different parameters were influenced by the change in water table level are presented. All the analyses were performed considering sand and silt hydraulic characteristics to evaluate the effect of different soil properties.

10.4.1. The Effect of G_0 Variations

Assuming Fine Sand Properties

The results of numerical site response analyses with different depths of water table, considering sand hydraulic characteristics, where only small-strain shear modulus (or corresponding shear wave velocity) was varied, are presented in this section. Observed surface/base RRS graphs as well as the predicted graphs with different depths of water table are shown in Figure 10-13 (a). In addition, the residual and normalized difference ratio of RRS graphs for different water table levels are shown in Figure 10-13 (b) and (c), respectively.

The predicted RRS values in shorter periods (i.e. less than almost 1 s) increased as a result of decreasing the water table height. However, for longer periods (i.e. higher than 1 s) decreasing the height of water table led to lower RRS values. The opposite trend was observed when water table was raised to the ground surface where RRS values decreased and increased within short- and long-period ranges, respectively. According to the amplification factor for a SDOF system (Equation 2-14), the small-strain shear modulus is inversely proportional to the acceleration amplification factor. Therefore, since the shear moduli for soil layers with water table at or 16 m below the ground surface were higher and lower than the reference values, respectively, the response of soil layers at shorter periods was not captured as anticipated from the analytical equations. A peak was observed in both $RRS_{Residual}$ and RRS_{Ratio} at almost 2 s period (i.e. around the fundamental period) for all the water table levels, indicating the incapability of the numerical models to capture the exact seismic response of soil profile regardless of depth of groundwater. This difference appears to be due to other uncertainties in 1-D site response such as 3-D effects, (where overpredicted response is obtained from 1-D modeling around the natural period) and

estimating soil properties through empirical correlations. Overall, a significant divergence in the RRS graphs, due to the change in small-strain shear modulus because of water table fluctuations, was observed.

Observed and predicted surface/base FFT Transfer Functions (TF) are presented in Figure 10-13 (a). The equivalent linear numerical models were capable to accurately predict different fundamental frequencies of the soil layer (acceptable predictions were observed for the first eight peaks). However, the predicted magnitudes of TF did not completely match the observed values, especially for the first two peak. This is, partly, due to smoothening process where the observed values of TF were averaged over spans of 10 data points. Figure 10-14 shows the surface/base FFT transfer functions with a focus on frequencies up to 4 Hz. Different predicted fundamental frequencies clearly increased as a result of lowering depth of water table, which reflects a stiffer soil profile for lower water table levels. Using the observed values, the residual FFT transfer function graphs as well as the normalized difference ratios were obtained for different water table heights, which are shown in Figure 10-13 (b) and (c), respectively. The residual TF graph does not show a meaningful trend, where all the numerical models regardless of the water table level over-predicted or under-predicted the TF values within different frequency ranges.

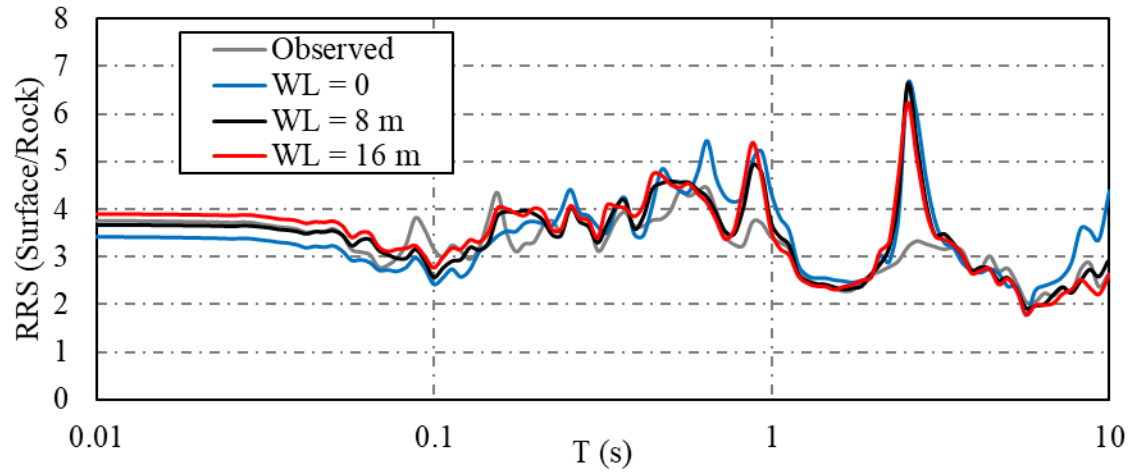

(a)

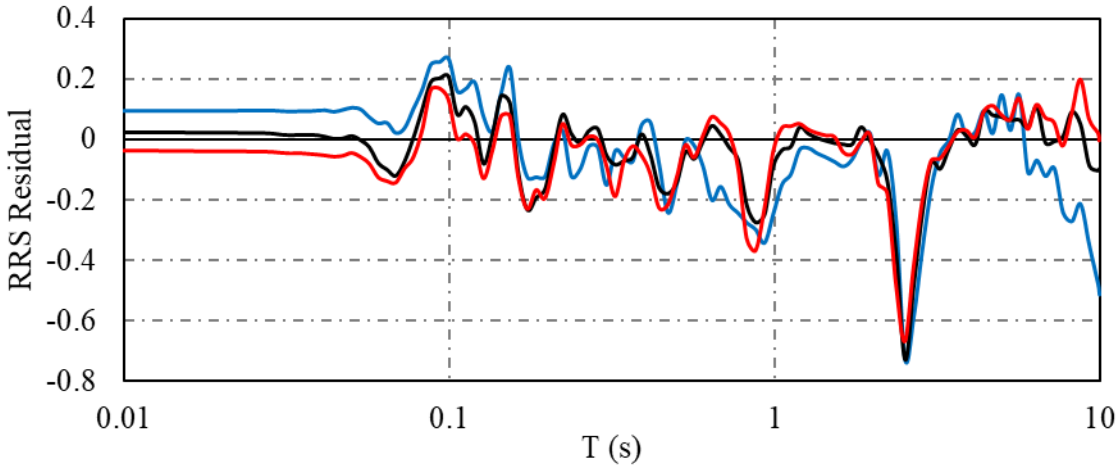

(b)

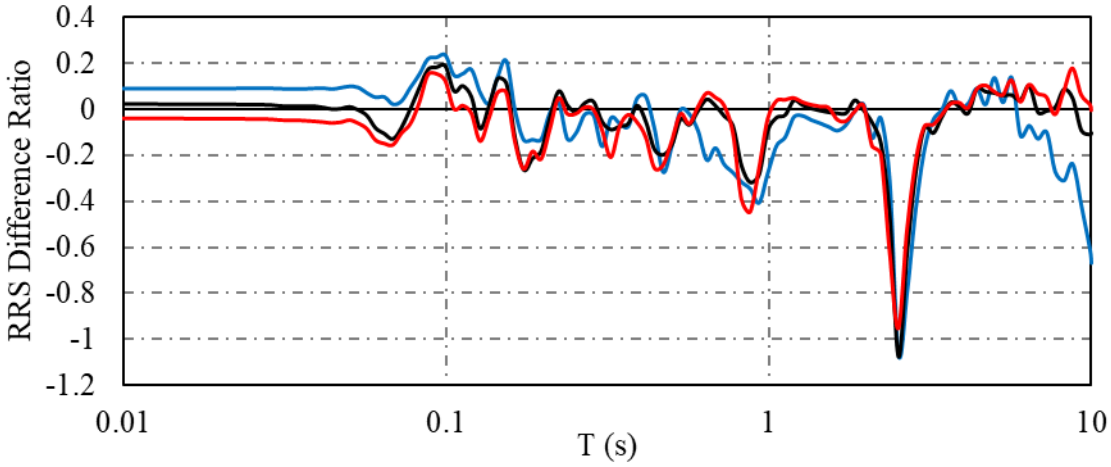

(c)

Figure 10-12. Variations of surface/base (a) Ratio of Response Spectra (b) RRS residual and (c) RRS normalized difference for soils with different water tables as a result of G_0 variations in sandy soil

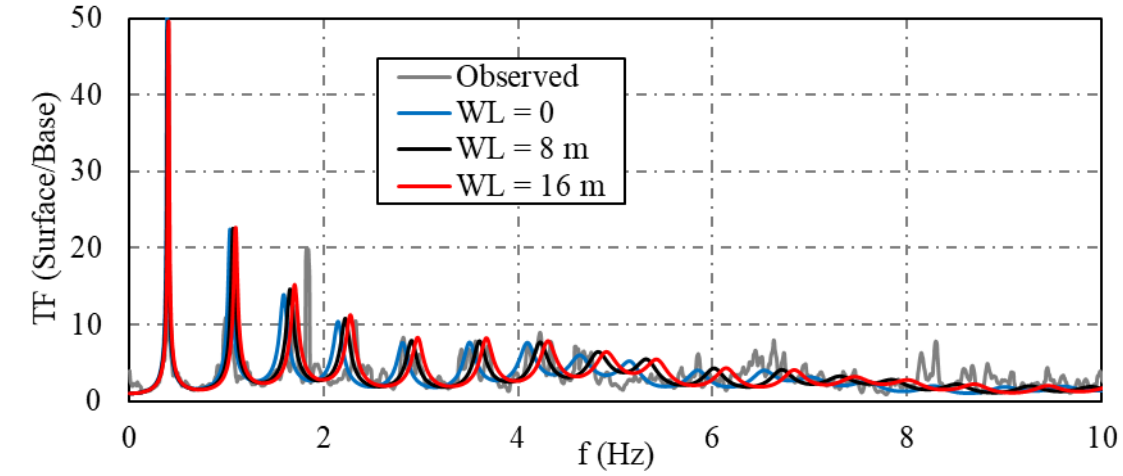

(a)

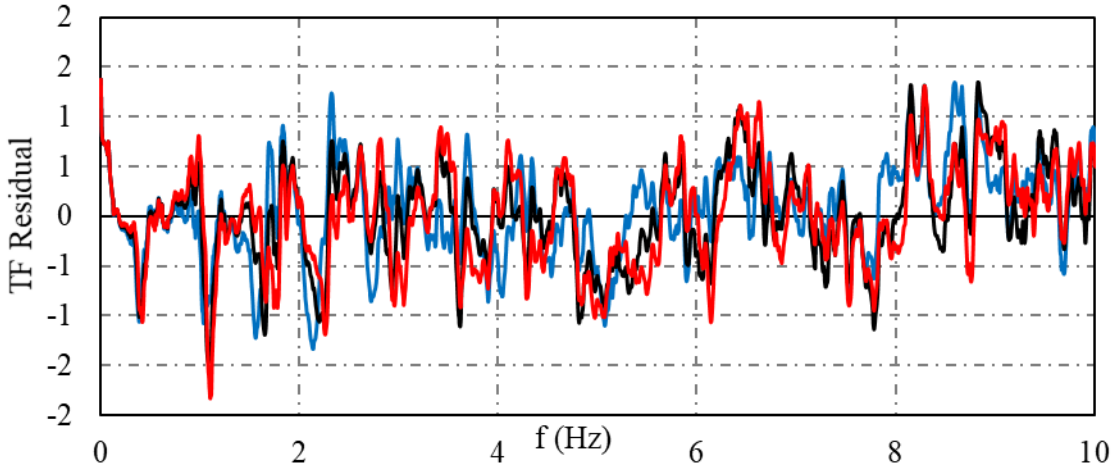

(b)

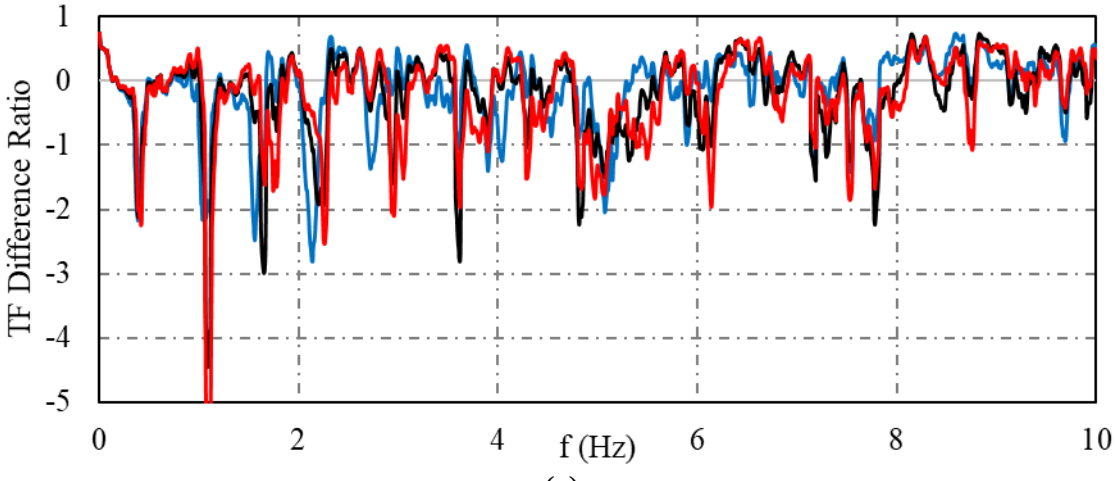

(c)

Figure 10-13. Variations of surface/base (a) FFT transfer function (b) FFT TF residual and (c) FFT TF normalized difference for soils with different water tables as a result of G_0 variations in sandy soil

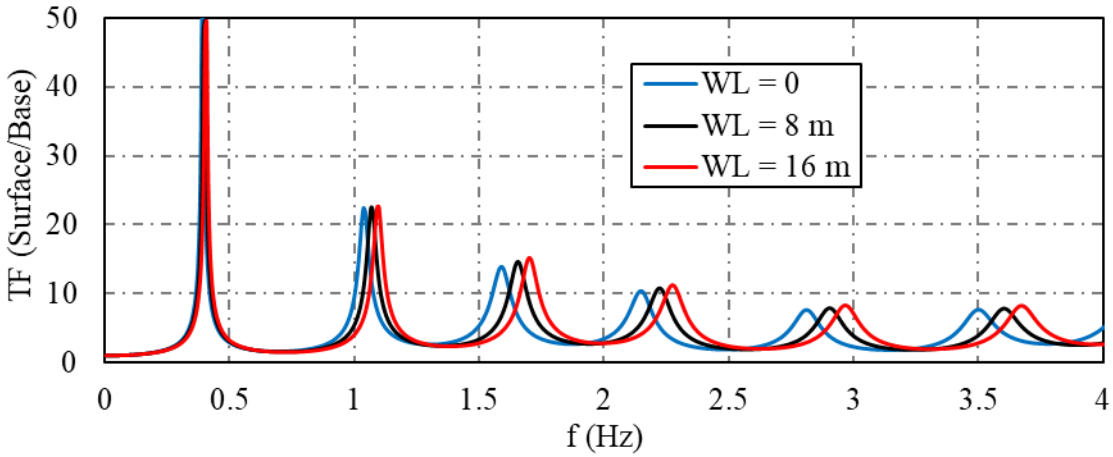

Figure 10-14. Variations of surface/base FFT transfer function for soils with different water tables as a result of G_0 variations in silty soil

Assuming Silt Properties

The results of numerical site response analyses with different depths of water table, considering silt hydraulic characteristics, where only small-strain shear modulus was varied, are presented in this section. Observed and predicted surface/base RRS graphs with different depths of water table are shown in Figure 10-15 (a). In addition, the residual and normalized difference ratio of RRS graphs for different water table levels are shown in Figure 10-15 (b) and (c), respectively. Although the values of $RRS_{Residual}$ and RRS_{Ratio} for soils with different depths of water table were closer in short periods (i.e. less than 0.1 s), the effect of water table fluctuation was more profound for silt layers than that for sand layers in periods higher than 0.1 s. For periods higher than 0.1 s, decreasing the height of water table led to substantially lower RRS values, which was indicated by higher residual values. The same peak in both $RRS_{Residual}$ and RRS_{Ratio} at almost 2 s period for all the water table levels was observed. Overall, a more significant divergence in the RRS graphs, due to the change in small-strain shear modulus because of water table fluctuation, was observed in silty soil than sandy layers. This is due to the different hydraulic characteristics

of silt and its higher values of matric suction/suction stress range than those in sand layers. In addition, the increase in matric suction values led to a response more similar to the expected one from analytical equation (i.e. higher and lower RRS values as a result of raising and lowering water table).

Observed and predicted surface/base FFT transfer functions are presented in Figure 10-16 (a), with a focus on the predicted values within frequencies up to 4 Hz shown in Figure 10-17. The observed increase in fundamental frequencies as a result of lowering depth of water table was more significant than those observed in sand layers. This is due to the higher stiffness and effective stress within the silt layers. The residual FFT transfer function graphs as well as the normalized difference ratios for different water table heights are shown in Figure 10-16 (b) and (c), respectively. Similar to the sandy site results, the residual and normalized difference of TF graphs do not show a meaningful trend over different frequency ranges.

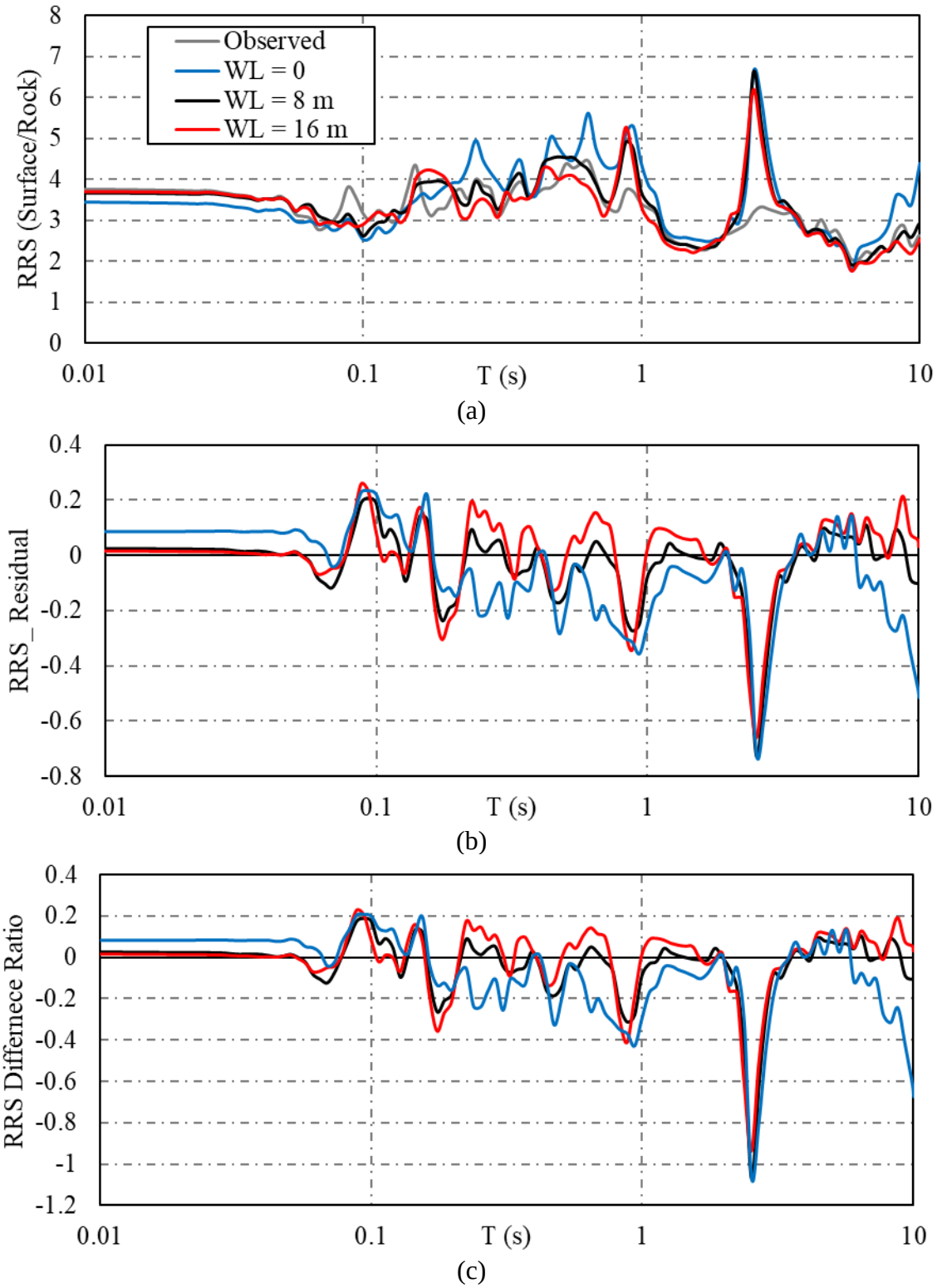

Figure 10-15. Variations of surface/base (a) Ratio of Response Spectra (b) RRS residual and (c) RRS normalized difference for soils with different water tables as a result of G_0 variations in silty soil

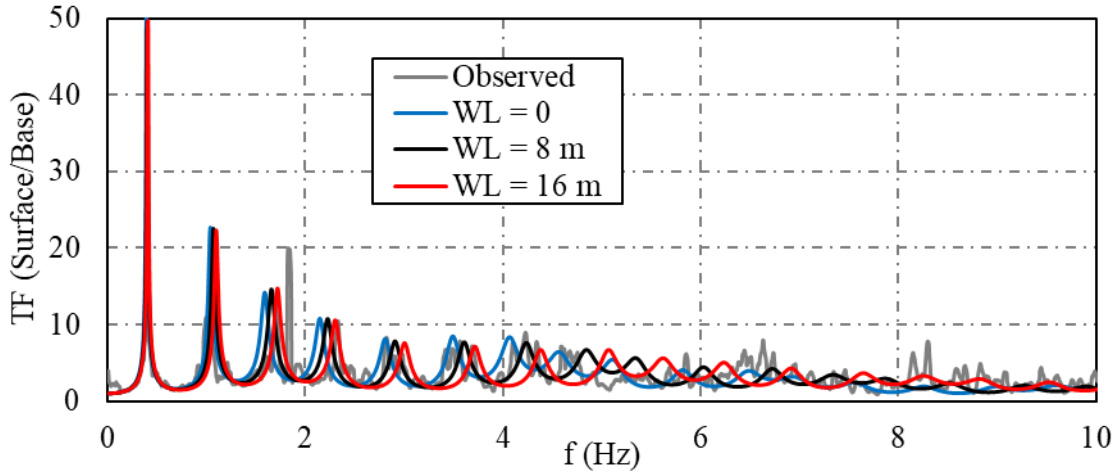

(a)

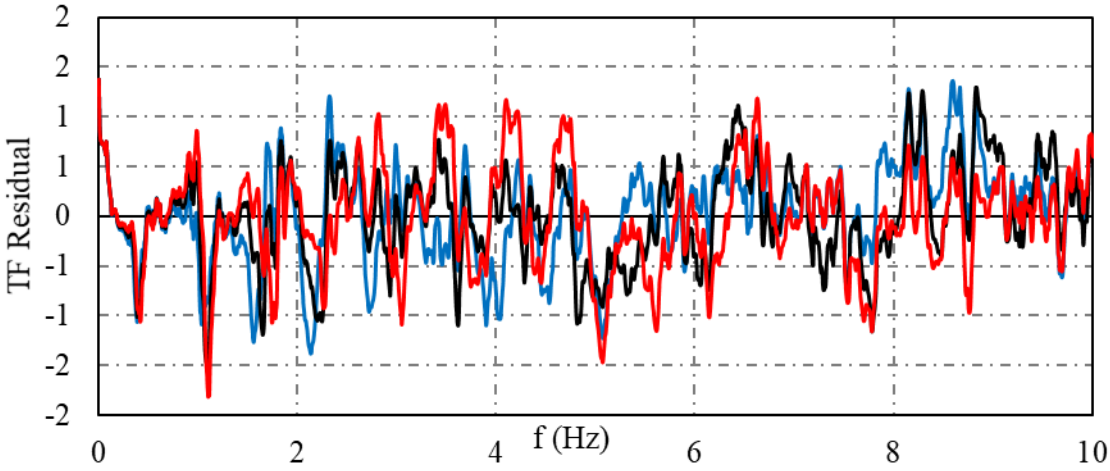

(b)

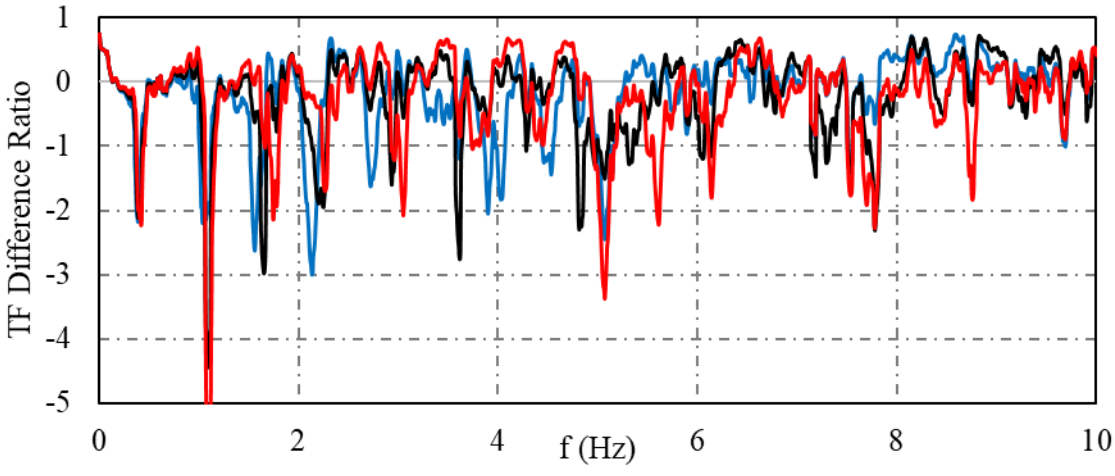

(c)

Figure 10-16. Variations of surface/base (a) FFT transfer function (b) FFT TF residual and (c) FFT TF normalized difference for soils with different water tables as a result of G_0 variations in silty soil

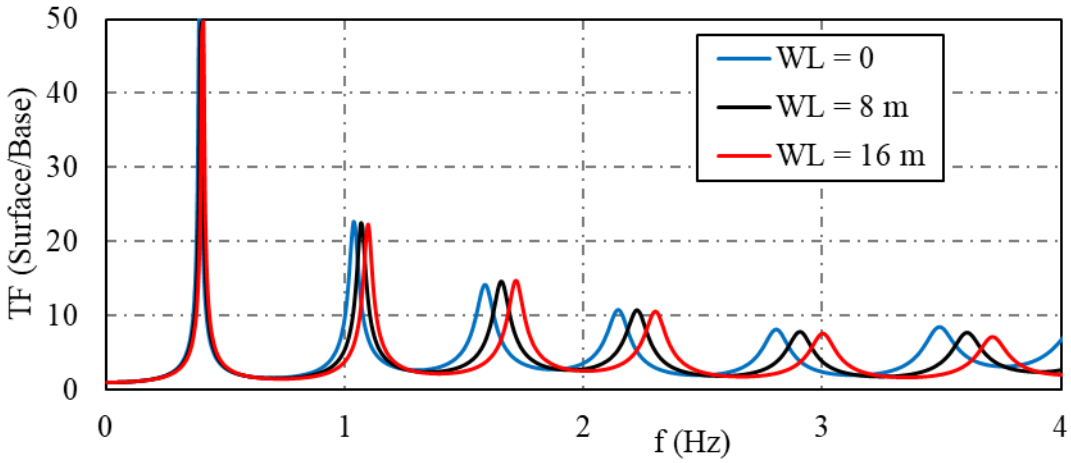

Figure 10-17. Variations of surface/base FFT transfer function for soils with different water tables as a result of G_0 variations in silty soil

10.4.2. The Effect of Damping Variations

Assuming Fine Sand Properties

The results of site response analyses with different depths of water table, considering sand hydraulic characteristics, where only damping was varied are presented in this section. Observed and predicted surface/base RRS graphs with different depths of water table are shown in Figure 10-18 (a). In addition, the residual and normalized difference ratio of RRS graphs for different water table levels are shown in Figure 10-18 (b) and (c), respectively. Lowering water table to 16 m below the ground surface led to slightly higher RRS values for almost all periods. However, a more significant change in RRS values was observed due to elevating water table to the ground surface, where the RRS values decreased for almost all the periods. The observed change in RRS for profiles with fluctuated water tables is consistent with the change in material damping for different water table levels in sandy soils, shown in Figure 10-5. According to Equation 2-14 for a simple SDOF system, material damping is inversely proportional to the acceleration amplification factors. The damping values in soil profiles with water table at and 16 m below the

ground surface were higher and lower than the reference values, respectively, which resulted in the reverse trend for RRS values in those profiles. In addition, less significant change in damping curves led to an insignificant variation in terms of RRS.

The extent of variations in predicted RRS values for the profiles with different water tables was appeared to be significantly lower. However more consistent trend within different period ranges was observed than the ones when the small-strain shear modulus varied. This is likely because of using a unified equation for predicting G_0 values in soil layers with different depths of water table while the employed equation for estimating damping was only capable of assessing the effect of partial saturation by increasing the effective stress. Therefore, in soil layers above the water table, where the difference in terms of effective stress was not significant due to relatively lower suction stresses, damping values did not show a substantial change between soils with water table at 8 m and 16 m below the ground surface. However, the equation for considering small-strain shear modulus incorporates the effect of partial saturation by changing both effective stress and degree of saturation. Hence, within the soil layers above the water table, although the change in effective stress was not substantial, degree of saturation of soil layers with fluctuating water table significantly varied; resulting in more profound variations in G_0 values even above the water table. For soil layers below the water table, the change in damping curves was more noticeable as the effective stress varied more significantly between the profiles with different depths of water table. The presented results clearly demonstrate the need for developing unified equations to estimate damping values in dry, unsaturated, and saturated soil condition.

Observed and predicted surface/base FFT transfer functions are presented in Figure 10-19 (a), with a focus on the predicted values within frequencies up to 4 Hz shown in Figure 10-20. The

residual FFT transfer function graphs as well as the normalized difference ratios for different water table heights are shown in Figure 10-19 (b) and (c), respectively. An insignificant change was observed in predicted fundamental frequencies and the TF magnitudes due to the damping variations, which could be observed through almost similar TF graphs and their residual and normalized difference ratios. This is also due to using equations, which were specifically calibrated using dry or saturated soils, for partially saturated soil layers.

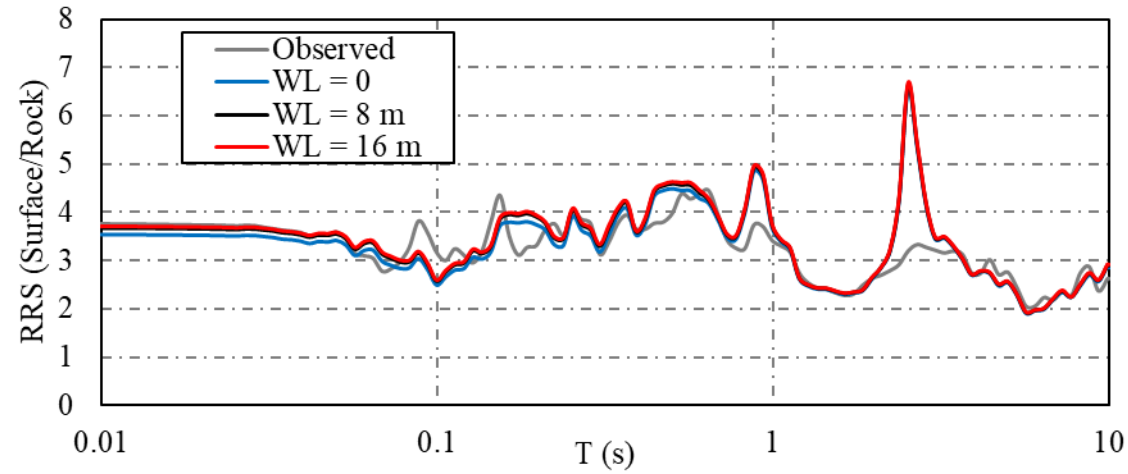

(a)

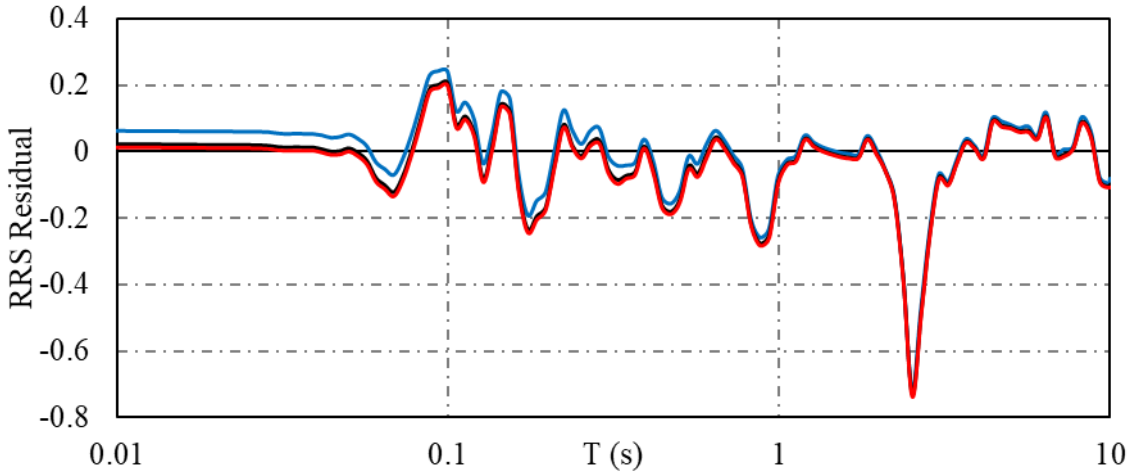

(b)

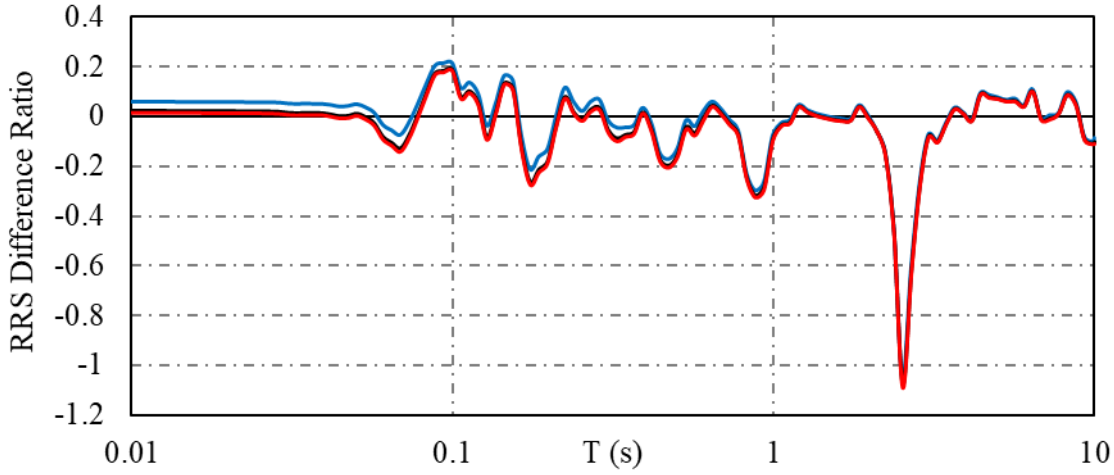

(c)

Figure 10-18. Variations of surface/base (a) Ratio of Response Spectra (b) RRS residual and (c) RRS normalized difference for soils with different water tables as a result of damping variations in sandy soil

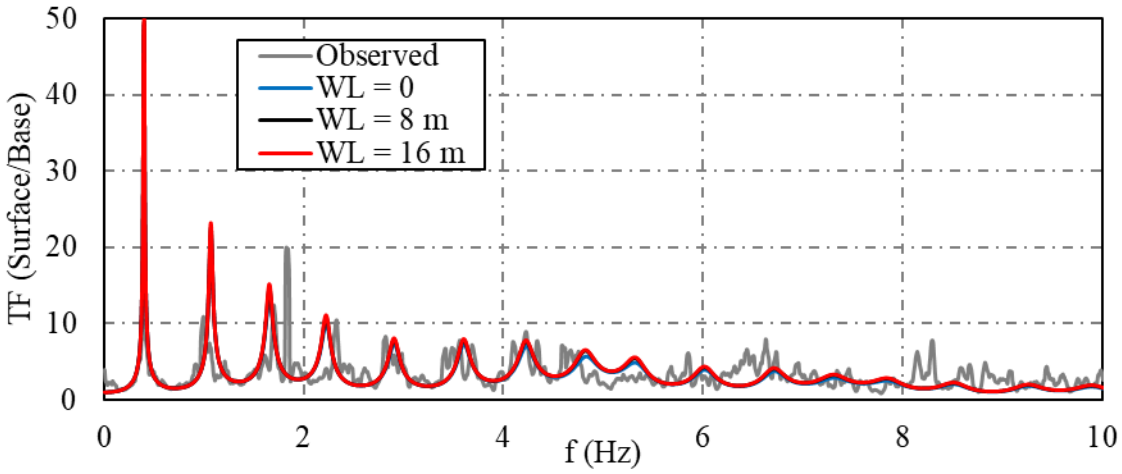

(a)

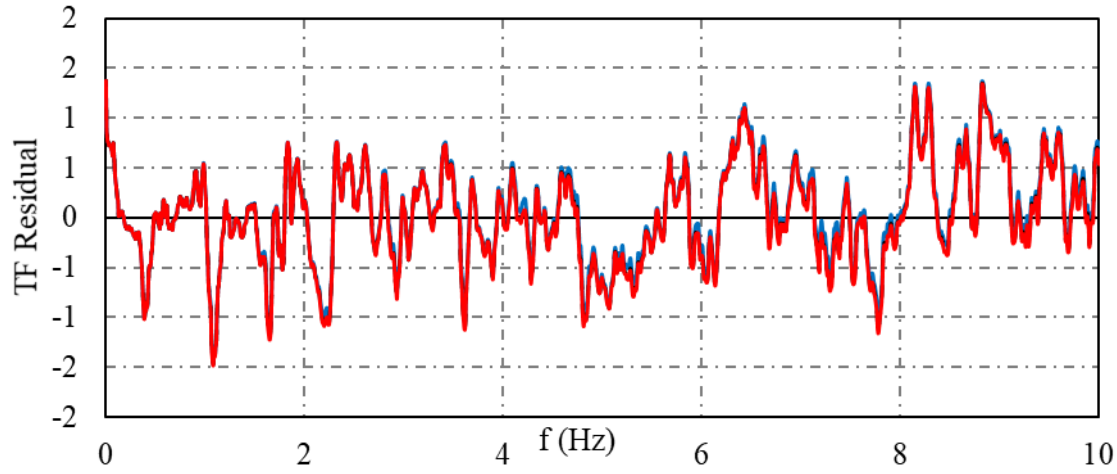

(b)

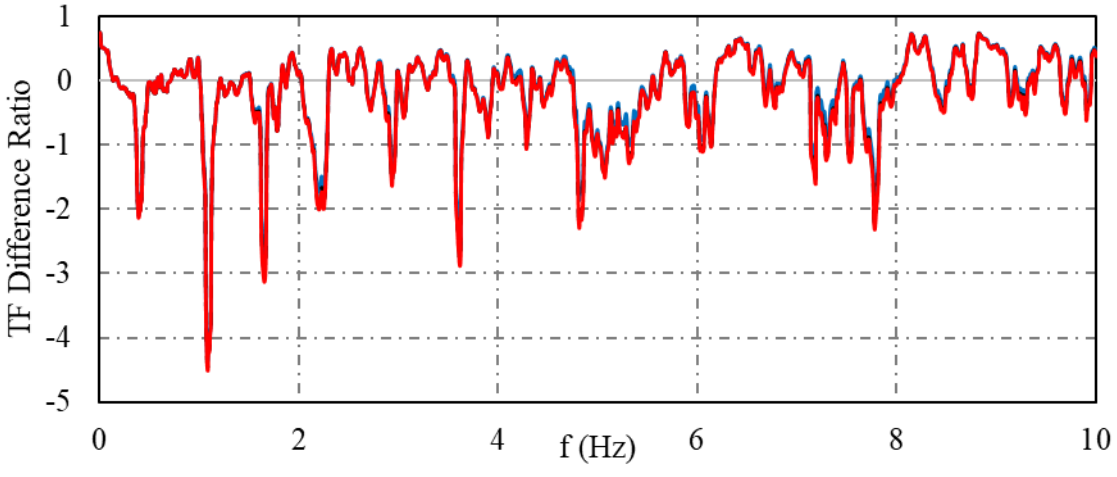

(c)

Figure 10-19. Variations of surface/base (a) FFT transfer function (b) FFT TF residual and (c) FFT TF normalized difference for soils with different water tables as a result of damping variations in sandy soil

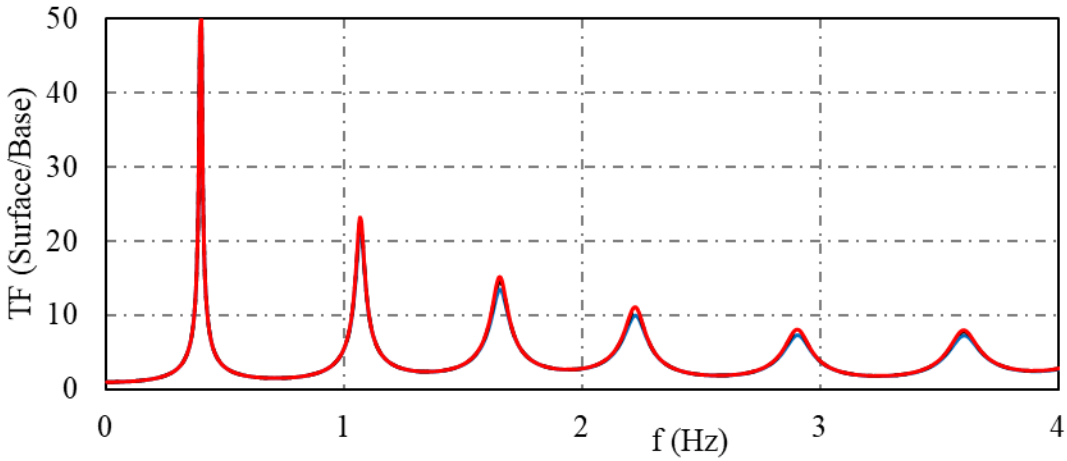

Figure 10-20. Variations of surface/base FFT transfer function for soils with different water tables as a result of damping variations in sandy soil

Assuming Silt Properties

The results of site response analyses with different depths of water table, considering silt hydraulic characteristics, where only damping was varied are presented in this section. Observed and predicted surface/base RRS graphs with different depths of water table are shown in Figure 10-21 (a). In addition, the residual and normalized difference ratio of RRS graphs for different water table levels are shown in Figure 10-21 (b) and (c), respectively. Similar to the results for the sand layers, the profiles with water table at the surface and 16 m below the ground surface showed a significant decrease and a slight increase in terms of RRS with respect to those with water table at 8, respectively. This trend was consistently observed for the total period range considered in this study. Because of the higher suction level in the silt layer, the change in RRS values between the soil layers with water table at 8 and 16 m below the ground surface was slightly higher than that considering sand hydraulic characteristics, especially for shorter periods

(i.e. less than 0.1 s). This is a result of a slightly higher divergence in terms of material damping between soil layers with different water table levels (Figure 10-6).

Observed and predicted surface/base FFT transfer functions are presented in Figure 10-22 (a), with a focus on the predicted values within frequencies up to 4 Hz shown in Figure 10-23. The residual FFT transfer function graphs as well as the normalized difference ratios for different water table heights are shown in Figure 10-23 (b) and (c), respectively. Similar to the effect of damping on the results of sand layers, an unnoticeable change was observed in terms of the TF graphs and their residual and normalized difference ratios between soil profiles with different water table levels. Since the effect of partial saturation on seismic site response of soils with higher suction levels is expected to be significantly higher, the presented graphs demonstrate the incompetency of the current damping formulations to be predictive of those values in unsaturated soils.

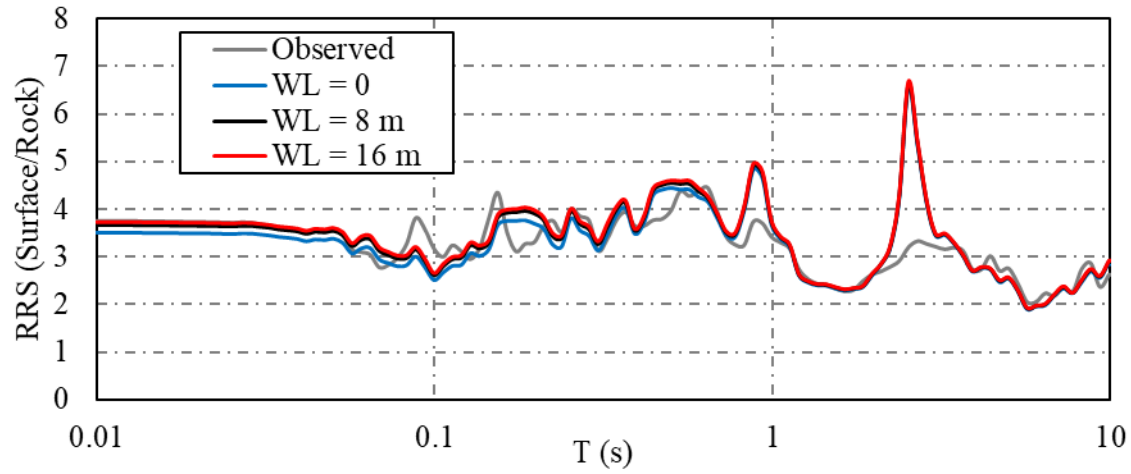

(a)

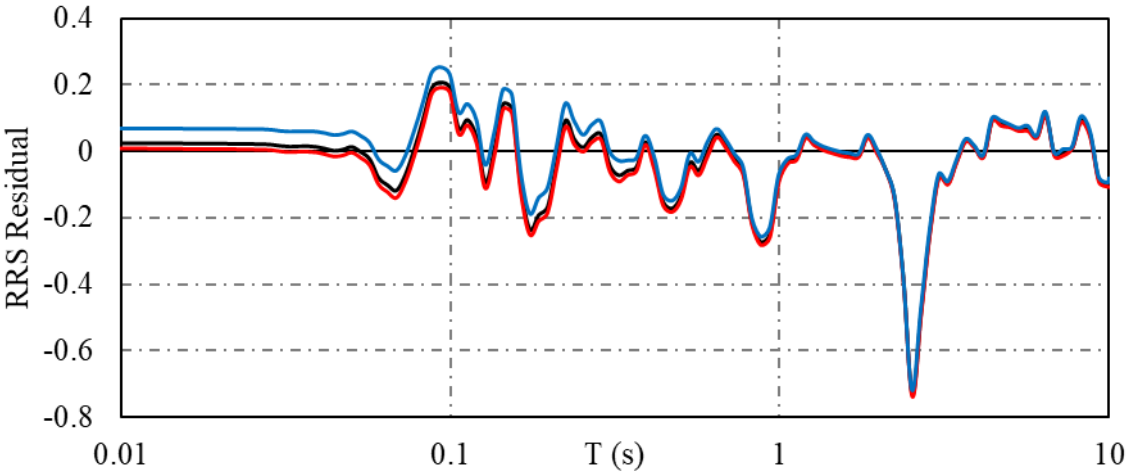

(b)

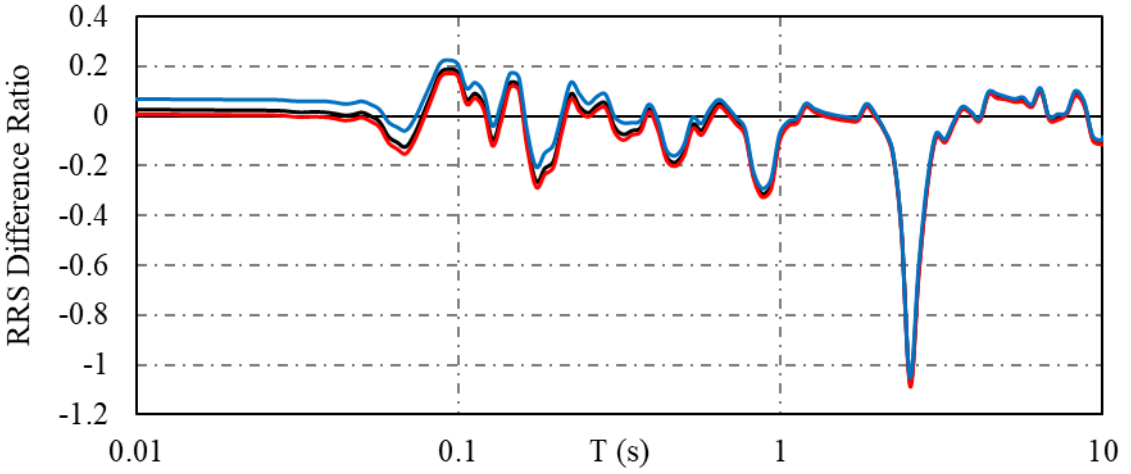

(c)

Figure 10-21. Variations of surface/base (a) Ratio of Response Spectra (b) RRS residual and (c) RRS normalized difference for soils with different water tables as a result of damping variations in silty soil

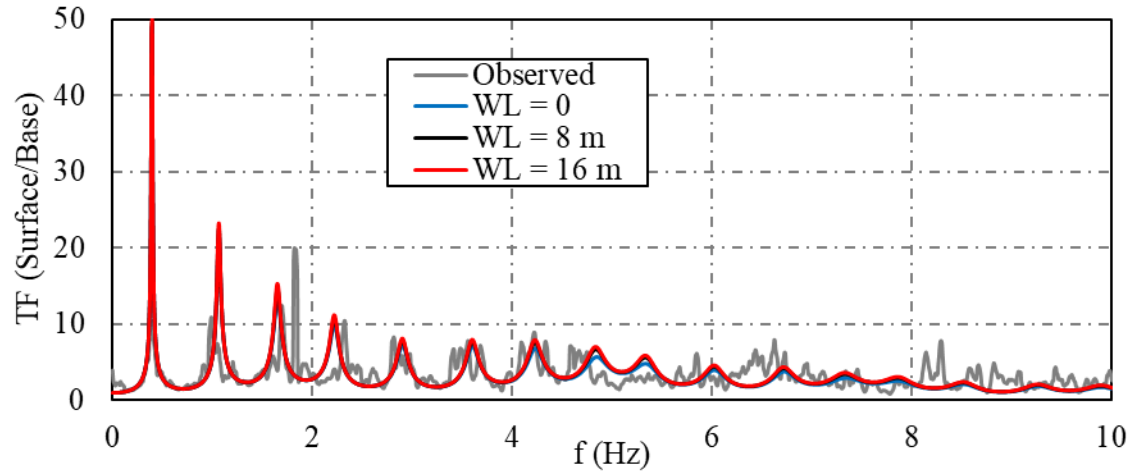

(a)

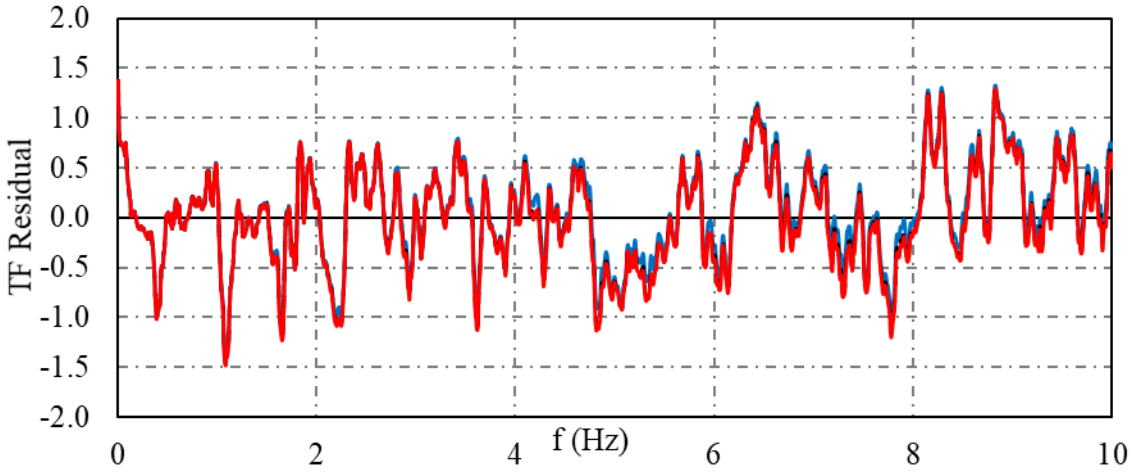

(b)

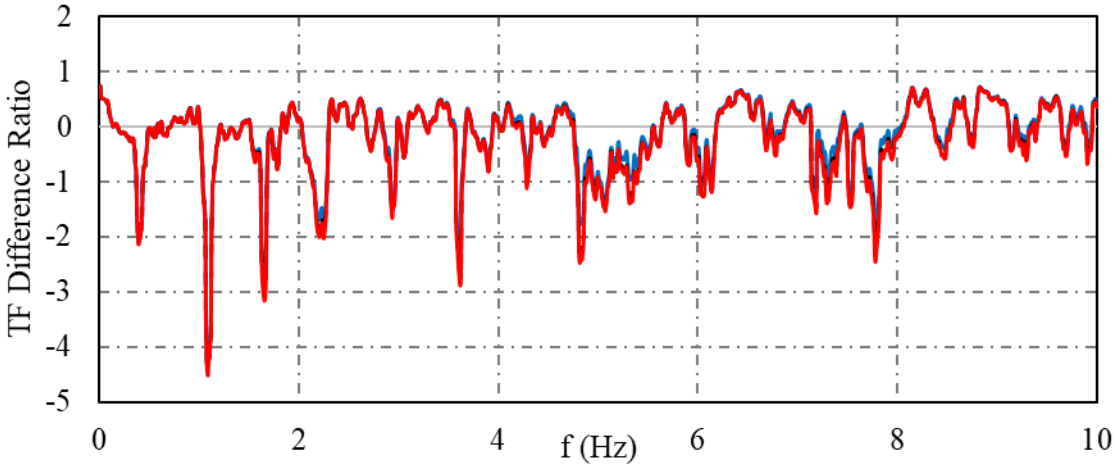

(c)

Figure 10-22. Variations of surface/base (a) FFT transfer function (b) FFT TF residual and (c) FFT TF normalized difference for soils with different water tables as a result of damping variations in silty soil

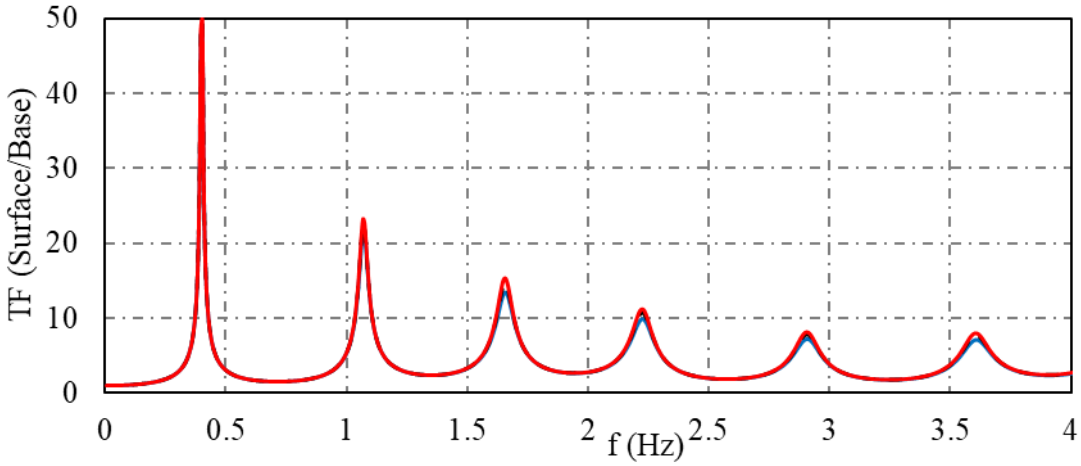

Figure 10-23. Variations of surface/base FFT transfer function for soils with different water tables as a result of damping variations in silty soil

10.4.3. The Effect of Modulus Reduction Factor Variations

Assuming Fine Sand Properties

The results of site response analyses with different depths of water table, considering sand hydraulic characteristics, where only modulus reduction factor was varied are presented in this section. Observed and predicted surface/base RRS graphs with different depths of water table are shown in Figure 10-24 (a). In addition, the residual and normalized difference ratio of RRS graphs for different water table levels are shown in Figure 10-24 (b) and (c), respectively. Elevating the water level was expected to lead to higher RRS values because of the lower modulus reduction factors in saturated conditions and the inverse proportionality between the acceleration amplification and shear modulus of soil layers (Equation 2-14). This was the main trend observed in terms of the RRS graphs, where a small increase in RRS values was observed for periods higher than 0.1 s. However, interestingly, elevating the water table to the ground surface led to a small decrease in terms of RRS within shorter period ranges, i.e. less than 0.1 s.

This trend is consistent with those obtained considering the change in G_0 values, although showing a significantly less magnitude in the observed change. Lowering water table to 16 m below the ground surface did not cause any significant change in RRS values, which was a reflective of those changes observed in modulus reduction curves due to lowering water table. Similar to the analyses considering damping variations, this was likely due to the inability of the equations of modulus reduction factors to capture the actual change in partially saturated condition by varying the effective stress. Similarly, for the soil layers above water table degree of saturation only had a small influence on the effective stress while playing a more important role on G_0 values by introducing a separate coefficient into the equations. The presented results indicate the need for developing unified equations to assess modulus reduction factors in dry, unsaturated, and saturated condition.

Observed and predicted surface/base FFT transfer functions are presented in Figure 10-25 (a), with a focus on the predicted values within frequencies up to 4 Hz shown in Figure 10-26. The residual FFT transfer function graphs as well as the normalized difference ratios for different water table heights are shown in Figure 10-25 (b) and (c), respectively. Although slightly higher than the change observed as a result of damping variation, the change in predicted fundamental frequencies and TF magnitudes was still very small, which is also due to employing platforms specifically calibrated for dry or saturated soils.

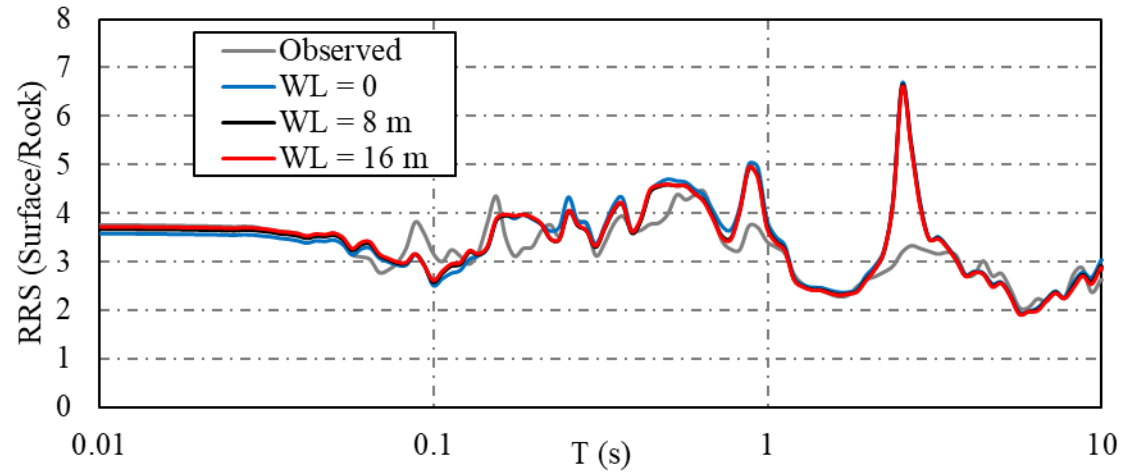

(a)

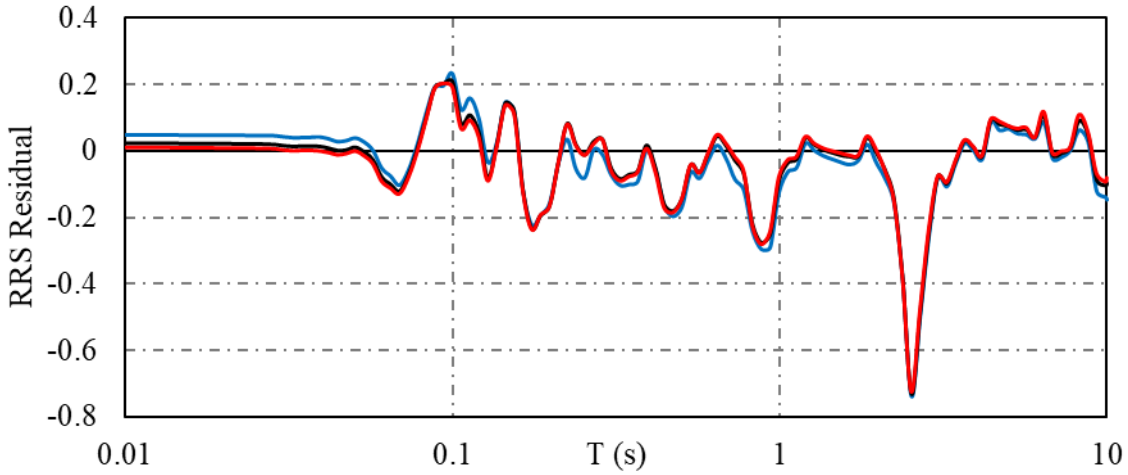

(b)

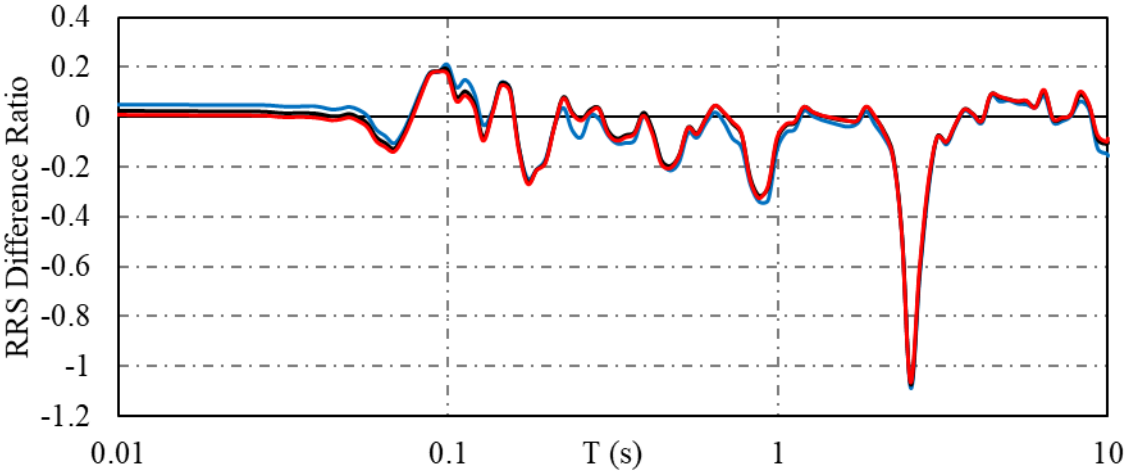

(c)

Figure 10-24. Variations of surface/base (a) Ratio of Response Spectra (b) RRS residual and (c) RRS normalized difference for soils with different water tables as a result of variations of modulus reduction factor in sandy soil

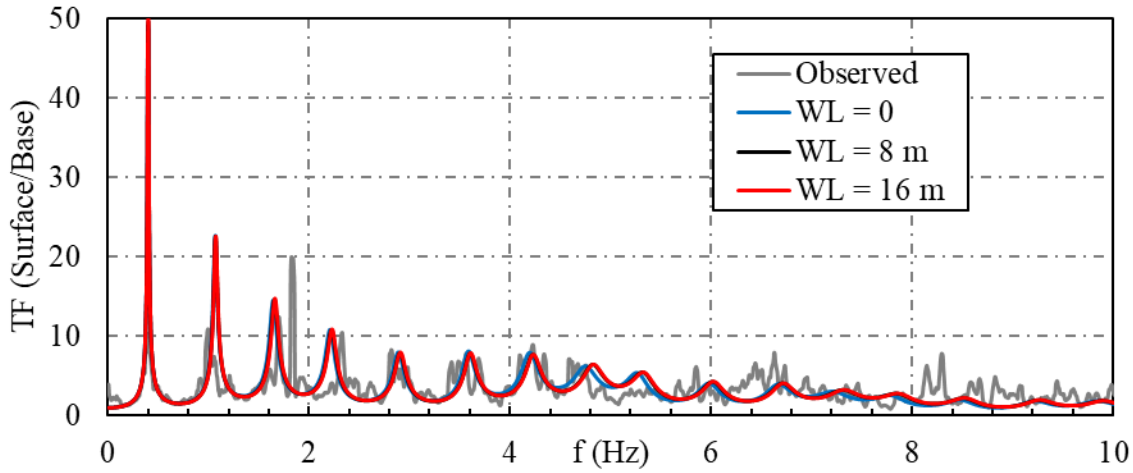

(a)

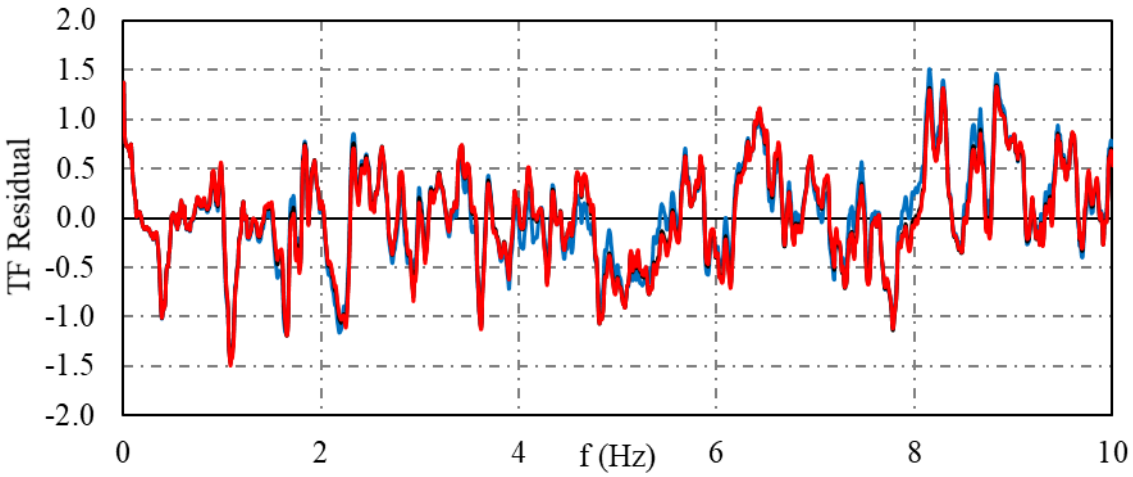

(b)

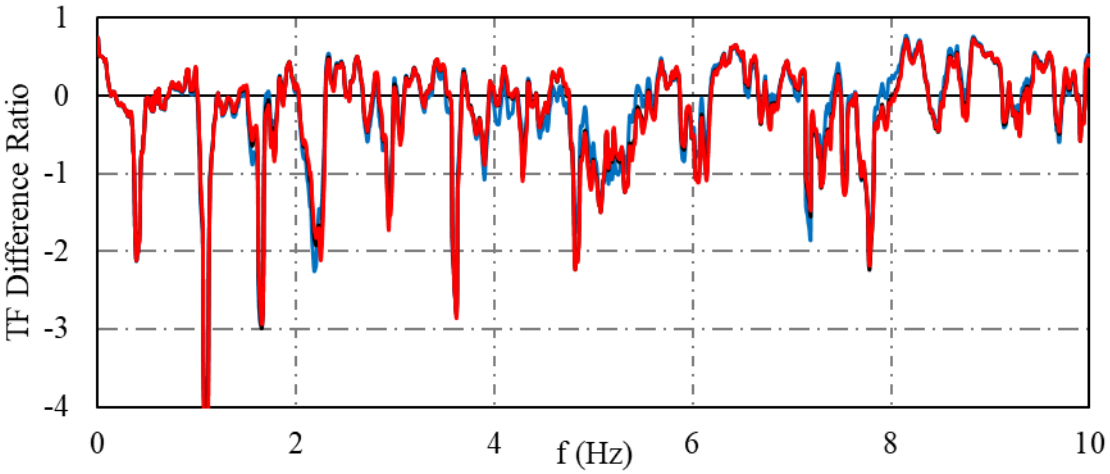

(c)

Figure 10-25. Variations of surface/base (a) FFT transfer function (b) FFT TF residual and (c) FFT TF normalized difference for soils with different water tables as a result of variations of modulus reduction factor in sandy soil

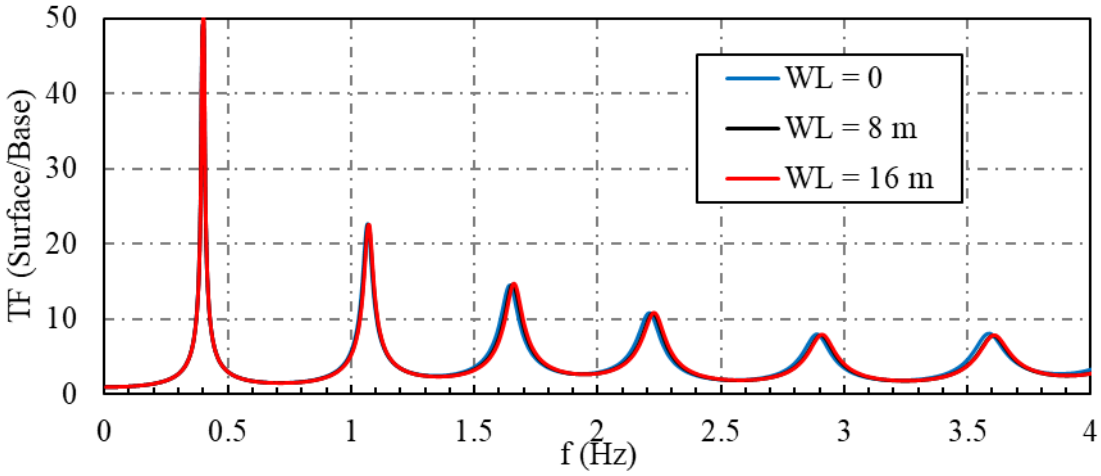

Figure 10-26. Variations of surface/base FFT transfer function for soils with different water tables as a result of variations of modulus reduction factor in sandy soil

Assuming Silt Properties

The results of site response analyses with different depths of water table, considering silt hydraulic characteristics, where only modulus reduction factor was varied are presented in this section. Observed and predicted surface/base RRS graphs with different depths of water table are shown in Figure 10-27 (a). In addition, the residual and normalized difference ratio of RRS graphs for different water table levels are shown in Figure 10-27 (b) and (c), respectively. Elevating the water table level to the ground surface led to slightly higher RRS values in silt layers within all period ranges than those predicted in sand layers. As a result, the increase in RRS values in saturated ground was more significant for periods higher than 0.1 s, while the decrease in shorter periods was less noticeable. This change makes the response of saturated soil layer closer to the expected trend (i.e. higher RRS values due to lower shear modulus values). Similar to the response of sand layers, models with water table at 16 m below the ground surface did not show any noticeable change in terms of RRS, which was due to the insignificant change

in modulus reduction factor curves. Since the response of unsaturated soils, especially with higher suction levels, is expected to be substantially different over different ranges of matric suction; the presented results demonstrate the incapability of current formulations to capture the values of modulus reduction factors in partially saturated condition.

Observed and predicted surface/base FFT transfer functions are presented in Figure 10-28 (a), with a focus on the predicted values within frequencies up to 4 Hz shown in Figure 10-29. The residual FFT transfer function graphs as well as the normalized difference ratios for different water table heights are shown in Figure 10-28 (b) and (c), respectively. The change in predicted fundamental frequencies as a result of water table fluctuations and changing shear modulus reduction factors appeared to be slightly higher than the change in sand layers. This was due to the higher suction stress in silty soils and, in turn, higher divergence in the modulus reduction curves of profiles with different water tables.

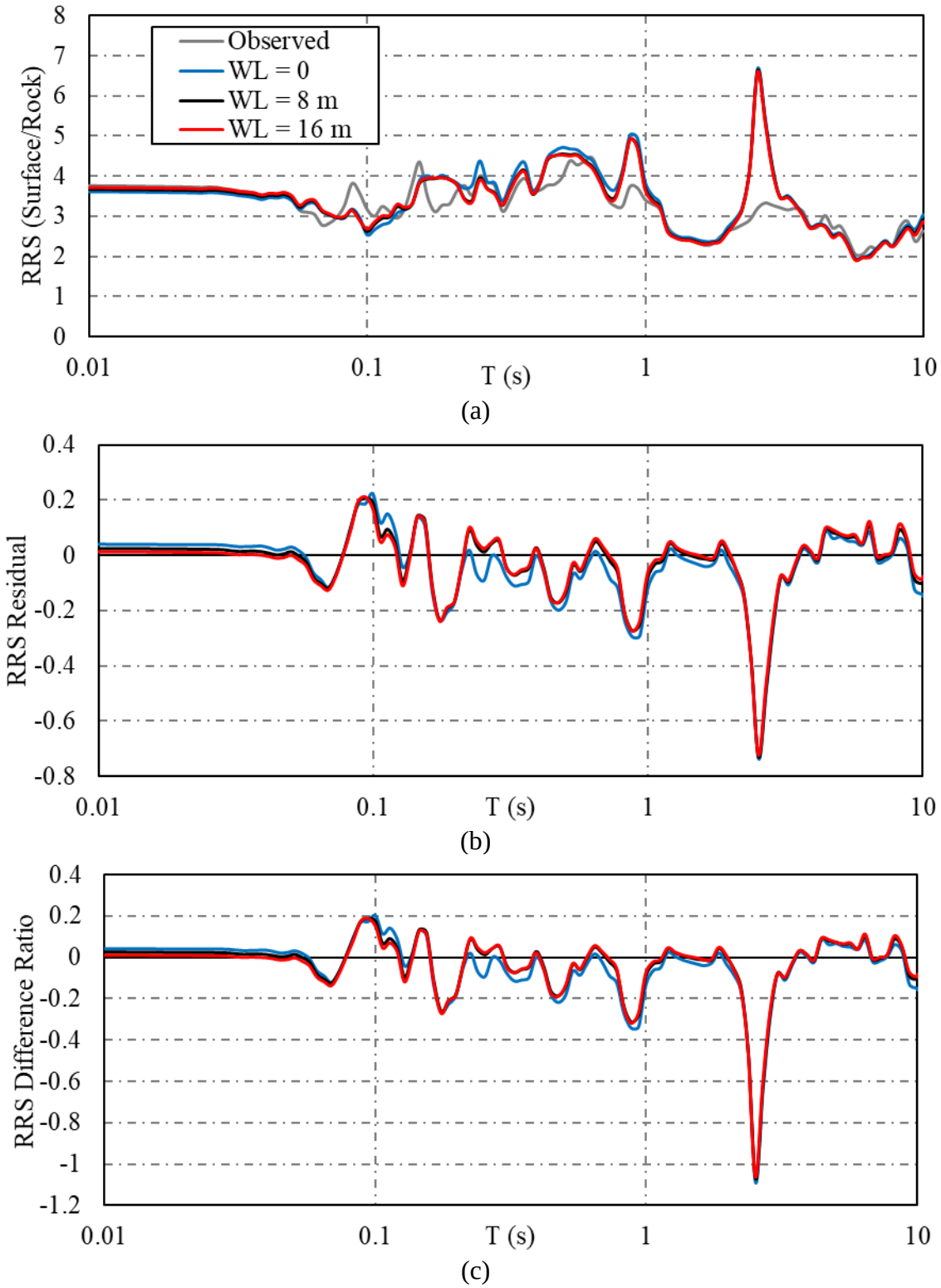

Figure 10-27. Variations of surface/base (a) Ratio of Response Spectra (b) RRS residual and (c) RRS normalized difference for soils with different water tables as a result of variations of modulus reduction factor in silty soil

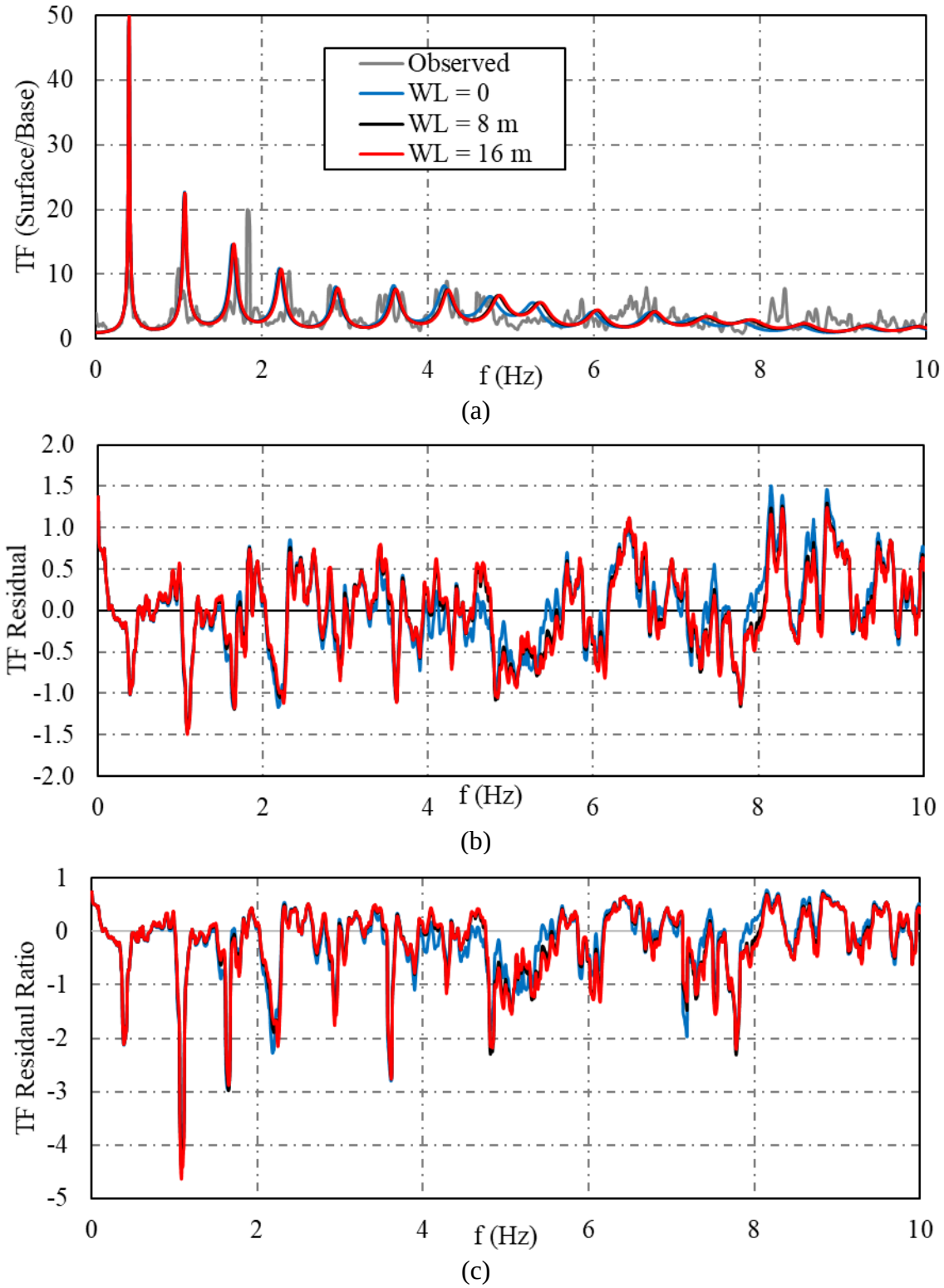

Figure 10-28. Variations of surface/base (a) FFT transfer function (b) FFT TF residual and (c) FFT TF normalized difference for soils with different water tables as a result of variations of modulus reduction factor in silty soil

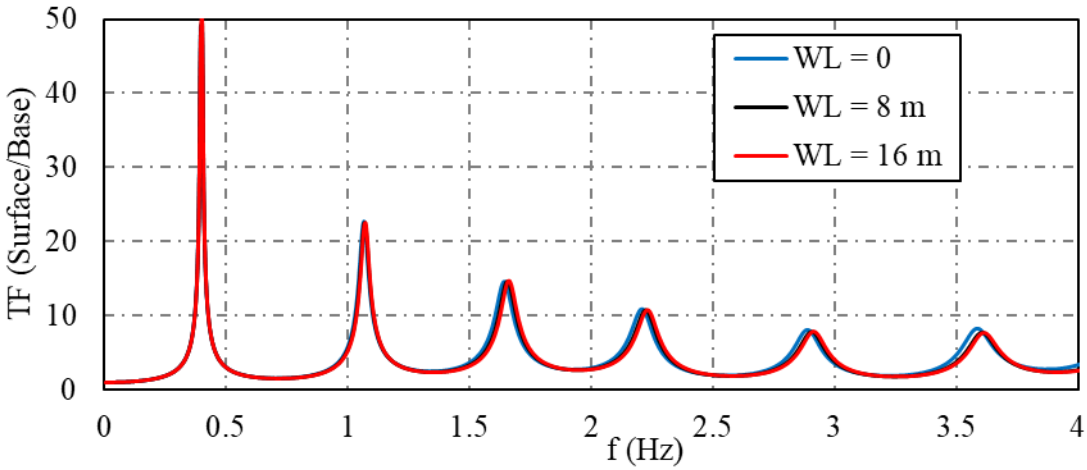

Figure 10-29. Variations of surface/base FFT transfer function for soils with different water tables as a result of variations of modulus reduction factor in silty soil

10.4.4. The Effect of Unit Weight Variations

Assuming Fine Sand Properties

The results of site response analyses with different depths of water table, considering sand hydraulic characteristics, where only unit weight was varied are presented in this section. Observed and predicted surface/base RRS graphs with different depths of water table are shown in Figure 10-30 (a). In addition, the residual and normalized difference ratio of RRS graphs for different water table levels are shown in Figure 10-30 (b) and (c), respectively. Similar to the effect of damping variations, changing unit weight in saturated ground led to lower RRS values, indicated by higher residuals and difference ratio, over the total analyzed period range. However, RRS values almost did not change when lowering the water table to 16 m below the ground surface, with the exception of period range between 0.2 s and 1 s. The observed trends highlight the effect of soil water-saturation at depths near the ground surface.

Observed and predicted surface/base FFT transfer functions are presented in Figure 10-31 (a), with a focus on the predicted values within frequencies up to 4 Hz shown in Figure 10-32. The residual FFT transfer function graphs as well as the normalized difference ratios for different water table heights are shown in Figure 10-31 (b) and (c), respectively. The change in the predicted fundamental frequency was relatively small, where the profile with the lowest water table showed the highest fundamental frequencies indicating a stiffer medium.

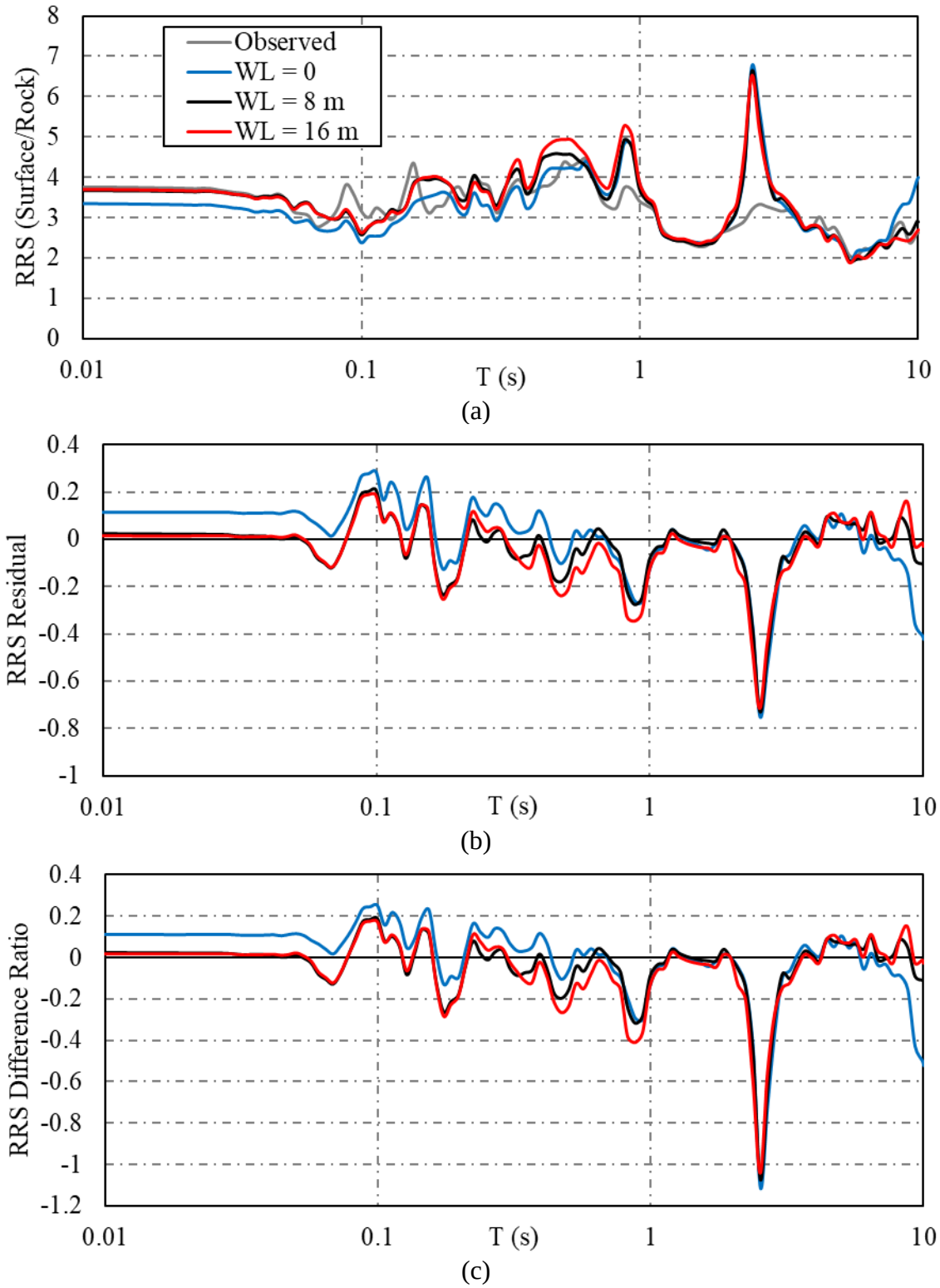

Figure 10-30. Variations of surface/base (a) Ratio of Response Spectra (b) RRS residual and (c) RRS normalized difference for soils with different water tables as a result of unit weight variations in sandy soil

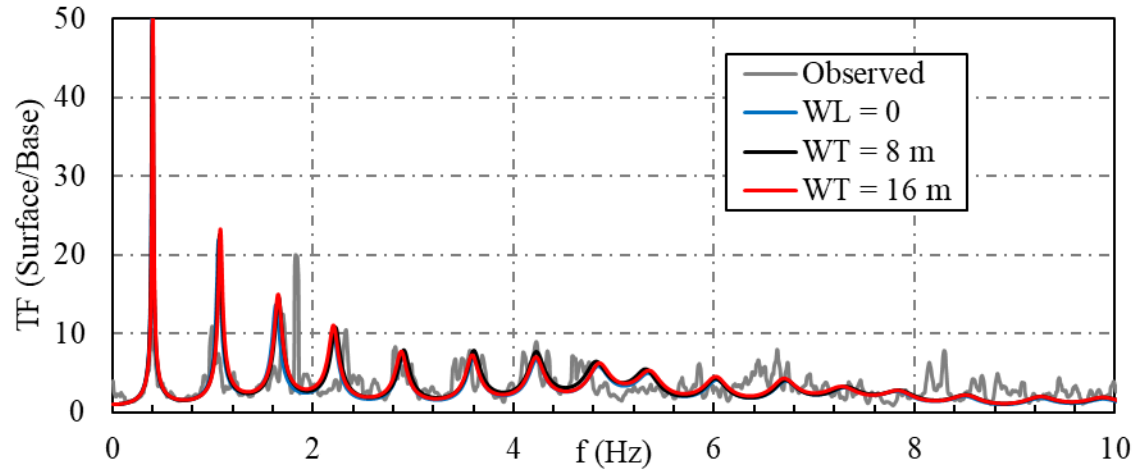

(a)

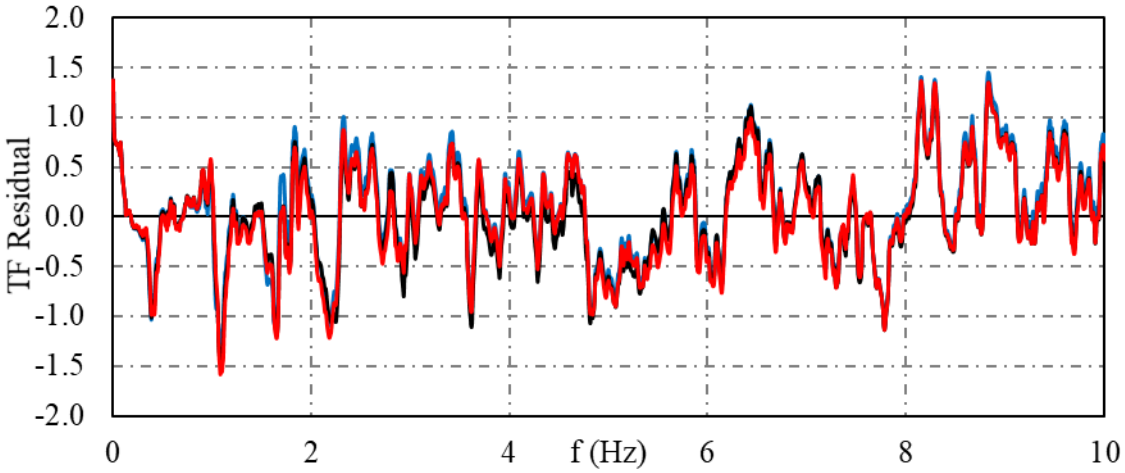

(b)

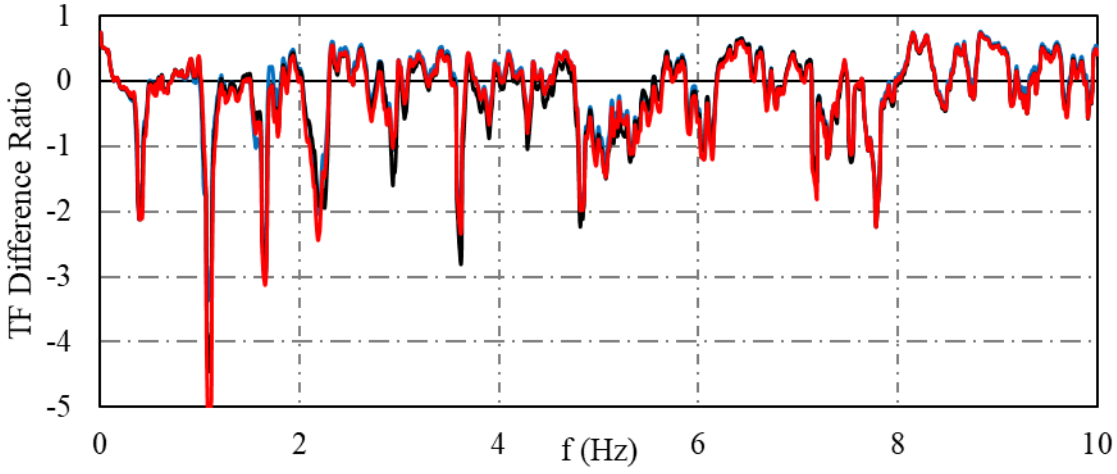

(c)

Figure 10-31. Variations of surface/base (a) FFT transfer function (b) FFT TF residual and (c) FFT TF normalized difference for soils with different water tables as a result of unit weight variations in sandy soil

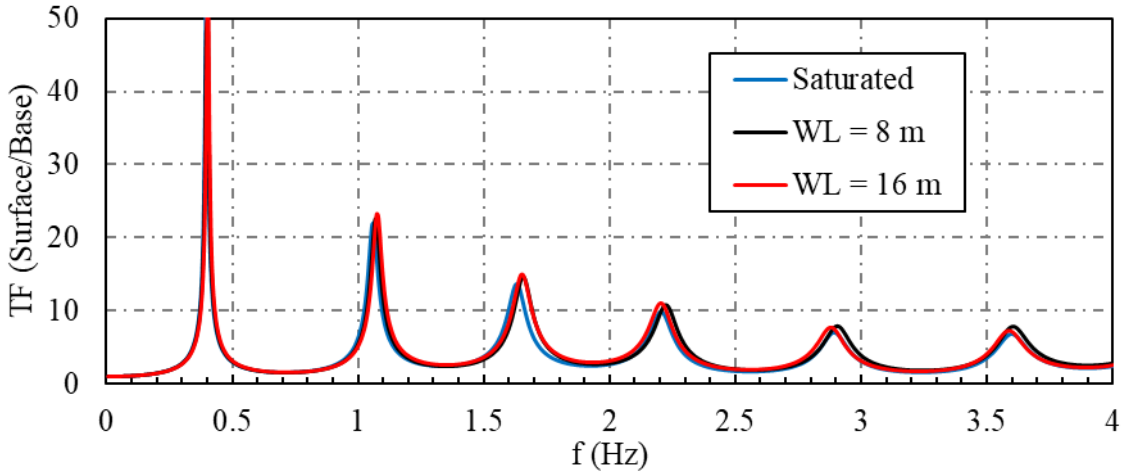

Figure 10-32. Variations of surface/base FFT transfer function for soils with different water tables as a result of unit weight variations in sandy soil

Assuming Silt Properties

The results of site response analyses with different depths of water table, considering silt hydraulic characteristics, where only unit weight was varied are presented in this section. Observed and predicted surface/base RRS graphs with different depths of water table are shown in Figure 10-33 (a). In addition, the residual and normalized difference ratio of RRS graphs for different water table levels are shown in Figure 10-33 (b) and (c), respectively. The variation in terms of RRS when the water table was elevated to the ground surface was less than those in sandy soils, which was due to the smaller change in unit weight occurred as a result of elevating the water table (Figure 10-3, b). However, since the unit weight profiles for water table at 16 m below the ground surface experienced a higher change than the reference one, the divergence observed in RRS graphs of that profile was slightly higher than that difference in sand layers. Similar to the effect of damping variations, profiles with water table at the ground surface and 16 m below the ground surface, showed lower and higher RRS values, respectively.

Observed and predicted surface/base FFT transfer functions are presented in Figure 10-34 (a), with a focus on the predicted values within frequencies up to 4 Hz shown in Figure 10-35. The residual FFT transfer function graphs as well as the normalized difference ratios for different water table heights are shown in Figure 10-34 (b) and (c), respectively. Only a small change in fundamental frequencies was observed as a result of changing the water table and unit weight profiles, which shows a less prominent influence of unit weight on the stiffness of soil layers.

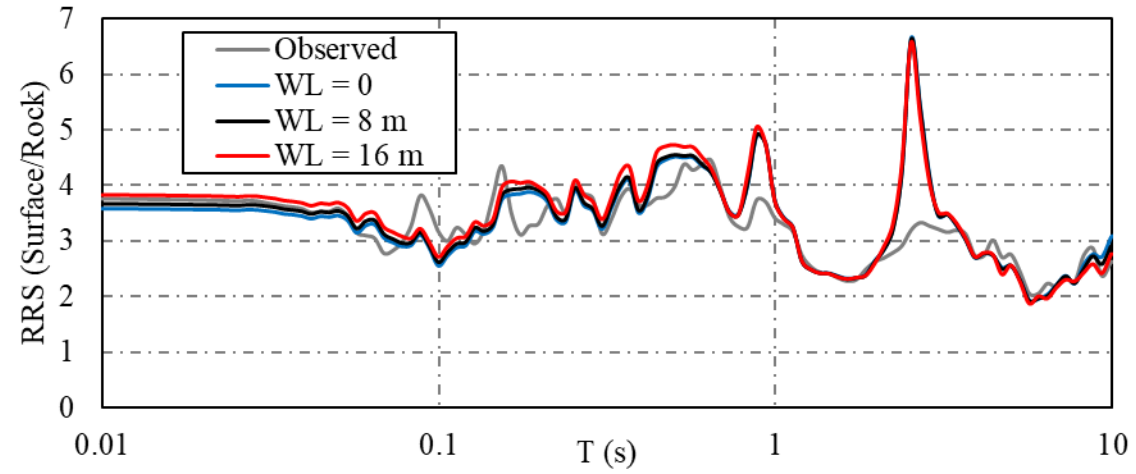

(a)

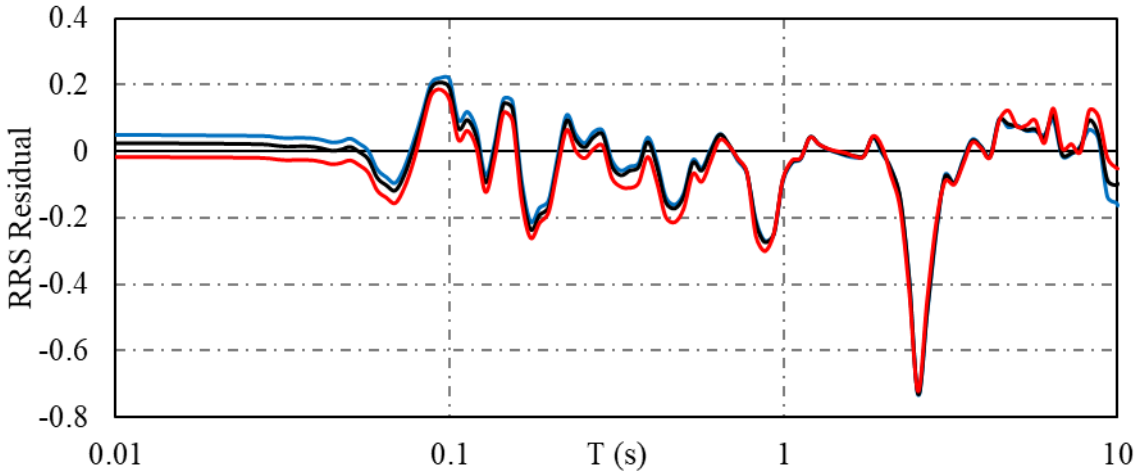

(b)

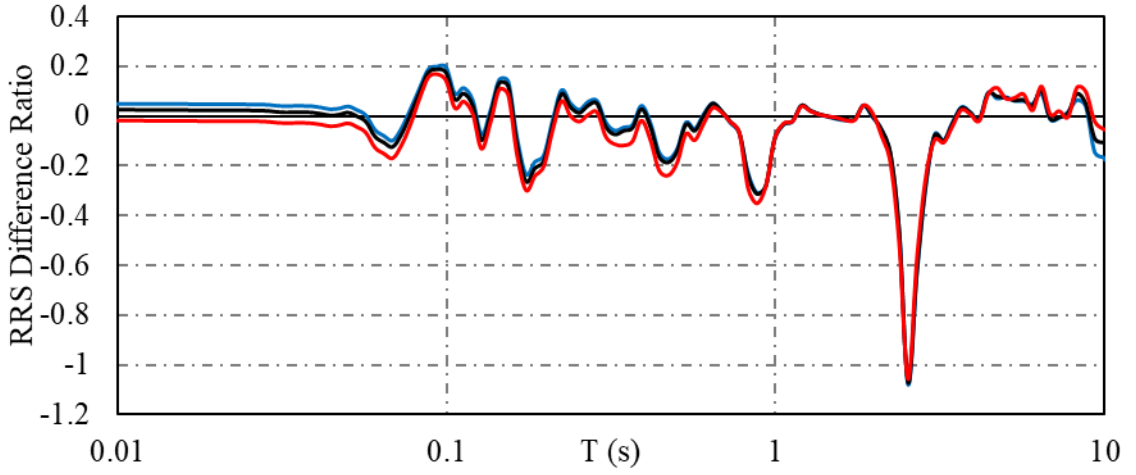

(c)

Figure 10-33. Variations of surface/base (a) Ratio of Response Spectra (b) RRS residual and (c) RRS normalized difference for soils with different water tables as a result of unit weight variations in silty soil

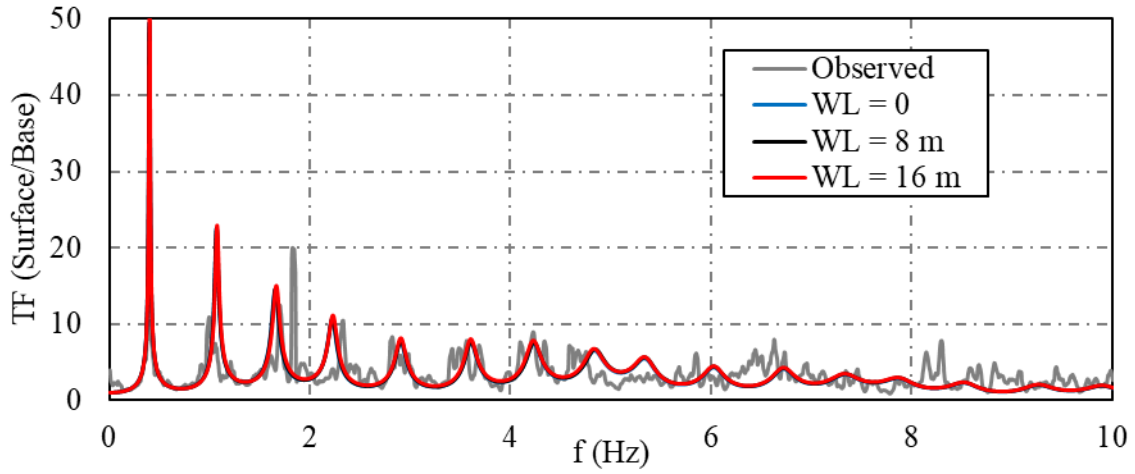

(a)

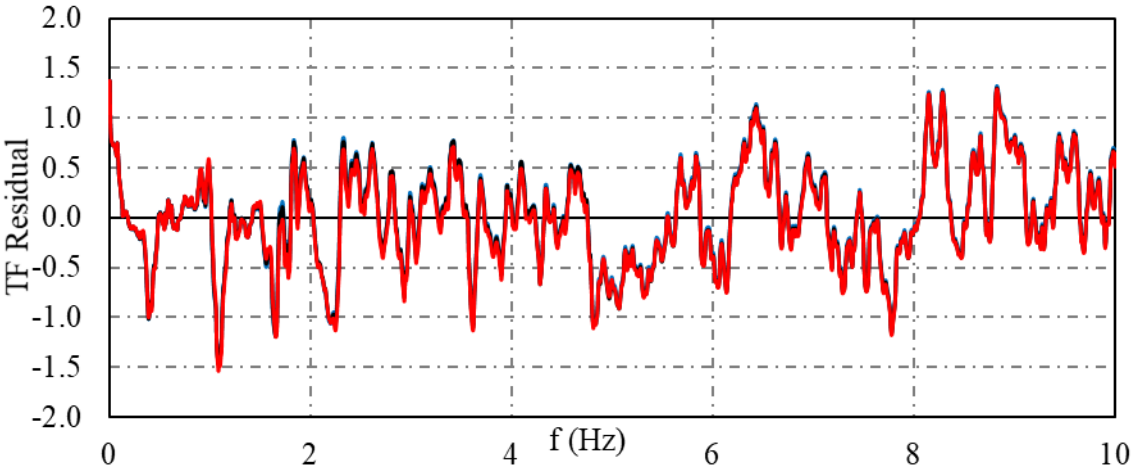

(b)

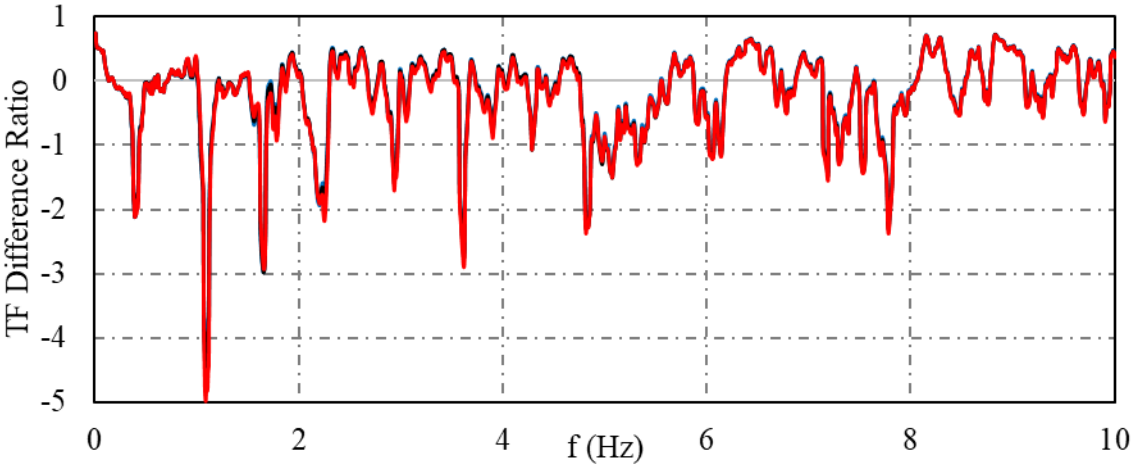

(c)

Figure 10-34. Variations of surface/base (a) FFT transfer function (b) FFT TF residual and (c) FFT TF normalized difference for soils with different water tables as a result of unit weight variations in silty soil

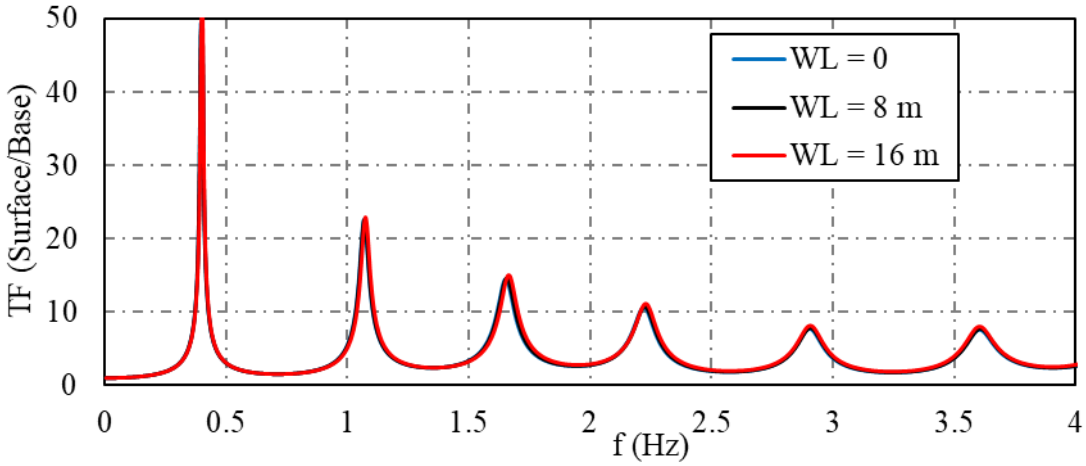

Figure 10-35. Variations of surface/base FFT transfer function for soils with different water tables as a result of unit weight variations in silty soil

10.4.5. The Combined Effect of Variations in All the Parameters

Assuming Fine Sand Properties

The results of site response analyses with different depths of water table, considering sand hydraulic characteristics, where all important soil parameters (i.e. small-strain shear modulus, damping, modulus reduction factor, and damping) were varied are presented in this section. Observed and predicted surface/base RRS graphs with different depths of water table are shown in Figure 10-36 (a). In addition, the residual and normalized difference ratio of RRS graphs for different water table levels are shown in Figure 10-36 (b) and (c), respectively. Elevating water table level to the ground surface led to significantly lower and slightly higher RRS values for periods less and higher than almost 0.5 s, respectively. Soil profiles with water table at 16 m below the ground surface showed higher RRS values for almost all periods. This is against the assumption of having lower amplification factors for unsaturated soils with higher stiffness. Although the profile with the 16 m depth of water table was stiffer than the reference profile, its

RRS values were higher than the ones for the soil profile with 8 m water table. These trends were observed due to interaction between the effects of variations in different input parameters. For the soil profile with water table at 16 m below the ground surface, while the increase in shear modulus profile led to lower RRS values, the counter-effects caused by lower damping and unit weight profiles caused an overall increase in terms of RRS than the reference ones. Further, the results show that water table fluctuation leads to a significant variation in terms of RRS for different period ranges, inducing a high level of uncertainty in site response analysis that has to be considered when using the results for design purposes.

Observed and predicted surface/base FFT transfer functions are presented in Figure 10-37 (a), with a focus on the predicted values within frequencies up to 4 Hz shown in Figure 10-38. The residual FFT transfer function graphs as well as the normalized difference ratios for different water table heights are shown in Figure 10-37 (b) and (c), respectively. Both fundamental frequencies and magnitude of FFT TFs increased as a result of lowering water table indicating a stiffer material in that case. However, as discussed earlier, the stiffer material with lower water table did not show a lower amplification factor due to the interaction between different soil parameters.

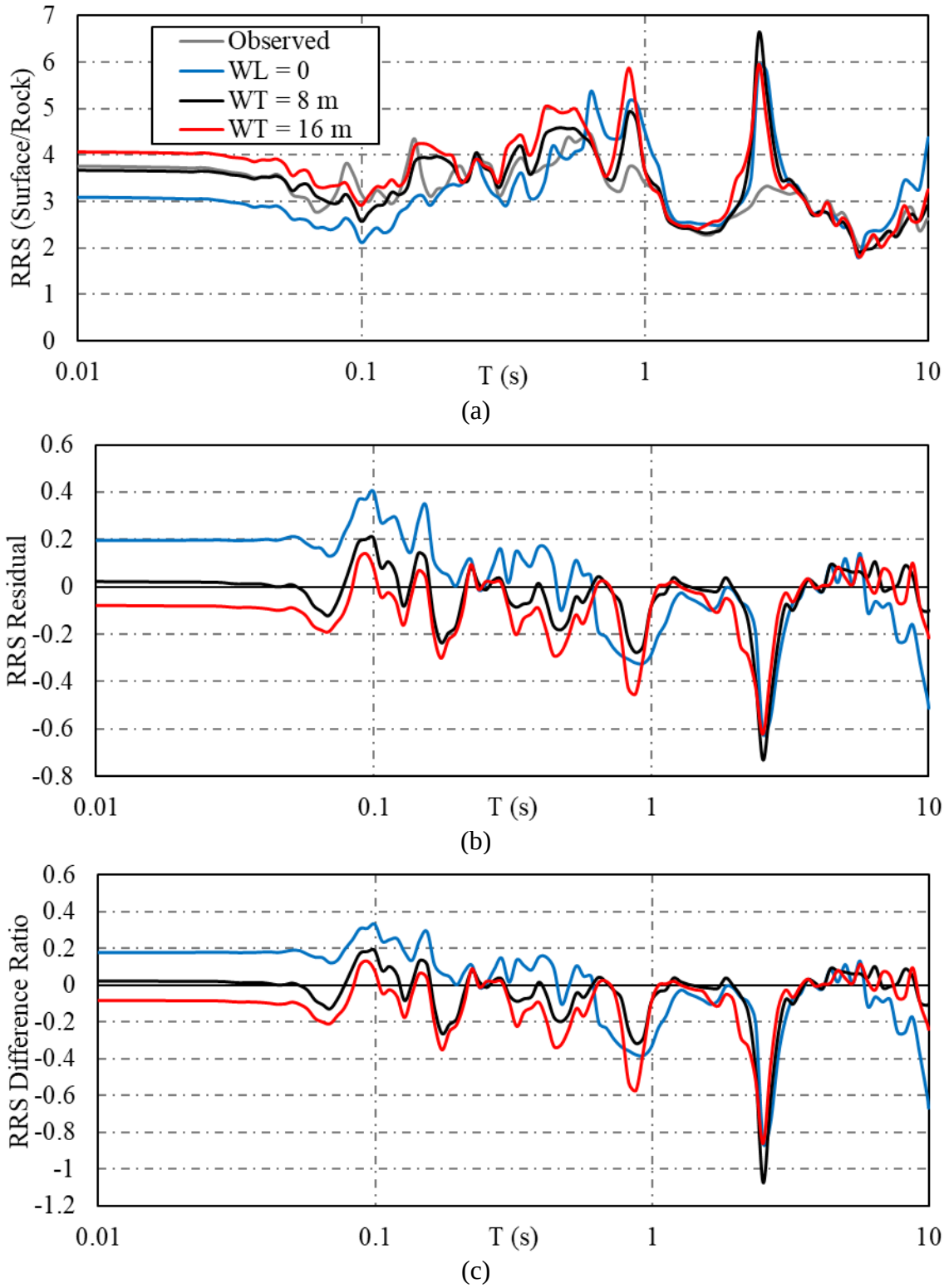

Figure 10-36. Variations of surface/base (a) Ratio of Response Spectra (b) RRS residual and (c) RRS normalized difference for soils with different water in sandy soil

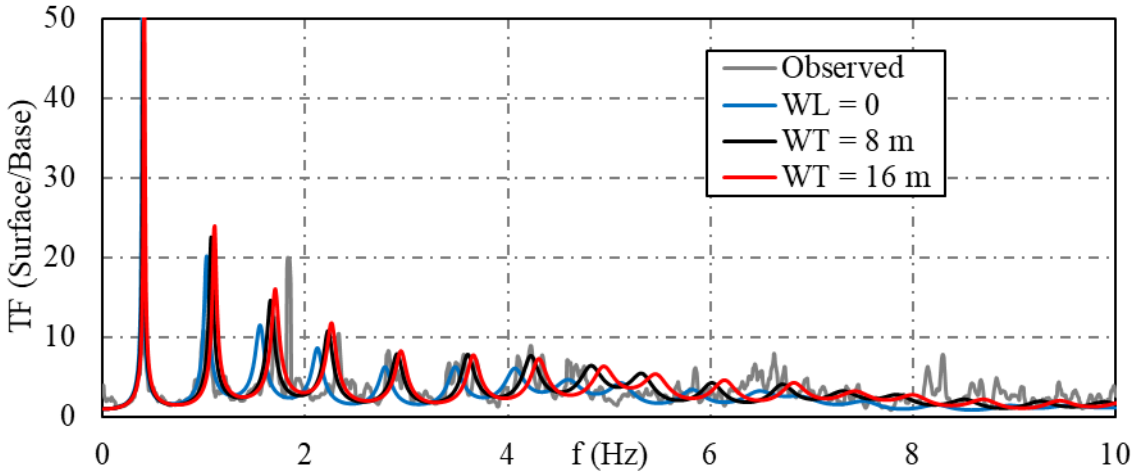

(a)

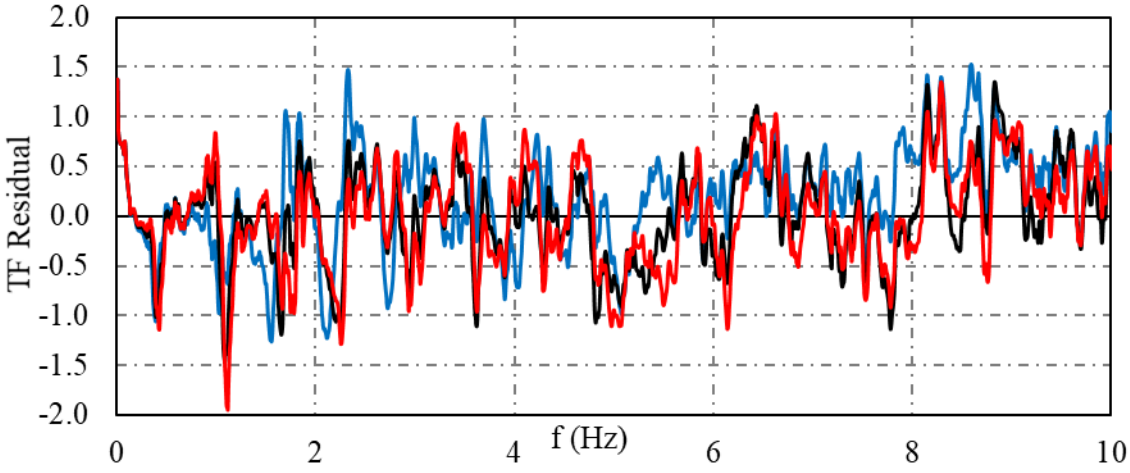

(b)

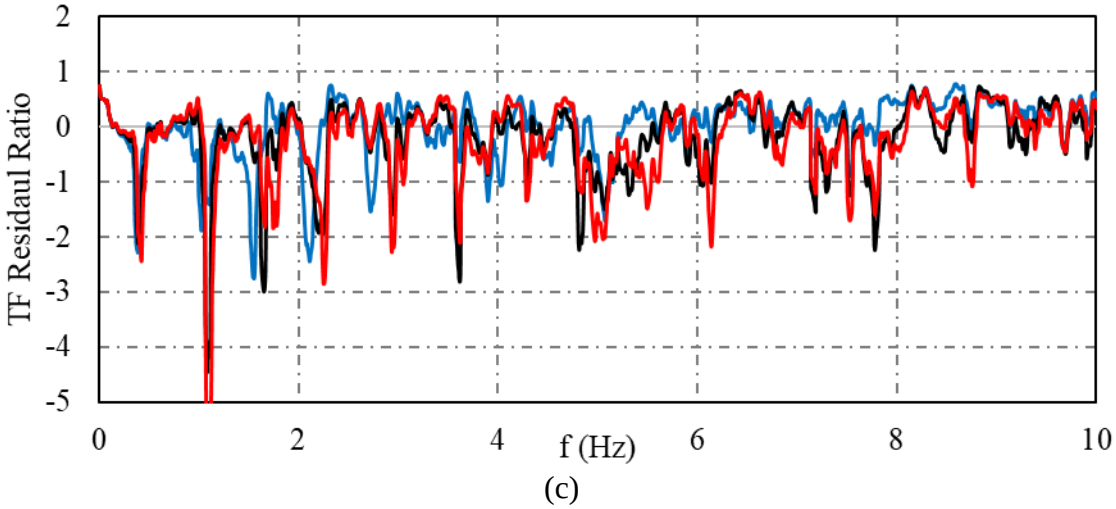

(c)

Figure 10-37. Variations of surface/base (a) FFT transfer function (b) FFT TF residual and (c) FFT TF normalized difference for soils with different water tables in sandy soil

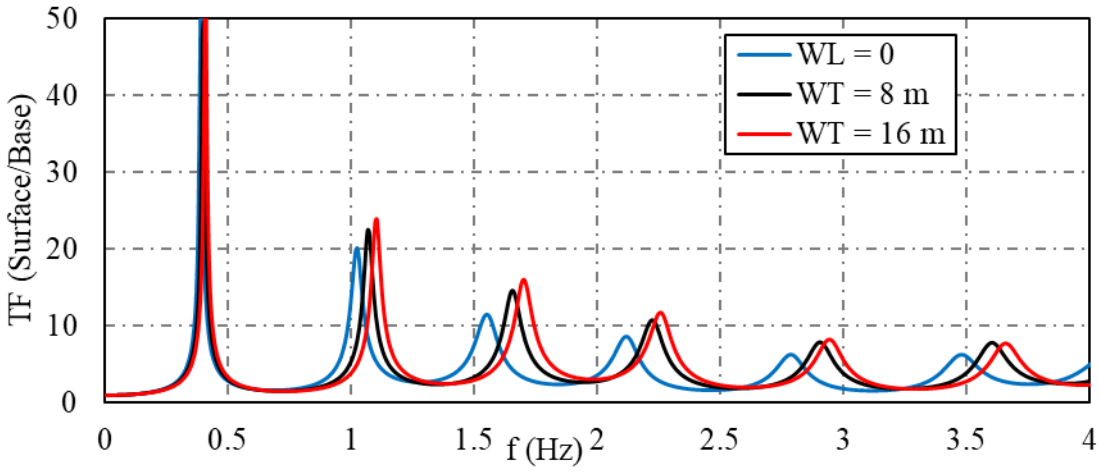

Figure 10-38. Variations of surface/base FFT transfer function for soils with different water tables in sandy soil

Assuming Silt Properties

The results of site response analyses with different depths of water table, considering silt hydraulic characteristics, where all important soil parameters (i.e. small-strain shear modulus, damping, modulus reduction factor, and damping) were varied are presented in this section. Observed and predicted surface/base RRS graphs with different depths of water table are shown in Figure 10-39 (a). In addition, the residual and normalized difference ratio of RRS graphs for different water table levels are shown in Figure 10-39 (b) and (c), respectively. For the models considering silt hydraulic characteristics, the RRS values of saturated ground slightly increased comparing to those in saturated sand layers. This led to higher RRS values of saturated ground than the one with reference water table for periods almost higher than 0.2 s. For periods shorter than 0.2 s, the analysis with water table at the ground surface still led to less RRS, although with an extent less than what was observed in sand layers. Lowering water table to 16 m below the ground surface led to less significant increase on the RRS values than its influence in sand

layers, where the RRS values even decreased within some mid-period ranges comparing to those of reference water table.

The observed trend is mainly due to the higher contribution of the effect of small-strain shear modulus on the site response of partially saturated silt than that in unsaturated sand layers. Variations of small-strain shear modulus as a result of elevating and lowering water table, led to higher and lower RRS values within a relatively long range of periods, respectively. However, variations in unit weight and damping due to the water table fluctuations caused counter-effects on RRS values. The values of small-strain shear modulus in silt layers experienced a more profound divergence as a result of water table fluctuations than damping or unit weight values due to the higher impact of effective stress on shear modulus formulation. Therefore, the effect of shear modulus variations as a result of water table fluctuation appeared to be more significant than that in sand layers. The different observations in sand and silt layers are consistent with the results of simplified numerical analysis, discussed earlier in Chapter 4 (Mirshekari and Ghayoomi 2015). According to the preliminary numerical analysis, partial saturation in sand layers (stiffer soils) led to higher amplification factors than dry condition, while unsaturated (stiffer) silt layers showed lower amplification factors than dry condition. Interestingly, although matric suction values in silt are considerably higher than those in sand, the extent of influence of water table fluctuation in silt layers appeared to be less significant than the observed change in sand layers. This demonstrates that considering the effect of partial saturation should not be limited to its influence on the stiffness (shear modulus) of ground layers. In fact, the predicted difference in the response of soil layers was shown to be more significantly affected by the variations of damping and unit weight due to water table fluctuation.

Observed and predicted surface/base FFT transfer functions are presented in Figure 10-40 (a), with a focus on the predicted values within frequencies up to 4 Hz shown in Figure 10-41. The residual FFT transfer function graphs as well as the normalized difference ratios for different water table heights are shown in Figure 10-40 (b) and (c), respectively. Similar to the response of sand layers, both fundamental frequencies and magnitude of TFs increased when lowering water table and generating a stiffer material. The observed change in different fundamental frequencies was higher than that in sand layers indicating stiffer characteristics for the silt layers with water table at 16 m below the ground surface.

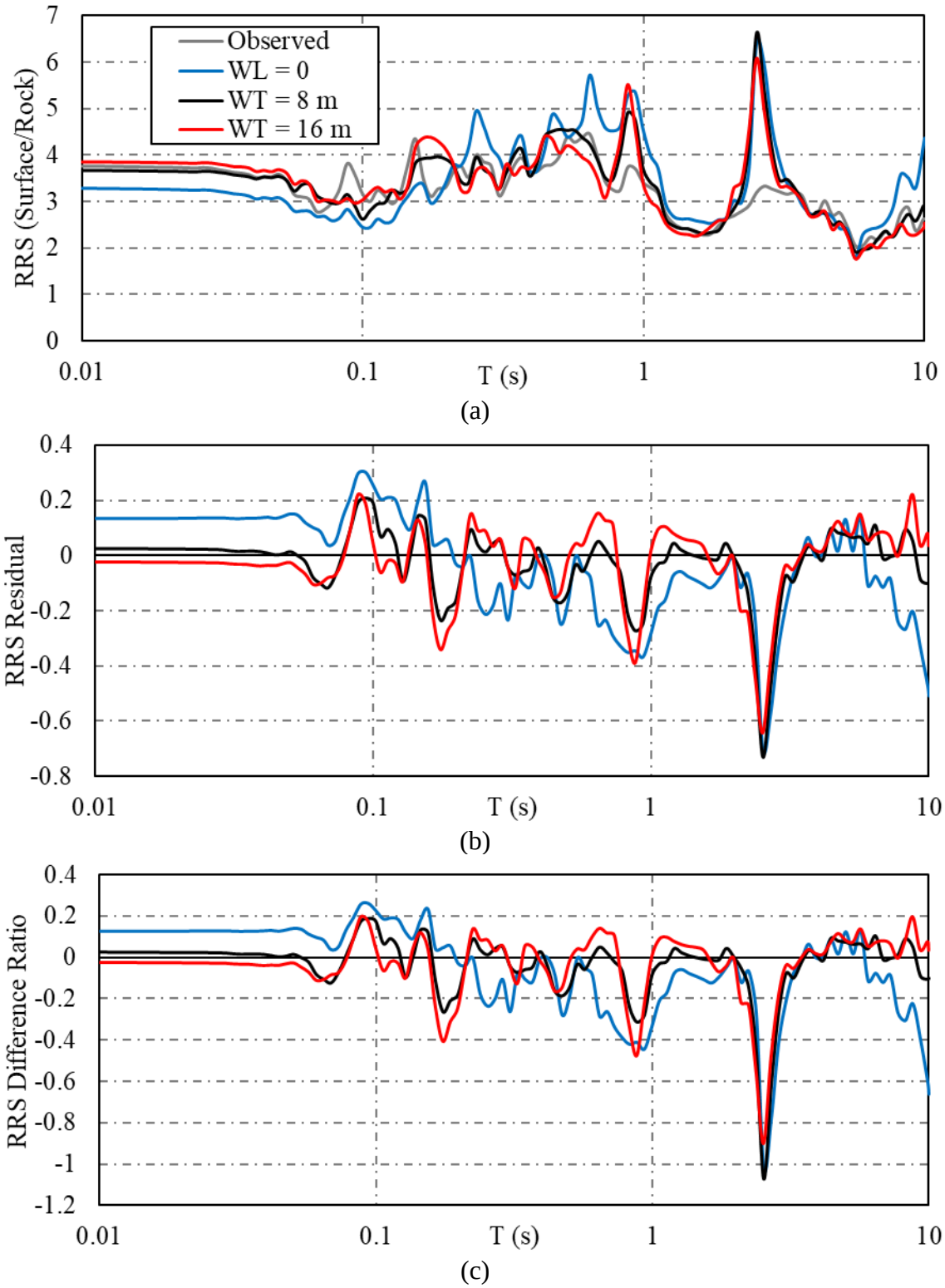

Figure 10-39. Variations of surface/base (a) Ratio of Response Spectra (b) RRS residual and (c) RRS normalized difference for soils with different water in silty soil

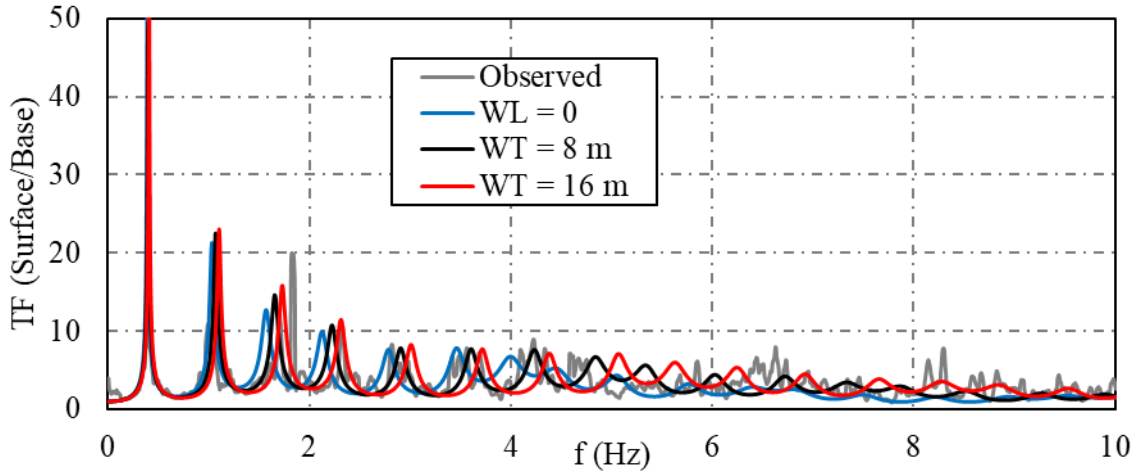

(a)

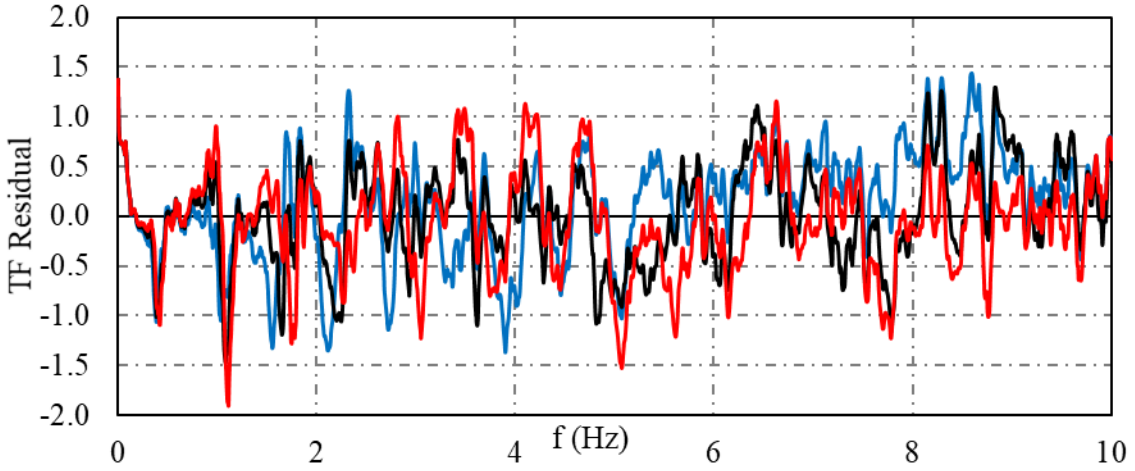

(b)

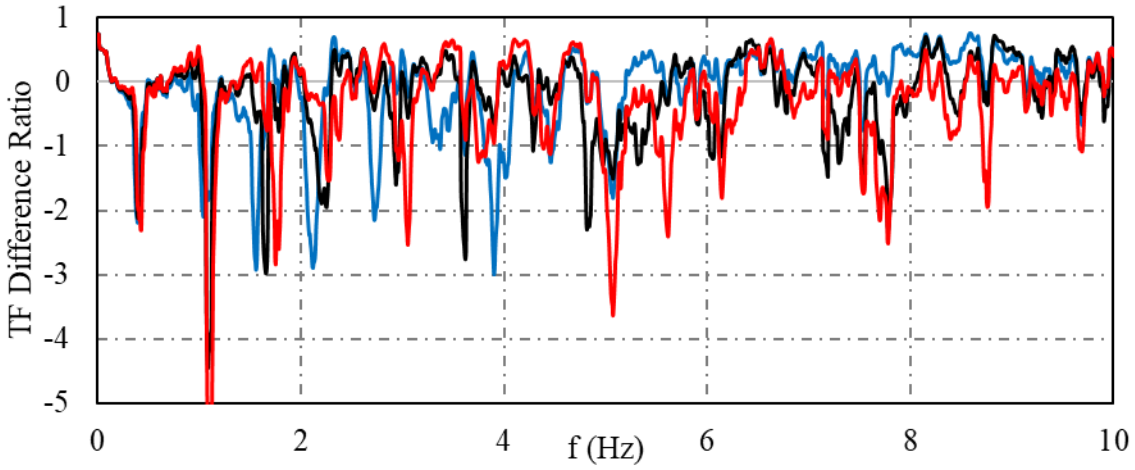

(c)

Figure 10-40. Variations of surface/base (a) FFT transfer function (b) FFT TF residual and (c) FFT TF normalized difference for soils with different water tables in silty soil

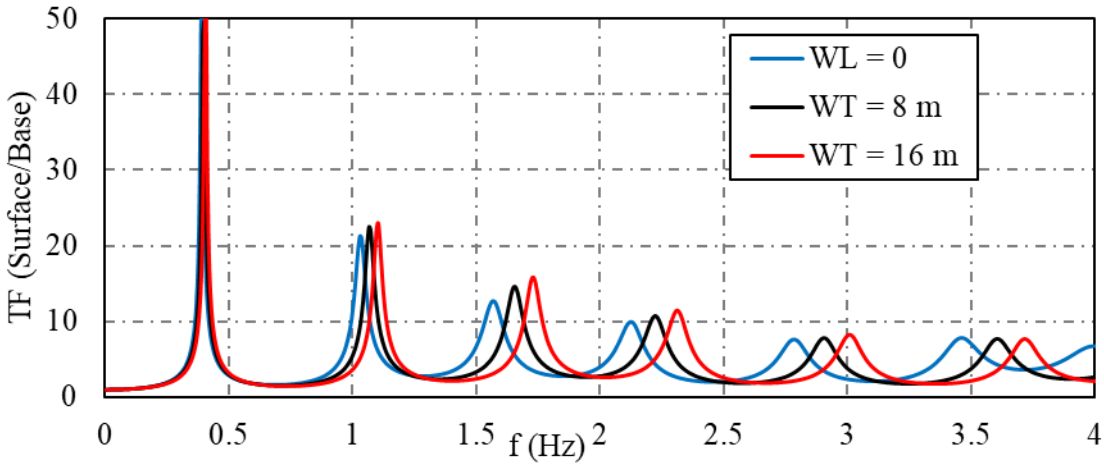

Figure 10-41. Variations of surface/base FFT transfer function for soils with different water tables in silty soil

10.5. Summary and Conclusions

The results of a parametric analysis were presented in this chapter where the effect of variations in different input variables, due to water table fluctuation, on seismic site response was evaluated. The soil profile in NMRH04 was selected from the sites in KiK-Net database in this study, and the depth of water table was altered from 8 m below the ground surface to the ground surface and 16 m below the ground surface as two extreme conditions. Empirical correlations were used to estimate the different input parameters (i.e. small-strain and strain-dependent shear modulus, damping, and unit weight) in sand and silt profiles with different depths of water table. The numerical modeling procedure was verified using the results of similar equivalent linear analysis from the software SHAKE2000 (Kaklamanos et al. 2015).

The variations of small-strain shear modulus, due to water table fluctuation, caused the highest influence on the intensity amplification. Since the effect of degree of saturation (or similarly matric suction) is not independently incorporated into the damping and shear modulus equations, the variations of these two parameters led to insignificant variations in terms of frequency- and

period-dependent acceleration amplification factors. As a result of the counter-effects on motion amplification, caused by variations in shear modulus as well as damping and unit weight, a considerable change in RRS and TF values were observed when all the parameters changed due to water table fluctuation. Interestingly, the RRS and TF magnitudes increased by lowering the water table (i.e. stiffer soil profile) and decreased by elevating the water table (i.e. softer soil profile). These changes were found to be higher in sand layers than those obtained in silt profiles. The effects of variations in different soil parameters, due to water fluctuation, on intensity amplification (i.e. the change in RRS and TF magnitudes) are summarized in Table 10-3.

Table 10-3. The effect of variations in different soil parameters, as a result of water table fluctuation, on intensity amplification

Depth of Water Table Variation (m)	**Soil Type**	**Parameter**	**Variation**	**Influence on Amplification Factor**
8 to 0	Sand and Silt	G_0	Decrease	Increase
		G/ G_0	Decrease	Increase
		Damping	Increase	Decrease
		Unit Weight	Increase	Decrease
		Total Change	-	Decrease
8 to 16	Sand and Silt	G_0	Increase	Decrease
		G/ G_0	Increase	Decrease
		Damping	Decrease	Increase
		Unit Weight	Decrease	Increase
		Total Change	-	Increase

CHAPTER XI

SUMMARY, CONCLUSIONS, AND RECOMMENDATIONS

11.1. Summary

The objective of this study was to assess the effect of partial saturation on seismic site response analysis of soil layers and introduce simplistic approaches to account for partially-saturated condition above the water table in conventional site response analysis. In addition, the effect of higher gravitational fields on Soil-Water Retention Characteristics was studied. Further, the uncertainty in seismic site response due to water table fluctuation was to be investigated. The mentioned objectives were accomplished through the following steps:

- Preliminary equivalent linear and nonlinear site response analyses were performed for partially saturated sand and silt layers with uniform suction profiles. The effect of partial

saturation was manually incorporated in the numerical procedure by increasing the effective stress in unsaturated layers with different degrees of saturation. The increase in effective stress, in turn, altered different input parameters including shear modulus, modulus reduction factor, damping, and unit weight. Various motion characteristics including the intensity amplification, spectral acceleration, and deformation, were monitored from the base to the ground surface in dry and unsaturated soil profiles.

- Steady state infiltration technique was implemented in a laminar container inside a Geotechnical centrifuge whereby matric suction (or alternatively degree of saturation) was controlled throughout the depth of the specimen. Uniform degree of saturation profiles were successfully obtained where different average degrees of saturation were obtained by varying the inflow discharge velocity. This technique was employed to evaluate the effect of different degrees of saturation on seismic site response of sand layers.
- The 1-g Soil Water Retention Curve (SWRC) of F-75 Ottawa sand was obtained along drying, wetting, and hysteresis paths using hanging column testing as well as tensiometeric technique.
- Centrifuge experiments were conducted where partially saturated condition was induced using steady state infiltration technique as well as capillary rise from an established water table (drying experiments) to study scaling laws regarding soil-water retention characteristics in high-g. The infiltration experiments were conducted under seven different discharges in this step, where for each discharge velocity the steady state condition was successively established in six different g-levels; ranging from 50 to 5 g.

The drying experiments were carried out by continuously lowering the water table in six different g-levels (i.e. 5, 10, 15, 20, 30, and 40 g).

- The scaling laws of capillary fringe height and hydrostatic pressure/suction profiles were investigated when water ascends from an identified water table in drying experiments.
- The effect of higher gravitational field on Soil Water Retention Curve during both drying and infiltration experiments was investigated.
- Dielectric sensors (for VWC), miniature PPTs (for pore water pressure), and miniature tensiometers (for pore water pressure/suction) were successfully deployed in steady state infiltration and drying experiments to validate SWRC measurements in higher gravitational fields.
- The in-flight shaking table was calibrated for two earthquake input motions; scaled 1994 Northridge motion with PGA of 0.3 g and scaled 1995 Kobe motion with PGA of 0.2 g.
- Seismic excitation simulating scaled Northridge and Kobe earthquake motions were applied to dry, saturated, and unsaturated specimens of loose Ottawa sand with uniform degrees of saturation in depth. The recorded data were used to assess the seismic site response under different water saturation profiles. In addition, the effect of shaking intensity on the site response of partially saturated soil layers was evaluated.
- Additional equivalent numerical analyses were carried out using DEEPSOIL software through which the uncertainty in site response analysis due to water table fluctuation was studied. Further, the effect of variations in each soil parameter, due to water table fluctuation, was assessed on seismic site response of ground layers. Surface and bedrock acceleration time histories recorded in NMRH04 vertical array, from the Kiban-Kyoshin network (KiK-net), were used as baseline data for validation and parametric study.

Hydrostatic matric suction variation was considered in this round of analysis, which similarly occurs in the nature as a result of capillary ascending in vadose zone. The water table was fluctuated from 8 m as the baseline depth to the ground surface and 16 m below the ground surface. Consequently, the input parameters (i.e. small-strain shear modulus, damping, modulus reduction factor, and unit weight, soil type) were changed, and the divergence in site response was recorded. The motion characteristics included Ratio of Response Spectra (RRS), Fast Fourier Transform Transfer Function (TF), and their residual values.

When using both numerical and experimental findings of this investigation, one has to pay attention to the following limitations of this work:

- In order to control degree of saturation in the centrifuge experiments, steady state infiltration technique was used, which resulted in uniform degree of saturation profiles. Although this technique is a suitable approach for evaluating the effect of degree of saturation on seismic site response, profiles of degree of saturation or matric suction follow a more complex pattern in the nature. Therefore, the results of centrifuge modeling were intended to be used as a proof-of-concept assessment of the effect of partial saturation on seismic site response.
- Although real earthquake motions were used in the experimental program, it should be noted that since the intensity of the motions were scaled and also due to the limited number of input motions in this study, the obtained conclusions could not be generalized to be predictive of the trends under all seismic events.

- F-75 Ottawa sand was selected for the experimental program in this study since its grain size distribution allowed the steady state infiltration to occur within the range of attainable discharge velocities using the infiltration setup. Thus, the experimental findings derived in this study are only the case for similar fine-grained poorly-graded sands. The seismic response of soil layers with different mechanical/hydraulic behavior would likely be different. The performed numerical analyses shed light on the extent of influence of partial saturation on site response of soils with higher suction levels.
- In the absence of numerical codes capable of considering partial saturation, it was simplistically incorporated into the numerical analysis by varying the input soil parameters. However, the majority of empirical equations of dynamic soil properties were obtained based on the results from completely dry or saturated materials and cannot precisely evaluate the variation of those parameters in unsaturated condition. In most cases, the effect of partial saturation on dynamic soil properties was only considered by adjusting the effective stresses in unsaturated condition. However, a more accurate assessment of those properties in unsaturated condition could be achieved by incorporating an independent term indicating the effect of matric suction or degree of saturation on that parameter.
- In addition to the limitations with respect to the selection of material dynamic properties in unsaturated condition, it should be noted that evaluating the seismic site response of unsaturated soil layers by changing the input soil parameters is a simplified approach. In order to more precisely predict the seismic response of unsaturated soils, different wave propagation mechanisms in partially saturated zones have to be considered.

11.2. Conclusions

Prior to conducting the target seismic centrifuge tests, a preliminary experimental program was carried out to address some challenging questions with respect to the soil-water retention scaling in higher gravities. The following conclusions were derived from this investigation:

- An approximate scaling factor of 1/N was found for the capillary fringe height, which is consistent with the analytical solutions from the "bundle of capillaries" approach. However, the capillary ascending might not occur uniformly within the soil layers due to the capillary fingers phenomenon where water rises along paths with different heights.
- The 1-g interchangeable relationship between the VWC and matric suction might be used for the results of higher g-levels since the captured SWRC of sand was analogous in different g-levels during the drying experiments. A slight difference was observed between the high-g and 1-g measurements, which could occur due to the small hysteresis effects accumulated during each drying experiment as well as small variations in density of the specimens.
- A significant hysteresis was observed during the steady-state infiltration experiments. As the tests, under each discharge, started at 50 g, the initially-saturated sand shifted along the drying path. Thereafter, the g-level was lowered while the discharge velocity was kept constant, which resulted in rewetting the specimen and moving the VWC-matric suction curve along a scanning path. This scanning path was in a good agreement with the 1-g data obtained from the tensiometeric technique.
- A parametric study on the equation proposed by Dell'Avanzi et al. (2004) revealed that the suction scaling factor during steady state infiltration can be simply represented by the

inverse of the uniformity factor. However, to project the measured model matric suctions to their prototype values, the stress scaling factor of 1 has to be used. In addition, the adequacy of back-calculating the degree of saturation or matric suction values in higher gravities only depends on the validity of 1-g SWRC in higher g-levels and is not a suction scaling problem.

- The SWRC of the sand obtained during the infiltration tests was not affected by the g-level. Although a complete scanning curve was not obtained from the data points of different discharges in each g-level, the coherency between the results of different g-levels indicate the independency of the SWRC from the g-level. This would permit the 1-g SWRC measurements to be used for back-calculation of degree of saturation or matric suction in higher g-levels.

The major objective of this research was to assess the effect of partial saturation on seismic site response. The following conclusions were obtained as a result of numerical as well as centrifuge physical modeling of seismic response of unsaturated soil profiles:

- The results of preliminary numerical analyses demonstrated the effect of partial saturation on seismic site response. The variations of different motion characteristics (i.e. PGA amplification factor, spectral accelerations, lateral deformation, and Arias intensity) depended on the suction level and the induced motion properties. For soils with higher suction level (e.g. 70 kPa) intensity amplification and deformation were higher in dry condition than the unsaturated cases. In the case of soils with low suction level (e.g. 10 kPa) the opposite trend was observed where unsaturated soils show higher amplification and deformation than the dry ones. This showed that although partial saturation generates

a stiffer medium, the amplification factors might be higher in unsaturated soils due to the interplay between different soil properties including shear modulus, modulus reduction factor, damping, and unit weight. In particular, the effect of reduced damping values as well as increased unit weights (and, in turn, applied force to the ground layers) in partially saturated condition played an important role in increasing the amplification factors.

- It is also shown that equivalent linear analysis results in significant higher amplification parameters. However, equivalent linear analysis resulted in lower deformation than in nonlinear analyses for Ottawa sand and higher deformation in Bonny silt, respectively.
- Through centrifuge seismic physical modeling, partial saturation was found to have a significant influence on seismic site response of sand layers. The effect of partial saturation on PGA amplification factor was shown to be a function of depth as well as the degree of saturation. Despite the commonly-practiced assumption that neglects the suction-dependency of seismic site response to be conservative, a higher PGA amplification at soil surface was observed as a result of partial saturation with an average increase of 16% (for the Northridge input motion). The PGA amplification factors proposed by seismic provisions were conservatively higher than the ones for the applied range of the degree of saturation. Amplification factors at soil surface decreased as the degree of saturation increased (i.e. lower matric suction and higher suction stress) where it became somewhat constant between the degrees of saturation of 45% and 70%. Suction stress correlated properly with the amplification factor, demonstrating a potentially promising parameter in evaluating the seismic behavior of unsaturated soils.

- The spectral acceleration in both low- and mid-period ranges were more amplified at soil surface as a consequence of partial saturation showing a more substantial change in the low-period amplification factor. The accumulated energy was intensified within the unsaturated soil layers indicated by a 6% increase in the surface to bedrock Arias intensity ratio, in the experiments with Northridge input motion. Despite higher intensity amplification in unsaturated soils, their lateral deformations were generally lower than the dry specimens with an average of 10% reduction in the experiments with Northridge input motion. Seismically-induced settlement reduced in unsaturated sand layers comparing with the dry ones, with a minimum settlement at a degree of saturation about 38% (in the experiments with Northridge input motion) due to the higher stiffness.
- Albeit unsaturated soils are stiffer than dry or saturated soils, which resulted in lower lateral deformation and surface settlement, partial saturation may trigger more intensity amplification as a result of interaction between different soil characteristics such as shear modulus, damping, and mobilized shear strain within the soil layers.
- The acceleration amplification, accumulated energy level, and seismic settlements in sand layers appeared to be a function of motion intensity. The surface/base amplification factors for Kobe motions were significantly higher than those obtained for Northridge motion due to lower PGA of the applied motion. Although the Kobe motion had a lower PGA, it caused a higher accumulated energy, indicated by the magnitude of Arias intensity, within the soil layers due to its higher FFT magnitude within the higher frequency ranges. The seismic settlements were higher in the sand layers triggered by Kobe motion due to its higher energy level.

As the last step of this research, a parametric study was performed to evaluate the induced uncertainty in site response analysis due to the water table fluctuations. The resulting conclusions of this step are as follow:

- Water table fluctuation substantially affected the site response of sand and silt layers. Interestingly, the extent of divergence in Ratio of Response Spectra and FFT Transfer Functions, appeared to be higher in sand layers comparing with the silt layers. This indicates that the effect of partial saturation on seismic site response is not limited to its influence on stiffness of ground layers, but it should be holistically studied considering the interaction between the effects caused by all the soil parameters.
- The effect of variations in different parameters (i.e. small-strain shear modulus, modulus reduction factor, damping, and unit weight) on the induced uncertainty in site response due to water table fluctuation was investigated. Changes of small-strain shear modulus due to water table fluctuations was shown to have the most profound influence on the site response among the considered variables. In addition, unit weight change caused slight variations in terms of the studied motion characteristics (i.e. RRS and TF). However, variations in damping and modulus reduction factor led to insignificant divergence in site response of both sand and silt layers. This demonstrated the incompetency of the current damping formulations to be predictive of those values in unsaturated soils.
- The variations in small-strain shear modulus due to elevating and lowering water table, mainly, led to higher and lower RRS values. This change was more pronounced in silt layers because of its higher level of matric suction. Variations in unit weight and damping, due to water table fluctuation, led to opposite effects on RRS values. These

counter-effects resulted in the overall trend of lower and higher RRS for soil layers with higher and lower water tables, respectively. In other words, stiffer ground (deeper water table) showed higher RRS values than softer layers (shallow water table). This conclusion is against the commonly-practiced assumption where stiffer soils are believed to cause lower acceleration amplification and recommends considering the change in all soil parameters when analyzing the response of partially saturated soils.

11.3. Recommendations for future work

Partially saturated condition was controlled using steady state infiltration technique in this study, which resulted in uniform degree of saturation profiles prior to the seismic events. It is recommended to further continue centrifuge seismic experiments on partially saturated soils following the capillary rise approach to generate a partially saturated zone above identified water tables. Generating partially saturated zone by capillary ascending of water is similar to the natural phenomenon occurring in the field. The results could be compared with those obtained in this study to investigate the influence of employed approach on the seismic response of unsaturated soil layers. Further, in order to capture the effect of different materials on site response of unsaturated soils, a variety of soil types in unsaturated state under a suite of earthquake motions is needed.

A recommendation would be to incorporate bender elements inside the laminar container whereby the small-strain shear modulus of unsaturated soils can be measured prior to the shaking events. Since the values of shear modulus can be back-calculated from the obtained results of seismic site response, shear modulus reduction factors could be estimated given the strain level at different depths obtained from side LVDT measurements. Due to the scarcity of shear

modulus reduction equations for partially saturated condition, obtaining such formulations under actual earthquakes would be of great value.

The parametric evaluation in this study could be employed as a preliminary step towards a comprehensive statistical analysis, which would study the uncertainty introduced in site response analysis as a result of water table fluctuation. Data from other vertical arrays, preferably instrumented with pore pressure transducers, which can precisely measure the depth of water table at the time of seismic events, will significantly improve the modeling assumptions in this study. It is suggested that similar numerical analyses will be performed with an emphasis on the parameters with higher impact, as demonstrated in this study (i.e. small-strain shear modulus and unit weight). Further, performing the analysis under different input motions and for different sites consisting of materials with a wide range of grain size distribution is suggested.

References

Afacan, K. B., Brandenberg, S. J., and Stewart, J. P. (2014) “Centrifuge modeling studies of site response in soft clay over wide strain range.” J. Geotech. & Geoenvir. Eng., ASCE, 140 (2), 04013003.

American Society of Civil Engineers, ASCE. (2010) “Minimum Design Loads for Buildings and Other Structures.” ASCE/SEI 7-10.

Allmond, J., and Wilson, D. (2012). "Analysis and Comparison of Various Pore Pressure Transducer Implemented in the JDA02 Centrifuge test." Department of Civil and Environmental Engineering College of Engineering, University of California at Davis.

Arias A. (1970) “A measure of earthquake intensity. In: Seismic design for nuclear power plants.” In: Hansen RJ, editor. Cambridge, MA. MIT Press.

Arulanandan, K., Anandarajah, A., & Abghari, A. (1983). “Centrifugal modeling of soil liquefaction susceptibility.” Journal of Geotechnical Engineering, 109(3), 281-300.

Arulanandan, K., Thompson, P., Kutter, B., Meegoda, N., Muraleetharan, K., and Yogachandran, C. (1988). "Centrifuge modeling of transport processes for pollutants in soils." *J.Geotech.Eng.*, 114(2), 185-205.

Assimaki, D., Li, W., Steidl, J., & Schmedes, J. (2008). “Quantifying nonlinearity susceptibility via site-response modeling uncertainty at three sites in the Los Angeles Basin.” Bulletin of the Seismological Society of America, 98(5), 2364-2390.

ASTM. (2001). “Standard test methods for determination of the soil water characteristic curve for desorption using a hanging column, pressure extractor, chilled mirror hygrometer, and/or centrifuge.” ASTM D6836, West Conshohocken, Pa.

Barry, D., Lisle, I., Li, L., Prommer, H., Parlange, J., Sander, G. C., and Griffioen, J. (2001). "Similitude applied to centrifugal scaling of unsaturated flow." *Water Resour.Res.*, 37(10), 2471-2479.

Bear, J., Corapcioglu, M. Y., and Balakrishna, J. (1984). "Modeling of centrifugal filtration in unsaturated deformable porous media." *Adv.Water Resour.*, 7(4), 150-167.

Biglari, M., Jafari, M.K., Shafiee, A., Mancuso, C., and d’Onofrio, A. (2011) “Shear Modulus and Damping Ratio of Unsaturated Kaolin Measured by New Suction-Controlled Cyclic Triaxial Device.” ASTM Geotechnical Testing Journal, 2011, 34 (5), 1-12.

Boore, D. M. (2016). “Determining Generic Velocity and Density Models for Crustal Amplification Calculations, with an Update of the Generic Site Amplification for Vs = 760 m/s.” Bulletin of the Seismological Society of America, 106(1), 313-317.

Boore, D. M., Joyner, W. B., and Fumal T. E. (1994) “Estimation of Response Spectra and Peak Accelerations from Western NorthAmerican Earthquakes: An Interim Report, Part 2.” U.S. Geological Survey Open-File Report. 1994, 94-127, 40 pp.

Borcherdt, R. D. (1994) “Estimates of Site-dependent Response Spectra for Design (Methodology and Justification).” Earthquake Spectra 10, 617-653.

Borcherdt, R. D. (2002) “Empirical evidence for site coefficients in building-code provisions.” Earthquake Spectra, 18, 189-218.

Borcherdt, R. D. and Glassmoyer, G. (1994) “Influences of Local Geology on Strong and Weak Ground Motions in the San Francisco Bay Region, California, and their Implications for Site-Specific Code Provisions.” The Loma Prieta Earthquake of October 17, 1989- Strong Ground Motion, R. D. Borcherdt, Ed. U.S. Geological Survey Professional Paper, 1994, 1151-A, A77-A108.

Briggs, L., and Mclane, J. (1907). "The moisture equivalent of soils. Washington, Department of Agriculture, 1907. 23p." *Bulletin,* 45 23.

Burkhart, S., Davies, M., Depountis, N., Harris, C., and Williams, K. (2000). "Scaling laws for infiltration and drainage tests using a Geotechnical Centrifuge." *Physical Modeling and Testing in Environmental Geotechnics,* 191-198.

Butterfield, R. (1999). "Dimensional analysis for geotechnical engineers." *Geotechnique,* 49(3), 357-366.

Caicedo, B., and Thorel, L. (2014). "Centrifuge modelling of unsaturated soils." *Journal of Geo-Engineering Sciences,* 2(1-2), 83-103.

Cargill, K. W., and Ko, H. (1983). "Centrifugal modeling of transient water flow." *J.Geotech.Eng.,* 109(4), 536-555.

Choi, Y. and Stewart, J.P. (2005) “Nonlinear site amplification as function of 30 m shear wave velocity.” Earthquake Spectra, 21 (1), 1-30.

Cobos, D. R., & Chambers, C. (2010). Calibrating ECH2O soil moisture sensors. Application Note, Decagon Devices, Pullman, WA.

Conca, J. L., and Wright, J. (1990). "Diffusion coefficients in gravel under unsaturated conditions." *Water Resour.Res.,* 26(5), 1055-1066.

Darendeli, M. B. 2001. “Development of a new family of normalized modulus reduction and material damping curves.” PhD dissertation, Univ. of Texas at Austin, Austin, Texas.

Darendeli M.B. and Stokoe K.H. (2001). Development of a new family of normalized modulus reduction and material damping curves, University of Texas, Geotechnical Engineering Report GD01-1.

Dell'Avanzi, E. (2004) "Unsaturated flow under increased gravitational field" Ph.D. Dissertation, University of Colorado at Boulder.

Dell'Avanzi, E., Zornberg, J. G., and Cabral, A. R. (2004). "Suction profiles and scale factors for unsaturated flow under increased gravitational field." *Soils and Foundations,* 44(3), 79-89.

Cooke, B., and Mitchell, R. (1991). "Physical modelling of a dissolved contaminant in an unsaturated sand." *Canadian Geotechnical Journal,* 28(6), 829-833.

Crançon, C., Pili, E., Dutheil, S., and Gaudet, J. (2000). "Modelling of capillary rise and water retention in centrifuge tests using time domain reflectometry." *Proceeding of the International Symposium on Physical Modelling and Testing in Environmental Geotechnics,* 199-206.

Depountis, N., Harris, C., and Davies, M. (2001). "An assessment of miniaturised electrical imaging equipment to monitor pollution plume evolution in scaled centrifuge modelling." *Eng.Geol.,* 60(1), 83-94.

Deshpande, S., and Muraleetharan, K. K. (1998). "Dynamic behavior of unsaturated soil embankments." *Geotechnical Earthquake Engineering and Soil Dynamics III:* ASCE, 890-901.

Dewoolkar, M. M., Ko. H. Y., Stadler, A. T., and Astaneh, S. M. F., A Substitute Pore Fluid for Seismic Centrifuge Modeling. ASTM Geotechnical Testing Journal, 1999, Vol. 22, No. 3, 196-210.

Dobry, R., Borcherdt, R. D., Crouse, C. B., Idriss, I. M., Joyner, W. B., Martin, G. R., Power, M. S., Rinne, E. E., Seed, R. B., New Site Coefficients and Site Classification System Used in Recent Building Seismic Code Provisions. Earthquake Spectra, 2000, Vol. 16(1), pp. 41- 67.

Dong, Y., Lu, N., and McCartney, J. S. (2016). Unified model for small-strain shear modulus of variably saturated soil. Journal of Geotechnical and Geoenvironmental Engineering, 142(9), 04016039.

D'Onza, F., d'Onofrio, A., and Mancuso, C. (2008) "Effects of unsaturated soil state on the local seismic response of soil deposits." Proc. 1st European Conf. on Unsaturated Soils, Durham, UK, 531- 536.

Esposito, G. (2000). "Centrifuge simulation of light hydrocarbon spill in partially saturated Dutch Dune Sand." *Bull.Eng.Geol.Env.,* 58(2), 89-93.

Federal Emergency Management Agency, FEMA. (2009) "NEHRP Recommended Seismic Provisions for New Buildings and Other Structures." FEMA P-750.

Gardner, R. (1937). "A method of measuring the capillary tension of soil moisture over a wide moisture range." *Soil Sci.,* 43(4), 277-284.

Gardner, W. (1958). "Some steady-state solutions of the unsaturated moisture flow equation with application to evaporation from a water table." *Soil Sci.,* 85(4), 228-232.

Garnier, J., Gaudin, C., Springman, S., Culligan, P., Goodings, D., Konig, D., Kutter, B., Phillips, R., Randolph, M., and Thorel, L. (2007). "Catalogue of scaling laws and similitude questions in geotechnical centrifuge modelling." *International Journal of Physical Modelling in Geotechnics*, 7(3), 1.

Garvey, R. and U. Ozbay (2013). "Assessing Coal Bumps from Excess Energy in Finite Difference Models." Proceedings of the 32nd International Conference on Ground Control in Mining. Morgantown, WV.

Ghayoomi, M. and Dashti, S. (2015) "Effect of Ground Motion Characteristics on Seismic Soil-Foundation-Structure Interaction", Earthquake Spectra, EERI, 31(3), 1789-1812.

Ghayoomi, M. and McCartney, J.S. (2011) "Measurement of small-strain shear moduli of partially saturated sand during infiltration in a geotechnical centrifuge." Special Issue on Advances in Experimental Characterization of Unsaturated Soils, Volume 1. ASTM Geotechnical Testing Journal, 34(5), 10 pg.

Ghayoomi,M. and McCartney, J.S. (2012) "Centrifuge Evaluation of the Impact of Partial Saturation on the Amplification of Peak Ground Acceleration in Soil Layers." Proceedings of GeoCongress 2012 (GSP 225). R.D. Hryciw, A. Athanasopoulos-Zekkos, and N. Yesiller, eds. ASCE. pp. 1968-1977.

Ghayoomi, M., McCartney, J.S., and Ko, H.-Y. (2011) "Centrifuge test to assess the seismic compression of partially saturated sand layers." ASTM Geotechnical Testing Journal, 34(4), 321-331.

Ghayoomi, M., McCartney, J.S., & Ko, H.-Y. (2013) "Empirical methodology to estimate seismically induced settlement of partially saturated sand." ASCE Journal of Geotechnical and Geoenvironmental Engineering, 139(3), 1-10.

Ghayoomi, M. and Mirshekari, M. (2014) "Equivalent Linear Site Response Analysis of Partially Saturated Sand Layers." UNSAT2014 conference, Sydney, Australia, 1-6.

Ghayoomi, M., Suprunenko, G., and Mirshekari, M. (2017) "Cyclic Triaxial Test to Measure Strain-Dependent Shear Modulus of Unsaturated Sand", ASCE International Journal of Geomechanics, Online, 1-11.

Gheibi, A. and Hedayat, A. (2018) "Ultrasonic investigation of granular materials subjected to compression and crushing." Ultrasonics, 87, 112-125.

Gibbs, J. F., Tinsley, J. C., and Joyner, W. B., Seismic Velocities and Geological Conditions at Twelve Sites Subjected to Strong Ground Motion in the 1994 Northridge California, Earthquake. U.S. Geological Survey Open-File Report 96-740, 1996, 103 pp.

Goforth, G. F., Townsend, F., and Bloomquist, D. (1991). "Saturated and unsaturated fluid flow in a centrifuge." *Proc. Centrifuge*, 497-502.

Goodings, D. (1982). "Relationships for centrifugal modelling of seepage and surface flow effects on embankment dams." *Géotechnique,* 32(2), 149-152.

Grelle, G., & Guadagno, F. M. (2009). “Seismic refraction methodology for groundwater level determination: Water seismic index. “Journal of Applied geophysics, 68(3), 301-320.

Haeni, F. P. (1986). “Application of seismic refraction methods in groundwater modeling studies in New England.” Geophysics, 51(2), 236-249.

Hardin, B. O. (1978) “The nature of stress-strain behavior of soils.” Proceedings, Earthquake Engineering and Soil Dynamics, ASCE Pasadena, California, Vol. 1, pp. 3-89.

Hardin, B.O. and Black, W.L. 1969. “Vibration Modulus of Normally Consolidated Clay; Closure.” J. Soil Mech. Found. Div. ASCE, Vol. 95, SM6, pp. 1531–1537.

Hardin, B.O., Drnevich, V.P. 1972. “Shear Modulus and Damping in Soils: Design Equations and Curves.” J. Soil Mech. Found. Div. Proc. ASCE 98, No. SM7, 667–692.

Hashash, Y. M. A., Dashti, S., Romero, M. I., Ghayoomi, M., and Musgrove, M. (2015) “Evaluation of 1-D Seismic Site Response Modeling of Sand using Centrifuge Experiments.” Soil Dyn. Earthquake Eng., 78, 19–31.

Hashash, Y.M.A., Musgrove, M.I., Harmon, J.A., Groholski, D.R., Phillips, C.A., and Park, D. (2016) “DEEPSOIL 6.1, User Manual.” Urbana, IL, Board of Trustees of University of Illinois at Urbana-Champaign.

Hasselström, B. (1969). “Water prospecting and rock-investigation by the seismic refraction method.” Geoexploration, 7(2), 113-132.

Hassler, G., and Brunner, E. (1945). "Measurement of capillary pressures in small core samples." *Transactions of the AIME,* 160(01), 114-123.

Heidari, M. and James, R. G. (1982). “Centrifugal Modeling of Earthquake Induced Liquefaction in a Column of Sand,” Proceedings of the Conference on Soil Dynamics and Earthquake Engineering, Vol. 1, Southampton, England, Taylor & Francis, New York, pp. 271–281.

Hoyos, L.R., Suescun-Florez, E.A., and Puppala, A.J. (2015) “Stiffness of Intermediate Unsaturated Soil from Simultaneous Suction-Controlled Resonant Column and bender Element Testing.” Engineering Geology,188, 10-28.

Hushmand, B. (1984) “Experimental Studies of Dynamic Response of Foundations.” PhD Dissertation, California Institute of Technology, CA, USA.

Hushmand, B., Scott, R. F., and Crouse, C. B. (1988) “Centrifuge Liquefaction Test in a Laminar Box.” Geotechnique, Vol. 38(2), pp. 253–262.

Idriss, I. M. (1990) “Response of Soft Soil Sites during Earthquakes.” Proceedings of the Symposium to Honor Professor H. B. Seed, Berkeley, May 1990, 273-289.

Idriss, I. M. (1991) “Earthquake Ground Motions at Soft Soil Sites.” Proceedings of the Second International Conference on Recent Advances in Geotechnical Earthquake Engineering and Soil Dynamics, St. Louis, MO, III, 1991, 2265-2273.

Idriss, I. M., Sun, J.I. (1992) “User's Manual for SHAKE91.” Center for Geotechnical Modeling, Dept. of Civil and Environmental Engineering, University of California, Davis, 1992.

International Code Council. (2011) “2012 international building code.” Country Club Hills, Ill: ICC.

Itasca Consulting Group. (2005) “FLAC, Fast Langrangian Analysis of Continua, Version 5.0.” Itasca Consulting Group, Minneapolis, Minnesota.

Iwasaki, T., Tatsuoka, F., and Yoshikazu, T. (1978). “Shear moduli of sands under cyclic torsional shear loading.” Soils and Foundations, Vol. 18, No. 1, 39-56.

Jarast, P., and Ghayoomi, M. (2017). “Numerical Modeling of Cone Penetration Test in Unsaturated Sand inside a Calibration Chamber.” International Journal of Geomechanics, 18(2), 04017148.

Jarast, P. (2017). “Numerical and Physical Modeling of Cone Penetration in Unsaturated Soils and Numerical Simulation of Fracture Propagation in Shale Rock during Brazilian Test” Doctoral dissertation, University of New Hampshire.

Joyner, W., Warrick, R., and Fumal, T. (1981) “The Effect of Quaternary Alluvium on Strong Ground Motion in the Coyote Lake, California, Earthquake of 1979.” Bull. Seism. Soc. Am., Vol. 71, No. 1, 1333-1349.

Kaklamanos, J., Baise, L. G., Thompson, E. M., and Dorfmann, L. (2015) “Comparison of 1D Linear, Equivalent-linear, and Nonlinear Site Response Models at Six KiK-net Validation Sites.” Soil Dynamics and Earthquake Engineering, 69, 207-219.

Ketcham, S. A., Ko, H.-Y. & Sture, A. (1991) “Performance of an Earthquake Motion Simulator for a Small Geotechnical Centrifuge.” Proceedings: Centrifuge 91. Boulder, CO.

Khademian, Z., Nakagawa, M., and Garvey, R. (2018). “Study on Seismic Events Induced by Loss of Fault Confinement due to Rock Temperature Decrease in EGS Reservoirs.” In 43rd Workshop on Geothermal Reservoir Engineering Stanford University. Stanford, California, Feb (pp. 12-14).

Khademian, Z., Nakagawa, M., and Ozbay, U. (2018). “Modeling injection-induced seismicity through calculation of radiated seismic energy.” Journal of Natural Gas Science and Engineering, 52, 582-590.

Khademian, Z., Nakagawa, M., Garvey, R., and Ozbay, U. (2017). “Role of fluid injection pressure in inducing seismicity.” In Proceedings (pp. 13-15).

Khanzode, R., Vanapalli, S., and Fredlund, D. (2002). "Measurement of soil-water characteristic curves for fine-grained soils using a small-scale centrifuge." *Canadian Geotechnical Journal,* 39(5), 1209-1217.

Khosravi, A., Ghayoomi, M., and McCartney, J.S. (2010) “Impact of effective stress on the dynamic shear modulus of unsaturated sand.” GeoFlorida 2010, West Palm Beach, Florida, USA. Feb. 20-24. CD-ROM.

Khosravi, A., Gheibi, A., & Rahimi, M. (2016c). “Impact of void ratio and state parameters on the small strain shear modulus of unsaturated soils.” Japanese Geotechnical Society Special Publication, 2(4), 241-246.

Khosravi, A. and McCartney, J.S. (2011) “Suction-controlled resonant column device for unsaturated soils.” ASTM Geotechnical Testing Journal 34(6). 1-10.

Khosravi, A., Mousavi, S., & Serej, A. D. (2016b). Hydraulic behavior of infilled fractured rocks under unsaturated conditions. In Geotechnical and Structural Engineering Congress 2016 (pp. 1708-1718).

Khosravi, A., Rahimi, M., Gheibi, A., and Shahrabi, M. M. (2017) “Impact of plastic compression on the small strain shear modulus of unsaturated silts.” ASCE International Journal of Geomechanics 18 (2), 04017138.

Khosravi, A., Serej, A. D., Mousavi, S. M., & Haeri, S. M. (2016a). Effect of hydraulic hysteresis and degree of saturation of infill materials on the behavior of an infilled rock fracture. International Journal of Rock Mechanics and Mining Sciences, (88), 105-114.

Kim, B., & Hashash, Y. M. (2013). “Site response analysis using downhole array recordings during the March 2011 Tohoku-Oki earthquake and the effect of long-duration ground motions.” Earthquake Spectra, 29 (s1), S37-S54.

Kizito, F., Campbell, C., Campbell, G., Cobos, D., Teare, B., Carter, B., and Hopmans, J. (2008). "Frequency, electrical conductivity and temperature analysis of a low-cost capacitance soil moisture sensor." *Journal of Hydrology,* 352(3), 367-378.

Knight, M., and Mitchell, R. (1997). "Modelling of light nonaqueous phase liquid (LNAPL) releases into unsaturated sand." *Canadian Geotechnical Journal,* 33(6), 913-925.

Knight, M., Cooke, A., and Mitchell, R. (2000). "Scaling of movement and fate of contaminant releases in the vadose zone by centrifuge modeling." *Physical Modeling and Testing in Environmental Geotechnics,* 233-242.

Ko, H.Y., (1988) “Summary of the state-of-art in centrifuge model testing”, Centrifuges in Soil Mechanics, Edited by Craig and Schofield, 11-18.

Kramer, S. L. (1996) “Geotechnical Earthquake Engineering.” Upper Saddle River, NJ: Prentice Hall. Print.

Lambe, P. C. and Whitman, R. V., (1982). “Scaling for Earthquake Loading Tests on Centrifuge,” Proc. of the Conference on Soil Dynamics and Earthquake Engineering, Vol. 1, Southampton, England, Taylor & Francis, New York, pp. 91–106.

Le, K., and Ghayoomi, M. (2017). "Cyclic Direct Simple Shear Test to Measure Strain-Dependent Dynamic Properties of Unsaturated Sand." *ASTM Getechnical Testing Journal*, (in press).

Lee, 1K. W. and W. D. L. Finn. (1978) “DESRA-2: dynamic effective stress response analysis of soil deposit with energy transmitting boundary including assessment of liquefaction potential.” Soil Mechanics Series, University of British Columbia, Vancouver, Canada.

Lord, A. (1999). "Capillary flow in the geotechnical centrifuge." *Geotechnical Testing Journal*, GTJODJ, Vol. 22, No. 4, December 1999, pp. 292–300.

Lu, N., Alsherif, N., Wayllace, A., & Godt, J. W. (2014). Closing the Loop of the Soil Water Retention Curve. Journal of Geotechnical and Geoenvironmental Engineering, 141(1), 02814001.

Lu, N., and Likos, W. J. (2004). *Unsaturated Soil Mechanics.* John Wiley & Sons, Hoboken, New Jersey.

Lu, N., and Likos, W. J. (2006) “Suction stress characteristic curve for unsaturated soils.” J. Geotech. Geoenviron. Eng., 1322, 131–142.

Lu, N., Godt, J. W., and Wu, D. T. (2010) “A Closed Form Equation for Effective Stress in Unsaturated Soil.” Water Resources Research, 46, W05515, 14pp.

Malengier, B., Di Emidio, G., Peiffer, H., Ciocci, M. C., and Kison, P. (2011) “Unsaturated permeability and retention curve determination from in-flight weight measurements in a bench-scale centrifuge,” Geotechnical Testing Journal, Vol. 38, No. 2, 2015, pp. 243‑254, doi:10.1520/ GTJ20140121. ISSN 0149-6115.

Mancuso, C., Vassallo, R., and d’Onofrio. A. (2002) “Small strain behavior of a silty sand in controlled-suction resonant column – torsional shear tests.” Canadian Geotechnical Journal, Vol. 39, No. 1, 22–31.

Marinho, E.A.M., Chandler, R.J., & Crilly, M.S. (1995) “Stiffness measurements on a partially saturated high plasticity clay using bender elements.” In Proc. of the 1 st Intl. Conf. on Unsaturated Soils, Paris, France, 6–8 September. A.A. Balkema, Rotterdam, the Netherlands, Vol. 2. 535–539.

Masing, G. (1926) “Eigenspannungen und Verfestgung Beim Masing,” Proceedings, Second International Congress of Applied Mechanics, pp.332-335.

Mason, H.B., Bray, J.D., Kutter, B.L., Wilson, D.W., and Choy, B.Y. (2010) “Earthquake Motion Selection and Calibration for Use in a Geotechnical Centrifuge.” 7th Int. Conf. on Physical Modeling in Geotechnics. Zurich, Switzerland.

Matasovic, N. (1993) “Seismic Response of Composite Horizontally-Layered Soil Deposits.” Ph.D. Thesis, University of California, Los Angeles, CA.

Mazzoni, S., F. McKenna, M. H. Scott and G. L. Fenves. (2006) “The OpenSees Command Language Manual.” Pacific Earthquake Engineering Research (PEER) Center: p. 451. Berkeley, California.

McCartney, J. S. (2007) “Determination of the hydraulic characteristics of unsaturated soils using a centrifuge permeameter” PhD Dissertation, The University of Texas at Austin.

McCartney, J. S. and Zornberg, J. G. (2010) “Centrifuge Permeameter for Unsaturated Soils. II: Measurement of the Hydraulic Characteristics of an Unsaturated Clay.” ASCE Journal of Geotechnical and Geoenvironmental Engineering, 136(8), 1064-1076.

Mendoza, C. E., Colmenares, J. E., and Merchan, V. E. (2005) “Stiffness of an unsaturated compacted clayey soil at very small strains.” Advanced Experimental Unsaturated Soil Mechanics, Taylor & Francis Group, London.

Menq, F. Y. (2003) “Dynamic Properties of Sandy and Gravelly Soils.” PhD Dissertation, the University of Texas at Austin.

Midorikawa, S., Matsuoka, M., and Sakugawa, K. (1994) “Site Effects on Strong-motion Records Observed during the 1987 Chiba-Ken-Toho-Oki, Japan Earthquake.” Proceedings of the 9th Japan Earthq. Eng. Symp., 3, E085-E090.

Mirshekari, M. and Ghayoomi, M. (2015) “Simplified Equivalent Linear and Nonlinear Site Response Analysis of Partially Saturated Soil Layers.” IFCEE 2015, Geotechnical Special Publication 256, M. Iskander, M.T. Suleiman, J.B. Anderson, D.F. Laefer eds., San Antonio, Texas, 2131-2140.

Mirshekari, M. and Ghayoomi, M. (2017) “Centrifuge Tests to Assess Seismic Site Response of Partially Saturated Sand Layers.” Soil Dynamics and Earthquake Engineering, Vol. 94, pp. 254-265.

Muraleetharan, K. K., and Granger, K. K. (1999). "The use of miniature pore pressure transducers in measuring matric suction in unsaturated soils." *Geotechnical Testing Journal*, GTJODJ, Vol. 22, No. 3, September 1999, pp. 226–234.

Ng, C. W. W., Leung, A. K., Kamchoom, V., and Garg, A. (2014). "A novel root system for simulating transpiration-induced soil suction in centrifuge." *Geotechnical Testing Journal*, Vol. 37, No. 5, 2014, pp. 1–15.

Ng, C.W.W., Xu, J. and Yung, S.Y. (2009) “Effects of imbibition-drainage and stress ratio on anisotropic stiffness of an unsaturated soil at very small strains.” Canadian Geotechnical Journal, Vol. 46, No. 9, 1062-1076.

Nimmo, J. R., and Akstin, K. C. (1988). "Hydraulic conductivity of a sandy soil at low water content after compaction by various methods." *Soil Sci.Soc.Am.J.*, 52(2), 303-310.

Nimmo, J. R., Akstin, K. C., and Mello, K. A. (1992). "Improved apparatus for measuring hydraulic conductivity at low water content." *Soil Sci. Soc. Am. J.*, 56(6), 1758-1761.

Nimmo, J. R., Rubin, J., and Hammermeister, D. (1987). "Unsaturated flow in a centrifugal field: Measurement of hydraulic conductivity and testing of Darcy’s law." *Water Resour.Res.*, 23(1), 124-134.

Ordonez, G. A. (2000). “SHAKE2000: A computer program for the 1D analysis of geotechnical earthquake engineering problems.” Geomotions, LLC, USA.

Parks, J. M., Stewart, M. A., and McCartney, J. S. (2011) “Validation of a centrifuge permeameter for investigation of transient infiltration and drainage flow processes in unsaturated soils.” Geotechnical Testing Journal, Vol. 35, No. 1, 182-192.

Petersen, M.D., Moschetti, M.P., Powers, P.M., Mueller, C.S., Haller, K.M., Frankel, A.D., Zeng, Y., Rezaeian, S., Harmsen, S.C., Boyd, O.S., Field, N., Chen, R., Rukstales, K.S., Luco, N., Wheeler, R.L., Williams, R.A., and Olsen, A.H. (2014) “Documentation for the 2014 update of the United States national seismic hazard maps” U.S. Geological Survey Open-File Report 2014–1091, 243 p., https://dx.doi.org/10.3133/ofr20141091.

Reatto, A., da Silva, E. M., Bruand, A., Martins, E. S., and Lima, Jorge Enoch Furquim Werneck. (2008). "Validity of the centrifuge method for determining the water retention properties of tropical soils." *Soil Sci.Soc.Am.J.*, 72(6), 1547-1553.

Reis, R. M., Sterck, W. N., Ribeiro, A. B., Dell’Avanzi, E., Saboya, F., Tibana, S., Marciano, C. R., and Sobrinho, R. R. (2011) “Determination of the Soil-Water Retention Curve and the Hydraulic Conductivity Function Using a Small Centrifuge.” ASTM Geotechnical Testing Journal, 34(5). 1-10.

Rezzoug, A., Konig, D., and Trantafylidis, T. (2000). "Numerical analysis of scaling laws for capillary rise in soils." *Physical Modeling and Testing in Environmental Geotechnics.*, 217-224.

Rezzoug, A., König, D., and Triantafyllidis, T. (2004). "Scaling laws for centrifuge modeling of capillary rise in sandy soils." *J.Geotech.Geoenviron.Eng.*, 130(6), 615-620.

Richards, L. A. (1931). "Capillary conduction of liquids through porous mediums." *Physics*, 1(5), 318-333.

Roesset, J. M., Soil Amplification in Earthquakes. Numerical Methods in Geotechnical Engineering, C. S. Desai and J. T. Christian, eds., McGraw Hill, New York, 1977, Chapter 19, 639-682.

Russell, M., and Richards, L. (1939). "The determination of soil moisture energy relations by centrifugation." *Soil Sci.Soc.Am.J.,* 3(C), 65-69.

Rutqvist, J., Rinaldi, A. P., Cappa, F., Moridis, G. (2013). "Modeling of Fault Reactivation and Induced Seismicity During Hydraulic Fracturing of Shale-Gas Reservoirs." Journal of Petroleum Science and Engineering 107: 31-44.

Sawangsuriya, A., Edil, T.B., and Bosscher, P.J. (2009). "Modulus-suction-water relationship for compacted soils in postcompaction state." Journal of Geotechnical and Geoenvironmental Engineering ASCE. Vol. 135, No. 10, 1390-1403.

Schubert, H. (1982). *Kapillaritat in porosen Feststoffsystemen.* Springer, Berlin.

Seed, H.B. and Idriss I.M. (1970) "Soil Moduli and Damping Factors for Dynamic Response Analyses." Rep. No. EERC70-10. Earthquake Eng. Res. Ctr., Univ. of California, Berkeley, Calif.

Seed, H. B., Murarka, R., Lysmer, J., and Idriss, I. M. (1976) "Relationships between Maximum Acceleration, Maximum Velocity, Distance from Source and Local Site Conditions for Moderately Strong Earthquakes." Bull. Seism. Soc. Am., 66, 1323-1342.

Silva, W., Darragh, R., Gregor, N., Martin, G., Abrahamson, N., and Kircher, C. (2000) "Reassessment of site coefficients and near-fault factors for building code provisions." USGS NEHRP program report 98-HQ-GR-1010.

Šimůnek, J., and Nimmo, J. R. (2005). "Estimating soil hydraulic parameters from transient flow experiments in a centrifuge using parameter optimization technique." *Water Resour.Res.,* 41(4),.

Stewart, J. P., and Kwok, A. O., Nonlinear seismic ground response analysis: Code usage protocols and verification against vertical array data. Proc., Geotechnical Engineering and Soil Dynamics IV, D. Zeng, M. T. Manzari, and D. R. Hiltunen, eds., ASCE Geotechnical Special Publication No. 181, ASCE, Reston, VA, 2008, 1–24.

Stewart, J.P., Liu, A.H., and Choi, Y. (2003) "Amplification Factors for Spectral Acceleration in Tectonically Active Regions." Bull. Seism. Soc. Am., 93 (1), 332-352.

Stewart, M. A., and McCartney, J. S. (2013). "Centrifuge modeling of soil-structure interaction in energy foundations." *J.Geotech.Geoenviron.Eng.,* 140(4), 04013044.

Stokoe, K. H., II, Hwang, S. K., Darendeli, M. B., and Lee, N. J. (1995a) "Correlation study of nonlinear dynamic soils properties." Final Rep. to Westinghouse Savannah River Company, Aiken, S.C.

Stokoe, K.H., III, Hwang, S.K., Lee, J.N.K, and Andrus, R.D. (1995b). “Effects of various parameters on the stiffness and damping of soils at small to medium strains” Proc. of Int. Symp. on Pre-Failure Deformation of Geomaterials Vol. 2, 785-816.

Suprunenko, G. (2015) “Suction-controlled cyclic triaxial test to measure strain-dependent dynamic shear modulus of unsaturated sand” M.Sc. thesis, University of New Hampshire.

Take, W., and Bolton, M. (2003). "Tensiometer saturation and the reliable measurement of soil suction." *Géotechnique*, 53(2), 159-172.

Tristancho, J., Caicedo, B., Thorel, L., and Obregón, N. (2011). "Climatic chamber with centrifuge to simulate different weather conditions."

van Genuchten, M. (1980) “A Closed Form Equation for Predicting the Hydraulic Conductivity of Unsaturated Soils.” Soil Sci. Soc. Am. J., Vol. 58, pp. 647–652.

Vucetic, M. and Dobry, R. (1991) “Effect of Soil Plasticity on Cyclic Response.” ASCE Journal of Geotechnical Engineering, Vol 117, No. 1, 89-107.

Whitman, R. V. and Lambe, P. C. (1986) “Effect of Boundary Conditions upon Centrifuge Experiments Using Ground Motion Simulation.” Geotech. Test. J., Vol. 9(2), pp. 61–71.

Whitman, R. V., Lambe, P. C., and Kutter, B. L. (1981). “Initial results from a stacked ring apparatus for simulation of a soil profile.” International Conferences on Recent Advances in Geotechnical Earthquake Engineering and Soil Dynamics. Paper 4.

Yang, J. (2006) “Frequency-Dependent Amplification of Unsaturated Surface Soil Layer.” ASCE Journal of Geotechnical and Geoenvironmental Engineering, 132(4), 526-531.

Yang, J. and Sato, T. (2000) “Effects of Pore-Water Saturation on Seismic Reflection and Transmission from a Boundary of Porous Soils.” Bulletin of the Seismological Society of America, 90 (5), 1313-1317.

Zeghal, M., Elgamal, A. W., Tang, H. T., and Stepp, J. C. (1995) “Lotung downhole array. II: Evaluation of soil nonlinear properties.” Journal of Geotechnical Engineering, Vol. 4 No. 363, 363–378.

Zhang J, Andrus R. D., and Juang, C. H. (2005) “Normalized Shear Modulus and Material Damping Relationships” Journal of Geotechnical and Geoenvironmental Engineering, 131 (453-464)

Zornberg, J. G., and McCartney, J. S. (2010). "Centrifuge permeameter for unsaturated soils. I: Theoretical basis and experimental developments." *J.Geotech.Geoenviron.Eng.*, 136(8), 1051-1063.